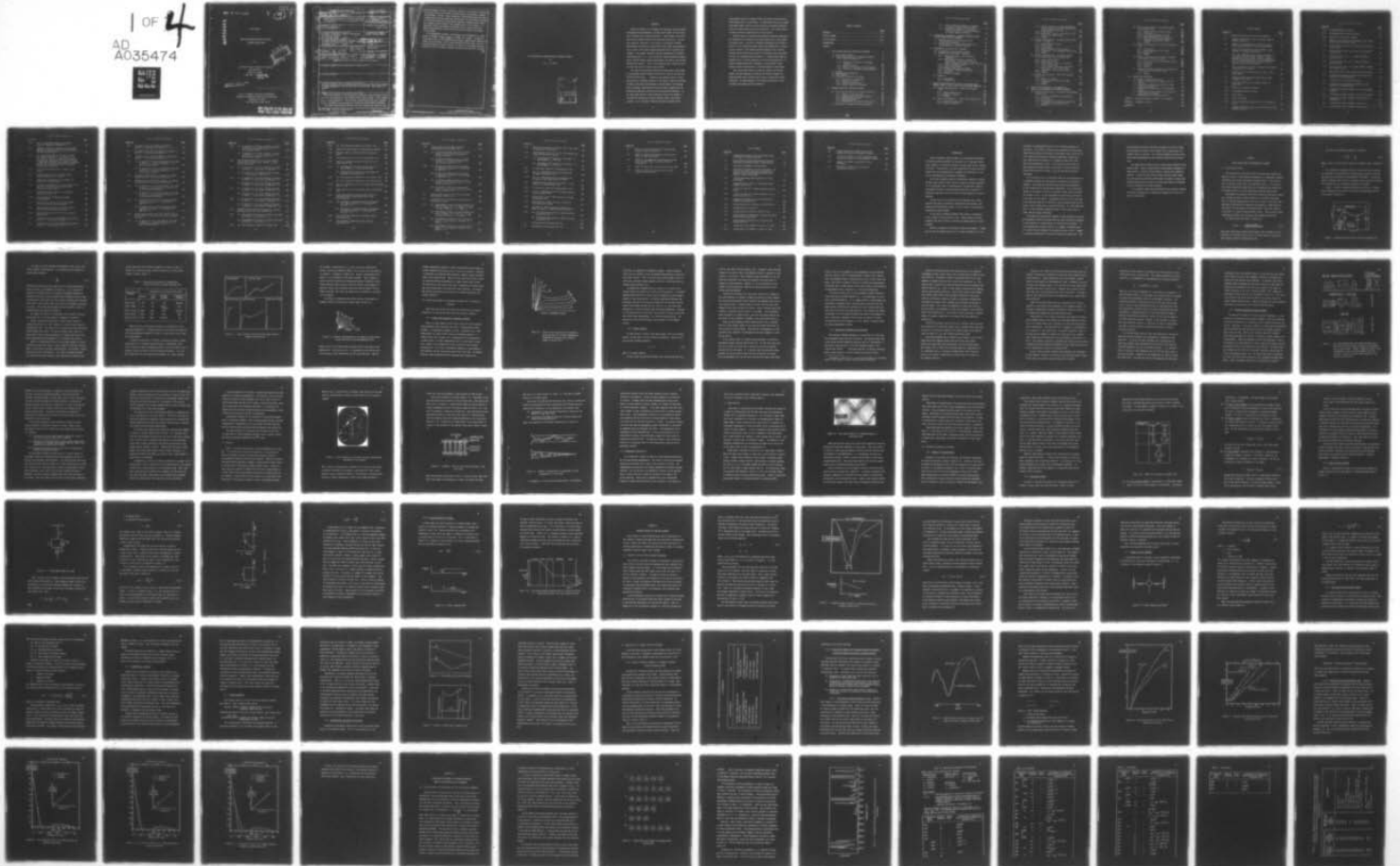


AD-A035 474

UTAH UNIV SALT LAKE CITY DEPT OF MATERIALS SCIENCE --ETC F/G 7/3  
MOLECULAR BEHAVIOR STUDIES OF GLASSY POLYMERS UNDER STRESS.(U)  
NOV 76 W O STATTON AF-AFOSR-2827-75  
UTEC-76-274 AFOSR-TR-77-0047 NL

UNCLASSIFIED

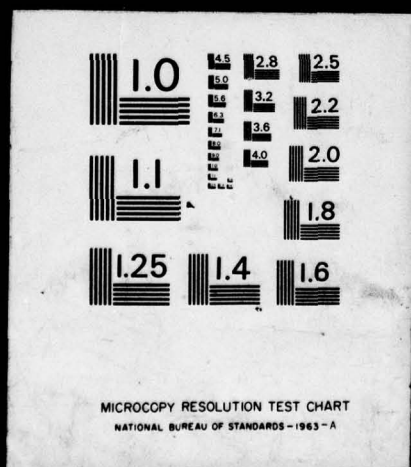
1 OF 4  
AD  
A035474





1 OF 4

AD  
A035474



UTEC 76-274  
November 23, 1976

AFOSR - TR - 77 - 0047

ADA035474

Final Report

MOLECULAR BEHAVIOR STUDIES OF GLASSY  
POLYMERS UNDER STRESS

to

Air Force Office of Scientific Research  
Bolling Field

Grant No. 75-2827

1 May 1975 - ~~1 October 1976~~

31 July 1976

Approved for public release;  
distribution unlimited.

Approved for public release;  
distribution unlimited.

Dr. W. O. Statton, Principal Investigator  
Department of Materials Science and Engineering  
University of Utah  
Salt Lake City, Utah 84112

COPY AVAILABLE TO DDC DOES NOT  
PERMIT FULLY LEGIBLE PRODUCTION



REPORT DOCUMENTATION PAGE		READ INSTRUCTIONS BEFORE COMPLETING FORM	
1. REPORT NUMBER <b>(18) AFOSR - TR - 77 - 0047</b>	2. GOVT ACCESSION NO.	3. RECIPIENT'S CATALOG NUMBER <b>(9)</b>	
4. TITLE (and Subtitle) <b>(6) MOLECULAR BEHAVIOR STUDIES OF GLASSY POLYMERS UNDER STRESS</b>		5. TYPE OF REPORT & PERIOD COVERED <b>FINAL rept. 1 May 1975 - 31 Jul 76</b>	
6. AUTHOR(s) <b>(10) William D. Statton</b>		7. PERFORMING ORG. REPORT NUMBER	
8. CONTRACT OR GRANT NUMBER(s) <b>AFOSR-75-2827</b>			
9. PERFORMING ORGANIZATION NAME AND ADDRESS <b>Department of Materials Science &amp; Engineering The University of Utah Salt Lake City, Utah 84112</b>		10. PROGRAM ELEMENT, PROJECT, TASK AREA & WORK UNIT NUMBERS <b>2303/A3, 61102F, 681303</b>	
11. CONTROLLING OFFICE NAME AND ADDRESS <b>AIR FORCE OFFICE OF SCIENTIFIC RESEARCH / NCL Building 410, Bolling Air Force Base Washington, D.C. 20332</b>		12. REPORT DATE <b>23 Nov 1976</b>	
13. NUMBER OF PAGES <b>239</b>		14. SECURITY CLASS. (of this report) <b>UNCLASSIFIED</b>	
14. MONITORING AGENCY NAME & ADDRESS (if different from Controlling Office) <b>(14) UREC-76-274</b>		15a. DECLASSIFICATION/DOWNGRADING SCHEDULE	
15. DISTRIBUTION STATEMENT (of this Report) <b>(15) ✓ AF-AFOSR-2827-75</b>		<b>(16) 2303 (17) A3</b>	
Approved for public release; distribution unlimited.			
17. DISTRIBUTION STATEMENT (of the abstract entered in Block 20, if different from Report)			
18. SUPPLEMENTARY NOTES			
19. KEY WORDS (Continue on reverse side if necessary and identify by block number) <b>Amorphous polymers, glassy polymers, molecular behavior under stress, dynamic infrared spectroscopy, fourier transform IR spectroscopy - Applications in polymers.</b>			
20. ABSTRACT (Continue on reverse side if necessary and identify by block number) <b>Molecular behavior of two structurally different glassy polymers, polystyrene and polycarbonate has been studied under tensile stress, cyclic fatigue and in crazing conditions. This has been accomplished by the use of dynamic fourier transform IR spectroscopy and standard characterization techniques. The study of polystyrene revealed that bulky phenyl side groups on the</b>			



polymer backbone dictate its mechanical behavior by partially interlocking the chains, causing distortions of phenyl groups and breakage of phenyl interlockings. Further, these interphenyl interferences have been found to depend on processing conditions particularly the orientation conditions. In cyclically fatigued PS films, better packing of polymer chains occurs even though serious molecular level damage occurs in the process. In unoriented films, bulky phenyl side groups highly restrict the chain mobility and therefore stress-relief occurs by crazing of the polymer at the surface.

In polycarbonate polymer, the stresses are distributed are a large number of polymer chains, because its higher free volume. Fatigued PC films show a shift of <sup>alpha</sup> and <sup>beta</sup> relaxation peaks towards lower temperatures indicating an increase in free volume through molecular chain scission. Fatigue-crazing and solvent-crazing in PC occurs via different molecular mechanism, with an extensive damage occurring during the cyclic fatigue.

UNCLASSIFIED

SECURITY CLASSIFICATION OF THIS PAGE(When Data Entered)

This Research was Conducted and the Report Written  
by  
Dr. S. K. Sikka

ACCESSION FOR	
NTIS	WATER SOURCE <input checked="" type="checkbox"/>
D.C.	BOTH SOURCE <input type="checkbox"/>
UNANNOUNCED	<input type="checkbox"/>
JUSTIFICATION .....	
BY .....	
DISTRIBUTION/AVAILABILITY CODES	
Dist.	AVAIL. AND/OR SPECIAL
A	



## ABSTRACT

Molecular behavior of two commercially important glassy polymers, polystyrene and polycarbonate, has been studied under tensile stress, cyclic fatigue and in crazing conditions. These polymers are different in their chemical structure and mechanical properties. The primary technique employed in this study is a new Dynamic Infrared Spectroscopy using both the conventional Perkin Elmer spectrophotometer, as well as the latest computer-equipped Fourier Transform spectrometer. This dynamic technique has been supplemented by standard characterizations, viz., X-ray scattering, dynamic mechanical measurements, tensile testing, density measurements and optical and scanning electron microscopies. Also, X-ray scattering under stress was used for the first time for these glassy polymers.

The study of polystyrene revealed that bulky phenyl side groups on the polymer backbone dictate its mechanical behavior by partially interlocking the chains. Therefore, any external stress is transmitted only to individual portions of the chains, causing distortions of phenyl side groups and breakage of certain phenyl interlockings. These interphenyl interferences have been found to depend upon the processing conditions, particularly the orientation conditions. It has been shown that the initial molecular state of the polymer is irreversibly affected by any small external stress, even before yielding. Cyclic fatigue of TRICITE (biaxially oriented) films



causes better packing of polymer chains even though serious molecular level damage occurs in the process. In unoriented films, bulky phenyl side groups highly restrict the chain mobility, preventing molecular chains to stress-relieve by plastic deformation. This causes chains to stress-relieve by creating crazes on the surface.

Applied stress to unoriented and uniaxially oriented polycarbonate (bisphenol A) was shown to distribute evenly over a large number of polymer chains. Cyclically fatigued polycarbonate films showed a shift of  $\alpha$  and  $\beta$  relaxation peaks toward lower temperatures, indicating an increase in free volume caused by molecular chain scission. Fatigue-crazing and solvent-crazing of polycarbonate have been found to occur via different molecular behavior. Fatigue-crazed material, though similar in surface appearance to solvent-crazed material, is actually damaged extensively throughout at the molecular level, whereas solvent-crazed material is affected mostly at the surface.

Thus, the present study has shown the viability of the new dynamic infrared technique to studying the molecular behavior in glassy polymers under varying tensile stress, fatigue and crazing conditions. An understanding of this molecular behavior is vital to explain and improve end use properties.

## TABLE OF CONTENTS

	<u>Page</u>
ABSTRACT.....	ii
LIST OF FIGURES.....	viii
LIST OF TABLES.....	xvii
INTRODUCTION.....	1
 CHAPTER	
I. STRESS STRAIN AND YIELD BEHAVIOR OF POLYMERS . . . . .	4
1.1 Stress-Strain Curves . . . . .	4
1.2 Stress-Strain Behavior of Amorphous Polymers and its Molecular Mechanism . . . . .	10
1.2.1 Stress-strain behavior of amorphous polymers . . . . .	10
1.2.2 Elastic response . . . . .	12
1.2.3 Theories of yielding and cold-drawing . .	14
1.2.4 Fracture of amorphous, glassy polymers .	18
1.3 Crazeing . . . . .	22
1.4 Inhomogeneous Deformation . . . . .	26
1.5 Shear-banding . . . . .	27
1.6 Viscoelastic Behavior of Polymers . . . . .	29
1.6.1 Concept of viscoelasticity . . . . .	29
1.6.2 Viscoelastic models . . . . .	30
1.6.3 Creep in glassy polymers . . . . .	33
1.6.4 Stress-relaxation in polymers . . . . .	38
II. INFRARED SPECTRA OF STRESSED POLYMERS . . . . .	40
2.1 Discussion of Peak Shift and Band Distortions . .	40
2.1.1 Change in force constants . . . . .	45
2.1.2 Bond angle and bond length changes . . . .	47
2.1.3 Conformational changes . . . . .	49
2.1.4 Defect mechanism . . . . .	50
2.1.5 Anharmonicity and phonon interactions . .	51
2.2 Application of Dynamic Infrared Technique . . . .	54



# TABLE OF CONTENTS (continued)

	<u>Page</u>
2.2.1 Study of molecular mechanics of polymer by dynamic infrared technique (DIR) . . . . .	54
2.2.2 Stress-strain behavior of oriented cry- stalline polymers. A molecular approach by dynamic infrared technique . . . . .	56
III. VIBRATIONAL ASSIGNMENTS OF INFRARED ABSORPTION BANDS OF POLYSTYRENE AND POLYCARBONATE . . . . .	66
3.1 Infrared Spectra of Polystyrene and its Vibrational Assignments . . . . .	66
3.2 Infrared Spectra of Polycarbonate (poly-4,4' dioxydiphenyl-2,2 propane carbonate) . . . . .	79
IV. EXPERIMENTAL AND ANALYTICAL TECHNIQUES . . . . .	90
4.1 Introduction to Experimental Program . . . . .	91
4.2 Equipment and Experimental Techniques . . . . .	91
4.2.1 Infrared equipment and experimental techniques . . . . .	91
4.2.2 Applications of Fourier transform IR spectroscopy in the study of stressed bonds in amorphous polymers (under tension). . . . .	97
4.2.3 X-ray diffraction studies . . . . .	109
4.2.4 Density measurements . . . . .	118
4.2.5 Dynamic mechanical measurements . . . . .	119
4.2.6 Differential scanning calorimetry . . . . .	122
4.2.7 Microscopy . . . . .	124
4.2.8 Fatigue in polymers . . . . .	124
4.3 Materials . . . . .	125
4.3.1 Polystyrene . . . . .	125
4.3.2 Polycarbonate . . . . .	126
V. RESULTS AND DISCUSSIONS OF ATACTIC POLYSTYRENE UNDER TENSILE STRESS, CYCLIC FATIGUE AND IN CRAZING CONDITION. . . . .	127
5.1 Results and Discussion: 0.0045" Thick TRICITE Film . . . . .	127
5.1.1 Stress-strain results . . . . .	127
5.1.2 Dynamic IR results . . . . .	131
5.1.3 Summary . . . . .	149
5.2 Results and Discussion: 0.003" Thick TRICITE Film. . . . .	152
5.2.1 Stress-strain results . . . . .	152
5.2.2 Dynamic IR results . . . . .	154

# TABLE OF CONTENTS (continued)

	<u>Page</u>
5.2.3 Fourier transform infrared spectroscopy results obtained from 3 mil TRICITE films under no stress and stress . . . . .	174
5.2.4 X-ray results . . . . .	180
5.2.5 Discussion: Molecular behavior of 3 mil TRICITE film under stress . . . . .	181
5.2.6 Summary . . . . .	190
5.3 Results and Discussion: Fatigued TRICITE Films of 3 mil. Thickness . . . . .	191
5.3.1 Load-elongation results . . . . .	191
5.3.2 FTIR results . . . . .	193
5.3.3 X-ray results . . . . .	197
5.3.4 Dynamic mechanical loss results . . . . .	197
5.3.5 Discussion: 3 mil fatigued TRICITE films. . . . .	197
5.3.6 Summary . . . . .	204
5.4 Results and Discussion: Unoriented Atactic PS Film Under Stress and in Crazed State . . . . .	205
5.4.1 Stress-strain results . . . . .	205
5.4.2 Dynamic IR results . . . . .	205
5.4.3 FTIR results: Crazed vs. uncrazed atactic polystyrene . . . . .	210
5.4.4 X-ray results: Unoriented atactic PS under stress and in crazed state . . . . .	212
5.4.5 Discussion: Unoriented PS films . . . . .	214
5.4.6 Summary . . . . .	215
5.5 Results and Discussion: Uniaxially Oriented Atactic PS . . . . .	215
5.5.1 Dynamic IR results . . . . .	215
5.5.2 Discussion of uniaxially oriented atactic PS . . . . .	216
5.5.3 Summary . . . . .	226
VI. RESULTS AND DISCUSSION OF POLYCARBONATE OR (POLY-4,4'-DIOXYDIPHENYL-2,2-PROPANE CARBONATE) . . . . .	227
6.1 Results and Discussion: Unoriented polycarbonate (LEXAN) Films . . . . .	227
6.1.1 Physical and mechanical measurements . . . . .	227
6.1.2 IR results . . . . .	229
6.1.3 X-ray results . . . . .	236
6.1.4 Discussion of the molecular behavior of unoriented PC film under stress . . . . .	238
6.1.5 Summary . . . . .	239



# TABLE OF CONTENTS (continued)

	<u>Page</u>
6.2 Results and Discussion: Unoriented Fatigue Polycarbonate Films . . . . .	241
6.2.1 Stress-strain and fatigue results . . .	241
6.2.2 FTIR results . . . . .	241
6.2.3 X-ray and birefringence results . . . . .	248
6.2.4 Dynamic mechanical loss results . . . . .	248
6.2.5 Discussion of molecular behavior of fatigued polycarbonate samples . . . . .	252
6.2.6 Summary . . . . .	259
6.3 Results and Discussion of Craze Polycarbonate Film . . . . .	260
6.3.1 FTIR results . . . . .	260
6.3.2 Dynamic mechanical loss results . . . . .	264
6.3.3 Discussion . . . . .	266
6.3.4 Summary . . . . .	267
6.4 Results and Discussion: Uniaxially Oriented Polycarbonate Films Under Stress . . . . .	267
6.4.1 Stress-strain and birefringence results .	267
6.4.2 IR results . . . . .	269
6.4.3 Discussion . . . . .	276
6.4.4 Summary . . . . .	277
6.5 Comparison of Molecular Behavior of Unoriented and Oriented PC Films Under Stress . . . . .	278
6.5.1 Summary . . . . .	279
VII. SUMMARY AND CONCLUSIONS . . . . .	280
7.1 Summary of Research Objectives . . . . .	280
7.2 Summary and Conclusions of Studies on Polystyrene . . . . .	281
7.3 Summary and Conclusions of Studies on Polycarbonate (bisphenol A) . . . . .	284
7.4 Comparison of Polystyrene and Polycarbonate Polymers . . . . .	286
7.5 Comparison of Present Studies with Studies on Semicrystalline Polymers . . . . .	286
7.6 Recommendations for Further Research . . . . .	294
APPENDIX A: MODELING OF BAND SPLITTINGS IN FTIR SPECTRA . . .	296
APPENDIX B: HYPOTHESIS TESTING . . . . .	302
REFERENCES . . . . .	305

## LIST OF FIGURES

<u>Figure No.</u>		<u>Page</u>
1.1	Generalized Stress-strain curve for polymers . . . . .	5
1.2	Tensile stress-strain curves for several types of polymeric materials . . . . .	8
1.3	Schematic representation of variation of stress- strain curves with strain rate and temperature . . . . .	9
1.4	Stress-strain diagram of solid amorphous, glassy polymers at different temperatures . . . . .	11
1.5	Top: Weak imperfections and strong structures on a molecular scale which appear important in the development of craze cracks. Bottom: Sequential steps in the development of voids, oriented polymer and craze cracks as a result of tensile stress applied in the vertical direction . . . . .	19
1.6	Crazes observed in cyclically fatigued polycarbonate (bisphenol A) film samples . . . . .	23
1.7	Schematic sketch of the molecular bundles in the craze region . . . . .	24
1.8	Schematic representation of mechanisms of crack propagation in a craze . . . . .	25
1.9	Shear band formation in a deformed sample of polystyrene . . . . .	28
1.10	Models for viscoelastic behavior . . . . .	31
1.11	A four-element model for creep . . . . .	34
1.12	Creep curves . . . . .	36
1.13	Stress relaxation . . . . .	38
1.14	The stress-relaxation modulus $G(t)$ as a function of time $t$ . . . . .	39
2.1	Schematic effect of stress on a band associated with backbone vibration . . . . .	42



# LIST OF FIGURES (continued)

<u>Figure No.</u>		<u>Page</u>
2.2	A simple harmonic oscillator . . . . .	45
2.3	IR frequency versus phase difference . . . . .	52
2.4	Density of state versus frequency . . . . .	52
2.5	Peak shift and distortion of skeletal $973\text{ cm}^{-1}$ band of PET under an external stress . . . . .	57
2.6	Stress-strain curves for PET films (A,B,C) obtained on an Instron . . . . .	59
2.7	Frequency shift versus stress plots for oriented PET films (A,B,C) . . . . .	60
2.8	F( $\nu$ ) curves for film C at 0, 5000 and 10000 psi external stress . . . . .	62
2.9	F( $\nu$ ) curves for film C at 0, 17000 and 21000 psi external stress . . . . .	63
2.10	F( $\nu$ ) curves for film C at 0, 40000, 52000 and 60000 psi external stress . . . . .	64
3.1	Approximate normal modes of monosubstituted benzene . .	68
3.2	IR absorption spectrum of atactic polystyrene film obtained on FTIR spectrometer . . . . .	70
3.3	A repeat unit of polystyrene molecule . . . . .	77
3.4	IR spectrum of polycarbonate (bisphenol A) film obtained on FTIR spectrometer . . . . .	81
3.5	IR spectrum of model compound--4,4'-isopropylidene- diphenol . . . . .	85
3.6	IR spectrum of model compound--2,2-Di-p-Tolylpropane . .	86
3.7	IR spectrum of model compound--2,2-Diphenyl-1,3- Propanediol . . . . .	87
3.8	IR spectrum of model compound--carbonic acid . . . . .	88
4.1	Loading system used in dynamic infrared tests . . . . .	92

# LIST OF FIGURES (continued)

Figure No.		Page
4.2	Pairs of functions related by the Fourier Integral Transforms in Equation 4.1 . . . . .	99
4.3	Schematic diagram of a Michelson interferometer showing the fixed mirror (A), the moving mirror (B) and beam splitter (C) . . . . .	101
4.4	(a) Superimposed $903\text{ cm}^{-1}$ IR band of TRICITE film under no stress (—) and stress (---); (b) $903\text{ cm}^{-1}$ IR band in subtraction spectrum - (stressed-80% unstressed); (c) $903\text{ cm}^{-1}$ IR band in subtraction spectrum-(stressed-88% unstressed); (d) $903\text{ cm}^{-1}$ IR band in subtraction spectrum - (stressed-90% unstressed) . . . . .	106
4.5	Film stretching device used in dynamic X-ray studies . . . . .	108
4.6	Cutaway diagram of small and medium-angle camera designed by W. O. Statton . . . . .	112
4.7	Dimensional relationship of the geometry of diffraction by the specimen . . . . .	113
4.8	Schematic representation of the diffraction from the internal standard of calibration (ZnO smeared on polymer sample) . . . . .	116
4.9	Densitometer trace of the X-ray scattering pattern of TRICITE film . . . . .	117
4.10	Block diagram of the Rheovibron dynamic viscoelastometer . . . . .	123
5.1	Stress-strain curve of 4.5 mil thick TRICITE film cut along the machine direction . . . . .	128
5.2	Stress-strain curve of 4.5 mil thick TRICITE film cut along transverse direction . . . . .	129
5.3	Stress-strain curve of 4.5 mil thick annealed TRICITE film . . . . .	130
5.4	IR spectra of 4.5 mil thick TRICITE film under no stress (—) and stress of 888 psi (---) . . . . .	133
5.5	IR spectra of 4.5 mil thick TRICITE film under no stress (—) and stress of 1776 psi (---) . . . . .	134



# LIST OF FIGURES (continued)

Figure No.		Page
5.6	IR spectra of 4.5 mil TRICITE film under no stress (—) and stress of 2666 psi (---) . . . . .	135
5.7	IR spectra of 4.5 mil thick TRICITE film under no stress (—) and stress of 3555 psi (---) . . . . .	136
5.8	IR spectra of 4.5 mil thick TRICITE film under no stress (—) and stress of 6222 psi (---) . . . . .	137
5.9	(a) IR spectra of 4.5 mil thick TRICITE film under no stress (—), stress of 8000 psi (---) and on stress removal (···) . . . . .	138
	(b) IR spectra of 4.5 mil thick TRICITE film under no stress (—), stress of 8000 psi (---) and on stress removal (···) . . . . .	139
5.10	Deformed IR band ( $1154\text{ cm}^{-1}$ ) fraction vs. applied stress plot for 4.5 mil thick TRICITE film . . . . .	142
5.11	Distorted IR band ( $1182\text{ cm}^{-1}$ ) fraction vs. applied stress plot for 4.5 mil thick TRICITE film . . . . .	145
5.12	(a) IR spectra of 4.5 mil thick TRICITE film under no stress (—) and stress of 7111 psi (---) in the transverse direction . . . . .	147
	(b) IR spectra of 4.5 mil thick TRICITE film under no stress (—) and stress of 7111 psi (---) in the transverse direction . . . . .	148
5.13	(a) IR spectra of 4.5 mil thick annealed TRICITE film under no stress (—) and stress of 6666 psi (---) . . . . .	150
	(b) IR spectra of 4.5 mil thick annealed TRICITE film under no stress (—) and stress of 6666 psi (---) . . . . .	151
5.14	Stress-strain curves of mil thick TRICITE films at strain rates of 2 in/min (Curve A) and 0.05 in/min (Curve B) . . . . .	153
5.15	(a) IR spectra of 3 mil thick TRICITE film under no stress (—), stress of 6333 psi (---) and on stress removal (···) . . . . .	155

# LIST OF FIGURES (continued)

Figure No.		Page
5.15	(b) IR spectra of 3 mil thick TRICITE film under no stress (—), stress of 6333 psi (---) and on stress removal (···) . . . . .	156
	(c) IR spectra of 3 mil thick TRICITE film under no stress (—), stress of 6333 psi (---) and on stress removal (···) . . . . .	157
5.16	Load-elongation behavior of 3 mil thick TRICITE film at various stress levels applied in steps during the IR scans . . . . .	161
5.17	(a) IR spectra of 3 mil thick TRICITE film under no stress (—) and stress of 2000 psi (---) . .	163
	(b) IR spectra of 3 mil TRICITE under no stress (—) and stress of 2000 psi (---) . . . . .	164
5.18	(a) IR spectra of 3 mil thick TRICITE film under no stress (—) and stress of 4000 psi (---). . .	165
	(b) IR spectra of 3 mil thick TRICITE film under no stress (—) and stress of 4000 psi (---). . .	166
5.19	(a) IR spectra of 3 mil thick TRICITE film under no stress (—) and stress of 6000 psi (---). . .	167
	(b) IR spectra of 3 mil thick TRICITE film under no stress (—) and stress of 6000 psi (---). . .	168
5.20	(a) IR spectra of 3 mil thick TRICITE film under no stress (—) and stress of 10000 psi (---) . .	170
	(b) IR spectra of 3 mil thick TRICITE film under no stress (—) and stress of 10000 psi (---) . .	171
5.21	Deformed IR band ( $1154\text{ cm}^{-1}$ ) fraction vs. applied stress plot for 3 mil thick TRICITE film . . . . .	173
5.22	(a) Superimposed FTIR spectra of TRICITE film under no stress (—) and stress (---) . . . . .	175
	(b) Superimposed FTIR spectra of TRICITE film under no stress (—) and stress (---) . . . . .	176
5.23	(a) FTIR subtraction spectrum of TRICITE film . . .	178



# LIST OF FIGURES (continued)

<u>Figure No.</u>		<u>Page</u>
5.23	(b) FTIR subtraction spectrum of TRICITE film . . . .	179
5.24	Approximate normal modes of monosubstituted benzene .	185
5.25	Molecular models of highly oriented polystyrene chains . . . . .	186
5.26	Load-elongation curve of 3 mil thick TRICITE film . .	192
5.27	Stress vs. number of cycles to failure for 3 mil thick TRICITE film . . . . .	194
5.28	(a) Superimposed FTIR spectra of unfatigued (—) and fatigued (---) 3 mil TRICITE film . . . . .	195
	(b) Superimposed FTIR spectrum of unfatigued and fatigued 3 mil TRICITE film . . . . .	196
5.29	(a) FTIR subtraction spectrum of 3 mil TRICITE film .	198
	(b) FTIR subtraction spectrum of 3 mil TRICITE film .	199
5.30	Tan $\delta$ vs. temperature plot for fatigued and unfatigued TRICITE films . . . . .	201
5.31	Stress-strain curve of unoriented atactic polystyrene film . . . . .	206
5.32	Crazes observed during stress-strain testing of unoriented atactic polystyrene films in the Instron machine . . . . .	207
5.33	(a) IR spectra of unoriented atactic polystyrene film under no stress (—) and stress of 3775 psi (---) . . . . .	208
	(b) IR spectra of unoriented atactic polystyrene film under no stress (—) and stress of 3775 psi (---) . . . . .	209
5.34	FTIR subtraction spectrum of unoriented atactic polystyrene film . . . . .	211
5.35	Creep response of 500% uniaxially oriented polystyrene film . . . . .	217

# LIST OF FIGURES (continued)

<u>Figure No.</u>		<u>Page</u>
5.36	Stress-strain curve of 500% uniaxially oriented atactic polystyrene film . . . . .	218
5.37	(a) IR spectrum of 500% uniaxially oriented atactic PS film under no stress and stress of 3375 psi . . . . .	219
	(b) IR spectra of 500% uniaxially oriented atactic PS film under no stress (—) and stress of 3375 psi (---) . . . . .	220
5.38	(a) IR spectra of 500% uniaxially oriented PS film under no stress (—) and stress of 5400 psi (---) . . . . .	221
	(b) IR spectra of 500% uniaxially oriented PS film under no stress (—) and stress of 5400 psi (---) . . . . .	222
5.39	(a) IR spectra of 500% uniaxially oriented atactic PS film under no stress (—) and stress of 8785 psi (---) . . . . .	223
	(b) IR spectra of 500% uniaxially oriented atactic PS film under no stress (—) and stress of 8785 psi (---) . . . . .	224
6.1	Stress-strain curve of 3 mil thick unoriented polycarbonate (LEXAN) film . . . . .	228
6.2	Creep behavior of unoriented polycarbonate film during the IR scans . . . . .	230
6.3	(a) Superimposed IR spectra of polycarbonate film under no stress, i.e., in Stage 1, (—) and a stress of 6166 psi, i.e., Stage 2 (---) . . . . .	231
	(b) Superimposed IR spectra of polycarbonate film under no stress, i.e., Stage 1, (—) and a stress of 6166 psi, i.e., Stage 2 (---) . . . . .	232
6.4	(a) Superimposed IR spectra of PC film under no stress (—) and stress of 7333 psi, i.e., Stage 3, (---) . . . . .	234
	(b) Superimposed IR spectra of PC films under no stress (—) and stress of 7333 psi, i.e., Stage 3 (---) . . . . .	235



# LIST OF FIGURES (continued)

<u>Figure No.</u>		<u>Page</u>
6.5	Models for the molecular behavior of PC films under no stress and on stressing . . . . .	240
6.6	Load-elongation curve of 3 mil PC film showing load limits for the cyclic fatigue . . . . .	242
6.7	(a) Superimposed FTIR spectra of unfatigued (—) and fatigued (···) PC films . . . . .	245
	(b) Superimposed FTIR spectra of unfatigued (—) and fatigued (···) PC films . . . . .	246
6.8	IR subtraction spectrum of polycarbonate films . . . . .	247
6.9	Tan $\delta$ vs. temperature plot for unfatigued and fatigued polycarbonate films . . . . .	250
6.10	Tan $\delta$ vs. temperature plot for unfatigued and fatigued (to over 5000 cycles) PC films . . . . .	251
6.11	Superimposed FTIR spectra of uncrazed (—) and crazed (---) polycarbonate films . . . . .	261
6.12	IR subtraction spectrum of polycarbonate films . . . . .	263
6.13	Tan $\delta$ vs. temperature plot for fatigue-crazed and solvent-crazed PC film . . . . .	265
6.14	Stress-strain curve of 300% uniaxially oriented polycarbonate film . . . . .	268
6.15	Creep behavior of 300% uniaxially oriented PC film during the IR scans . . . . .	270
6.16	IR spectra of 300% uniaxially oriented PC film under no stress (—) and stress of 11100 psi (---) . . . . .	271
6.17	(a) FTIR subtraction spectrum of 300% uniaxially oriented PC film . . . . .	273
	(b) FTIR subtraction spectrum of 300% uniaxially oriented PC film . . . . .	274
7.1	FTIR spectrum of unstressed PET film . . . . .	292
7.2	FTIR spectrum of unstressed PET film . . . . .	293

# LIST OF FIGURES (continued)

<u>Figure No.</u>		<u>Page</u>
A.1	Model for single band splitting resulting from change in peak distribution . . . . .	297
A.2	Model for double band splitting resulting from change in peak distribution . . . . .	297
A.3	Model for non-symmetrical single band splitting resulting from change in peak distribution and position . . . . .	298
A.4	Model for double band splitting due to peak shift . .	299
A.5	Model for single band splitting due to band resolving and peak shift . . . . .	301



# LIST OF TABLES

<u>Table No.</u>		<u>Page</u>
1.1	Characteristic Features of Stress-Strain Curves as Related to Polymer Properties . . . . .	7
2.1	Major Molecular Differences Resulting from Two Macroscopic Deformation Modes in Polypropylene . . . . .	55
3.1	Absorption Assignments for Polystyrene . . . . .	71
3.2	Vibrational Frequencies and their Assignments for Helical (Isotactic) and Planar (Syndiotactic) Sequences Along with Experimentally Observed IR Bands in Atactic Polystyrene . . . . .	75
3.3	Infrared Absorption Band Frequencies and Their Assignments . . . . .	82
5.1	Band Distortion of $1154\text{ cm}^{-1}$ Band Under Stress: 0.0045" TRICITE Film . . . . .	141
5.2	Fraction of $1182\text{ cm}^{-1}$ IR Band Deformation Due to Stress . . . . .	144
5.3	Fraction of $1154\text{ cm}^{-1}$ IR Band Deformation Due to Stress on TRICITE Film . . . . .	172
5.4	Frequency Shifts Observed from FTIR Spectra of TRICITE Films Under Stress . . . . .	180
5.5	Stress-affected Infrared Bands of TRICITE Films . . . . .	188
5.6	Fatigue Data of PS Specimens . . . . .	193
5.7	Fatigue-affected IR Bands of TRICITE Films . . . . .	200
5.8	Bragg Distances in Unstrained, Strained and Stress Crazed Atactic Polystyrene . . . . .	213
6.1	Bragg Distances Calculated for Unstrained and Strained PC Film . . . . .	237
6.2	Fatigue Data of PC Samples 0.5" Wide x 4" long . . . . .	243
6.3	Fatigue Data of PC Samples 1" Wide x 4" long . . . . .	244

# LIST OF TABLES (continued)

<u>Table No.</u>		<u>Page</u>
6.4	Changes Observed with Bands from the FTIR Subtraction Spectra on Fatigued PC Samples . . . . .	249
6.5	Position and Shifts of $\alpha$ and $\beta$ Relaxation Peaks of Samples Fatigued to Varying Number of Cycles. . . .	253
6.6	Changes in IR Bands of Stressed PC Films (Oriented) . . . . .	275
7.1	Comparison of Atactic Polystyrene and Polycarbonate Polymers . . . . .	287



## INTRODUCTION

Several amorphous, glassy polymers are exceptionally important in providing useful materials for everyday life. They have limitations, however, of developing crazes and cracks under stress, leading to failure. This process is now well understood by recent excellent studies from the phenomenological viewpoint but the process is not at all understood from the molecular viewpoint.

Our is the pioneering study of the molecular behavior of glassy polymers under tensile stress, cyclic fatigue and crazing conditions. It is indisputable that an understanding of the molecular behavior in polymeric materials under the above conditions is essential if mechanical properties and service life of these materials are to be improved.

The way stress is distributed over the polymer chains under external load must be intimately connected with the polymer's morphology and microstructure, which, in turn, dictate the mechanical properties of these polymers.

In the case of amorphous polymers there exists a controversy on the subject of microstructure [1,2]. Several models have been proposed from time to time to represent the microstructure of these polymers.

There are essentially two opposing views on the subject. Proponents of one view support the idea of a random coil model, i.e., the

existence of disordered microstructure for amorphous polymers in bulk state. Their model is based on the measurements of mean square length and the radius of gyration of the polymer chains by the use of X-ray scattering and neutron scattering techniques, respectively. The other view on the subject is in support of some local order among the macromolecular chains. The existence of such order has been proposed by several authors on the basis of their results obtained from electron microscopy, X-rays and electron diffraction techniques.

As it stands to date, no particular model for the microstructure in amorphous polymers has been proved or disproved or universally accepted. Each model has some merits and explains some properties of the polymers while leaving other unexplained. Thus, controversy remains as to whether any kind of structure exists in the structureless polymer or not. In this dissertation no particular microstructural model will be favored. The emphasis here will lie in the study of the molecular behavior of amorphous, glassy polymers under tensile stress, cyclic fatigue and in crazing conditions. It is believed that this is a more fruitful approach and may, in fact, give a new insight into the larger controversy.

The novelty of the molecular approach is made possible by the use of new dynamic infrared technique which has been successfully employed in our laboratory in recent studies of semicrystalline polymers. In this technique the infrared spectrum of a polymer is obtained while it is under load and compared to the spectrum under no load. Changes in shapes and frequencies of certain IR bands occur under load. From



the knowledge of various vibrational assignments of these IR bands one can monitor the changes which polymer chains undergo when this external stress is applied. This technique becomes even more informative when supplemented by other standard characterization techniques.

Two commercially important glassy polymers were selected for the present study: atactic polystyrene and polycarbonate (bisphenol A). These provide a contrast in both chemical structure and mechanical behavior. It was felt that study of these materials would answer the basic questions about the distribution of external stresses over polymer chains and give insight as to how these chains are affected by cyclic fatigue and crazing conditions.

It is naturally hoped that understanding this molecular behavior will help in seeking ways to improve the properties of plastics in specific applications.

## CHAPTER I

### STRESS STRAIN AND YIELD BEHAVIOR OF POLYMERS

#### 1.1 Stress-Strain Curves

The stress-strain curves most simply illustrate the strength properties of solids. They describe the behavior of a homogeneous specimen of uniform cross section subjected to external stress. Stress-strain test is the most widely used of all mechanical tests. It is also the most widely studied and sought-after test to determine the suitability of polymeric materials in the engineering design and applications.

Measurements are generally made under tension by uniaxially stretching a polymer specimen of known dimensions at a uniform, continuous rate in a tensile-testing machine such as the Instron. The force, thus developed on the material is measured simultaneously. These tests are continued to the point where the specimen breaks. Data thus received is generally in a form of load-elongation curves. These curves are then transformed to stress-strain curves by the following definitions.

For tensile tests the stress is defined as:

$$\text{Stress } \sigma = \frac{\text{Force or load } F}{\text{Cross sectional area } A} \quad (1.1)$$

The stress calculations based on the original cross sectional area are referred to as the engineering stress, so called because of being the most commonly applied in engineering field.



The strain for engineering purpose is defined as:

$$\epsilon = \frac{L - L_0}{L_0} = \frac{\Delta L}{L_0} \quad (1.2)$$

where  $L_0$  and  $L$  are the original length and stretched length, respectively.

The standard test methods relating to tension testing of plastics are described in the publications of the American Society for Testing and Materials [3] (ASTM D412, ASTM D638-64T, ASTM D882). In addition, several reference books [4-11] are available on this subject of testing and of mechanical and viscoelastic properties of polymers.

Figure 1.1 depicts a generalized stress-strain curve for thermoplastic materials and is used to illustrate the terminology used for stress-strain testing [12].

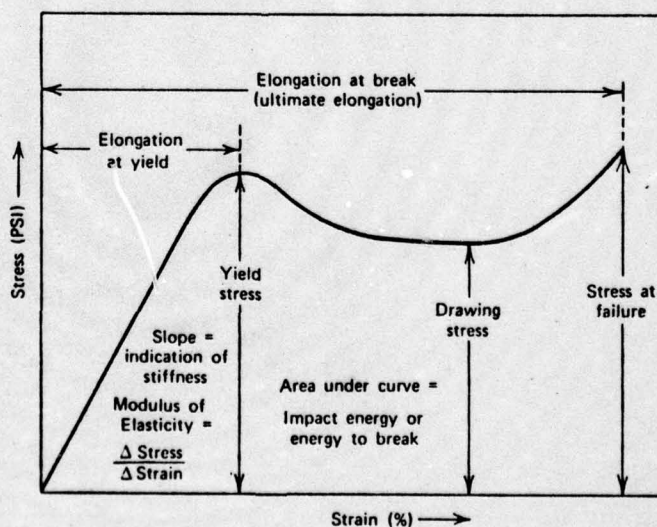


Figure 1.1 Generalized stress-strain curve for polymers [12].

The slope of initial straight line portion of this curve is the elastic modulus of the material. In a tensile test this modulus is called Young's modulus,

$$E = \frac{d\sigma}{d\epsilon} \quad (1.3)$$

The maximum in this curve also referred to as a yield point denotes stress at yield  $\sigma_y$  and elongation at yield  $\epsilon_y$ .  $\sigma_y$  is a measure of strength of a material and its resistance to permanent deformation. Following yield point, stress decreases with increasing strain to some limiting value, after which the stress remains constant with increasing strain over a fairly large region of strain and is denoted as the drawing stress. End of the curve denotes failure of material, which is characterized as the tensile strength  $\sigma_B$ .

Area under the entire curve represents work required to fracture the specimen and is a rough measure of toughness of a material.

Another term usually encountered in these tests is known as "necking" and refers to a local reduction in cross sectional area of a specimen under test. This shows up as the region just past yield point on the stress-strain curve. The nearly constant stress region in a stress-strain curve is due to progressing of necked region until the entire gage length of the specimen is of a uniform cross section.

Shape of a stress-strain curve for any polymer depends on several structural and molecular factors, such as chemical structure, molecular weight, crosslinking, branching, plasticization, crystallinity, crystal structure and chain configuration. As a result, different polymers show varied stress-strain behavior under similar test conditions and



can be classified into different categories as listed in Table 1.1. Figure 1.2 illustrates various classifications of the stress-strain behavior listed in Table 1.1.

Table 1.1 Characteristic Features of Stress-Strain Curves as Related to Polymer Properties [5]

Description of Polymer	Characteristics of Stress-Strain Curve			
	Modulus	Yield Stress	Ultimate Strength	Elongation to Breakage
Soft, weak	low	low	low	moderate
Soft, tough	low	low	(yield stress)	high
Hard, strong	high	high	high	moderate
Hard, tough	high	high	high	high
Hard, brittle	high	none	moderate	low

Materials used in the present research are polystyrene and polycarbonate (bisphenol A). Polystyrene exhibits hard and brittle behavior while polycarbonate (bisphenol A) follows a stress-strain curve of hard and tough polymers.

In addition to the above structural and molecular factors, stress-strain behavior of a polymer depends strongly on temperature, time, rate of straining, type of deformation (shear, tensile or biaxial, etc.), thermal history and nature of the surrounding environment. It is now well established that the temperature dependence for stress response

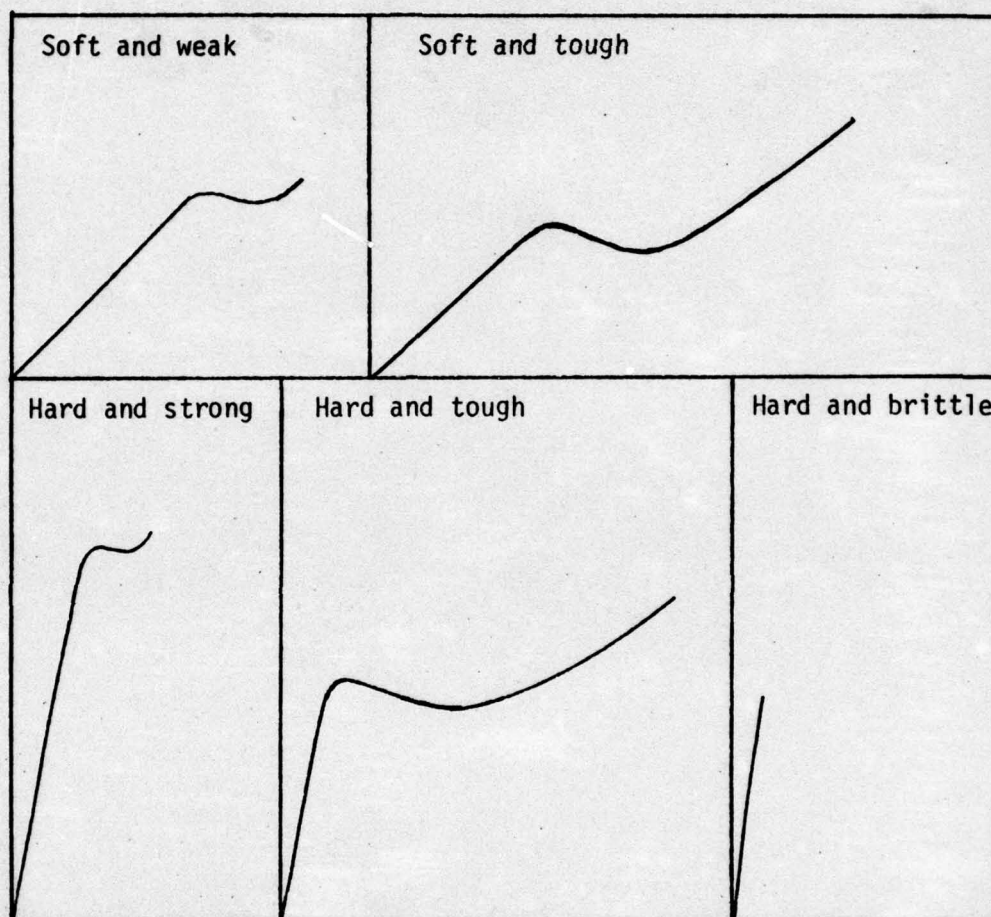


Figure 1.2 Tensile stress-strain curves for several types of polymeric materials [5].



of a polymer is governed by its  $T_g$  (glass transition temperature) [5-12]. Below  $T_g$  the material behaves like a glassy solid and above  $T_g$  its behavior is leathery or rubber-like. However, polycarbonate (bisphenol A) is an exception to the above statement. Their response to rate of testing is based upon relaxation processes of molecular chains. Slower straining rates allow more time for internal rearrangements of molecular chains and the material shows more ductile behavior than at higher straining rates where not enough time is available for the material to respond.

The effects of temperature and strain rate are illustrated by a schematic family of stress-strain curves shown in Figure 1.3.

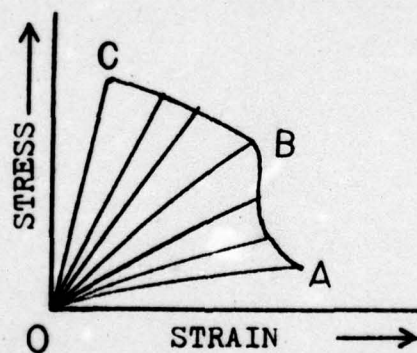


Figure 1.3 Schematic representation of variation of stress-strain curves with strain rate and temperature [13].

Higher curves of the family belong to higher strain rates and/or lower temperatures. The curve OA in Fig. 1.3 represents an equilibrium condition attained at high temperatures and slow straining rate. Ideally,

further temperature increase or strain rate decrease should produce no further movement of the curve, but it is not so in practice. Actually, it represents the condition where molecular segments respond instantaneously to the applied load. There is no lag caused by internal viscosity operative during the generation of higher stress-strain curves. The end point of each curve of the family represents an ultimate stress and strain appropriate to the particular test condition. The envelop ABC joining these points show variation of ultimate properties with testing conditions.

## 1.2 Stress-Strain Behavior of Amorphous Polymers and its Molecular Mechanism

Under this main section the stress-strain behavior of amorphous polymers will be discussed, mostly from the molecular viewpoint.

### 1.2.1 Stress-strain behavior of amorphous polymers

Figure 1.4 shows general stress-strain curves for solid amorphous (glassy) polymers and illustrates the effect of temperature on these polymers. At temperatures between  $T_g$  (glass transition) and  $T_f$  (flow temperature) the stress-strain curve of an amorphous polymer is S-shaped (curves 6-8 in Figure 1.4), corresponding to the appearance of a rubbery state. At these temperatures and at a given rate of extension, rubbery strains develop due to the straining of the flexible macromolecules. As a result, deformation reached at a given moment of time decreases and the curve bends towards the strain axis. On further extension, when macromolecules have exhausted their capacity for



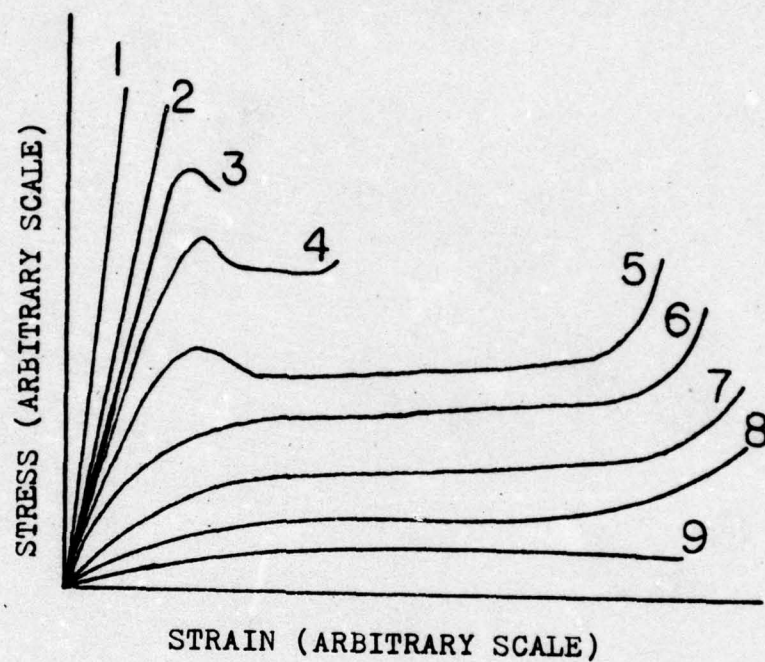


Figure 1.4 Stress-strain diagram of solid amorphous, glassy polymers at different temperatures. (Temperature increases with ascending number of curves [14].)

straining, the mechanism of deformation changes. Further extension occurs only by extension of the straightened macromolecules, requiring very large stresses. That is why the curve passes through a point of inflection and bends sharply upwards, ending at a point where the extended polymer specimen fails.

At temperatures somewhat below  $T_g$  (curves 3-5 in Figure 1.4) a "forced rubber-like elasticity" [14] or cold flow appears, its outward manifestation being that in glassy state an amorphous polymer becomes capable of very large strains. On further temperature decreases the horizontal section of the curve rises gradually and the entire stress-strain curve becomes shorter (curves 3 and 4), i.e., the space from deformation to failure decreases with decreasing temperature. Eventually, the specimen fails at the very first section of stress-strain curve with rather small deformations, i.e., brittle fracture occurs. The theories of yield and cold drawing are discussed in the following section.

### 1.2.2 Elastic response

An ideal elastic isotropic solid obeys Hooke's law, which relates stress  $\sigma$  to the strain  $\epsilon$  for the uniaxial deformation. Hooke's law is given by the following equation:

$$\sigma = E\epsilon \quad (1.4)$$

where  $E$  is Young's modulus.

In most linear uncrosslinked polymers this relation may hold true



only for very small strains (usually  $\leq 2\%$ ). Although in some cases the response is not quite linear, yet complete recovery is possible on load release in this region. Such a behavior shown by polymers has not yet been fully unraveled, thus making it impossible (at this point) to present its exact mechanism. However, it will be discussed at some length in this dissertation, based on the results obtained on polystyrene and polycarbonate.

According to Billmeyer [15], the linear elasticity is related to the glassy behavior of polymers in which the motions of chain segments are restricted and external stress stretches the backbone bonds and deforms the bond angle. Roylance [16] also favors this view that small nondestructive stress distorts the valence bonds of polymer chains and produces a reversible elastic strain in the sample. This explanation seems reasonable in polymers below  $T_g$  but does not clearly explain the occurrence of this phenomena in polymers close to and above their  $T_g$ .

Above  $T_g$  chain segments possess enough mobility for an external stress to cause polymer chains to slip past one another and orient in the direction of applied stress. Such internal rearrangements are non-reversible and, therefore, the deformation does not disappear on removing the stress.

If the valence bonds in a sample do get distorted, it should be detectable through infrared spectroscopy [17]. On the other hand, such low level strains may affect only a fraction of the chain segments, leaving the rest unstressed. It is possible that the molecular entanglements and Van der Waal's forces act here as physical crosslinks.

These entanglements bear the low level stresses which means fewer bonds

(that are part of the segment on the entanglement) are overstressed. When the external load is increased beyond a certain level, some of these entanglements break, transferring the stress to other chain segments. Any further increase of stress will break more entanglements and Van der Waal's bonds and thus orient these chains in the direction of the applied stress, resulting in a non-elastic deformation.

The author believes that in glassy amorphous polymer with bulky rigid side groups on their backbone (viz., in polystyrene), this process is different below  $T_g$ . It is suggested that in such polymers the side-groups on adjacent chains interfere and/or interlock with each other and thus distribute the applied stress over several chain segments and also restrict the chain mobility. By so sharing the stress and keeping it off the polymer backbone (and hence in the Hookean region), the polymer undergoes strain recovery on removal of stress. This mechanism will be discussed in a later chapter at length, based on various experimental evidence.

### 1.2.3 Theories of yielding and cold-drawing

Most polymers, whether amorphous or crystalline, will cold draw. This phenomenon occurs past the yield point. The specimen necks down in one region and the stretching continues until all the material is cold-drawn, stopping only at a critical elongation known as the "natural draw ratio".<sup>1</sup> Cold-drawn material, on further stretching, shows a rapid increase in stress followed by an abrupt rupture.

---

<sup>1</sup>The "natural draw ratio" is a ratio of the length of a cold-drawn region to the length of undrawn material before stretching.



During cold-drawing process great changes occur in the molecular arrangement and the polymer chains tend to become highly oriented in the draw direction. Orientation requires considerable mobility of large segments of polymer molecules which cannot occur much below  $T_g$ . This implies that, in some way, orientation mechanism brings the polymer temporarily above its  $T_g$ . There are many theories explaining this concept but the issue remains unresolved. Janckel [18], Marshall and Thompson [19], Mueller [20], Deanin [21] and Newman [22] believe that due to internal friction the mechanical energy of stretching a polymer gets converted into thermal energy, thereby locally heating the polymer in the neck region. This raises the temperature at weak spots above  $T_g$  and facilitates a rearrangement of large chain segments, thus relieving them of the imposed stress. This theory has been questioned in general except at cryogenic temperatures for polymers with low temperature secondary  $T_g$ .

Vincent [23] proposes that the stress on a polymer lowers the softening temperature at which the drawing occurs, evidence being that large stresses on a viscoelastic material will greatly reduce the relaxation times and lower its  $T_g$  or the softening temperature [24].

Byrant [25] suggests that an applied stress reduces  $T_g$  to the test temperature where segments become fully mobile and yield occurs.

Andrews and Kazama [26] have explained the idea more quantitatively. They suggest that  $T_g$  should not be regarded just as a temperature but as a phenomenon that is a function of temperature, stress level and time, as an increase in temperature or stress causes an increase in the segmental mobility.

There are still others [5,27-29,37,42,43] who envisage yield as a process of progressive breakdown of interaction points between the adjacent molecules. These interactions can be the secondary valence forces or the geometrical entanglements or both. Although it is possible that such processes occur, it is not clear as to what extent they determine the level of yield stress. However, such a process can explain the rapid strain-softening that occurs after yield. The breakdown of such interactions need not be permanent but may reform after a rest period [5].

Brady and Yeh [30] suggest that at a temperature well below  $T_g$  yielding is controlled by the cooperative local segmental motion. An increase in temperature increases the degree of this motion until  $T_g$  is reached where cooperative long chain motions occur.

Robertson [31], in his theory, postulates that normally the molecular segments making up the polymer are distributed between a population of cis (high energy) and a population of trans (low energy) molecular conformations. The population of cis segments in equilibrium at  $T_g$  is frozen-in in the glassy state. The effect of applied stress is to cause certain segments to change over from trans to cis conformation, increasing the population of cis sufficiently to cause yield to occur. Such changes in molecular conformations, before and after yield, in highly drawn poly (ethylene terephthalate) have indeed been observed in our laboratories by Mocherla and Statton [32].

Finally, there are other theories which emphasize the importance of free radicals formation on breaking of over-stressed polymer chains at the start of necking or fracture processes [17,33-35].



According to these theories, the broken chains relax quickly by transferring the stress to other chains. The stressed probability of chain rupture,  $P_b$ , is mathematically represented by the following equation:

$$P_b = W_0 \exp[-(\Delta H - \Lambda \sigma_c)/kT] \quad (1.5)$$

where  $W_0$  is a collision parameter,  $\Delta H$  is the energy of activation,  $\Lambda$  is the activation volume,  $\sigma_c$  is the stress on the polymer chain (as opposed to stress on the specimen), and  $k$  is the Boltzmann's constant. This probability equation is stress-biased so that the taut chains break first. Stress is then redistributed among the remaining chains [34]. This relaxation of stress at points of stress concentration may favor cold-drawing. Another possibility is that free radicals formed by breaking of one chain may catalyze fracture of other chains around it by a chain reaction mechanism. Thereby, a void develops in regions where new chain-ends contract, as the stress on them is removed [35]. This small void may nucleate a craze-crack which leads to either yielding or failure.

It is not yet certain which of the above theories can actually be applicable during "yielding" and "cold-drawing," although all have some merit. It can be said that "yielding" and "cold-drawing" may take place through several mechanisms and the relative importance of different mechanisms may vary in different polymers. It is probable that on a molecular level something like the following takes place in the glassy polymers. Polymers are not homogeneous and consist of weak and strong spots. The weak spots can be the aggregates of chain-ends,

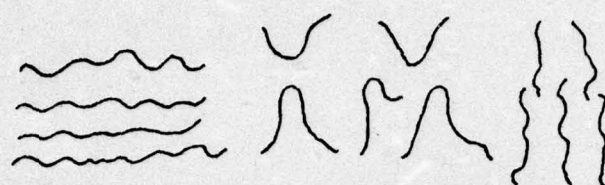
unentangled loops from different chains in close proximity and regions with clusters of several chain segments oriented in a perpendicular direction to the applied stress direction. In addition, those fully extended chains surrounded by slack chains also act as weak spots because such taut chains will be the first to break or pull apart on further stressing in its axial direction [34,35]. This creates sub-microscopic cracks and voids, as illustrated in Figure 1.5. The initial voids can grow into large voids and their size can vary from 20 to several hundred Angstrom units. Under the influence of continued stress such voids can coalesce and form visible crazes and cracks.

#### 1.2.4 Fracture of amorphous, glassy polymers

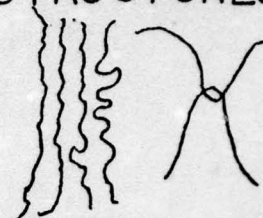
The subject of fracture is of great practical importance. In any practical or engineering application of polymeric solids the conditions of fracture inevitably set a limitation, both to design and service conditions. Therefore, it has been a subject of a great many investigations. Several theories have been proposed to explain the complex sequences that lead to failure. There is the "fracture mechanics" approach, which can be described as a "theory of fracture of solids viewed as continuous media." Under this approach Griffith [36] developed a "theory of strength of brittle materials" in which cracks were assumed to be the determining factor of the strength of such materials. This same theory was extended by Smith [37] for viscoelastic materials and has been applied to amorphous polymers, too. The theory postulates an existence of "flaws" and that fracture occurs by crack propagation through these flaws. Flaws in polymeric solids can be visualized as structural



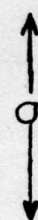
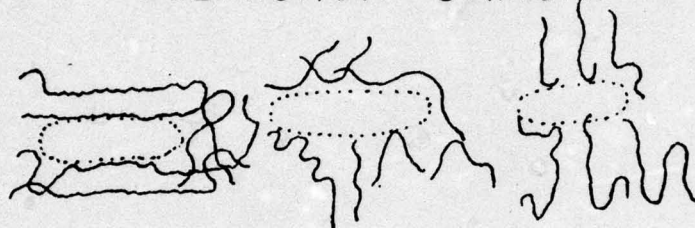
## WEAK IMPERFECTIONS



## STRONG STRUCTURES



## SUBMICRON CRACKS



## CRAZE

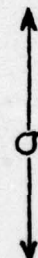
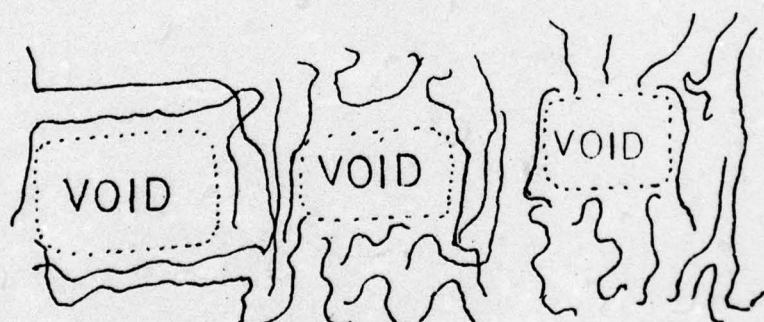


Figure 1.5 Top: Weak imperfections and strong structures on a molecular scale which appear important in the development of craze cracks. Bottom: Sequential steps in the development of voids, oriented polymer, and craze cracks as a result of tensile stress applied in the vertical direction [7].

defects such as dirt inclusions, air bubbles, surface scratches, impurities like water and dissolved monomer, voids and chain ends (Predecki and Statton [38]). Besides these, there is also a microscopical and a molecular approach to fracture behavior. Microscopical approach considers the structure of materials on a very fine scale and the way in which these structures affect (and are affected by) the fracture process [39]. Crazing and microvoiding are examples of microscopical features arising during the fracture process and will be discussed in the next section.

The molecular approach has been explained in terms of kinetic theories [40-42] of mechanical fracture of solids. Based on this, the polymer fracture can be divided into three stages from the molecular viewpoint:

- (i) Overstressing of interatomic bonds by mechanical stress so that the net bonding interaction is reduced.
- (ii) Breakage of overstressed bonds (primary valence bonds within the molecule or secondary bond between them) by thermal fluctuations, thus creating free radicals.
- (iii) Accumulation of bond rupture to the point of breakdown and fracture of macroscopic sample.

An experimental evidence of bond rupture or a chain scission of interatomic bonds under deformation has been presented by the use of Electron Spin Resonance (ESR) technique. This technique was first used by Zhurkov [42] and later by Statton et al. [43] and DeVries et al. [44, 45]. DeVries et al. have shown that in highly oriented Nylon 6 fibers under mechanical stress (60% of the fracture strength and above) a homolytic scission of polymer backbone chains occur and free radicals are formed. They also suggest that the rate of free radical generation



increases exponentially with increasing tensile stress and temperature. However, these researchers were not successful in observing free radicals due to bond rupture in polystyrene and poly(methyl methacrylate). This was justified on the basis of a low number of free radicals ( $<10^{14}$ ) generated /cm<sup>3</sup> in these polymers [46] and thus not being within the detectability of their ESR instrument.

The sensitivity of the instrument may indeed be an important factor in the detection of the free radicals. ESR spectra have been obtained by Kawashima and coworkers [42] on mechanically fractured poly(methyl methacrylate) and the free radicals formation due to backbone chain bond-scissions have been demonstrated.

The primary free radicals once formed can interact with neighboring chains to produce further chain scission. This initiates local fracture causing submicro-cracks which can grow as more chains rupture. Once a certain limit is reached, they coalesce to form macroscopic cracks which rapidly spread across the entire cross-section of the polymer sample, causing a fracture. DeVries [48] and Peterlin [49] suggest that cracks grow through a path of least resistance, i.e., through the regions with defects and flaws so that a least number of chains have to be ruptured.

To summarize, it can be said that the strength of a polymer in its glassy state is that of a physically crosslinked network of main chains. Initially, all primary bonds are in the unbroken state. Under load, small chain ends may be pulled loose, segments and side groups will slip past each other, closed loops can be opened and the backbone chains are stressed until they break or slip past each other.

The exact mechanism of fracture in polymers may depend on the test conditions, structure and temperature. For instance, at very low temperatures fracture of glassy polymers may occur by chain scission of overstressed bonds and some chain slippage, causing micro-cracks, leading to macroscopic crack formation and growth. At relatively high temperatures this may occur through breaking chain entanglements, chain slippage and large-scale molecular rearrangements.

Experimental evidence for the existence of overstressed backbone bonds in crystalline polymers, such as polypropylene and poly (ethylene terephthalate), through the use of a new Dynamic Infrared Technique has been shown by Wool and Statton [50] and Mocherla and Statton [51].

The present study will investigate the existence of such overstressed bonds on loading amorphous polymers, such as atactic polystyrene and polycarbonate (commercial Lexan<sup>®</sup>) films.

### 1.3 Crazing

Crazes in polymers have been well studied phenomenologically [52-54]. It is under tensile stress and especially in the presence of active environments [55-56] that many glassy polymers develop a fine network of surface cracks prior to fracture. These are aligned in the same direction and often arranged in nearly parallel planes normal to the direction of the major principal tensile stress. Figure 1.6 shows the crazes varying in length from 20 microns to 200 microns on a 0.003" thick film of polycarbonate fatigued to over 5000 cycles for our research. Crazes differ from true cracks; in a crack there is no continuity of the material, whereas a craze is plastically deformed



material [57]. Crazed material can support some fraction of the load borne by uncrazed material whereas cracked material will fracture on loading.

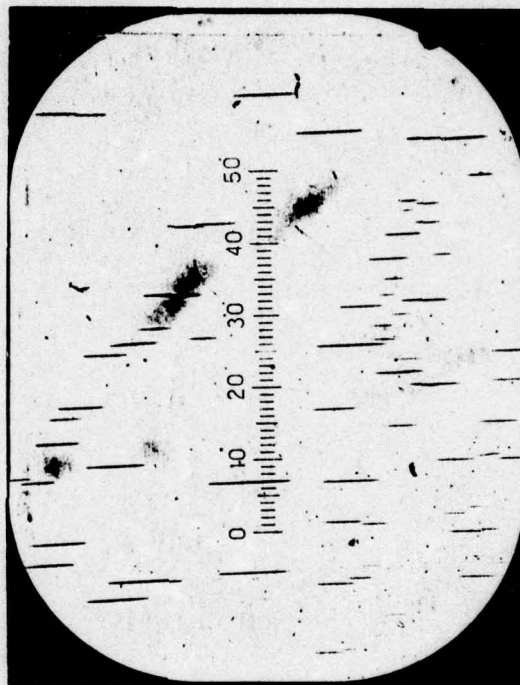


Figure 1.6 Crazes observed in cyclically fatigued polycarbonate (bisphenol A) film samples

When a stress is maintained on a material for a period of time cracks originate, preferably in the weaker, crazed material.\* Thus, crazes generally cause a premature fracture. Such fracture is termed brittle because an overall deformation is small, even though the material

within the craze has undergone a large extension of 100% or more.

Since crazes develop in localized regions, it is reasonable to suppose that these are initiated at stress-raising flaws, which may be surface cracks or scratches. Stress-raising flaws can also be regions of elastic inhomogeneity within the material (these can arise, e.g., from local fluctuations in molecular orientation). High resolution electron microscopy [58-60] has shown that crazes consist of interconnecting fibrillar network, which are aligned perpendicular to the craze matrix interface. The orientation of polymer chains in the craze matter is aligned in the direction of the applied stress and is shown in Figure 1.7.

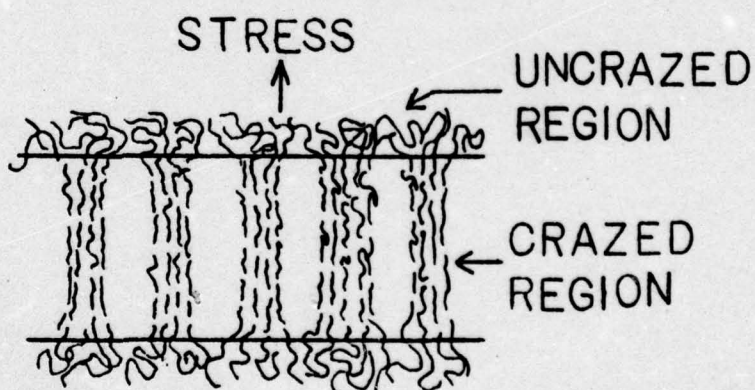


Figure 1.7 Schematic sketch of the molecular bundles in the craze layer

These observations confirm that a craze is a region of very large local strain and support the measurement of Kambour [61] which indicates



that there is a large increase in volume, i.e., decrease in polymer density in the crazed region.

Murray and Hull [62] and Hull [63] based their work on crazing and fracture of polystyrene and have proposed that the following two processes may be involved in a crack propagation in preformed craze:

- (i) cavitation of craze and final separation by tearing of the material in the craze layer,
- (ii) splitting of the material along the interface between the crazed and uncrazed material.

These two processes are illustrated schematically in Figure 1.8.

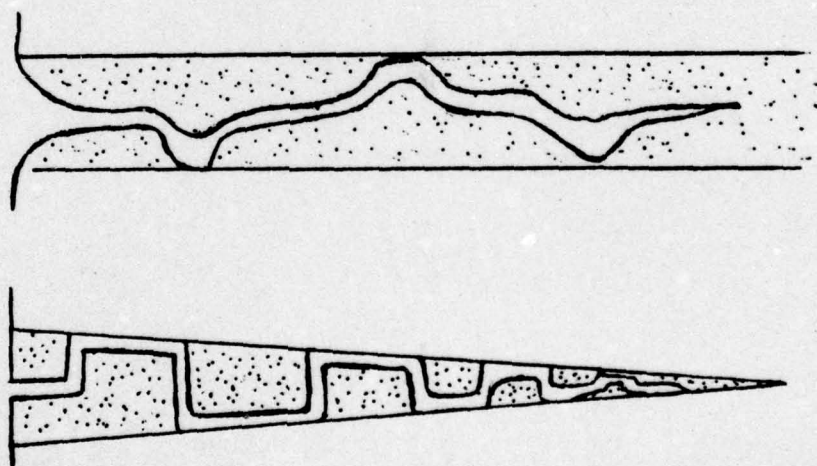


Figure 1.8 Schematic representation of mechanisms of crack propagation in a craze [63].

To summarize, it is now well-established that a link between

crazing and fracture exists and crazes generally cause a premature fracture of the material. Crazes have been accepted to be precursors to fracture. Although there are many phenomenological observations made on crazing behavior of glassy polymers, not enough is known about it from the molecular viewpoint. It has been suggested [64] that large-scale changes in chain conformation can and do occur in glassy polymers under stress. The inhomogeneous character of such deformation implies that segmental mobility sufficient to produce domains of high deformation exists only at discrete locations in a solid. In contrast, however, low stress and long-time homogeneous creep yielding [65] is indicative of segmental mobility throughout the sample. Both homogeneous and inhomogeneous yielding phenomena may, in fact, be manifestation of the same molecular process, but differing in degree and localization as proposed by Sternstein [66]. The molecular process in the crazing behavior will be discussed later in this dissertation, based on the experimental evidence.

#### 1.4 Inhomogeneous Deformation

It is known that a number of materials, when deforming plastically, do not always deform homogeneously. The strain in certain local regions increases more rapidly than it does in the specimen as a whole. The inhomogeneous deformations occur because homogeneous deformation becomes unstable. This can be due to the geometrical features of the specimen, such as slight variation in width or thickness of the sample, and strain softening. These strain inhomogeneities cause "shear-band" formation in materials that exhibit strain softening. Since materials



used in this research do show "shear-band" formation, this phenomenon is briefly introduced in the following section.

### 1.5 Shear-banding

Shear bands in unoriented glassy polymers have been the subject of a number of investigations [67-70] after they were first observed by Whitney [71] in compressed polystyrene. The initiation of shear bands can be well accounted for on the basis of phenomenological theory of Bowden [68], in which localization of "shear strain" is viewed as an inevitable consequence of "strain softening" which is characteristic of "yield" in glassy polymers. Since all amorphous glassy polymers strain-soften to some extent, they all have a tendency to form shear bands but in some polymers this tendency is much stronger than in others. The character of bands differ in different polymers. For example, in poly (ethylene terephthalate) and polystyrene the bands are as thin as 50 nm and shear strain in them is approximately 2.5.

Shear bands in polymers are similar to the Lüder bands in metals, where the bands form an angle of nearly  $45^\circ$  to the direction of tensile stress. However, the inclination of shear bands in amorphous glassy polymers differs slightly from  $45^\circ$ , when measured in relaxed specimens. The value of  $\beta$  (i.e., the angle between the tensile stress direction and the shear band) is always greater than  $45^\circ$ . For polystyrene, Argon and coworkers [67] measured a value of  $\beta$  of  $53^\circ$  for the bands formed in compression near a stress-concentrating notch. Figure 1.9 shows the shear bands formed in the deformed sample of polystyrene [39],

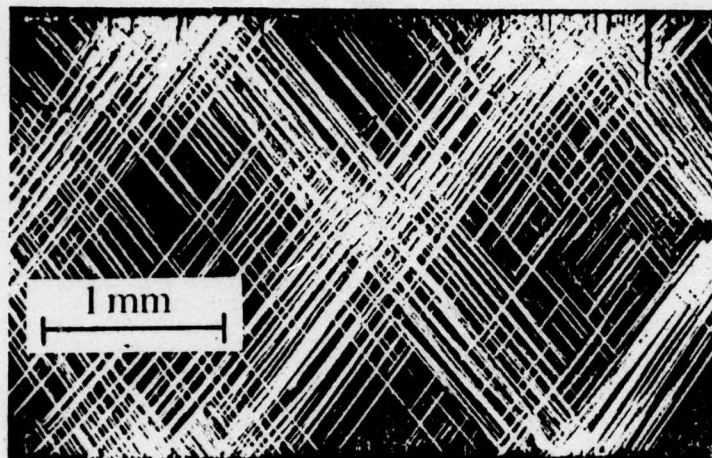


Figure 1.9 Shear band formation in a deformed sample of polystyrene [39]

Brady and Yeh [72] discuss the similarities between the craze morphology and shear band morphology in polystyrene. They report that it is similar in both cases and depends initially upon the relative shear displacement of  $100\text{-}1000\text{\AA}$  domains. As a deformation continues and orientation increases, fibrils varying from  $50\text{-}700\text{\AA}$  are formed within the deformation zone. Both shear-band formation and crazing strongly depend on the tie-molecules between these domains.

Sultan and McGarry [73] also suggest that both crazing and shear banding involve the same basic mechanism: a slippage of molecules and molecular segments past one another and the changes in the molecular configuration under the applied stress. However, each requires different activation energies and volume values and depends strongly on the



physical state of the glassy polymer, as well as on the stress system applied.

Shear-bands are located deep in the sample and can be distinguished from crazes which result from surface inhomogeneities and stress concentrations. Crazes propagate from the surface to the interior of the sample. Shear-bands are controlled by the shear stress which actually encourages lateral movement and thus prevents void formation. Crazing is controlled by a tensile stress and, therefore, fibrous matrix contains voids which result from restricted lateral Poisson's contraction.

Shear bands have been observed to be fairly regular in their width which is in the order of  $10^{-2}$  to  $10^{-3}$  nm. With continued deformation individual bands do not widen, instead more bands form inside the original bands with a high degree of molecular orientation in these newer bands.

## 1.6 Viscoelastic Behavior of Polymers

### 1.6.1 Concept of viscoelasticity

According to the theory of elasticity, the mechanical properties of solids are described in terms of Hooke's law. Similarly, the classical theory of hydrodynamics deals with the properties of viscous liquids for which, in accordance with Newton's law, stress is directly proportional to the rate of strain but independent of the strain itself. These categorizations of material behavior are really idealizations. While the behaviors of many solids and liquids approaches conformity (at small strains or rates of strain) to Hooke's law and Newton's law,

respectively, under other conditions significant deviations occur.

First, when finite strains are imposed on solids the stress-strain relations are found to depart from linearity (i.e., become non-Hookean) while for liquids under finite rates of strain their behavior is often observed to depart significantly from Newton's law (i.e., they exhibit non-Newtonian flow). Secondly, even if both strain and rate of strain are infinitesimal, a system may exhibit behavior which combines liquid-like and solid-like characteristics. For example, a body which is not quite solid does not maintain a constant deformation under the application of a constant stress but rather continues to deform slowly with time (i.e., creeps). When such a body is constrained at constant deformation, the stress required to maintain this deformation decreases with time. On the other hand, a body which is not quite liquid may, while flowing under constant stress, store some of the energy input rather than dissipate it as heat, and it may recover part of its deformation when the stress is removed.

Materials whose behavior exhibits such characteristics described above are called viscoelastic. If both strain and rate of strain are small, we have a linear viscoelastic behavior. The properties of viscoelastic materials are strongly time and temperature dependent. All polymeric materials come in the category of viscoelastic materials by virtue of their properties.

#### 1.6.2 Viscoelastic models

In order to describe and simulate the viscoelastic behavior of polymers, several models have been developed. Figure 1.10 [74]



describes four basic models which are only very briefly described here since a detailed description can be found in several textbooks on polymers. In these models  $E$  denotes the modulus or stiffness of the spring and  $\eta$  the viscosity of dashpot.


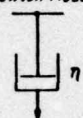

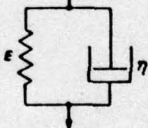
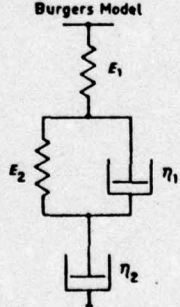
NUMBER OF ELEMENTS IN MODEL	MODEL	
1	Hooke Model	Newton Model
		
2	Maxwell Model	Voigt Model
		
3	Burgers Model	
		

Figure 1.10 Models for viscoelastic behavior [74].

- (a) The ideal elastic element is represented by a spring which obeys Hooke's law (with a defined modulus of elasticity). The elastic

deformation is instantaneous. An ideal rubbery solid exhibits such a simple behavior.

- (b) The ideal viscous element can be represented by a dashpot filled with a Newtonian fluid whose deformation is linear with time while the stress is applied and is completely irrecoverable (Newton element). The stress is exactly 90° out of phase with strain.
- (c) The Maxwell element (elastic deformation plus flow) is represented by a spring and a dashpot in series. It describes a material which can respond elastically to stress, but can also undergo viscous flow. The two contributions to the strain are additive in this model

$$\epsilon = \epsilon_{\text{elastic}} + \epsilon_{\text{viscous}} \quad (1.6)$$

The strain will be out of phase with stress, with a phase angle between 0° and 90°.

- (d) The Voigt element (retarded elastic response) is represented by a spring and a dashpot in parallel. The elastic response is not instantaneous but retarded by a viscous resistance. The two contributions to stress are additive in this model.

$$\sigma = \sigma_{\text{elastic}} + \sigma_{\text{viscous}} \quad (1.7)$$

Besides these four basic models there are many models consisting of springs and dashpots. The three components (4 units) which make up the simplest behavior of an actual polymer sample in creep can be represented by the so-called 4 parameter model, which



combines a series of Maxwell and Voigt elements in series. Such a model is described under the next section, which is on creep.

Finally, there are so-called extended models involving an instantaneous elastic response, viscous flow and a large number of Voigt elements, each with its own modulus and retardation time. Although these models exhibit the chief characteristics of viscoelastic behavior of polymers and lead to a spectrum of relaxation and retardation times, they are of limited value (valid for very small deformations). The flow behavior of real polymers cannot be characterized by discrete relaxation or retardation times but requires a wide range of such times to describe all phases of its behavior. Thus, these models are only a qualitative representation of the polymer behavior.

Creep and stress-relaxation are both manifestations of viscoelastic nature of polymers and both of these are observed in the materials used for this research. Therefore, the following two sections describe, very briefly, the creep and stress-relaxation behavior and their measurements in polymeric materials.

#### 1.6.3 Creep in glassy polymers

Creep is a characteristic feature of the macroscopic behavior of polymeric materials and is described by a four-element model shown in Figure 1.11.

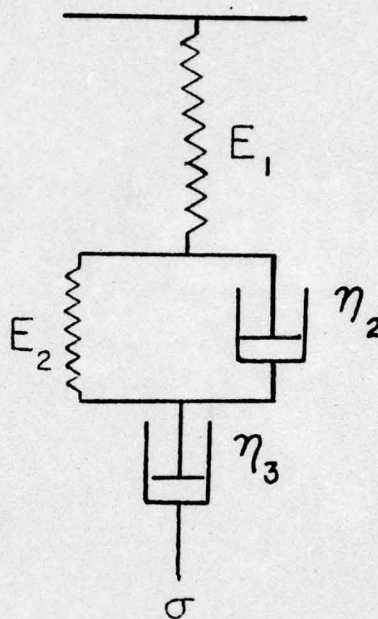


Figure 1.11 A four-element model for creep

When a constant load is applied, initial elongation comes from the single spring with modulus  $E_1$ . Later elongation comes from spring  $E_2$  and dashpot  $\eta_2$  in parallel and from the dashpot with viscosity  $\eta_3$ . Total elongation of the model is the sum of individual elongation of these three parts. Thus,

$$\epsilon = \frac{\sigma}{E_1} + \frac{\sigma}{E_2} (1 - e^{-t/\tau}) + \frac{\sigma}{\eta_3} t \quad (1.8)$$

where



$\sigma$  is applied stress

$\tau$  is retardation time defined by

$$\tau = \eta_2/E_2 \quad (1.9)$$

In a recovery test, after all the load is removed, creep is all recoverable except from the viscous part due to dashpot  $\eta_3$ . Instant elongation reduction on removing the load comes from single spring with elasticity  $E_1$  and is equal to  $\sigma_0/E_1$ .

Experimentally, the creep test can be carried out in tension, compression or shear. A tensile creep test is the most widely used one. In such a test stress is applied on the sample and elongation is measured periodically. Creep curves may be plotted in different ways, such as strain vs. time, elongation vs. time or log of elongation vs. time. A strain vs. time curve is illustrated in Figure 1.12.

If a viscoelastic material was subjected to a constant stress of  $\sigma$ , its length, in general, would increase as a function of time,  $\ell(t)$  the strain at any time is defined as

$$\epsilon(t) = \frac{\ell(t) - \ell_0}{\ell_0} \quad (1.10)$$

where  $\ell(t)$  is the length at time  $t$ , and  $\ell_0$  is the original (unstretched) length. If stress is removed at time  $t = t_1$ , the resulting  $\epsilon(t)$  vs.  $t$  curve will be approximately a mirror image of the  $\epsilon(t)$  curve prior to time  $t_1$ . At any time the ratio of strain  $\epsilon(t)$  to applied stress,  $\sigma_0$ , defines a quantity called "compliance" as follows:

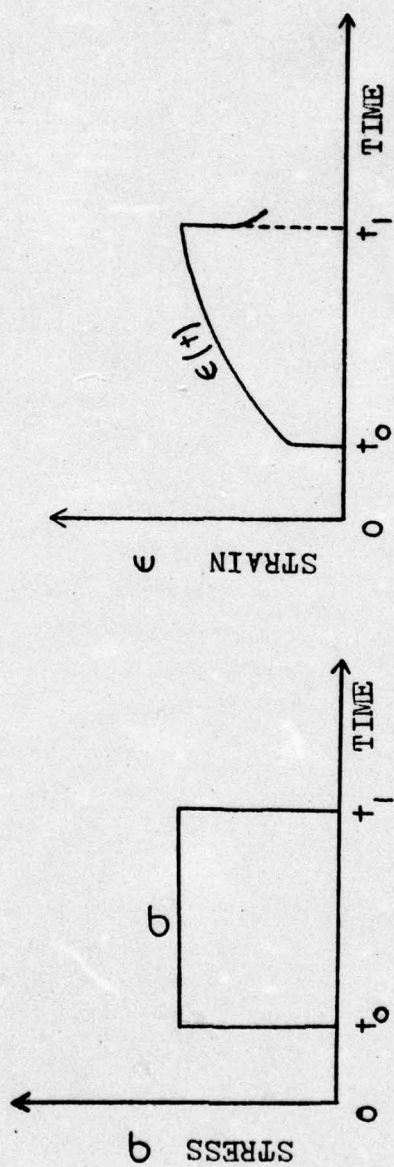


Figure 1.12 Creep curves.



$$D_{\text{crp}}(t) = \frac{\epsilon(t)}{\sigma_0} \quad (1.11)$$

Creep properties of a polymer are very dependent upon temperature. At temperatures well below  $T_g$  the polymer is rigid with high modulus or low compliance. If the temperature is so low that segmental movement of polymer chains cannot occur, very little creep will occur, even after long periods of time. As the temperature is raised, not only does elongation or compliance increase, but also the rate of creep increases since some segmental molecular motion can take place. As long as a chain segment is frozen in a fixed position, the stress on it cannot be internally relieved. However, a chain segment under stress will move so as to relieve the stresses whenever possible. Stresses removed from one segment are added to others, thus stretching them a little more. The other chain segments, in turn, move to relieve stresses from time to time. The result is a gradual increase in length of the test specimen with time. The stress on a segment of a polymer chain can be relieved if the chain can slide with respect to its neighbors. This type of motion is similar to viscous flow. Stress can also be removed if the polymer chain breaks. This occurs if the chains are overstressed and rupture under load, or if chemical reaction such as oxidation takes place during creep test. These concepts will be explained on the basis of experimental evidence in polystyrene and polycarbonate polymers in later chapters of this dissertation.

#### 1.6.4 Stress-relaxation in polymers

A simple model for stress-relaxation is a Maxwell model, which consists of a Hookean spring and a Newtonian dashpot, as already described in Figure 1.10. Stress-relaxation can be considered to be counterpart of creep, where the sample is subjected to constant strain  $\epsilon$ , and the decay of stress  $\sigma(t)$  is observed. This is illustrated in Figure 1.13. Assuming a linear behavior, the stress relaxation modulus  $G(t)$  can be defined by equation (1.12)

$$G(t) = \frac{\sigma(t)}{\epsilon} \quad (1.12)$$

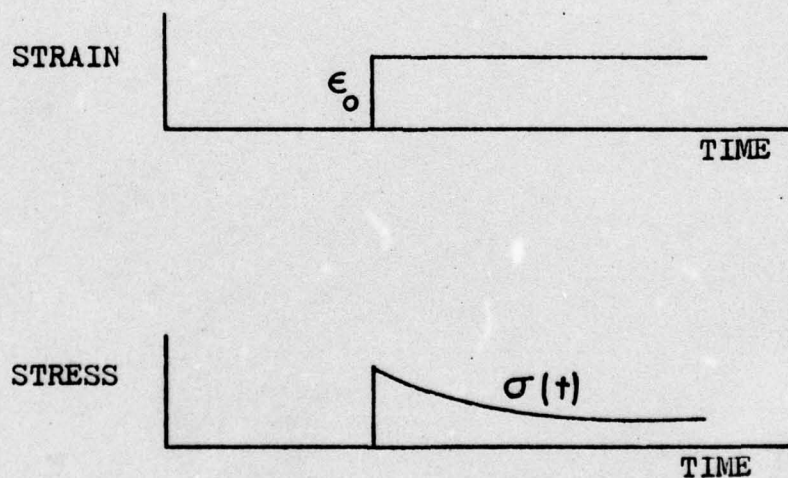


Figure 1.13 Stress relaxation [8]



In case of stress relaxation, presence of viscous flow affects the limiting value of stress. If viscous flow occurs, stress can decay to zero at sufficiently long times. If no flow occurs, the stress decays to some finite value and one obtains an equilibrium or relaxed modulus at infinite time. Figure 1.14 is a schematic graph of stress-relaxation modulus as a function of time. The regions of behavior, viz., glassy viscoelastic rubbery and flow, can be identified and also a transition time  $\tau$  can be defined. Transition time characterizes the time-scale of viscoelastic behavior.

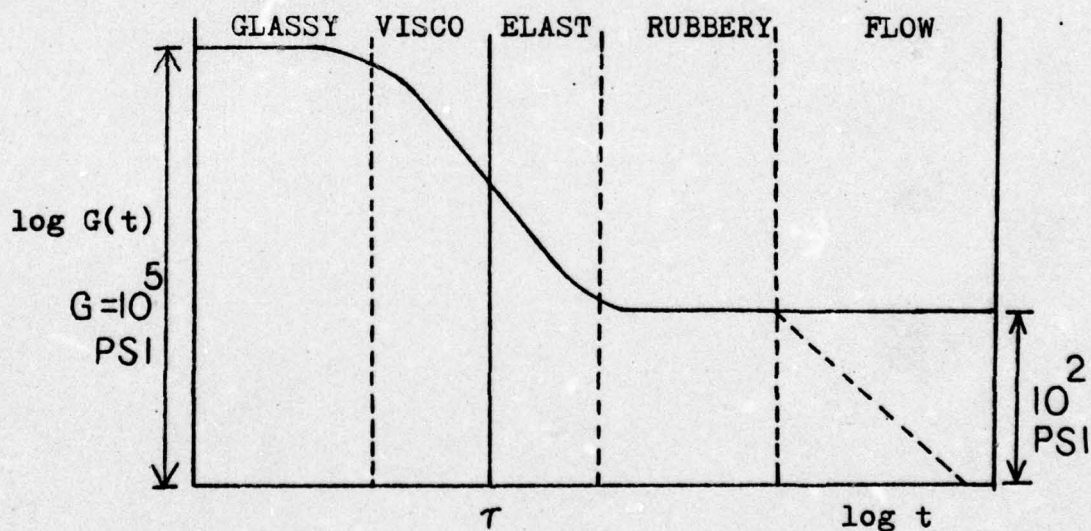


Figure 1.14 The stress-relaxation modulus  $G(t)$  as a function of time  $t$ .  $\tau$  is the characteristic time (the relaxation time).

## CHAPTER II

### INFRARED SPECTRA OF STRESSED POLYMERS

Basic theory of infrared spectroscopy and its applications to the studies of polymers have been very well described by Zbinden [75]. In this chapter the author will discuss up-to-date application of infrared spectroscopy in determining the molecular state of a polymer subjected to tension and/or cyclic fatigue.

#### 2.1 Discussion of Peak Shift and Band Distortions

The infrared vibrational frequency of a molecule is known to depend on force constants (which are determined by the strength of the atomic bonding) and bond angles. It is well known that the deformation of atomic bonds and their angles under stress can result in a shift of skeletal vibration. The amount of shift can provide a measure of the magnitude of the mechanical stress acting on the polymer chain. Zhurkov and coworkers [76] made use of these principles to learn about the overstressed bonds, true stresses and stress distribution in oriented films in polypropylene, poly (ethylene terephthalate) and Nylon 6.

In their experiments Zhurkov and coworkers [76] loaded the sample along the axis of orientation while the sample remained in the beam of the infrared spectrometer and recorded the spectra. Then, on comparison of the IR absorption spectra of a load-free specimen and



that of a specimen under load, they found that the mechanical stress had shifted the peak of the absorption band of polypropylene and poly (ethylene terephthalate) towards the lower frequencies. The absorption bands which showed this effect were due to vibrational frequency of C-C (backbone) bonds in the polymer chain. By measuring shifts at various stresses on the polymer, they related peak shift to the applied stress by the following equation:

$$\nu_0 - \nu_\sigma = \sigma\alpha \quad (2.1)$$

or

$$\Delta\nu = \sigma\alpha$$

where  $\nu_\sigma$  and  $\nu_0$  are the frequencies of absorption band peaks under stress  $\sigma$  and without it.  $\Delta\nu$  is the shift in frequency.  $\alpha$  is the proportionality constant.

These researchers [76] also postulate that distortion in IR band shape on the low frequency (tail-end) region is caused by a non-uniform stress distribution on the atomic bonds. Thus, a small portion of chains in the polymer are highly stressed, as compared to the rest of chains. These highly-stressed bonds absorb at much lower frequencies and show up on the tail-end side as a shoulder or a distortion. Figure 2.1 illustrates deformation behavior of such a band when polymer experiences a tensile stress. The shift of IR absorption peak and an appearance of shoulder toward the lower frequency are both obvious in Figure 2.1 [77].

The experimentally found linear relationship between "peak shift" (shift in the maxima of IR absorption band on stressing) and stress

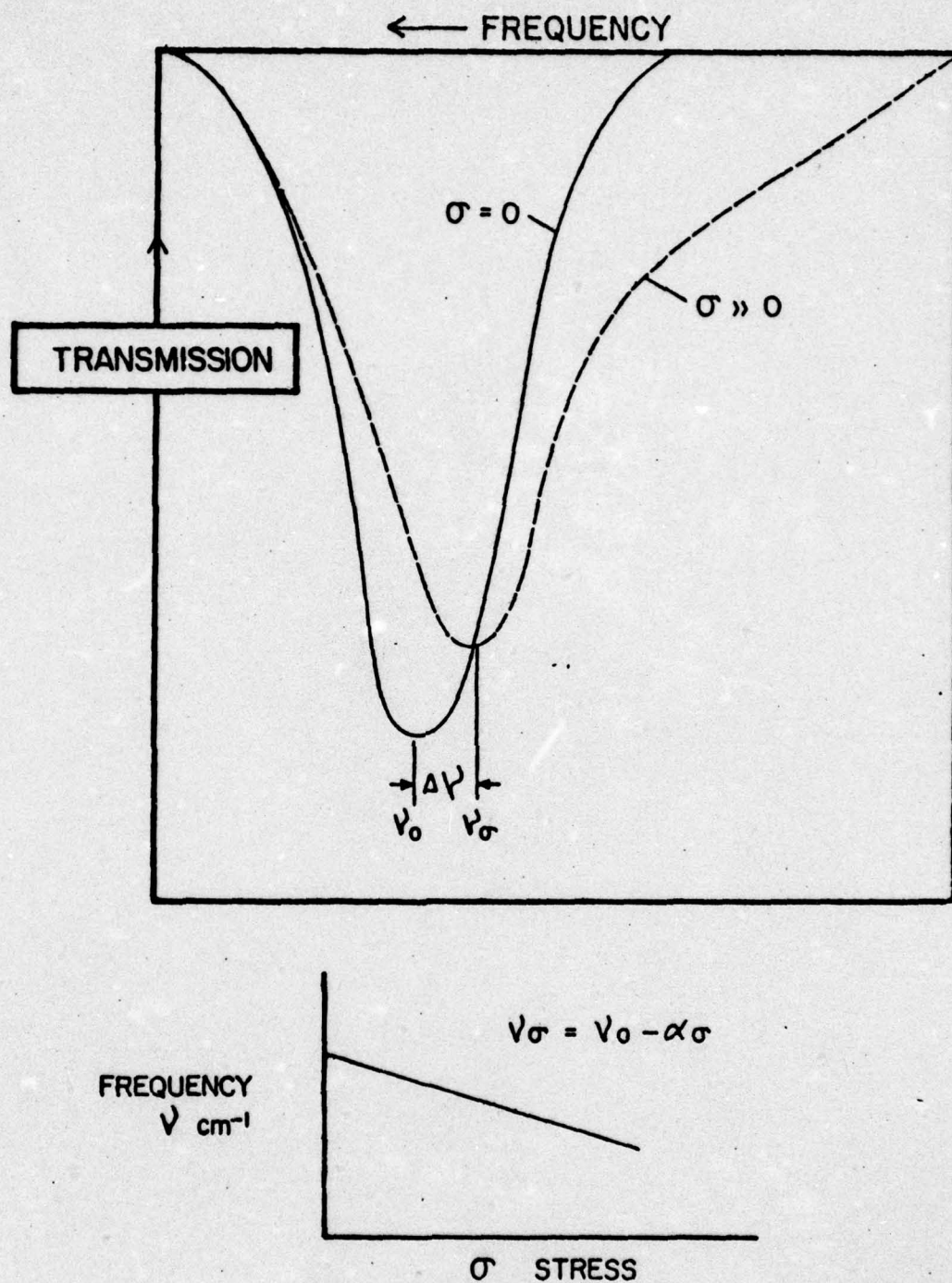


Figure 2.1 Schematic effect of stress on a band associated with backbone vibration [77].



has been theoretically predicted in Gubanov's publications [78,79] which show the validity of relation over a wide range of stresses up to breaking stress. By extrapolation of this linear relationship to frequencies of strongly overstressed bonds, Zhurkov and coworkers [76] were able to determine true stresses on overstressed bonds.

This technique has been used by several researchers [32,77, 80-82] to determine atomic stress distributions in various semicrystalline polymers. It is now, for the first time, being extended by the present author to amorphous, glassy polymers to investigate the load-bearing mechanism and molecular behavior of polymer chains under stressed conditions.

Based on the above basic theory, Wool [77] and Vettegren and coworkers [80] evolved a technique to obtain molecular stress distribution. In this a deformed band  $D(\nu)$  is expressed by a convolution integral

$$D(\nu) = \int_{-\infty}^{\infty} F(\xi) U(\nu) d\xi \quad (2.2)$$

where  $F(\xi)$  is a distribution of the stressed oscillators,  $U(\nu)$  is the shape of normalized deformed band and  $\xi$  a dummy variable. In this integral, if the form for  $U(\nu)$  is assumed, it is possible to evaluate  $F(\xi)$  since  $D(\nu)$  is measured and, therefore, known. The distribution of stressed oscillators is then converted to a stress distribution on the molecular bonds by using constant  $\alpha$  and making other assumptions, the details of which will not be discussed here and are available in reference 32 and reference 77.

Zhurkov and coworkers in their later publication [81] discuss another method of determining the fraction of overstressed bonds. This method involves first separating the symmetrical band from the overall band and then measuring the area under both, the symmetrical as well as the distorted portion of the absorption band. A ratio of the area under the distorted portion to the area under the symmetrical band gives an estimate of a fraction of non-uniformly stressed atomic bonds in the polymer.

In this publication [81] Zhurkov et al. also discussed a probable mechanism for "peak-shift" as well as band distortion. They suggest that loading does not lead to an appearance of any new oscillators whose vibrational frequencies would superimpose upon band under consideration and thus change its form. The mechanical stress only alters the energy state of oscillators, leading to a shift of their vibrational frequencies toward the low wavenumbers. Further, the load-induced band-broadening is related to inhomogeneity of energy state caused by structural inhomogeneities of polymers. On loading a polymer specimen, certain bonds in polymer chains are overstressed and their vibrational frequencies shift toward lower frequency. Superposition of such bands on the rest of the absorption band thus shows up as deformation of the IR band.

Since there can be several other explanations for "peak shifts" and "band distortion" in polymers, a few discussed by Wool [77] in his dissertation will be discussed here briefly. According to Wool, when a polymer is stressed, the macromolecular chains rearrange themselves in order to accommodate the imposed load. The chains also



experience stress which can cause bond stretching, bond angle distortion and even conformational transitions. When large numbers of chains are involved, it is possible that long-range order may also be changed. As a result of any of the above changes, it is possible that molecular orbitals and bonding energies are also affected and thus an altered IR spectra is observed.

Five possible mechanisms that can cause "band shift" and "band distortion" are discussed in the next section.

#### 2.1.1 Change in force constants

A vibrational mode of a molecule is most conveniently represented by vibrations of a single mass attached by a flexible bond, i.e., by a spring to a fixed system as shown in Figure 2.2.

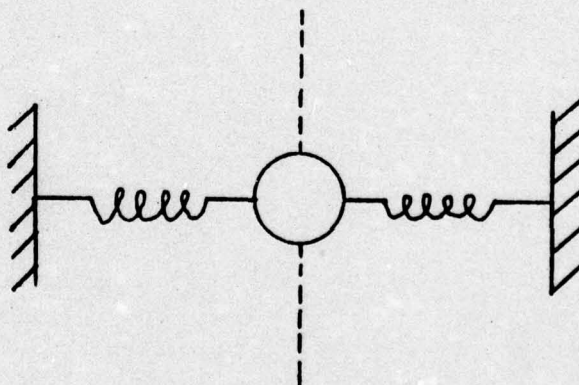


Figure 2.2 A simple harmonic oscillator

Vibrational characteristics of such a particle are determined by the mass of the particle and the nature of the spring (of a chemical bond at the molecular level). The vibrational frequency of such a system is given by

$$\nu = \frac{1}{2\pi c} \sqrt{\frac{k}{m}} \quad (2.3)$$

where  $\nu$  = frequency

$k$  = force constant

$m$  = mass

$c$  = velocity of light

It is obvious from equation (2.3) that frequency is independent of stress but is related to force constant ( $k$ ). Therefore, any decrease in  $k^2$  will be directly related to the decrease in frequency. Gubanov and coworkers [78,83] applied this principle of varying the force constant to a polypropylene chain and showed that some vibrational frequencies can shift toward the lower frequencies while the others can shift toward higher frequencies. Similar results have been obtained by Reynolds and Sternstein [84] for hydrogen bonding in polyvinyl alcohol and Cooper [85] for polyurethanes. A change in force constants of a body can be caused by a change in internuclear distance and molecular orbital interactions, both of which also affect the bond strength.

Badger and Gordy [86] have suggested an empirical formula for  $k$  for a diatomic molecule which is:



$$k = a N \left[ \frac{x_a \cdot x_b}{d^2} \right]^{3/4} + b \quad (2.4)$$

where  $a$  and  $b$  are both constants, depending on the positions of two atoms in the periodic table.  $N$  = number of covalent bonds between the two atoms,  $d$  = internuclear distance, and  $x_a$  and  $x_b$  are the electronegativities of the two atoms.

If a change in force constant is indeed the mechanism for band shifts and band distortions, then skeletal bonds are expected to be most affected by the stress and there will be very little or no change in the side group frequencies.

The above mechanism is directly applicable to polymers since a long polymer chain, when stressed, will experience stress along its backbone bonds resulting in a change of force constants along its length.

Zhurkov and coworkers [76] have also suggested this to be the prime mechanism leading to "band shifts" and "band distortions" in stressed polymers.

### 2.1.2 Bond angle and bond length changes

It is quite obvious that an application of stress on a polymer chain will tend to extend it in the direction of applied stress. Such extension is accompanied by stretching of valence bond length and distortion of bond angles. It is known that infrared frequency calculations based on valence force field and normal mode analysis take

into account the following variables (symbols given for convenience):

- (a) Mass of the constituent atoms -  $m$
- (b)  $k$  - the bond force constant
- (c)  $k_\theta$  - angle bending force constant
- (d)  $d$  - equilibrium internuclear distance
- (e)  $\theta$  - angle between any two bonds

Therefore, any changes in  $d$  and/or  $\theta$  can cause a shift or a change in vibrational frequency. Wool [77] used the following symbols for different bending and stretching modes in his frequency calculations on a simple nonlinear triatomic molecule:

- $\nu_1$  - symmetric stretching
- $\nu_2$  - symmetric bending
- $\nu_3$  - asymmetric stretching

and suggested that for small deformations angle bending is likely to be a dominant mode of deformation and it will vary with stress as

$$\theta(\sigma) = \sin^{-1} \left[ \sin \theta_0 \left\{ 1 + \sigma \left( \frac{d^2}{k_\theta} \right) \right\} \right] \quad (2.5)$$

where  $\theta_0$  corresponds to undeformed angle.

Using convenient values for  $m$ ,  $k$ ,  $k_\theta$ ,  $d$  and  $\theta_0$ , Wool [77] demonstrated that  $\nu_1$  is most sensitive to stress and shifts to lower frequencies, whereas  $\nu_2$  and  $\nu_3$  show positive shifts (to higher frequencies). In all cases shift is approximately linear with stress for small deformations. A similar analysis for changes in bond distance showed that only symmetric bending vibration was affected, leaving other modes unchanged. The changes in bond distances and angles were



dependent on stress, i.e., they would revert to their equilibrium position on removal of stress. Thus, only elastic deformation was considered.

The above discussion and analysis for a simple system can be extended to long polymeric chains and it can be said that elastic deformation of chains can themselves cause frequency shifts (i.e., even if force constants are assumed to be unchanged).

### 2.1.3 Conformational changes

Another factor responsible for observed stress effects on IR absorption bands can be due to conformational transitions in polymer chains under stress. A polymer chain adopts a series of conformational isomers determined by an energy balance of intermolecular and intramolecular interactions. Boyd and Breitling [87] demonstrated that a polypropylene molecule, when uniaxially deformed, can assume one of a series of metastable conformations that would not normally be adopted in the unoriented state. Some of these strain-stabilized conformations may differ only very slightly in their internal rotational angles from those of unstressed state. Thus, new conformations may cause additional infrared bands to occur at very close, but different, frequencies from the previous state.

Miyazawa [88] investigated the effect of internal rotation on the skeletal frequencies of several polymers. He showed that both positive and negative shifts can occur and these are approximately linear function of the internal rotation angle for small deformation.

But, if some bands exist that are conformationally insensitive, i.e., they show the same characteristics in melt or solid and are not affected by orientation and crystallinity, then it is possible to assume that the frequency shifts may not be due to the conformational changes. However, many bands are sensitive to the above-mentioned factors and it is difficult to separate conformationally sensitive bands from the insensitive ones. It is not clear whether all chains show metastable conformations with stress; it is also possible that such intermediate states are energetically unfavored. If theoretical calculations do show such metastable states, this mechanism cannot be ruled out completely. However, such conformational transitions have to be reversible in order for the frequency shifts to disappear on release of external stress. Also, these transitions must occur synchronously with varying angle, force constants and bond stretching effects.

#### 2.1.4 Defect mechanism

Real polymer chains or crystal lattices are known to contain many defects. Some of these defects can be:

Chemical defects--incomplete polymerization, crosslinks, branching, impurities, etc.

Morphological defects--chain ends, crystal defects, chain folds, voids

Steric and  
Conformation defects--presence of different isomers and lack of homogeneous tacticity.

All of these defects can affect the vibrational spectrum. As previously discussed, in an infinitely long polymer chain, all the



oscillators must be in-phase to cause a net change in dipole moment and thus be infrared active. In Figure 2.3 the frequencies of two hypothetical infrared bands, A and B, are shown as a function of phase difference. The density of states  $g(\nu)$  for this process is obtained by integrating Figure 2.3 for each  $\Delta\nu$  interval to generate Figure 2.4. The singularities of  $g(\nu)$  are the usually observed infrared peaks in the spectrum. Several regions of  $g(\nu)$  may be infrared active but, when stressed, previously inactive vibrations may be brought into resonance to form the tail region of the band.

Theoretically, the defect mechanism may explain the tail-end distortion but it does not explain the "band shifts" as observed experimentally. More so, it is not yet certain whether defect mechanism is indeed involved in the tail-end distortions. Mocherla [32] in his dissertation attempted to clarify the situation. Since some of the above mentioned defects (particularly the morphological and conformational) are heat sensitive, Mocherla [32] heat treated (annealed) poly (ethylene terephthalate) (PET) samples and obtained IR spectra of these, under stress. His results showed that heat treatments did not eliminate the tail-end distortions in the absorption bands of the stressed PET samples. This means that either the defects are not heat sensitive or the contribution of the defect mechanism to the tail-end distortions is very small.

#### 2.1.5 Anharmonicity and phonon interactions

Anharmonicity and phonon interactions can also cause band broadening of IR absorption bands. This is a well-known fact in IR

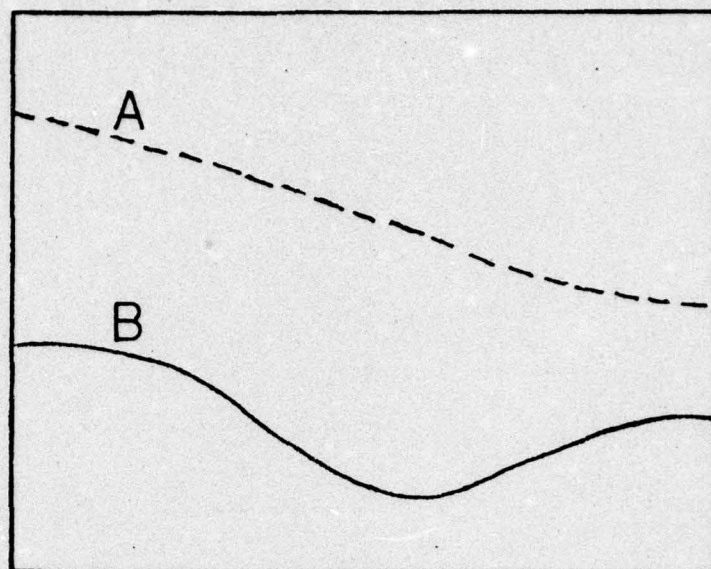


Figure 2.3 IR frequency versus phase difference

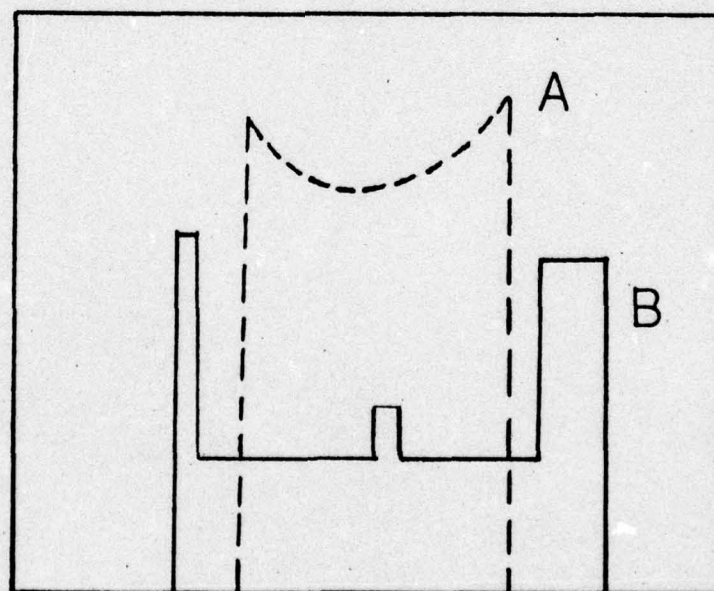


Figure 2.4 Density of state versus frequency [77].



absorption spectra of crystals. There the basic theory of IR predicts that diatomic cubic crystals should show single and rather narrow absorption band but, in practice, a broad absorption band is observed. Also, contrary to IR theory, weak but well pronounced bands are observed for nonpolar crystal (viz., diamond, silicon and germanium) [89-90]. Such discrepancies may be due to higher order effects neglected in the basic theory, namely, anharmonic terms in the potential energy and nonlinear terms in dipole moment. The latter arises from the fact that in course of lattice displacement or vibrations the electron shells are deformed and, as a result, the polarization is not exactly proportional to the lattice displacement but also contains terms which are of second, third, etc., order in displacement coordinates.

Anharmonicity effects and phonon interactions have been dealt in great detail for crystals using quantum mechanical calculations [89-91]. In polymers, so far, there have been only two publications on this subject. In one of these [92] the effects of anharmonicity on half width of IR absorption bands have been studied as a function of temperature, which is not applicable to the present work. In the other publication Kosobukin [93] investigated the effect of anharmonic damping of phonon interactions and concluded that line broadening was primarily due to quasi-elastic force constants rather than anharmonic damping of phonons. These effects will not be developed in this dissertation but have been very recently investigated by Mitra et al. [94].

## 2.2 Application of Dynamic Infrared Technique

In the following two sections a brief review of Wool's [77] and Mocherla's [32] work is presented to demonstrate the versatility of this technique to study changes occurring at the molecular level.

### 2.2.1 Study of molecular mechanics of polymer by dynamic infrared technique (DIR)

As previously discussed, dynamic infrared technique was pioneered by Zhurkov and coworkers [76] in USSR. Statton and Wool [50] were the first researchers in this country to build a loading device which would enable recording of infrared spectra of a polymer under load while its creep and stress-relaxation response is simultaneously measured.

In this research group Wool [77] was the first researchers to investigate the molecular mechanics of highly oriented polypropylene during stress-relaxation and creep by using DIR techniques. He studied "band shifts" and "band distortions" of polypropylene under stress and demonstrated, for the first time, the mechanism of stress distribution on individual molecules. Wool [77] concluded on the basis of this technique that there were major molecular differences resulting from two macroscopic deformation modes in polypropylene. These are listed in Table 2.1.

Wool, in his dissertation, evaluated the creep behavior of the highly-stressed bonds and fractured chains by several theoretical and experimental methods and found a good correlation. Thus, DIR



Table 2.1 Major Molecular Differences Resulting from Two Macroscopic Deformation Modes  
in Polypropylene

Stress Relaxation	Creep
1. The number of highly-stressed bonds decreases with time.	The number of highly-stressed bonds increases with time.
2. The number of intermediately-stressed bonds increases with time.	The number of intermediately-stressed bonds decreases with time.
3. Helix bands decrease.	Helix bands increase.
4. Orientation decreases.	Orientation increases.
5. Small number of fractured bonds.	Large number of fractured bonds.

technique has an obvious advantage.

### 2.2.2 Stress-strain behavior of oriented crystalline polymers.

#### A molecular approach by dynamic infrared technique.

Following Wool's [77] work involving the use of dynamic infrared technique, Mocherla [32] applied this method to investigate another important aspect of polymers--the stress-strain behavior of polymers on a molecular basis. He studied highly oriented poly (ethylene terephthalate) films. Highlights of his work are the following:

- (a) Discussion of "peak shift" and "band distortion" and its dependence on sample morphology.
- (b) Proposition of a morphological model based on the observed infrared data calculation of the molecular stress distribution by numerical deconvolution of the observed infrared bands of PET under different stress conditions.
- (c) Proposal of a morphological model based on observed infrared data, as well as on molecular stress distribution calculations.

2.2.2.1 Peak shifts and band distortions in PET. Mocherla [32] suggests a strong dependence of peak shifts and band distortions on the morphology of a polymer sample. Figure 2.5 shows the effect of stress on highly oriented PET film showing peak shift, tail-end distortion (or a shoulder on lower frequency side) and a slight broadening of the absorption band. Peak-shift has been described by this author to be due to similar stress effect on the majority of oscillators. He ascribed tail-end distortions to small numbers of oscillators experiencing much higher stresses. Zhurkov and others [76,80,95] point out that peak shift was caused by uniformly stressed crystalline chains. Mocherla [32] extends this view by stating that



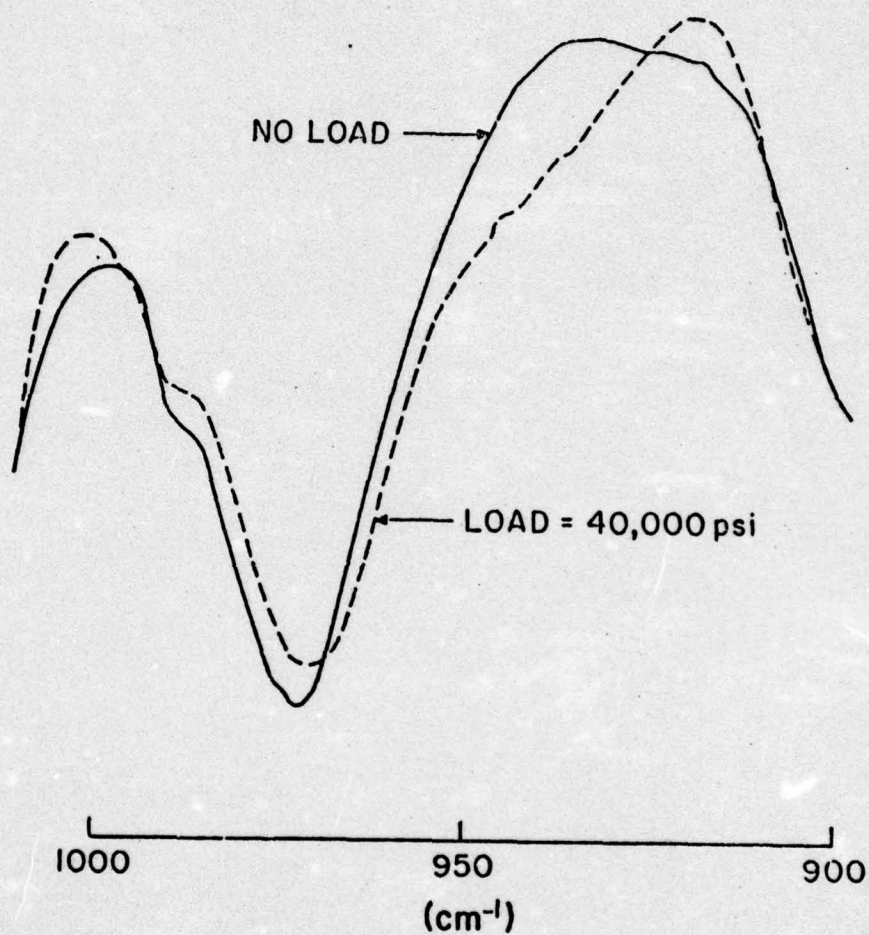


Figure 2.5 Peak shift and distortion of skeletal  $973\text{ cm}^{-1}$  band of PET under an external stress [32].

there are also some noncrystalline chains experiencing uniform stresses because of their arrangement in the morphological matrix. Thus, they also participate in the band shift phenomena.

Mocherla [32] postulates that not all bonds may be stressed to exactly the same level. A small variation in stresses will cause various oscillators to absorb at slightly different frequencies and the overall result of this is probably a broadened IR band.

Mocherla [32] also studied three morphologically different PET samples for peak-shifts as a function of stress. Stress-strain curves for these samples are shown in Figure 2.6. Peak shifts as a function of stress are shown in Figure 2.7, which indicates that no peak shift occurs at low level stresses but it increases with increasing load after a threshold value. This had not been observed by previous researchers. As a result, the following constraints have been applied to equation (2.1):

$$\begin{array}{ll} \Delta\nu = 0 & 0 \leq \sigma \leq \sigma_t \\ \Delta\nu = \alpha \sigma & \sigma_t < \sigma \end{array}$$

where  $\Delta\nu$  = shift in peak frequency

$\sigma$  = stress on the sample

$\sigma_t$  = threshold stress beyond which peak shift occurs

$\alpha$  = the response of majority of chain segments in a polymer to a unit stress.

No shift region at low level stresses has been related to Hookean behavior of the polymer where stress and strain are linearly related



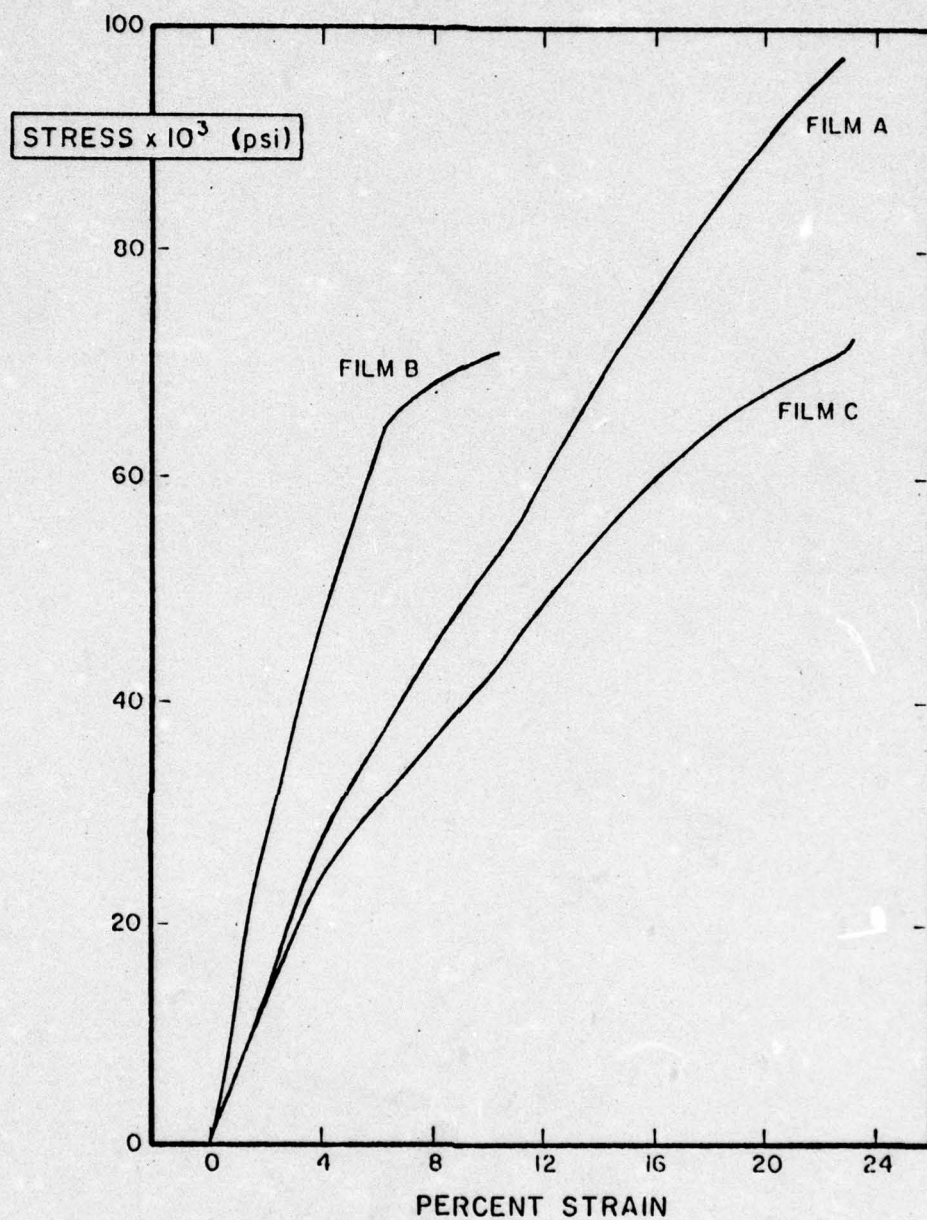


Figure 2.6 Stress-strain curves for PET films (A,B,C) obtained on an Instron.

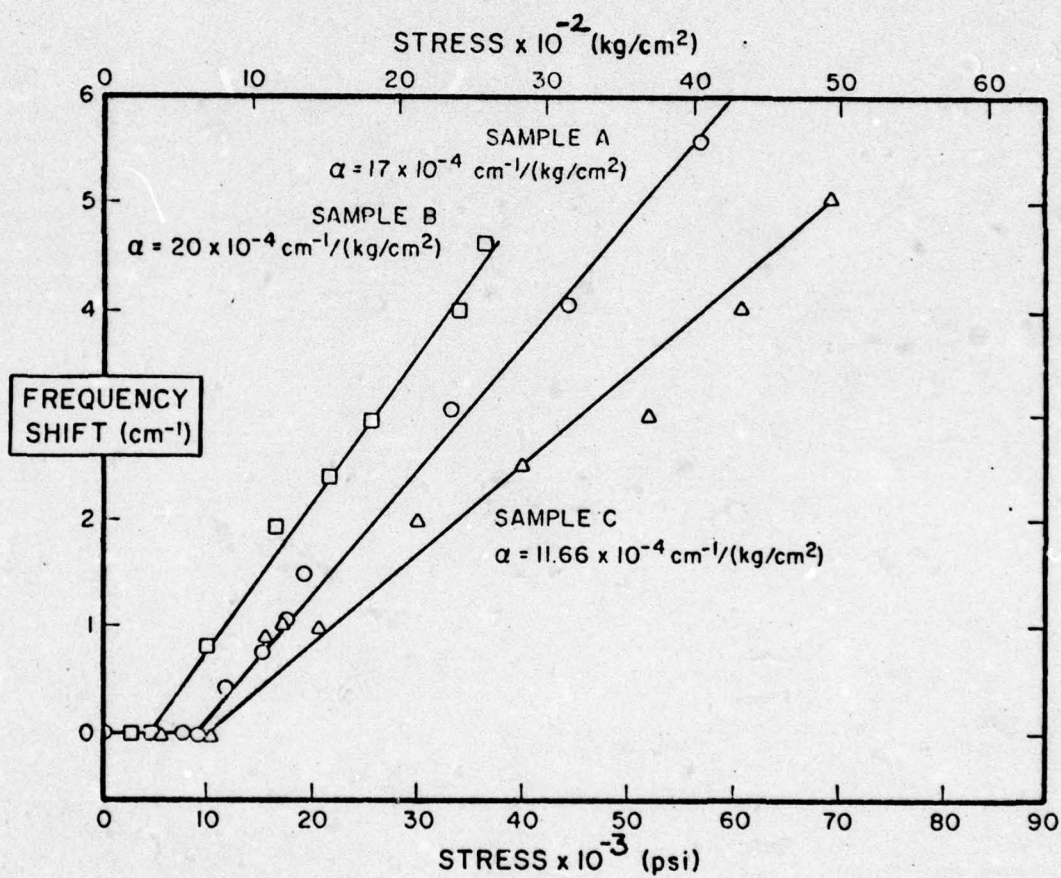


Figure 2.7 Frequency shift versus stress plots for oriented PET films (A,B,C) [32].



and reversible. Beyond the threshold stress the material starts yielding and stresses are borne by the rest of the molecular chains in addition to tie molecules. Heat treatment of PET films showed the following:

$$\alpha_{\text{unannealed}} > \alpha_{\text{constraint-annealed}} > \alpha_{\text{slack-annealed}}$$

This led to the belief that  $\alpha$  is a measure of stresses on all uniformly loaded chain segments and is mainly influenced by crystalline chain segments.

2.2.2.2 Molecular stress-distribution in PET. Mocherla [32] numerically deconvoluted IR absorption bands and thus obtained a molecular stress-distribution corresponding to various points on the stress-strain curve. Figure 2.8 shows that at low stress levels, i.e., in Hookean region, no peak shift occurs and there is only a minor change in low frequency side of overstressed region. Figure 2.9 shows that past the Hookean region changes in the distribution start taking place and these become significant. Figure 2.10 shows that at very high stresses, i.e., close to fracture, peak shift increases with a decrease in the fraction of overstressed bonds in the low frequency region. This is so because some overstressed bonds may have fractured at such junctures on stress-strain curve.

Another important outcome of the DIR technique, as demonstrated by this researcher, is that a morphological model for semicrystalline polymers, viz., PET, can be proposed based on observed peak shifts and band distortions.

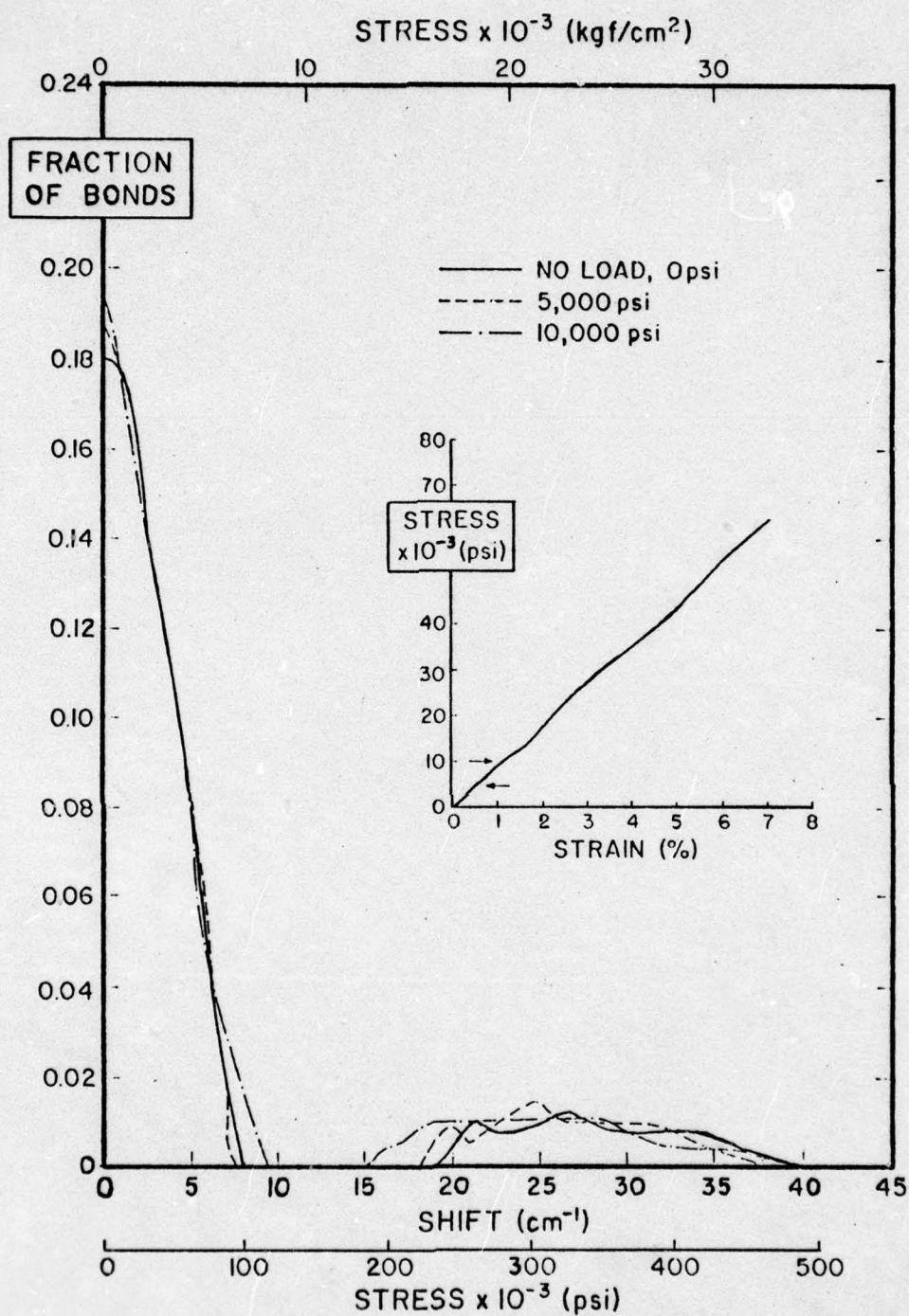


Figure 2.8  $F(v)$  curves for film C at 0, 5000 and 10000 psi external stress [32].



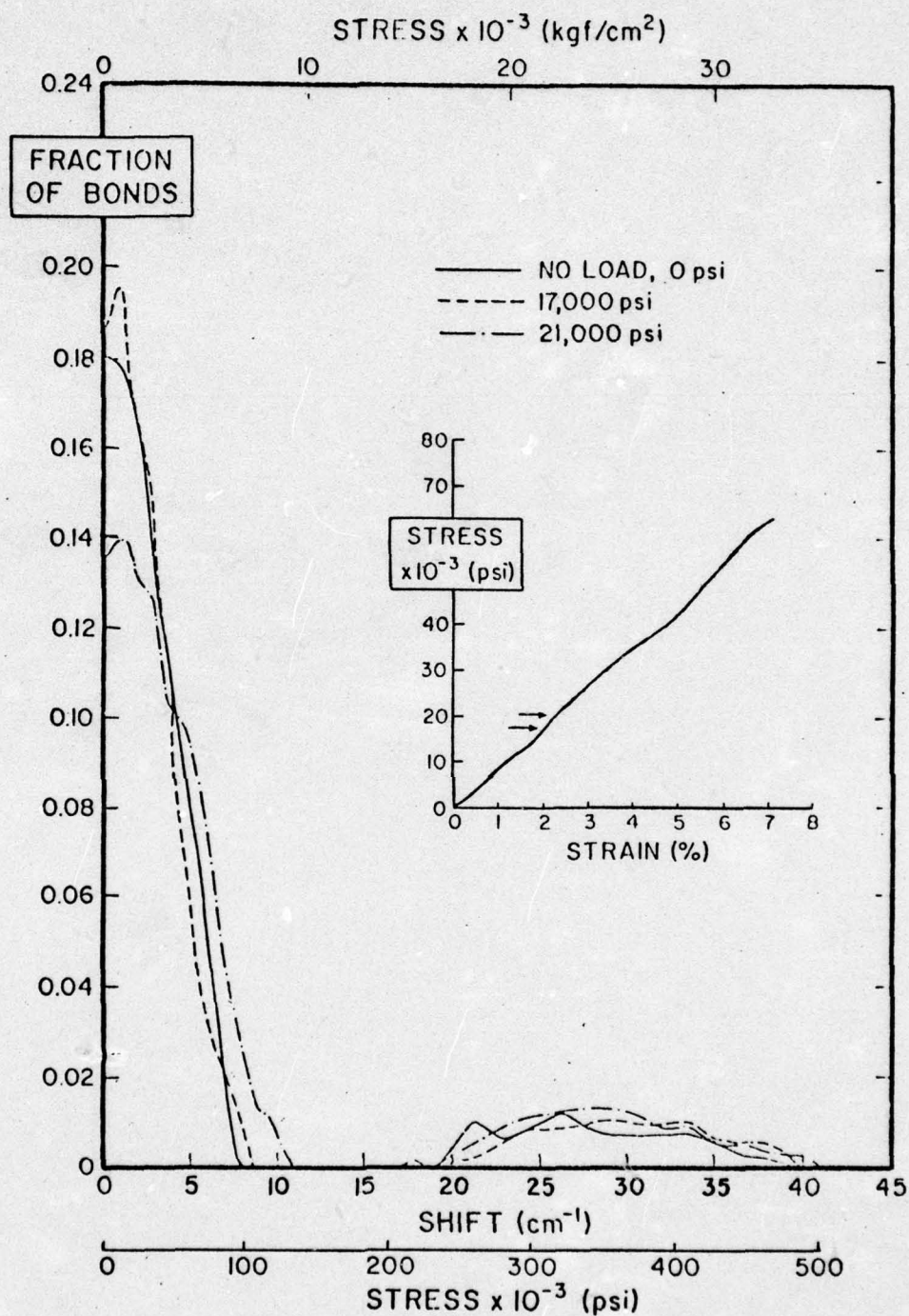


Figure 2.9  $F(v)$  curves for film C at 0, 17000 and 21000 psi external stress [32].

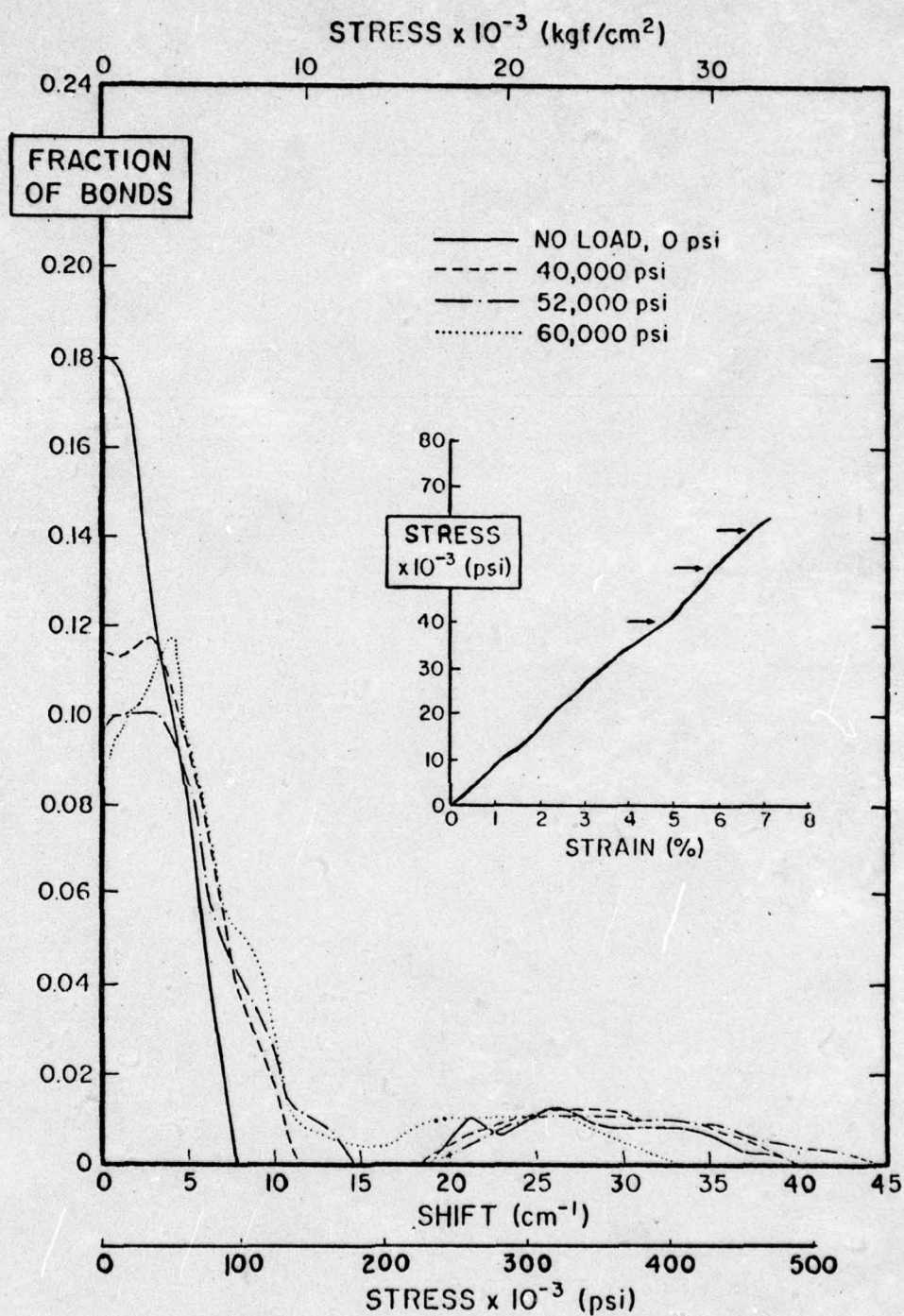


Figure 2.10  $F(v)$  curves for film C at 0, 40000, 52000 and 60000 psi external stress [32].



Finally, the versatility of the DIR technique has been demonstrated by this author in the studies of the molecular behavior of amorphous, glassy polymers, viz., polystyrene and polycarbonate, under static tension, cyclic fatigue and in crazing conditions.

## CHAPTER III

### VIBRATIONAL ASSIGNMENTS OF INFRARED ABSORPTION BANDS OF POLYSTYRENE AND POLYCARBONATE

#### 3.1 Infrared Spectra of Polystyrene and its Vibrational Assignments

Although several scientists have studied the infrared spectra of polystyrene, Liang and Krimm [96] seem to have come up with a most comprehensive of all calculations of infrared absorption band frequencies and their vibrational assignments. Their calculations are based upon normal mode analysis of phenyl,  $\text{CH}_2$  and CH groups which are parts of a monomer unit of polystyrene, i.e.,  $[\text{CH}_2-\underset{\text{C}_6\text{H}_5}{\text{CH}}]$ . In a long polymer these repeat units are linked to each other in a head-to-tail arrangement, i.e., phenyl groups are attached alternately to carbon atoms. The orientation of these phenyl groups appears to be random as indicated by X-ray diffraction studies [97,98] which show that the polymer is completely amorphous. The polystyrene chain is probably stiffened somewhat due to interference among the neighboring phenyl groups [99] but there is an indication [100] that no regularity exists along the carbon backbone. This implies that for spectroscopic purposes there are no specific interactions among monomeric units in the chain. (This has been actually shown by recent Russian researcher [101] on polystyrene.) Therefore, Liang and Krimm [96] assumed that the normal vibrations of phenyl,  $\text{CH}_2$  and CH groups may be considered separately and



a complete spectrum of polystyrene can be interpreted as a linear superposition of the contribution of these parts.

In order to simplify the normal mode analysis of phenyl groups, these researchers [96] considered monosubstituted benzene with an assumption that the substituent lacked any special symmetry. Symmetry analysis of the monosubstituted benzene shows that it belongs to ( $C_{2v}$ ). The character table for this point group shows a possibility of 30 internal vibrations which are distributed as:  $11A_1 + 3A_2 + 10B_1 + 6B_2$ , where  $A_1$ ,  $A_2$ ,  $B_1$ ,  $B_2$  are the symmetry species. The  $A_2$  modes are inactive in IR for  $C_{2v}$  symmetry. However, since the symmetry is not strictly followed in this case, these modes may be active but with a weak intensity. Approximate normal modes for monosubstituted benzene are shown in Figure 3.1.

The  $CH_2$  modes of polystyrene monomer units have been assigned on the basis of IR studies on polyethylene [102]. The stretching mode of a lone CH group is generally too weak to be identified [96] and is not observed in polystyrene. The only other CH mode that might be expected is the CH bending- $\delta(CH)$ , which appears with reasonable intensity in the region of  $1250-1380\text{ cm}^{-1}$ . In polystyrene this mode may be contributing to the band at  $1376\text{ cm}^{-1}$ . However, such modes can mix with some of the ring vibrations, thus causing frequency shift and intensity changes.

The skeletal chain stretching mode of planar zig-zag carbon chain has been studied previously [103] and specific frequencies are predicted in the vicinity of  $1100$ ,  $400$  and  $200\text{ cm}^{-1}$ . In the present case the carbon chain is random and some of these frequencies may not be differ-

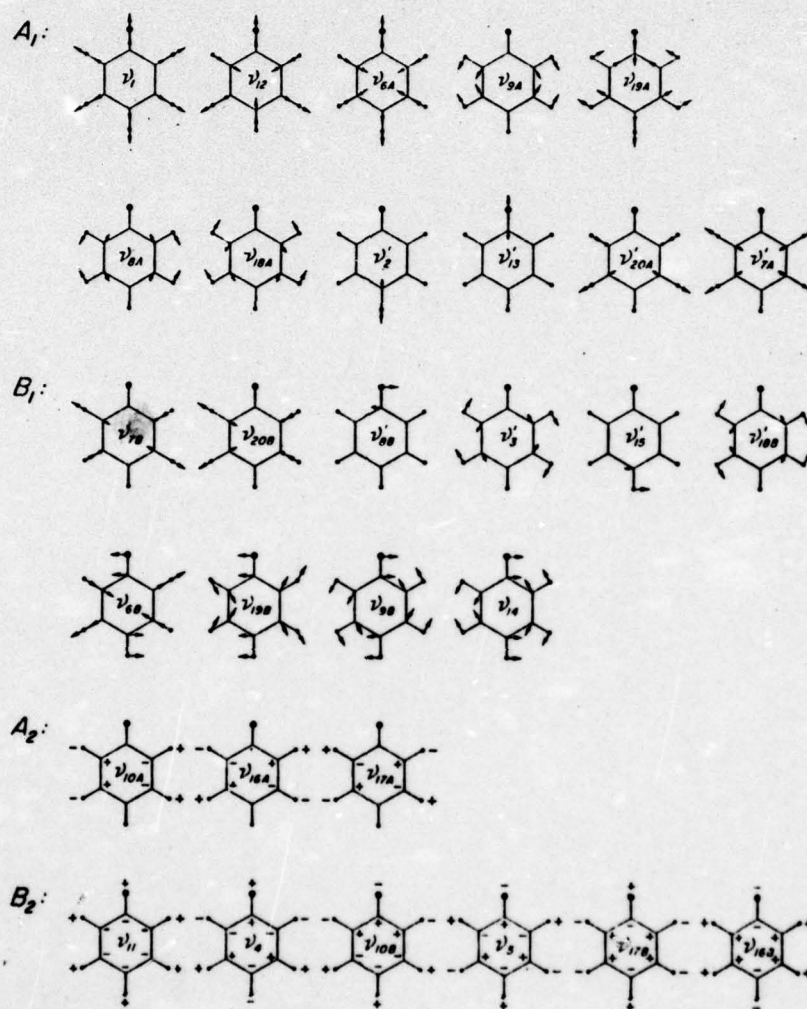


Figure 3.1 Approximate normal modes of monosubstituted benzene [96].



entiable. Such is the case in amorphous polyethylene where a band at  $1080\text{ cm}^{-1}$  is observed. On this basis Krimm [96] assigned a part of the medium intensity polystyrene band at  $1070\text{ cm}^{-1}$  to a skeletal chainstretching mode.

An IR spectrum of atactic polystyrene is shown in Figure 3.2. Complete vibrational assignments of these absorption bands are listed in Table 3.1 [96,104]. The IR spectrum of isotactic polystyrene differs only slightly from that of atactic polymer. Since these spectra may be needed as a reference while discussing the microstructure of atactic polystyrene, additional bands arising due to isotactic structure are also included in Table 3.1 in parenthesis. There are also some differences in the band intensities of two structures. Any increase or decrease in intensity of IR bands in the isotactic polymer is, therefore, indicated by (+) or (-), respectively. Along with these differences, Table 3.1 also shows the dichroism of bands in isotactic polystyrene.

Backing to some of these vibrational assignments is available in a recent study on calculations and assignments of IR bands, conducted by Russian researchers [101]. They employed models of polystyrene with 12 to 300 repeat units per polymer segment in helical and planar (syndiotactic) conformations. These frequencies for helical, planar and atactic conformations, along with their assignments, are listed in Table 3.2. Various notations used in this table are shown in Figure 3.3.

In addition to vibrational assignments, it is important to know the kind of sequences, viz., isotactic and syndiotactic, present in an atactic polystyrene chain. This could give us a better understanding

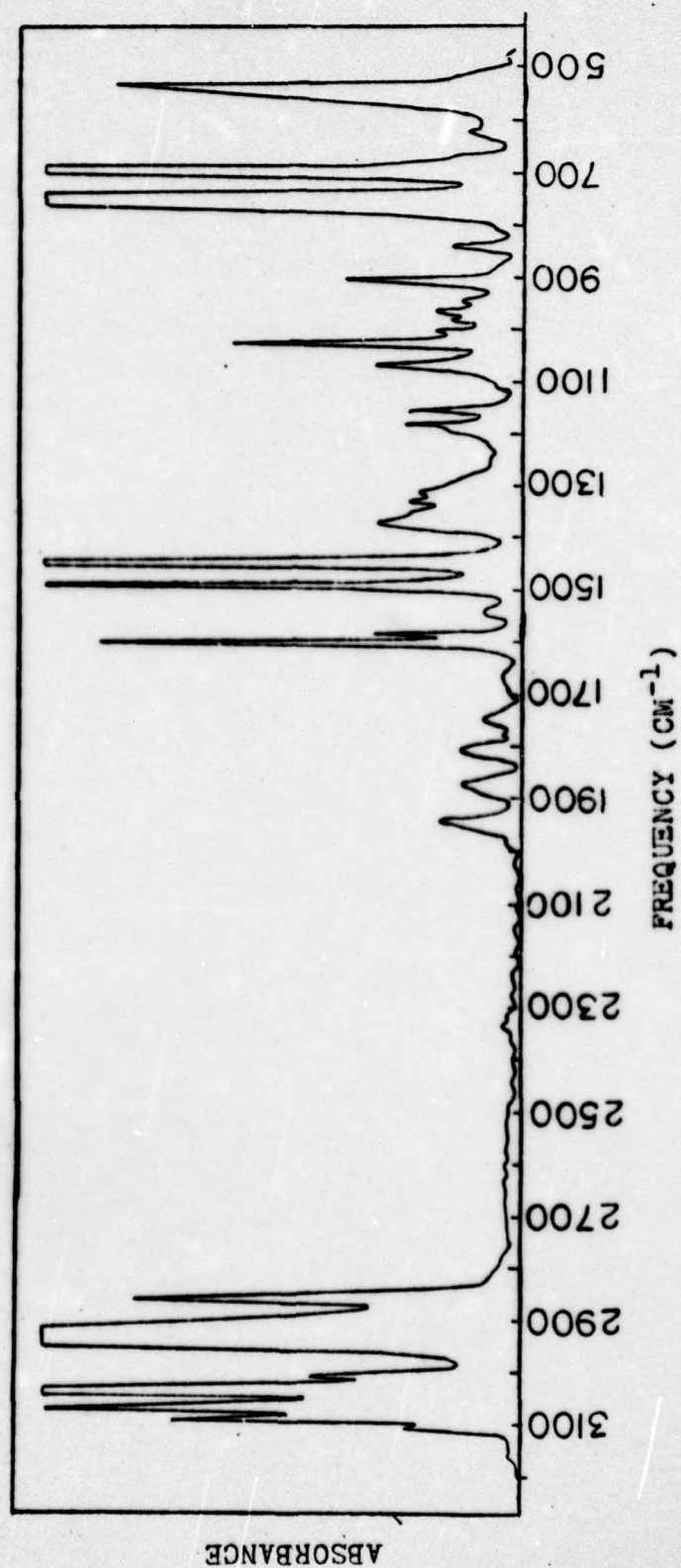


Figure 3.2 IR absorption spectrum of atactic polystyrene film obtained on FTIR spectrometer.



Table 3.1 Absorption Assignments for Polystyrene

Symbols used in this table and their meaning:

<u>Vibration modes</u>	<u>Symmetry species</u>	<u>Band Intensities</u>
$\nu$ - stretching	$A_1, B_1, A_2, B_2, \dots$	vs - very strong
$\delta$ - bending		m - medium
$\gamma_w$ - wagging		w - weak
$\gamma_t$ - twisting	<u>Polarization</u>	vvw - very very weak
$\gamma_r$ - rocking	$\pi$ - parallel	
	$\sigma$ - perpendicular	

Other symbols

- ( ) : new band appearing in spectrum of isotactic polystyrene
- (+), (-) : corresponding bands of atactic polystyrene which increase or decrease in intensity from the isotactic polymer. All other bands occur at common frequencies in both polymers.
- ? : indicates uncertainty in assignment, etc.

Combination bands are denoted by listing all constituents, e.g.,  $\nu_{10A} + \nu_{16B} = 978$ . The unprimed modes are benzene modes while the primed ones are derived from benzene

IR Absorption Band ( $\text{cm}^{-1}$ )	Relative Intensity	Polarization	Assignments of vibrational modes by Liang and Krimm's calculations (112)
216	w		$\nu_{16B}(B_2)$
325	vw		$\delta(\text{CCC})$
410	w		$\nu_{16A}(A_2)$
446	w		$\delta(\text{CCC})$
542	s		$\nu_4(B_2)$
(550)	s	$\sigma$	$\nu_4(B_2) - E ?$
(567)	s	$\pi$	$\nu_4(B_2) - A$
(589)	vw		
622	vw		$\nu_{6B}(B_1)$
670	vvw		

Table 3.1 (continued)

IR Absorption Band (cm <sup>-1</sup> )	Relative Intensity	Polarization	Assignments of vibrational modes by Liang and Krimm's calculations (112)
700	680	s	$\nu_{11}(B_2) - A$
	vs		$\nu_{11}(B_2)$
	689	s	$\nu_{11}(B_2) - E$
760	vs	$\pi$	$\nu_{10B}(B_2) - A$
	(787)	vvw	$\nu_{10B}(B_2) - E$
842	mw	$\sigma$	$\nu_{10A}(A_2)$
906	898	m	$\nu_{17B}(B_2) - A$
	m		$\nu_{17B}(B_2)$
	920	m	$\nu_{17}(B_2) - E$
945	(-)	vw	$\nu_4 + \nu_{16A} = 950 (B_1)$
965	w	$\sigma$	$\nu_{17A}(A_2)$
982	(+)	m	$\left\{ \begin{array}{l} \nu_5(B_2) \\ \nu_{10B} + \nu_{16B} = 978 (A_1) \end{array} \right.$
1005		vw	$\pi(?)$
1027	(+)	ms	$\nu_{18A}(A_1)$
1070	1048	m	$\nu(CC)_{\text{helix}} ?$
	1080	m	$\nu'_{18B}(B_1)$
1110	vvw	$\sigma$	$\nu_{11} + \nu_{16A} = 1110 (B_1)$
1154	mw	$\sigma$	$\nu'_{15}(B_1)$
1182	(+)	mw	$\nu(CC)_{\text{helix}} ?$
1195	vvw	?	$\nu_{8A}(A_1)$
1240	(+)	w	$\nu_{10A} + \nu_{16A} = 1247 (A_1)$



Table 3.1 (continued)

IR Absorption Band (cm <sup>-1</sup> )	Relative Intensity	Polarization	Assignments of vibrational modes by Liang and Krimm's calculations (112)
(1297)	m		$\gamma_t(\text{CH}_2)$ - A
1310	(-)	m	$\left\{ \begin{array}{l} \nu_{14}(\text{B}_1) \\ \gamma_t(\text{CH}_2) \end{array} \right.$
(1314)	ms	$\sigma$	$\gamma_t(\text{CH}_2)$ - E
1328	(+)	ms	$\nu'_3(\text{B}_1)$
(1364)	s	$\sigma$	$\delta(\text{CH})$
1376	(-)		$\delta(\text{CH})$
(1390)	vw	$\sigma$	$\nu_5 + \nu_{16A} = 1392 (\text{B}_1)$
(1440)	mw	$\sigma$	$\delta(\text{CH}_2)$
1450	vs	$\sigma$	$\left\{ \begin{array}{l} \nu_{19B}(\text{B}_1) \\ \nu_{11} + \nu_{10B} = 1460 (\text{A}_1); \\ \nu_4 + \nu_{17B} = 1446 (\text{A}_1) \end{array} \right.$
1493	vs	$\sigma$	$\nu_{19A}(\text{A}_1)$
1543	w	$\sigma$	$\nu_{11} + \nu_{10A} = 1542 (\text{B}_1)$
1585	(+)	m	$\nu_{9A}(\text{A}_1)$
1602	s	$\sigma$	$\nu_{9B}(\text{B}_1)$
1675	w	$\sigma$	$\nu_{10B} + \nu_{17B} = 1668 (\text{A}_1)$
1745	mw	$\sigma$	$\nu_{10A} + \nu_{17B} = 1749 (\text{B}_1)$
1800	mw	$\sigma$	$\nu_{10A} + \nu_{17A} = 1807 (\text{A}_1)$
1875	mw	$\sigma$	$\nu_{17B} + \nu_5 = 1889 (\text{A}_1)$
1945	mw	$\sigma$	$\nu_{17A} + \nu_5 = 1947 (\text{B}_1)$
2851	ms	$\pi?$	$\nu_s(\text{CH}_2)$
2923	vs	$\sigma$	$\nu_a(\text{CH}_2)$

Table 3.1 (continued)

IR Absorption Band (cm <sup>-1</sup> )	Relative Intensity	Polarization	Assignments of vibrational modes by Liang and Krimm's calculations (112)
3029	s	$\sigma$	$\nu'_2(A_1)$
3061	ms	$\sigma$	$\nu'_{20A}(A_1)$
3083	w		$\nu_{20B}(B_1)$



Table 3.2 Vibrational Frequencies and their Assignments for Helical (Isotactic) and Planar (Syndiotactic) Sequences Along with Experimentally Observed IR Bands in Atactic Polystyrene (116)

Theoretical Calculations for		Experimentally Observed Bands in Atactic Structure (cm <sup>-1</sup> )	Assignments*
Helical Structure (cm <sup>-1</sup> )	Planar Structure (Syndiotactic) (cm <sup>-1</sup> )		
1615	1613	1602	$\nu_{CC} + \delta_{CCH} (ar)$
1577	1577	1585	$\nu_{CC} + \delta_{CCH}$
1493	1487	1493	$\nu_{CC} + \delta_{CCH}$
1472	1465	1450	$\nu_{C-C_{ar}} + \delta_{CCH} (par)$
1444	1440		$\nu_{CC} + \nu_{C-C_{ar}} + \delta_{CCH} (ar) + \delta_{CCH} (par)$
1373	1375	1376	$\nu_{C-C} + \delta_{CCH} (par)$
1363	1362		$\nu_{CC} + \delta_{CCH} (ar)$
1318	1317	1328	$\nu_{CC} + \nu_{C-C} + \delta_{CCH} (ar) + \delta_{CCH} (par)$
1309	1309	1310	$\delta_{CCH} (ar) + \delta_{CCC} (ar) + \delta_{CCH} (par) + \delta_{CCC} (par)$
1241	1218	1240	$\nu_{C-C_{ar}} + \delta_{CCH} (par)$
1197	1211	1195	
		1180	$\nu_{C-C_{ar}} + \nu_{C-C} + \delta_{CCH} (ar) + \delta_{CCH} (par)$
1150	1149	1154	$\delta_{CCH} (ar)$
1118	1127		$\nu_{C-C} + \delta_{CCH} (par)$

AD-A035 374

UTAH UNIV SALT LAKE CITY DEPT OF MATERIALS SCIENCE --ETC F/G 7/3  
MOLECULAR BEHAVIOR STUDIES OF GLASSY POLYMERS UNDER STRESS.(U)  
NOV 76 W O STATTON

AF-AFOSR-2827-75

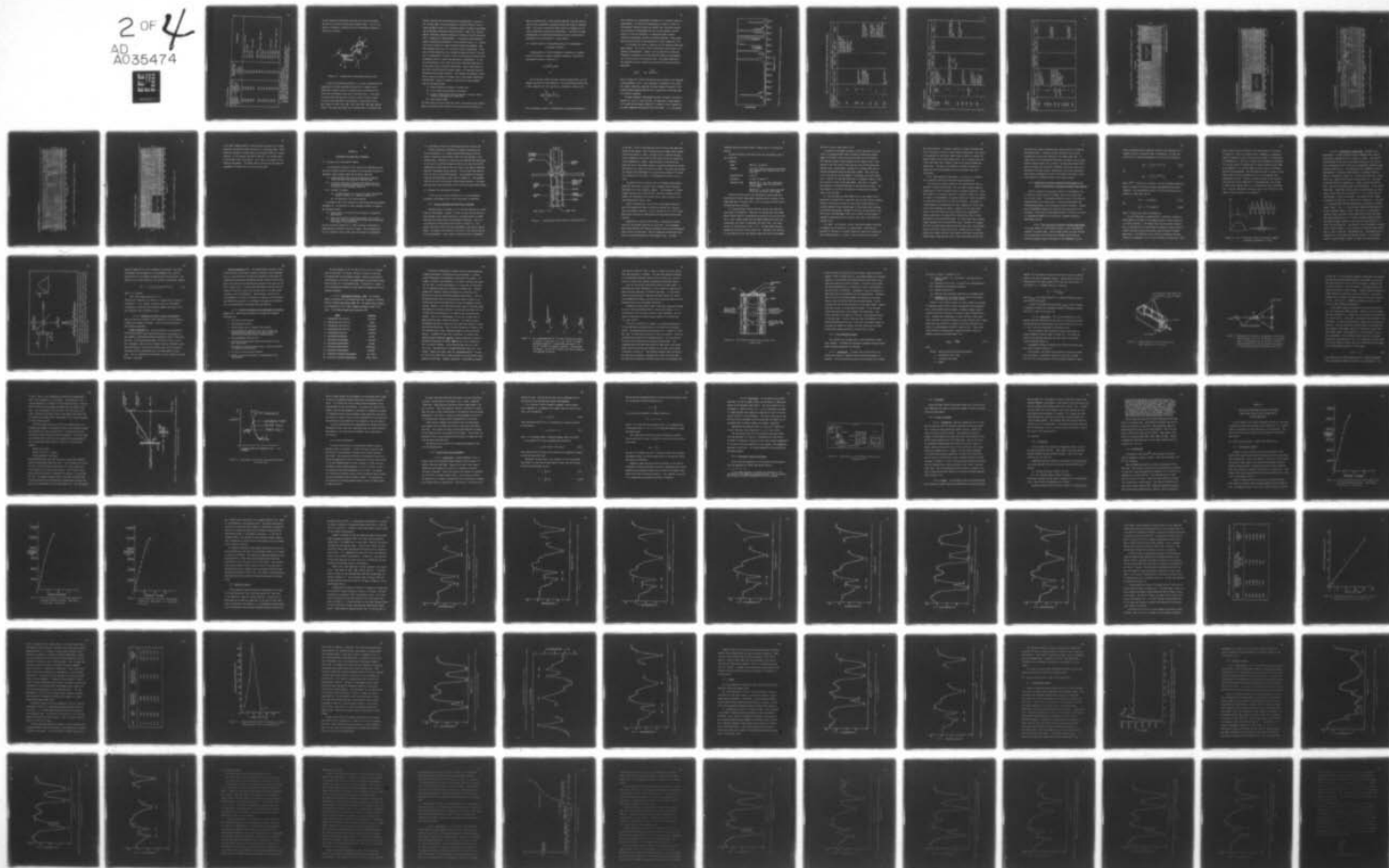
UNCLASSIFIED

UTEC-76-274

AFOSR-TR-77-0047

NL

2 OF 4  
AD  
A035474





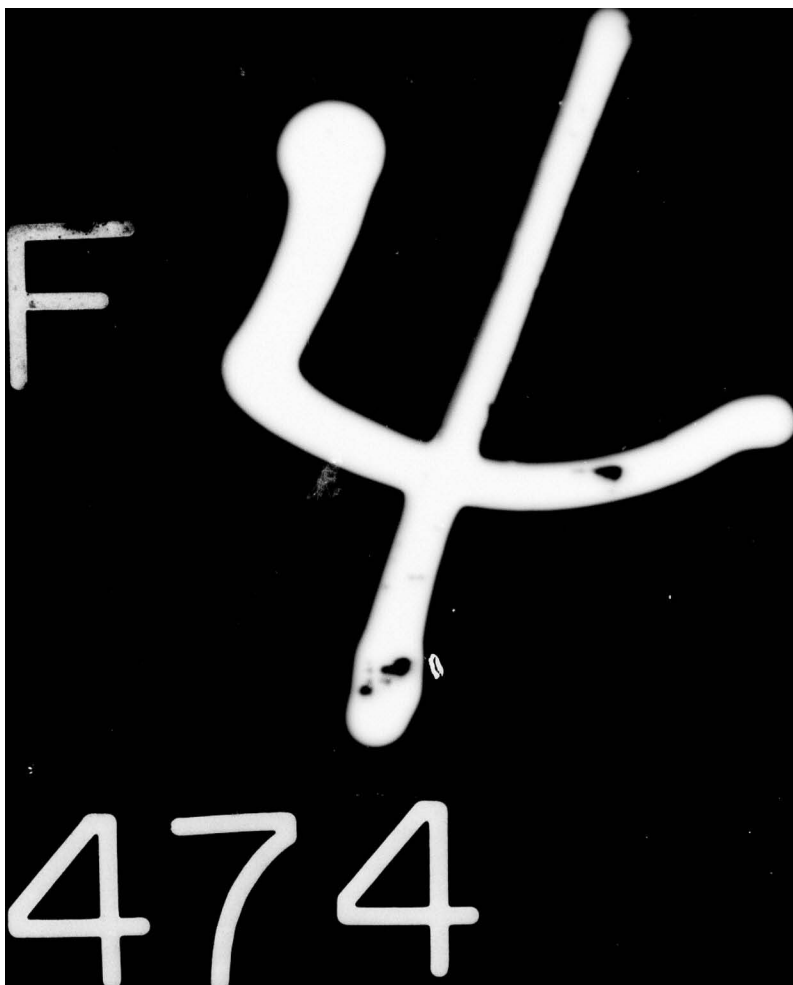


Table 3.2 (continued)

Theoretical Calculations for		Experimentally Observed Bands in Atactic Structure (cm <sup>-1</sup> )	Assignments*
Helical (Isotactic) Structure (cm <sup>-1</sup> )	Planar (Syndiotactic) Structure (cm <sup>-1</sup> )		
1099	1100	1110	$\nu_{CC} + \delta CCH (ar) + \delta CCC (ar)$
1063	1070	1070	$\nu_{CC} + \delta CCH (par)$
1048	1048	1027	$\delta CCH (ar)$
1024	1030	1005	$\delta CCH (ar) + \delta CCH (par)$
950	972	980	
		945	$\delta CCH (par)$
862	872	842	$\nu C-C_{ar} + \delta CCH (ar) + \delta CCH (par)$
703	677	670	$\delta CCH (par)$
630	632	622	$\delta CCC (ar)$
523	524	540	$\delta CCC (ar)$
421	402	410	$\delta CCH (par) + \delta CCC (ar)$
358	329	325	$\delta CCH (par)$
243	242	216	$\delta CCH (par) + \delta CCC (par) + \delta CCC (ar)$
	184	196	$\delta CCH (par)$

\* $\nu$  denotes the stretching vibrations.

$\delta$  denotes the bending vibrational modes.

par refers to the paraffin (chain) of the polystyrene repeat unit.

ar refers to the aromatic group on the polystyrene repeat unit.

Various angles used in assignments have been described in Figure 4.3.



of the interchain-interactions that might exist and the way these may affect the stress-distribution on polymer chains. It will also enable us to monitor configurational and conformational changes on application of stress.

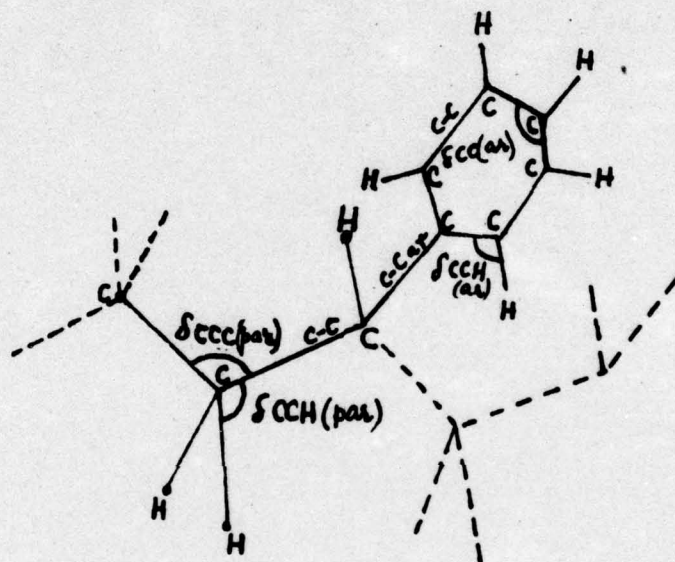


Figure 3.3 A repeat unit of polystyrene molecule [101]

Isotactic polystyrene crystallizes in a helical conformation with trans-gauche alternate conformation along the C-C backbone chain. Syndiotactic sequence exists in a planar zig-zag conformation with trans-trans conformation along the C-C backbone chain. It has been shown [105,106] that there are certain IR bands sensitive to these (isotactic and syndiotactic) conformations of polystyrene chains. The IR bands at 1364, 1312, 1261, 1194, 1084, 1053, 920, 898, 783 and 758  $\text{cm}^{-1}$  have been shown [105] to be characteristic of isotactic (TG)

helical structure and are associated with intramolecular interaction. All of these bands, with the exception of 1261 and 1194  $\text{cm}^{-1}$ , are already included in Table 3.1 as absorption bands of isotactic polystyrene. Out of the above listed helix bands the bands at 1364, 1312, 1194 and 898  $\text{cm}^{-1}$  have been related to sequences of helices within the same chain [107]. Takeda et al. [106] obtained IR spectra of three different types of crystalline polystyrenes in four different forms, i.e., crystalline solid, solution (in carbon disulfide) molten and quenched. They then compared these with an IR spectrum of atactic polystyrene. On the basis of these comparisons they assigned the bands at 1070  $\text{cm}^{-1}$  and 543  $\text{cm}^{-1}$  to characteristic vibration of the C-C chain which has mainly trans conformation along C-C chain from syndiotactic configuration. It has also been observed in this study that certain absorption bands persist in the molten state of isotactic polystyrene. Some of these bands, in particular the helix-sensitive bands, appear in IR spectrum of atactic polystyrene with reduced intensity. This suggests the presence of small helical sections of about six monomer units in the atactic polystyrene [104,105,107]. Besides IR evidence, information has been gathered from the following sources:

- (a) general structural features of polymer chain
- (b) X-ray scattering from atactic polystyrene
- (c) change of many dilute solution properties of atactic and/or isotactic polystyrene with temperature
- (d) high resolution NMR.

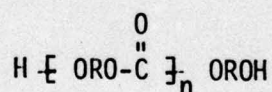
All these lead to the conclusion that atactic polystyrene chains contain short, less perfect (than isotactic polystyrene) helical sections of



about six monomer units. High resolution NMR data indicates the presence of short syndiotactic sequences besides the isotactic sequences [107]. Thus atactic polystyrene chains consist of sequences of isotactic, syndiotactic and atactic conformations. The effect of these conformations on interchain-interactions and stress distribution in polystyrene will be discussed in a later chapter.

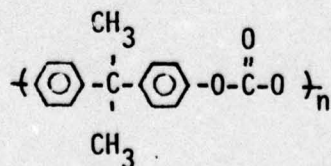
### 3.2 Infrared Spectra of Polycarbonate (poly-4,4' dioxydiphenyl-2,2 propane carbonate)

Polycarbonates are linear thermoplastic polyesters of carbonic acid with aliphatic or aromatic dihydroxy compounds. These may be represented by general structure (I).



(I)

By far the best studied and most versatile polycarbonates are the aromatic type derived from bisphenol A. The polycarbonate polymer used in this research is of this type and its structure is shown as (II).

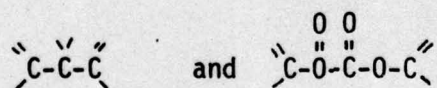


(II)

This polycarbonate (poly-4,4' dioxydiphenyl-2,2 propane carbonate) is

also referred to as polycarbonate (bisphenol A) or hereafter simply as polycarbonate. IR spectrum of polycarbonate is shown in Figure 3.4. An extensive literature survey has revealed that vibrational analysis of IR spectrum of polycarbonate has not yet been studied in detail. Table 3.3 lists the frequencies of absorption bands and their vibrational assignments available at present [108,109]. These assignments are mostly based on the characteristic group frequencies in IR.

It is evident from Table 3.3 that not all the absorption bands have been assigned. This is due to lack of theoretical calculations of IR spectra of polycarbonate. Though it will be beneficial to know the vibrational assignments of all the absorption bands of polycarbonate, it is not so crucial to the present study. The valence bonds which are expected to be most affected by the external stress are the backbone bonds



The C-C stretch for  $\text{C}-\text{C}-\text{C}$  bond had not been assigned to any frequency in polycarbonate, so far. This assignment is important in this study. This author, therefore, undertook its study through IR spectra of four different model compounds and was able to assign this vibrational mode to a definite frequency.

The model compounds investigated and their IR spectra are shown in Figures 3.5, 3.6, 3.7, and 3.8 [110]. On comparison of these spectra, it is found that the band at  $1080 \text{ cm}^{-1}$  is present in the IR spectra of all model compounds containing  $\text{C}-\text{C}-\text{C}$  valence bonds. It is not present



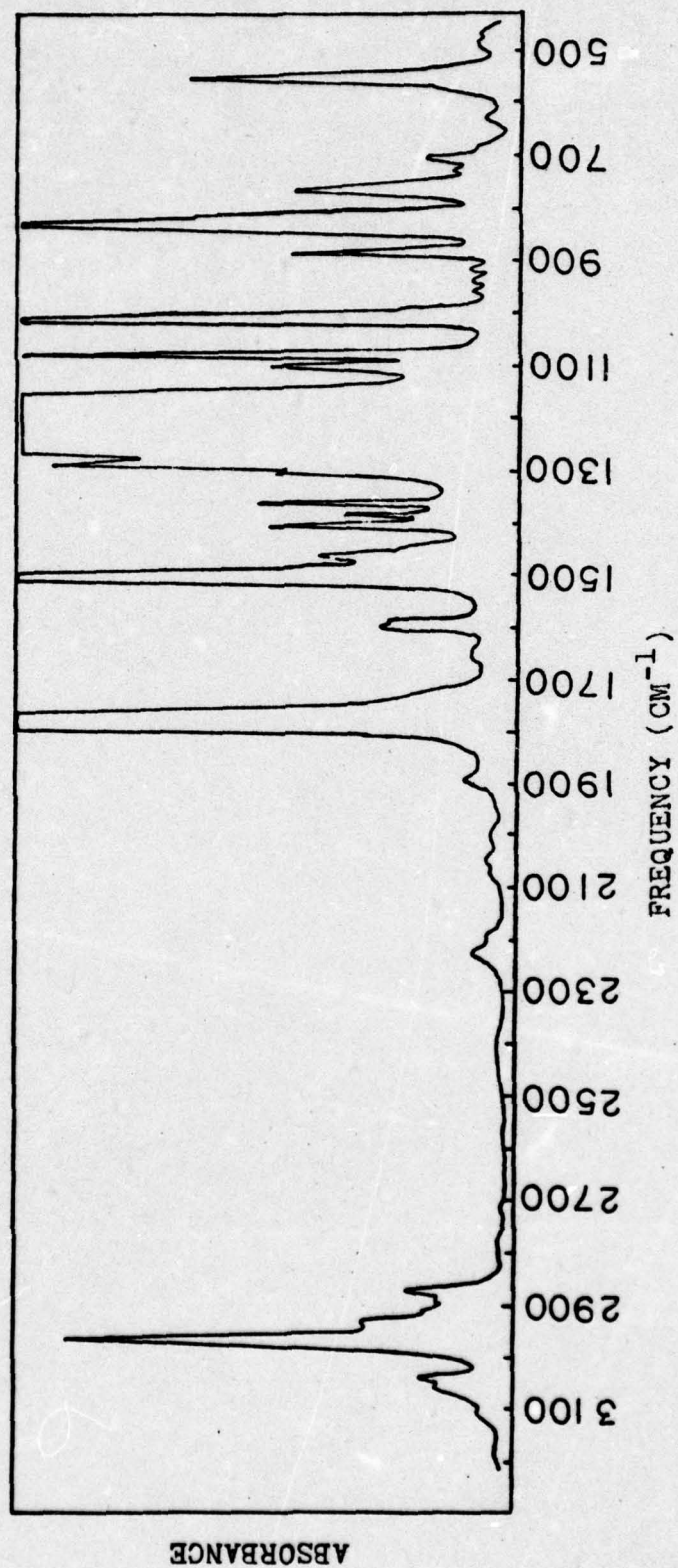


Figure 3.4 IR spectrum of polycarbonate (bisphenol A) film obtained on FTIR spectrometer.

Table 3.3 Infrared Absorption Band Frequencies and Their Assignments

IR Absorption Band Frequency ( $\text{cm}^{-1}$ )	Intensity	Assignments Due To		
		Schnell (123)	Brügel (124)	Hummel (85) Others
555	s			
629	wv			Out of plane bending vibration of p-disubstituted benzene ring
706	wv			Deformation vibration of -O-C-O- group
768	m	Non-coordinated bands		" O
828	vs	Out of plane bending of H atoms of p-disubstituted benzene		
1012	s			B <sub>1</sub> species modes of the benzene ring (119)
1078	vs			A <sub>1</sub> species mode of the benzene ring (119)
1100	m	Non-coordinated band		Asymmetric C-C stretch of central C atom (present author)



Table 3.3 (continued)

IR Absorption Band Frequency ( $\text{cm}^{-1}$ )	Intensity	Assignments Due To		
		Schnell (123)	Brügel (124)	Hummel (85)
$\left\{ \begin{array}{l} 1150 \\ \text{to} \\ 1268 \end{array} \right.$	Broad band	C-O valence vibration of the $\text{C-O-C-O-C}$ group		
			Characteristic of $\begin{array}{c} \text{CH}_3 \\   \\ -\text{C}-\text{CH}_3 \\   \\ \text{group} \end{array}$	
1288	s			
1362	m	Aliphatic CH valence vibration		In-phase symmetrical methyl bending mode
1384	w			Out of phase bending mode
1408	m	Non-coordinated band		
1464	w (shoulder)			
1502	vs	C=C skeletal in plane ring vibrations		
1590	w	Skeletal in plane ring vibrations		

Table 3.3 (continued)

IR Absorption Band Freq- cy (cm <sup>-1</sup> )	Intensity	Assignments		
		Schnell (123)	Brügel (124)	Due To Hummel (85)
1600	w	C=C skeletal in plane ring vi- bration		
1895	vW	The configuration at the central C- atom of the 4,4'- dihydroxyl-diphen- yl alkales has its effect in this range		CH <sub>3</sub> symmetric stretch (84)
2226	wV			
2872	w			
2890	vW (shoulder)			
2910	vW (shoulder)			
2932	w			
2968	s			
3038	w			
3054	vW			CH <sub>3</sub> asymmetric stretch (84)



4,4'-ISOPROPYLIDENEDIPHENOL

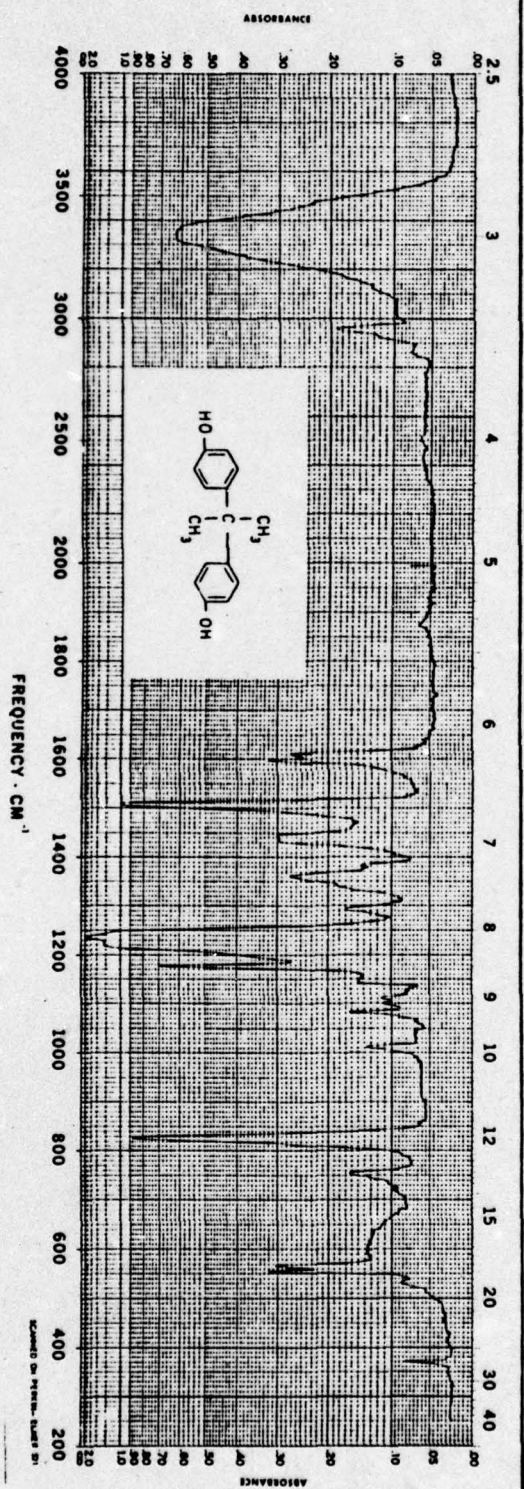


Figure 3.5 IR spectrum of model compound--4,4'-isopropylidenediphenol.

4,4'-ISOPROPYLIDENEDIPHENOL

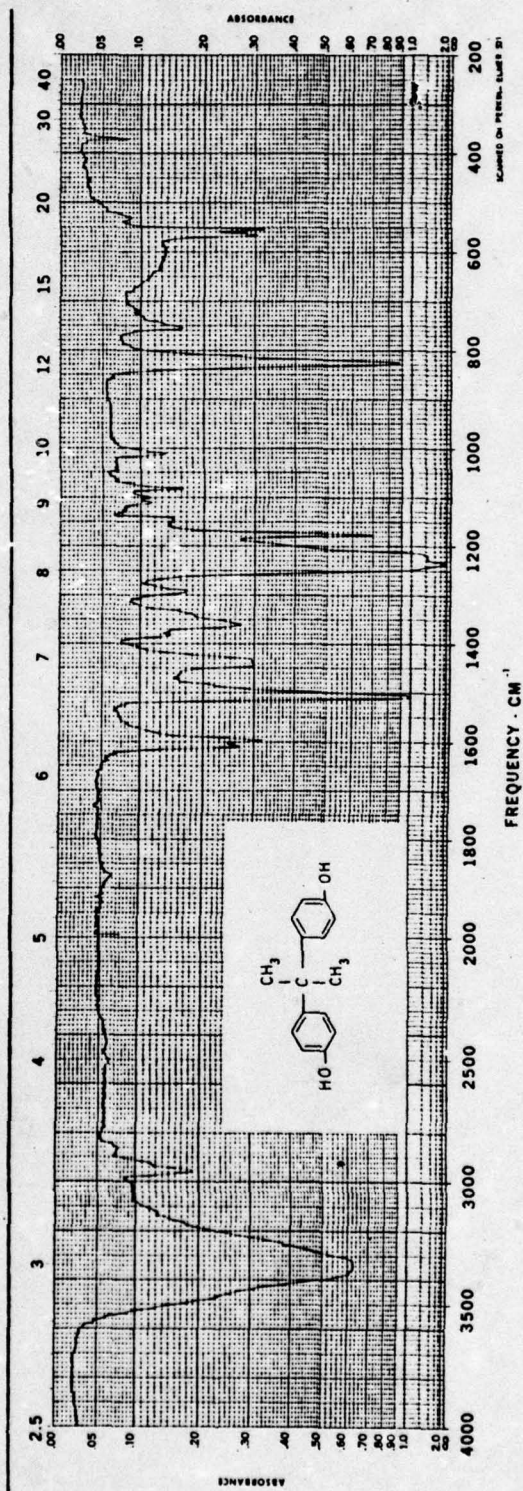


Figure 3.5 IR spectrum of model compound--4,4'-isopropylidenediphenol.



## 2,2-DI-p-TOLYLPROPANE

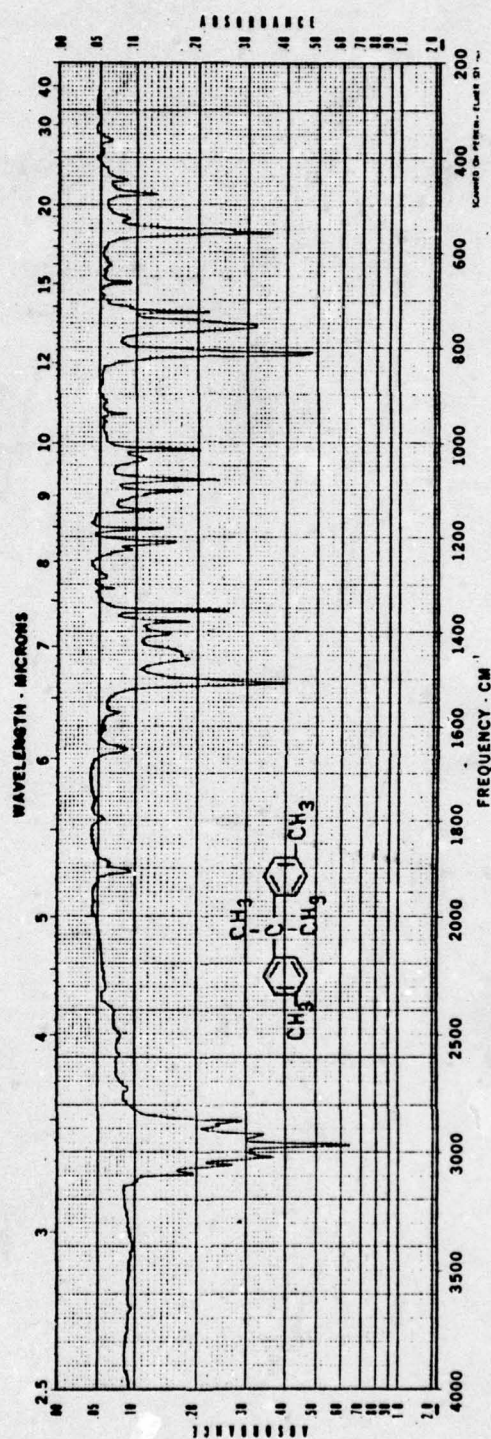


Figure 3.6 IR spectrum of model compound--2,2-Di-p-Tolylpropane.

2,2-DIPHENYL-1,3-PROPANEDIOL

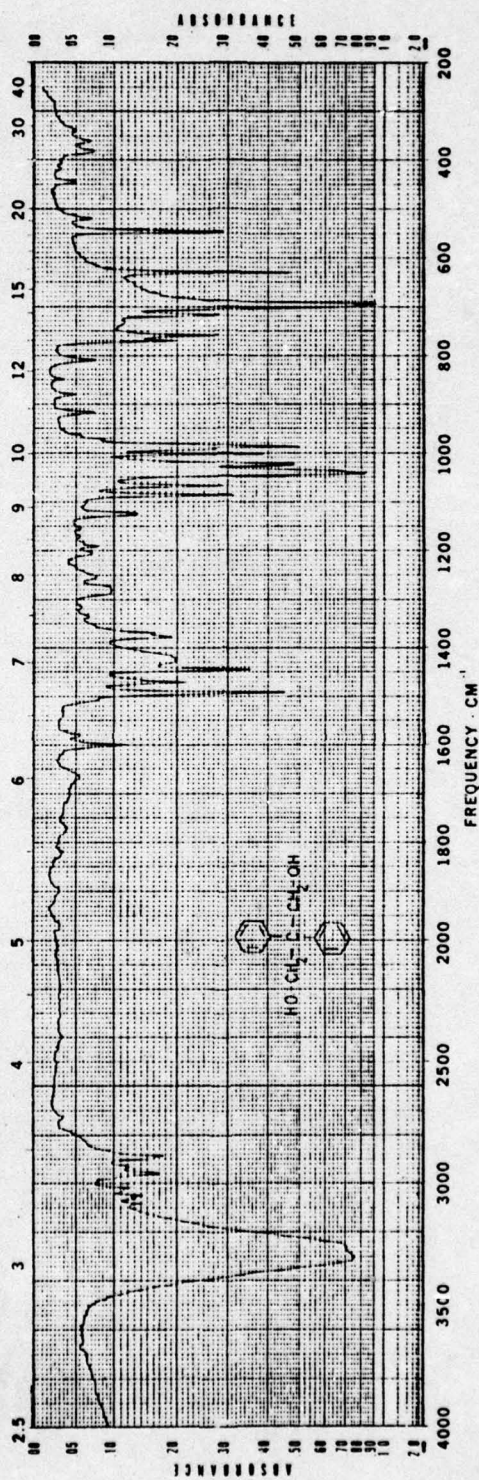


Figure 3.7 IR spectrum of model compound--2,2-Diphenyl-1,3-Propanediol.



CARBONIC ACID, DI-m-TOLYL ESTER

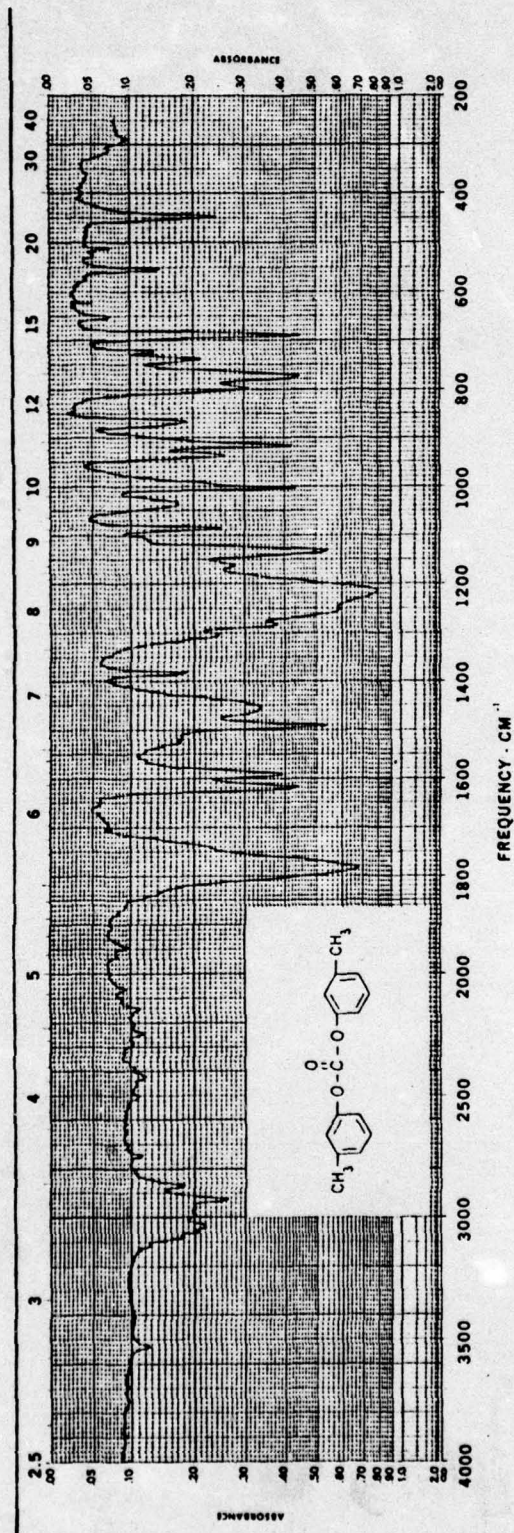


Figure 3.8 IR spectrum of model compound--carbonic acid.

in the model compound shown in Figure 3.8 which contains -O-C-O- bond. Therefore, the author assigns this band to C-C stretching mode. Krimm [104] has assigned C-C stretch mode to an IR band at  $1078\text{ cm}^{-1}$  in polyethylene. He also assigns the band at  $1080\text{ cm}^{-1}$  to  $B_1$  species modes of the benzene ring in polystyrene. Thus, there is an anomaly in his [104] own assignments. The author tends to believe that the  $1078\text{ cm}^{-1}$  assignment is actually due to chain stretching mode.



## CHAPTER IV

### EXPERIMENTAL AND ANALYTICAL TECHNIQUES

#### 4.1 Introduction to Experimental Program

The experimental program for this research was undertaken to examine and ultimately explain the molecular level processes occurring in amorphous, glassy polymers under the following conditions:

- (i) loading polymer films to varying load levels--starting from a zero level and going up to fracture load.
- (ii) cyclically fatiguing (in tension) film samples and thus simulating the repeated load-unload situations that occur in practical use of polymeric materials.
- (iii) crazing film samples
  - (a) by loading these to a critical load level and applying organic solvents, viz., methanol, ethanol, etc.
  - (b) by fatiguing in the Instron machine.

The polymers used in this research are polystyrene and polycarbonate (bisphenol A). The selection of these amorphous polymers is based on two important factors:

- (i) These polymers are versatile and of practical engineering applications.
- (ii) They are of chemically different structure, (viz., with bulky side groups on polymer chains on one hand and non-bulky side groups on the other hand).

This was especially planned so, in order to create a broad base in understanding the molecular behavior in depth. These polymers were, in turn, studied in their various types and states of orientations,

i.e., unoriented, uniaxially oriented and biaxially oriented, etc.

Besides conventional techniques of polymer characterization, two new techniques, i.e., Dynamic Infrared Spectroscopy (DIR) and Fourier Transform IR spectroscopy (FTIR) have been employed in the present study. Although our laboratories have employed DIR extensively in the case of crystalline polymers [32,50,51,77], both DIR and FTIR techniques are being used for the first time in the study of molecular behavior of amorphous, glassy polymers. FTIR has never been used before, not even on crystalline polymers. The application of DIR technique has been explained at some length in Chapter II. The equipment used for this will be described in the following sections. The equipment and experimental techniques used in FTIR are being discussed below.

#### 4.2 Equipment and Experimental Techniques

In this section a brief introduction of all the experimental techniques and equipment used in these experiments is described.

##### 4.2.1 Infrared equipment and experimental techniques

Infrared spectra of polymers in film form were obtained on a Perkin Elmer 521 spectrometer. However, in order to obtain the IR spectra of these polymers under loaded condition, a stretching device is needed that does not interfere with the spectrometer operation. Such a device was built by Wool [50,77] and is shown in Figure 4.1. This entire unit runs on wheel and track arrangement, supported by a gantry frame. The design of this device is such that it can slide in and out of the spectrometer's cavity without interfering with its operation



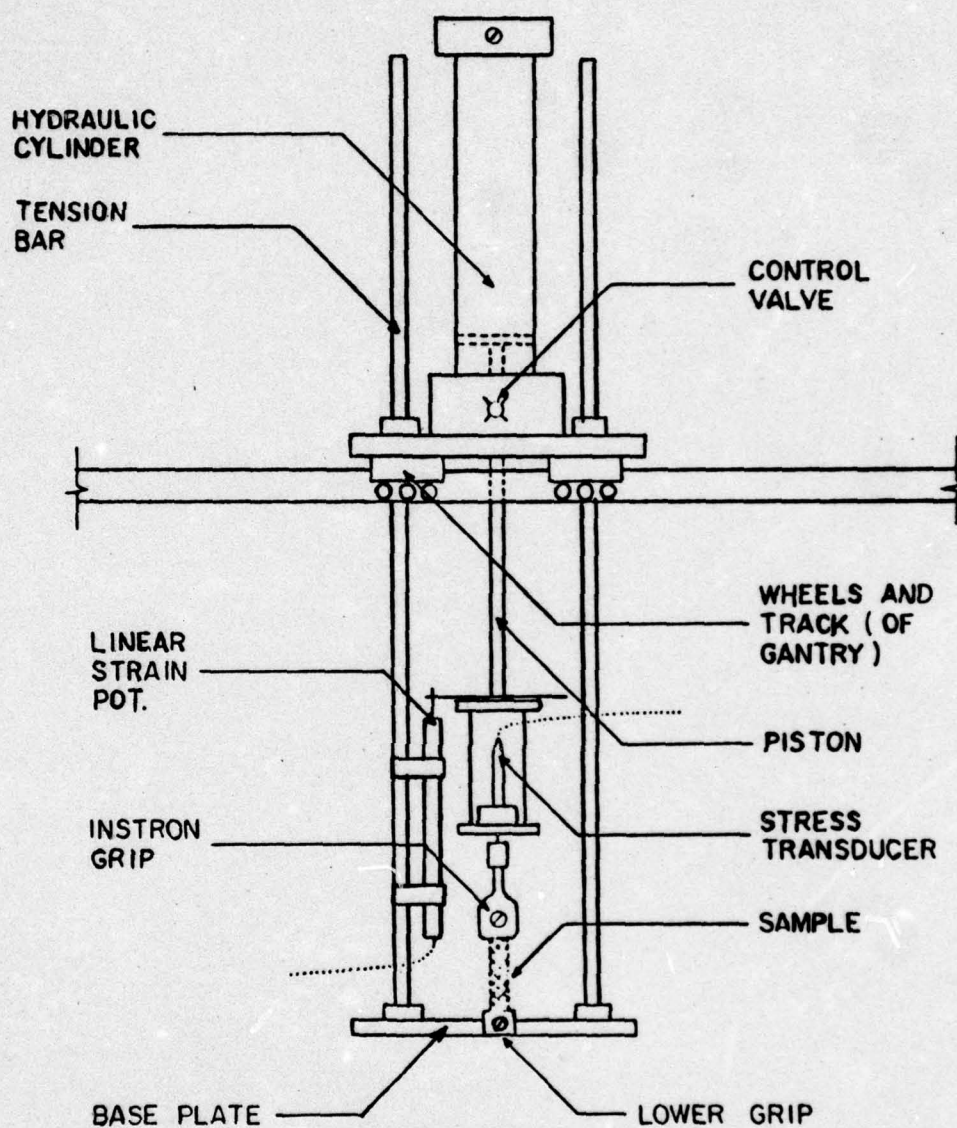


Figure 4.1 Loading system used in dynamic infrared tests [77]

in any way. It has a fixed lower grip and an Instron type upper grip which can move upward. Both of these grips have rubber-lined surfaces in which the sample is fixed. The upper grip is connected through a stress transducer to the piston of the cylinder which has connections to the compressed air supply. Upward movement of the piston and, hence the load on the polymer sample, is controlled manually by varying the amount of air supply let into the cylinder. The piston and cylinder are Schrader model 30003-0080 with a maximum displacement of 12 inches and a diameter of 3.25 inches. Its performance efficiency is 8 to 1 ratio.

The applied force is directly read on a Stratham Analog Readout, Model UR5, which gets its signal from a Stratham Stress Transducer, Gold Model UC-3, with a 1000 lbs. adapter. The transducer is located between the upper grip and the piston. Both the transducer and the readout are calibrated on the Instron tensile tester to give a full-scale deflection of 100 lb. load.

Strain is measured by a linear strain potentiometer mounted on one of the support bars with its slide rod attached to a cross-bar atop the transducer mounting. It has a sensitivity of  $1 \times 10^{-3}$  inches. Both stress and strain are monitored on an Omniscribe flat-bed chart recorder.

Compressed air supply to the cylinder is regulated by a manual control of the bleeder valve with an on-off tap. This arrangement facilitates constant load (creep) or constant strain (stress-relaxation) tests, as well as ramp input. Rate of loading can be made nearly uniform by a careful manipulation of the bleeder valve. For tests



conducted during the present study a loading rate of 10 lbs/min was applied.

The specifications of the Perkin Elmer 521 spectrometer used in this study are:

Frequency

Range	4000 $\text{cm}^{-1}$ to 250 $\text{cm}^{-1}$
Accuracy	$\pm 0.5 \text{ cm}^{-1}$ (higher accuracies are possible with frequency scale expansion and a low scan rate)
Reproducibility	0.25 $\text{cm}^{-1}$
Resolution	0.3 $\text{cm}^{-1}$ at 1000 $\text{cm}^{-1}$
Scattered light	4000-500 $\text{cm}^{-1}$ : max 1/4% transmittance with an average value less than 0.1% T in this range. 500-200 $\text{cm}^{-1}$ : max 2% T with an average value less than 0.25% in this range.

Polarized infrared spectra were obtained by using an AgBr Wire Grid Polarizer (Perkin Elmer Number 186-0241) which is mounted in the common beam before entrance slits. This is the most efficient type of infrared polarizer available.

It is possible that infrared radiation can heat the sample and thus change its properties. Therefore, the temperature in the sample beam of Perkin Elmer 521 spectrometer was measured and found to be 30°. This is only slightly higher than the ambient temperature and it was assumed that such effect is negligible for short scans. The cross-section of infrared beam is 0.25" x 1.0". The gage length (distance between the grips) was fixed at about 2.0". Therefore, 0.5" wide and 4" long samples were cut from polymer sheets and firmly fixed between

the grips to give a gage length of 2.0".

A complete IR experiment consisted of first obtaining an IR spectrum of an unloaded polymer sample followed by loading the polymer sample to different loads and obtaining another set of IR spectra. The loads were roughly spaced between zero and fracture load. Fresh samples of the same material were used each time the IR spectrum was obtained from a loaded sample. Through this technique there were no previous deformation effects on the polymer sample. Thus, there was a set of IR spectra for each sample--in unstressed state and stressed state. However, to study the effect due to incremental loading, stress was increased in steps on the same sample. Here again, IR spectra were obtained in unstressed state and in varying stressed states. The main objective of obtaining the spectra in unstressed and stressed state is the following:

(i) The instrument may show slight shift in wave numbers due to operational irregularities or conditions from one time period to another. Therefore, one cannot rely upon the chart paper reading entirely to read wave numbers of the infrared bands of the polymer sample recorded at different time periods. Because, in this way, one may observe small shifts due to the instrument itself, the IR spectra of each sample is recorded in both unstressed and stressed state, which eliminates this possible error.

(ii) Beer's law expresses a direct relationship between absorption of radiation by the sample and its concentration. Therefore, any variation in thickness of a polymer sample will affect the intensity of the IR absorption band. In polymer films and sheets such variations



are usually present. In addition, variation in local orientation may also exist which can cause a slight change in band shape. As a result, an IR spectrum of a particular sample cannot be used as a control for another sample from the same polymer sheet. This is particularly true in our study where small changes in peak shifts and band shapes are sought after. Therefore, this method of recording IR spectra for unstressed and stressed polymers each time eliminates such small differences.

(iii) Superimposing of two spectra is a quick and a convenient way of measuring peak shifts and observing band distortions.

The stressing of polymer samples in our experiments was done by applying a constant load on them. This can cause a polymer sample to creep because of the viscoelastic nature of polymeric materials. Since the response of viscoelastic materials to external stimuli (viz., stress or strain) is time dependent, the polymer sample can "creep" concurrently during the IR scan, which can take 10-15 minutes. The amount of "creep" depends on the magnitude of stress, temperature, rate of loading and the morphology of a sample. Therefore, at low load levels, creep is not significant but as the fracture load is approached, it becomes significant. We cannot fully eliminate the effects of this phenomenon but can only minimize them. It is well known that a polymer creeps exponentially to an equilibrium value. Therefore, by allowing some time to elapse before recording the spectrum, major time dependent stresses can reach an equilibrium value. Certain scans of stressed samples were indeed carried out when samples had already crossed their rapid-response stage and were close to their equilibrium values, while

the others were actually obtained under creep situations to study the overstressed bonds. Creep was visually monitored from the chart, recording the stress-strain response of the sample under load. If creep effect is to be completely eliminated, one needs to use an instantaneous scanning system, such as Fourier Transform Spectrometer (FTS) which was indeed used for certain experiments during this study and is discussed in the next section. Nevertheless, the results obtained on Perkin Elmer spectrometer are valid and valuable to the study of molecular behavior in amorphous polymers under external stress.

#### 4.2.2 Applications of Fourier transform IR spectroscopy in the study of stressed bonds in amorphous polymers (under tension)

Fourier transform IR spectroscopy (FTIR) is a very powerful tool to study the infrared spectra of polymers under stress, where time is a critical factor. FTIR became available for use at this University toward the end of the present study. A great many experiments had already been performed on the conventional grating instrument. However, the few experiments conducted on FTIR have proven the worth of this instrument. Even visually unobservable changes of IR bands of stressed vs. unstressed polymers can be detected by a computer subtracted (difference) spectra.

##### 4.2.2.1 Basic principles of Fourier transform spectroscopy.

As the name implies, FT spectroscopy involves a special mathematical treatment of spectral data. Fourier series allows a periodic function to be represented as an infinite sum of harmonic oscillations at definite frequencies equal to multiples of the fundamental, so the



Fourier transform allows an aperiodic function to be expressed as an integral sum over a continuous range of frequencies. It turns out certain pairs of functions denoted by  $h(\nu)$  and  $g(\delta)$  are related as:

$$h(\nu) = \int_{-\infty}^{\infty} g(\delta) e^{i2\pi\nu\delta} d\delta \quad (4.1a)$$

and

$$g(\delta) = \int_{-\infty}^{\infty} h(\nu) e^{-i2\pi\nu\delta} d\nu \quad (4.1b)$$

where  $e^{+i2\pi\nu\delta} = \cos(2\pi\nu\delta) + i\sin(2\pi\nu\delta)$ . The use of complex expressions makes it convenient to carry out certain manipulations with Fourier integrals. The transformations given in (4.1a) and (4.1b) can be expressed in a functional form as:

$$h(\nu) = F(\nu, \delta)[g(\delta)] \quad (4.2a)$$

and

$$g(\delta) = F^{-1}(\delta, \nu)[h(\nu)] \quad (4.2b)$$

where  $F^{-1}$  denotes the inverse transformation.

It can be seen that in equation (4.2a)  $F$  transforms a function  $g$  which depends on variable  $\delta$  into another function  $h$ , which depends on a different variable  $\nu$ . This means that if we can perform a measurement to determine  $g(\delta)$  for some range of variable  $\delta$ , we may be able to recover  $h(\nu)$  more rapidly and accurately than we could by directly measuring it. The functions  $g$  and  $h$  which are related by the transformations of equations (4.1) or (4.2) are known as Fourier pairs. Two

sets of Fourier pairs of interest in FT spectroscopy are illustrated in Figure 4.2. The  $h(\nu)$  in Figure 4.2(a) represents a monochromatic signal of frequency  $\nu_0$  ( $\text{cm}^{-1}$ ) and its Fourier partner is a cosine wave of wavelength  $1/\nu_0$ . The  $h(\nu)$  in Figure 4.2(b) represents a polychromatic or white source of radiation and its Fourier partner can be viewed as the addition of an infinite number of cosine waves of a different amplitude and wavelengths. The transformation given in equation (4.1a) implies that all of the information in  $h(\nu)$  can be obtained from a determination of  $g(\delta)$ . However, the range of values of the variable  $\delta$  over which  $g(\delta)$  can be determined in a measurement has to be limited to some interval smaller than  $(-\infty \text{ to } \infty)$  specified by the  $\delta$  transformation. Thus the experimental limitation results in a truncation in the number of terms included in the integration.

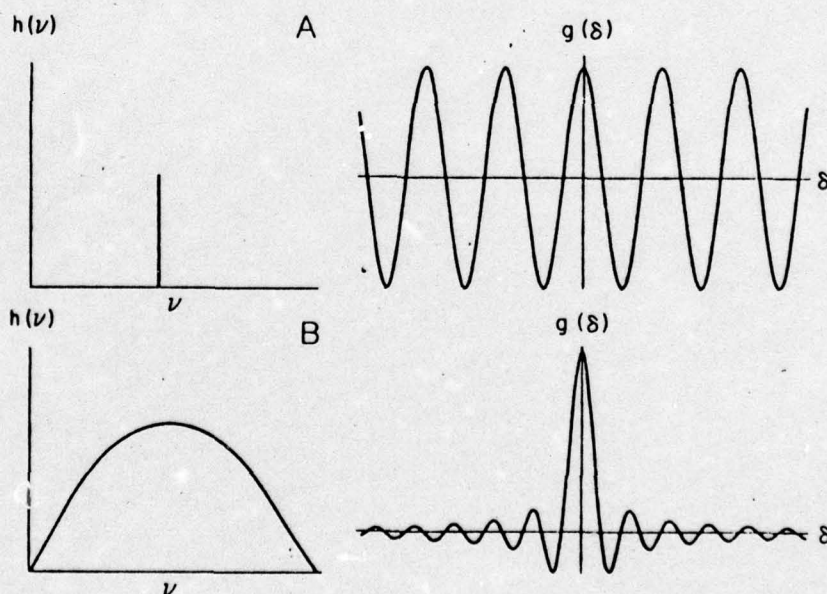


Figure 4.2 Pairs of functions related by the Fourier Integral Transforms in Equation 4.1 [111]



4.2.2.2 Interferometric spectroscopy. Basically, an FT spectrometer is a device having an optical component which, from an input source, produces  $g(\delta)$  over a range of  $\delta$  values. These results can be obtained in the form of transformed spectrum,  $h(\nu)$  by the use of its own computer which carries out the mathematical operation represented in equation (4.1). The principal optical component of an FTIR spectrometer is a Michelson interferometer, a schematic diagram of which is illustrated in Figure 4.3. Its three basic parts are a fixed mirror (A), a moving mirror (B) and a beam splitter (C). The center of the beam splitter is denoted by O. Figure 4.3 shows the optical path, a parallel light beam through the interferometer. If the initial length (OB) = length (OA), then the optical path difference,  $\delta$ , introduced by moving the mirror a distance L is  $\delta = 2L$ . If the input to interferometer is beam of wavelength  $\lambda$ , the output will be a signal illustrated in Figure 4.2a. If the mirror B is moved by  $L = \lambda/4$ , then  $\delta = \lambda/2$  and two beams interfere destructively, resulting in no output signal. When  $L = \lambda/2$ ,  $\delta = \lambda$  and two beams combine constructively at O to give a maximum intensity signal. When input is a polychromatic source of light, the output is more complicated and the input waves add constructively only at  $\delta = 0$  to give a maximum intensity signal. The input and output signals for this case are illustrated both in Figure 4.2b and Figure 4.3. The output of the interferometer is measured as a signal intensity, I, as a function of the optical path difference,  $\delta$ , and is called the interferogram  $I(\delta)$ . Interferogram  $I(\delta)$  is characteristic of the source and the beam splitter. If the output signal is passed through a sample, the sample will absorb certain

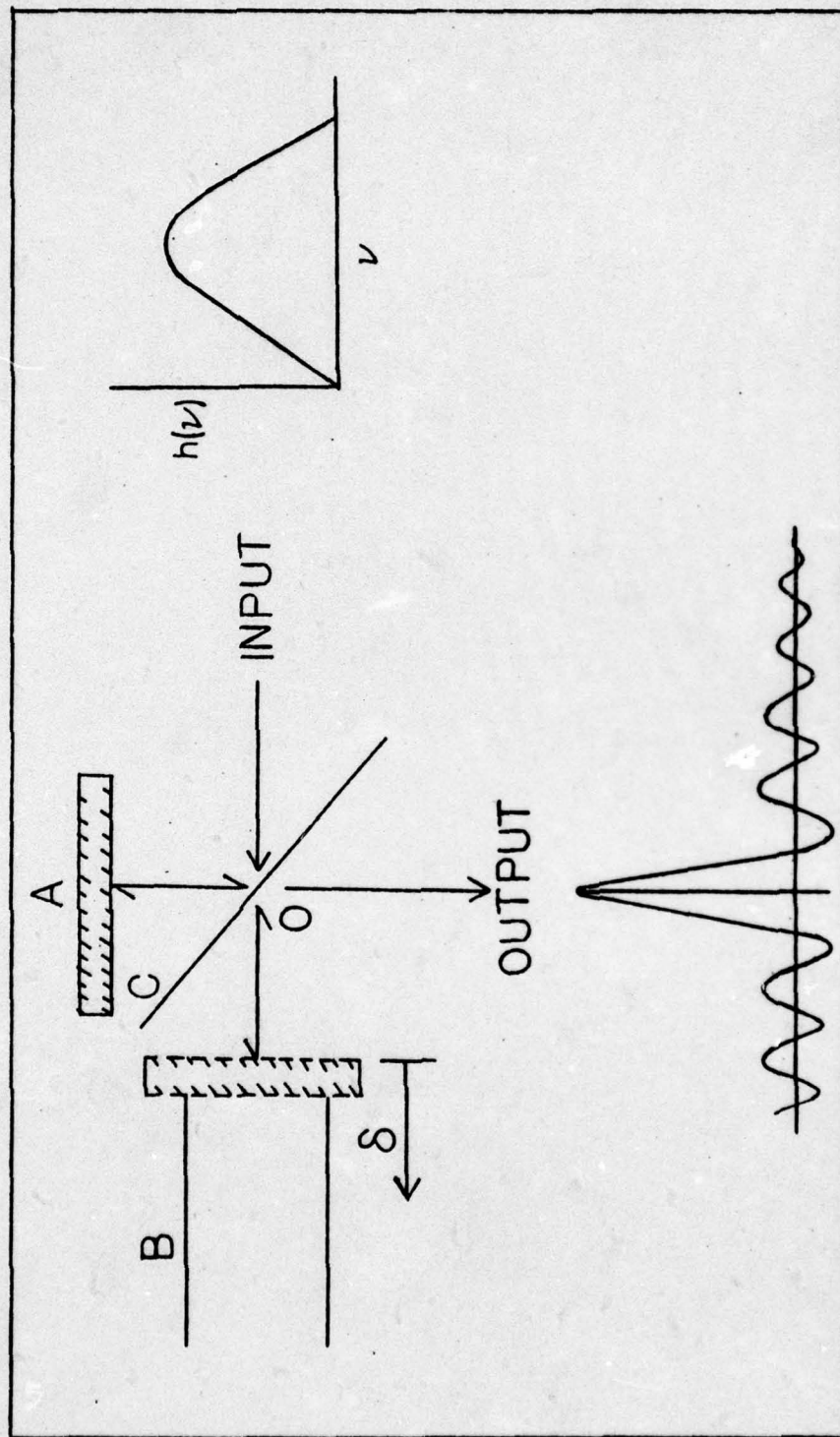


Figure 4.3 Schematic diagram of a Michelson interferometer showing the fixed mirror (A), the moving mirror (B) and beam splitter (C). The optical path is shown by the arrows. The interferogram output of the broad band input source is shown with a triangular apodization function [111]:



spectral components from  $I(\delta)$ , depending on its nature. The signal that emerges from the sample is an interferogram,  $\bar{I}(\delta)$ , which is characteristic of the sample, the beam splitter and the source. The spectrum  $S(\nu)$  is then related to  $I(\delta)$  by means of the Fourier integral

$$S(\nu) = C \int_{-\infty}^{\infty} [\bar{I}(\delta) \frac{1}{2} \bar{I}(0)] e^{i2\pi\nu\delta} d\delta \quad (4.3)$$

where  $C$  is a constant

$\bar{I}(0)$  is the signal intensity at  $\delta = 0$ .

Theoretically, equation (4.3) specifies a spectrum  $S(\nu)$  in which no information is lost, whereas in practice there are instrumental limitations to extend the path difference between the limits  $(-\infty, \infty)$  and, therefore, some information is lost.

#### 4.2.2.3 Advantages of Fourier transform spectrometer.

There are two major concepts of basic advantages in an FTS, known as Fellgett and Jacquinot advantages. These are briefly described in the following paragraphs.

Fellgett Advantage [112]. An interferometer receives information from an entire range of a given spectrum during each time element of a scan whereas a conventional grating spectrometer receives information from only a very narrow region which lies within the exit slit of the instrument. Thus, the interferometer receives information about the entire spectral range during an entire scan, while the grating instrument receives information only in a narrow band at a given time. This is a statement of the Fellgett, or also referred to as the multiplex, advantage.

Jacquiot Advantage [111]. The interferometer can have a large circular source at the input or entrance aperture of the instrument with no strong limitation on resolution, whereas the resolution of a conventional grating-type spectrometer depends linearly on the instrument's slit width and the detected power depends on the square of the area of equal slits. A grating-type spectrometer requires long and narrow slits which can never have the same area for the same resolving power as the interferometers. Quantitatively, the ability of interferometers to collect large amounts of energy at high resolution was expressed by Jacquiot as a throughput advantage of interferometers over spectrometers and thereby Jacquiot advantage.

4.2.2.4 Specific advantages and disadvantages of interferometers [111]. Additional advantages from Fellgett and Jacquiot advantages are:

1. Very large resolving power.
2. High wavenumber accuracy.
3. Vastly reduced stray or unwanted flux problems.
4. Fast scanning time (sometimes less than 1 second) and computer storage capability allows several spectra to be recorded at one time (almost instantaneously).
5. Large wavenumber range per scan.
6. Possibility of making weak-signal measurements at millimeter wavelengths.
7. Measurement in amplitude spectroscopy of complex reflection or transmission coefficients.
8. Low cost of basic optical equipment.
9. Smaller size and lower weight of interferometers than spectrometers.



Few disadvantages of FTS are that the basic cost of the equipment is quite high. At present, the cost is almost in the range of \$100,000 with its own computer system. Another disadvantage of interferometers is the error in transmittance or reflectance measurements of about 5% of the absolute value. If the error is random, it can be minimized by recording a large number of repeated spectra and computer-averaging.

4.2.2.5 Experimental technique: FTIR. The infrared spectra of polymers for the present study were recorded on a Digilab Fourier Transform Spectrometer Model 14B. The spectra were recorded at a resolution of  $2\text{ cm}^{-1}$  after computer-averaging a total of 20 scans. The following samples were studied on FTS:

<u>Sample</u>	<u>Condition</u>
1. Polystyrene film (TRICITE)	No stress
2. Polystyrene film (TRICITE)	Stress
3. Polystyrene film (TRICITE)	Unfatigued
4. Polystyrene film (TRICITE)	Fatigued
5. Unoriented polystyrene	Uncrazed
6. Unoriented polystyrene	Crazed
7. Unoriented polycarbonate	Uncrazed
8. Unoriented polycarbonate	Crazed
9. Unoriented polycarbonate	Unfatigued
10. Unoriented polycarbonate	Fatigued
11. Uniaxially oriented polycarbonate	No stress
12. Uniaxially oriented polycarbonate	Under stress

In addition to FTIR spectra recorded under the above conditions, "computer-subtracted" FTIR spectra were also obtained. In these a certain percentage of one spectrum is subtracted from another. For example, to monitor the differences in IR bands resulting from stressing the films, a certain percentage of an IR spectrum of unstressed film is subtracted from the IR spectrum of stressed film. The main purpose for choosing a certain percentage for subtraction is to minimize any intensity differences between the two spectra. This can be achieved rather easily by monitoring the spectra visually on an oscilloscope and then deciding upon the actual percentage to be subtracted. However, at the time of the present study oscilloscope attachments were not available; therefore, subtractions were made by trials in which varying percentages of one spectrum were subtracted from another. This, too, is advantageous to pick out any additional IR bands resulting from a subtraction process. For example, certain IR bands may decrease in intensity while others may increase in intensity during subtractions. Thus, the ones increasing in intensity can be associated with a larger remaining component in the subtraction spectra. In addition to such small differences in infrared bands caused by sample conditions, certain visually unobservable changes in absorption frequencies of various IR bands can also be detected by the "subtraction" spectra. Such differences may show up as band splittings. The advantages of computer-subtracted spectra are illustrated in Figure 4.4a, which shows the superimposed  $903\text{ cm}^{-1}$  IR band of TRICITE film under stress (shown by broken line) and without stress (shown by solid line). Computer subtracted: (stress-80% unstressed)



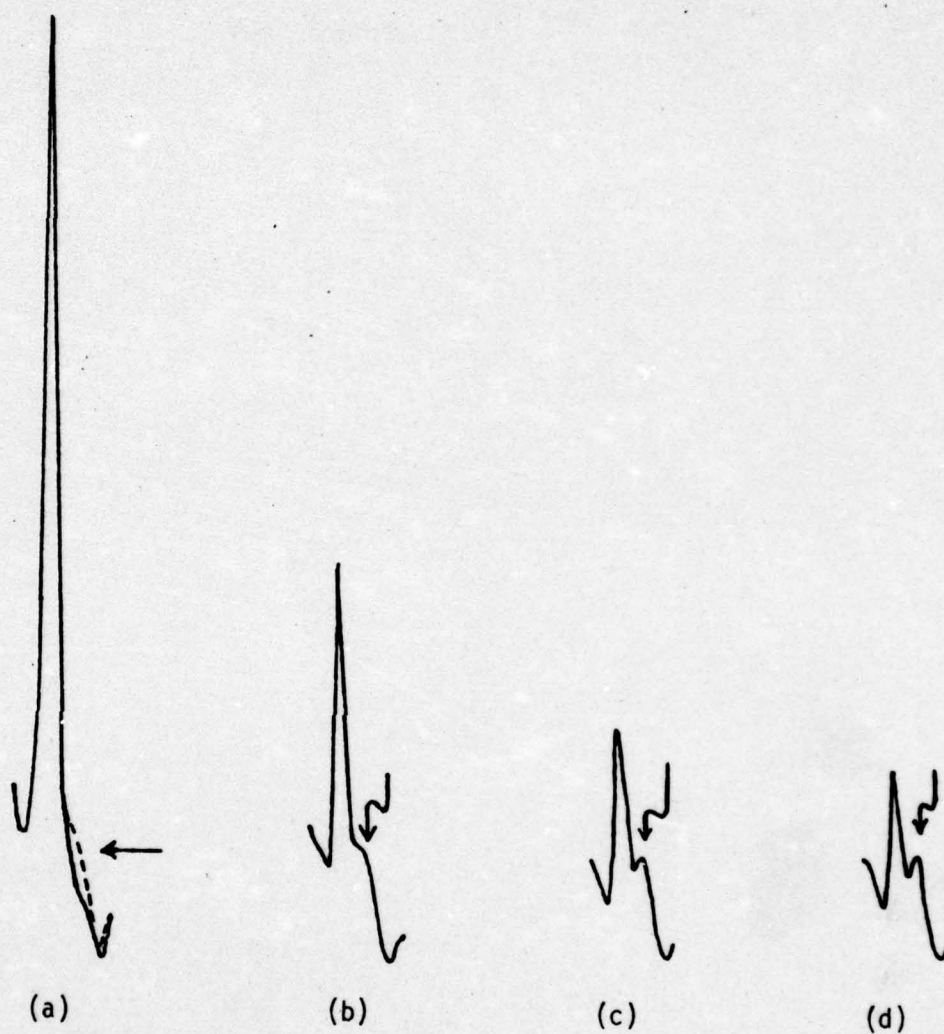


Figure 4.4 (a) Superimposed  $903\text{ cm}^{-1}$  IR band of TRICITE film under no stress (—) and stress (---). (b)  $903\text{ cm}^{-1}$  IR band in subtraction spectrum - (stressed-80% unstressed). (c)  $903\text{ cm}^{-1}$  IR band in subtraction spectrum - (stressed-88% unstressed). (d)  $903\text{ cm}^{-1}$  IR band in subtraction spectrum - (stressed-90% unstressed).

FTIR spectra of  $903\text{ cm}^{-1}$  band is shown in Figure 4.4b, which shows a weak band emerging as a shoulder. This weak band becomes pronounced in (stressed-88% unstressed) spectra shown in Figure 4.4c, and even more so in Figure 4.4d, showing (stressed-90% unstressed) spectra.

Thus, we can see that subtraction spectra are quite useful in monitoring very small differences in the IR spectra of samples which might have been subjected to different conditions. In the present study we obtained several "computer-subtracted" spectra for each of the aforementioned samples, but only those subtraction spectra will be presented which yield the maximum information.

Fatigued and crazed samples used in the above study were obtained by cyclic loading-unloading process in the Instron machine, i.e., in the same way as for IR studies on Perkin Elmer instrument. The procedure of obtaining cyclically-fatigued samples will be described in a later section.

The stress on polymer film samples in the above experiments on FTS was applied by stretching these in a modified film stretching device. The stretching device manufactured by W. H. Warhus Co. [113] had thus far been used exclusively in the X-ray studies. Figure 4.5 illustrates the original film stretching device. This was modified for use on FTS by removing the collimator holding plate. This stretching device did serve the purpose to some extent, even though better results would have been obtained by using the loading system illustrated in Figure 4.1. The difference between these two devices was that one was pneumatic, equipped with a stress type grip while the other was a mechanical stretching device with no arrangements for



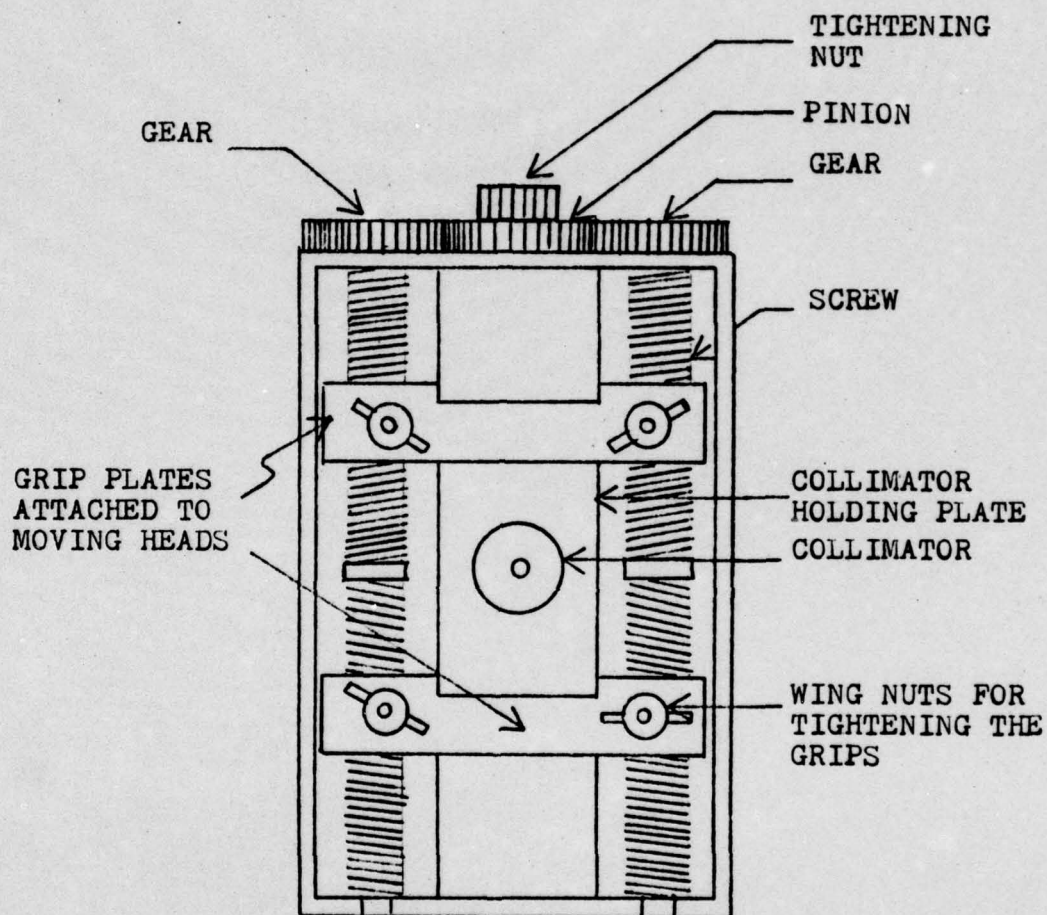


Figure 4.5 Film stretching device used in dynamic X-ray studies [113].

direct reading of stress and with grip plates, unable to hold the samples firmly at higher strains. The polymer samples were stressed manually in the modified film stretching device and strain on the sample was measured by Vernier calipers. The stress on the sample was then determined from its stress-strain curve, corresponding to the strain due to stretching. Furthermore, it was not possible to apply high loads on the modified film stretching device. Therefore, most IR spectra of stressed polymers were obtained at low loads. Though it was not the most efficient stressing system, it had to be borne with for lack of accessibility to the other system. However, there was one plus in having used this system. It was the same stretching device used in our dynamic X-ray experiments. Thus, strains applied on the samples in FTIR and X-ray experiments were in the same range. Finally, there were some disadvantages of the modified stretching device, yet it did serve the present purpose of stressing the samples for dynamic infrared studies and thus demonstrating the changes occurring in IR bands due to stress.

#### 4.2.3 X-ray diffraction studies

This section is an introduction to X-ray diffraction of amorphous polymers. Following the introduction equipment used and experimental techniques employed are discussed.

4.2.3.1 Introduction. In either film or fiber form X-ray diffraction studies are important characterization techniques in polymers. The X-ray scattering patterns thus obtained from a polymer



can yield a variety of information, viz.,

- (i) Type of polymer, i.e., crystalline, semicrystalline or amorphous.
- (ii) Dimensions of unit cell if crystalline or semicrystalline.
- (iii) Interchain and intrachain distances.
- (iv) Percent crystallinity.
- (v) Structure and orientation condition of the polymer chain.
- (vi) Inhomogeneities in polymers such as voids or microvoids--determined from small angle studies.

However, in the present research our basic concern is the study of amorphous polymer films of atactic polystyrene and of polycarbonate. Unlike semicrystalline polymers, amorphous polymers exhibit diffused rings (also referred to as halos) in their diffraction pattern. Although their measurement is rather difficult, there does exist a maximum of scattered intensity in these diffused rings. These maxima have been ascribed to frequently occurring interatomic distances in a predominantly disordered material [114]. These interatomic distances (corresponding to observed diffused rings) are commonly obtained by applying Bragg's law:

$$d_{\text{Bragg}} = \frac{n\lambda}{2\sin\theta} \quad (4.4)$$

where

- $d_{\text{Bragg}}$  = Bragg distance for crystalline material
- $\lambda$  = wavelength of the X-rays
- $\theta$  = scattering half angle
- $n$  = integer

However, the interatomic distances thus obtained are only an approximation in the case of amorphous polymers. Application of X-ray scattering function on liquids suggests [115] that the true distance in the glass (i.e., in random state)  $d_g$ , is given by

$$d_g = 1.22 d_{\text{Bragg}}$$

where  $d_{\text{Bragg}}$  is the Bragg distance for a crystalline material having the same scattering angle.

In spite of the approximation involved,  $d_{\text{Bragg}}$  is still popularly employed to denote the interatomic distance in amorphous polymers and will be used in this study, too.

4.2.3.2 Experimental. All X-ray scattering data in the present study were obtained from flat film X-ray diffraction patterns. Both polystyrene and polycarbonate films being studied were too thin ( $\sim 3$  mil) to give any measurable diffractometer trace.

Flat film patterns were obtained by using an evacuable box camera designed by Statton (shown in Figure 4.6). The camera was simple to use and both wide angle and small angle X-ray patterns could be obtained through it.

The geometry involved in producing the diffraction pattern from this setup is shown in Figure 4.7.

Since present X-ray studies were conducted to essentially determine the changes in interatomic distances on stressing a polymer film, the film stretching device (film-stretcher) sketched in Figure



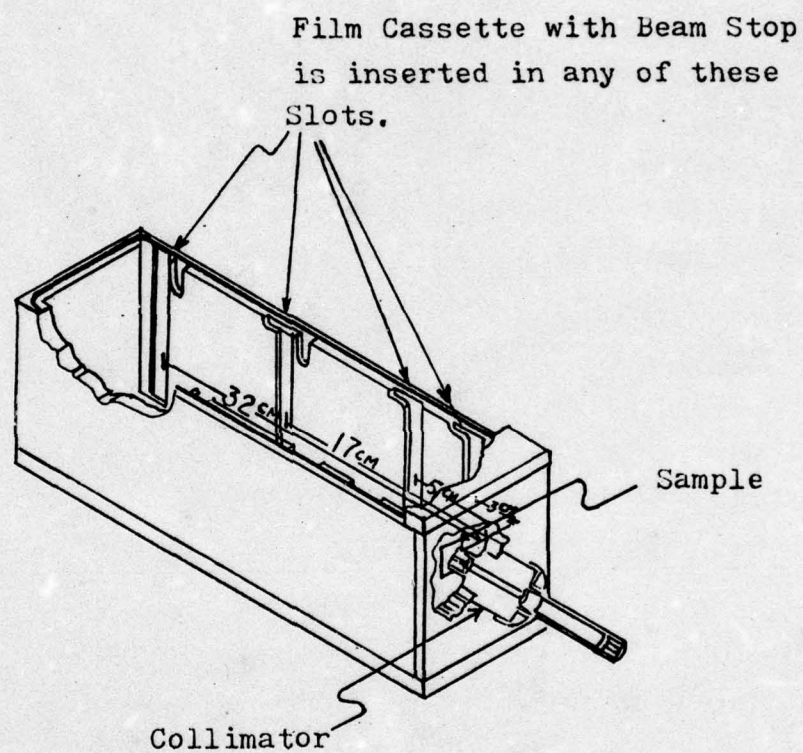


Figure 4.6 Cutaway diagram of small and medium-angle camera designed by W. O. Statton.

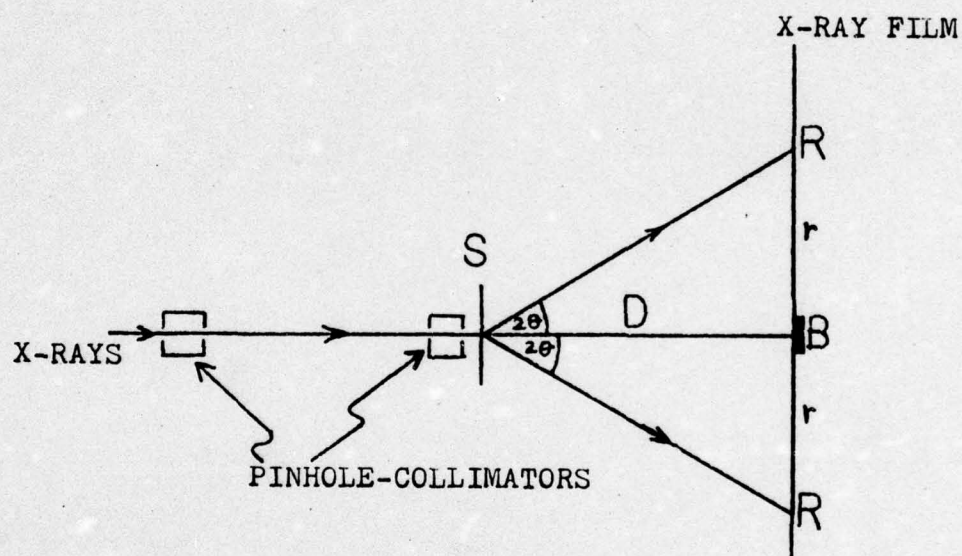


Figure 4.7 Dimensional relationship of the geometry of diffraction by the specimen. Here S is the specimen, B is the beam stop, R is diffraction spot or ring and r is the distance between spot or ring and center of the pattern. D is the distance between the specimen and the film.



4.5 was used. As the diffraction patterns of the same films under unstressed and stressed conditions were to be obtained, the film samples were secured each time in the film stretcher, irrespective of its stress condition. The film-stretcher is equipped with its own pinhole collimator of 0.020" diameter. Another pinhole collimator of 0.025" diameter was used close to the X-ray source. X-rays were produced from Cu target at a voltage setting of 50 kV and a current of 20 mA. The  $\text{CuK}_{\alpha}$  ( $\lambda = 1.5405\text{\AA}$ ) was obtained by using a nickel filter in these diffraction experiments.

In the present setup the distance (D) from the X-ray source to the film cassette was known precisely. However, the film stretcher could move outwards (i.e., towards the film cassette) on evacuation of air from the camera. Since precise measurements were essential in our experiments, an internal calibration for sample-to-film distance was necessary. This was achieved by smearing polymer film samples with small amounts of ZnO powder, which gives three most intense reflections ((100), (002), (101)) appearing as three concentric rings on the X-ray pattern. The d spacing of these rings can be obtained through the X-ray diffraction file, X-ray wavelength is known, therefore, the  $2\theta$  values for these rings can be determined from the geometrical relationship of Figure 4.7, which shows

$$\tan 2\theta = \frac{r}{D} \quad (4.5)$$

Thus, obtaining  $2\theta$  through computations and  $r$  through measurement from the diffraction pattern, distance  $D$  can be calculated. Thus,

if ever  $D$  varies,  $r$  will undoubtedly be affected correspondingly. Since  $r$  can be measured,  $D$  is calculable. The distance  $D$  in our case was measured on a lighted X-ray film measuring device. The diameter of the ZnO ring was measured between the outer edges of the ring. This was essential since the outer rim of the ring is due to the diffraction from ZnO closest to the sample (see Figure 4.8). To eliminate any random errors, the diameter of the ring was measured at eight different points.

Since the primary objective of the X-ray studies here was to determine any changes in interatomic distance, the diffraction pattern was obtained first from unstressed films. The same film was then strained and another diffraction pattern obtained. X-ray films under two different strain conditions were exposed for the same number of hours and developed under identical conditions in the following sequence:

Washed for 1 minute

Placed in fixer for 4 minutes

Finally washed for 15 minutes.

These developed films were then scanned by a Joyce-Loebl automatic recording densitometer (Model MD 111CS). This instrument has a resolution of 1 micron at optical densities up to 2.0 and reaches full-scale response in less than one half second. In all scans of polystyrene and polycarbonate film patterns, an aperture of 30 microns was used. The maximum intensity point in the outer diffused rings of both polystyrene and polycarbonate was determined by drawing tangents on the densitometer traced peaks (Figure 4.9). The intersecting



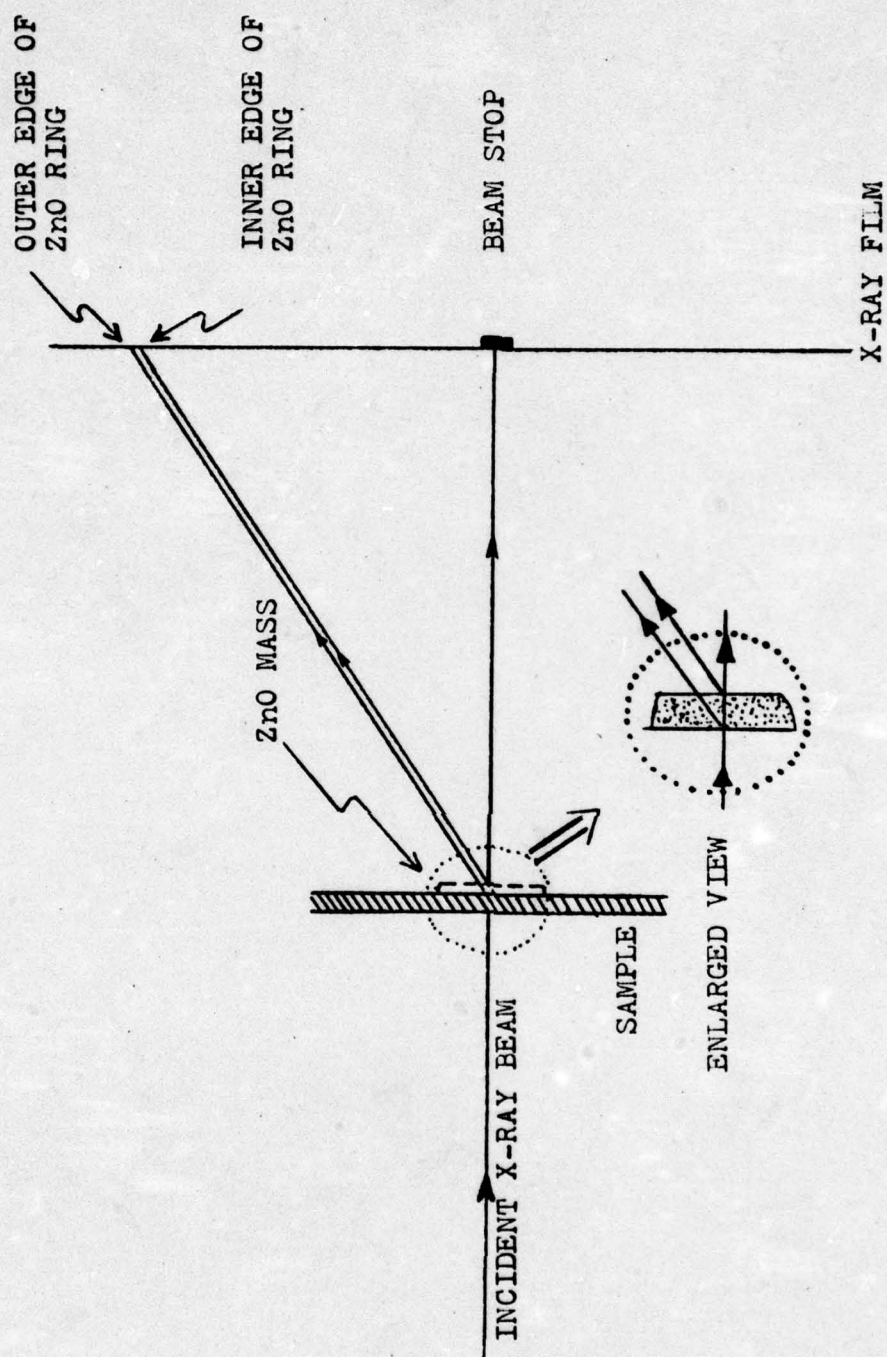


Figure 4.8 Schematic representation of the diffraction from the internal standard of calibration (ZnO smeared on polymer sample).

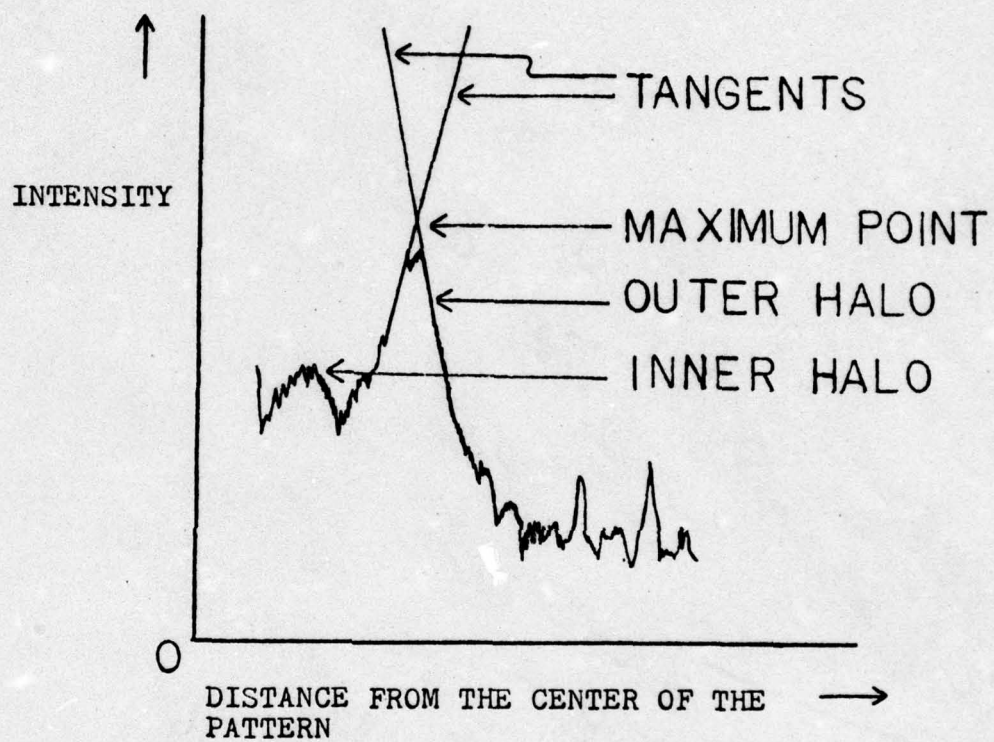


Figure 4.9 Densitometer trace of the X-ray scattering pattern of TRICITE film.



point of these tangents was considered to be the maximum point, based on which a corresponding Bragg distance was calculated by Equation (4.4). To eliminate any errors, at least eight densitometer traces were obtained for each film pattern. The points were chosen on the equator, meridian and diagonals of the pattern to observe any changes in intensities arising from orientation, which might have occurred on application of stress. Various results obtained from X-ray studies on polystyrene and polycarbonate will be discussed in the next chapter.

It may be mentioned here that measurements of interchain distances obtainable from the inner halo would have been very useful but such measurements in our study were not possible, due to experimental difficulties.

#### 4.2.4 Density measurements

To measure the densities of polycarbonate samples a density gradient column was prepared. To obtain the desired density range two different concentrations of aqueous sodium bromide solutions were mixed. The concentrations and their corresponding densities at various temperatures are given in International Critical Tables [116]. In our case concentrations of 15 and 26 weight % of NaBr were used to obtain a density gradient between 1.121 and 1.232 g/ml. at 30°C-- the constantly maintained temperature of the column. The aqueous salt solution was purposely used to avoid any swelling and/or dissolution of polycarbonate films in organic liquids. The procedure for the preparation of density-gradient column is given in ASTM bulletin (D 1505-58 of 1971).

The above described column was calibrated by the use of calibrating balls, the densities of which were 1.1317, 1.1843, 1.2000 and 1.2248 g/ml. These densities covered the entire range between 1.121 and 1.232 g/ml. Since the procedure involved in filling this column does not allow a linear interpolation of the densities from the marked graduations of the column, a graph was plotted between the densities of calibrated balls versus position (graduations) on the column.

Small pieces of samples (whose density was to be determined) were dropped into the column and allowed to reach their equilibrium positions. This usually took about an hour and thereafter no change in the sample position was observed up to 24 hours. At that point the position of these samples were noted and the density of sample was read from the above mentioned graph.

The density results obtained for fatigued polycarbonate films will be presented later.

#### 4.2.5 Dynamic mechanical measurements

4.2.5.1 Introduction. Dynamic mechanical tests, in general, give more information about multiple relaxation peaks of a material than any other tests. Dynamic tests over a wide range of temperature and frequency are sensitive to chemical and physical structure of polymers. These tests measure the response of a material to a sinusoidal or other periodic stress. Since stress and strain are generally not in phase, two quantities can be determined--a modulus and a phase angle or a damping term. The sinusoidal stress can be in



tension or shear. Only the tension case will be discussed here because we are using the Rheovibron Dynamic Tensionometer.

If a sinusoidal strain of angular frequency  $\omega$  and of maximum strain amplitude  $\epsilon_0$  is imposed on the sample, then the strain at any time  $t$  will be given by:

$$\epsilon = \epsilon_0 \sin \omega t \quad (4.6)$$

Their resulting stress ( $\sigma$ ) for a viscoelastic or a glassy solid can be described by

$$\sigma = \sigma_0 \sin (\omega t + \delta) \quad (4.7)$$

where  $\delta$  is the phase angular difference between stress and strain.

This equation (4.7) can be expanded and rewritten as

$$\sigma = \sigma_0 (\cos \delta \sin \omega t + \sin \delta \cos \omega t) \quad (4.8)$$

which implies that the stress can be resolved into components in-phase and out of phase with strain.

Defining  $E'$  as the ratio of the in-phase stress to the in-phase strain and  $E''$  as the ratio of amplitudes of stress  $1/2\pi$  out of phase to the strain amplitude, we have

$$E' = \frac{\sigma_0}{\epsilon_0} \cos \delta \quad (4.9)$$

$$E'' = \frac{\sigma_0}{\epsilon_0} \sin \delta \quad (4.10)$$

The ratio of the maximum amplitudes of stress and strain during a cycle can be defined as complex modulus  $E^*$  and

$$E^* = \frac{\sigma_0}{\epsilon_0}$$

or it can also be expressed in complex notation as

$$E^* = E' + i E''$$

where  $E'$  is a real part of the modulus and  $E''$  is an imaginary part of the modulus and  $i = \sqrt{-1}$ ,  $E''$  is also called the damping or energy dissipation term.

The angle which reflects the time lag between the applied stress and strain is  $\delta$  and is defined by a ratio called the dissipation factor

$$\tan \delta = \frac{E''}{E'}$$

The  $\tan \delta$  is a damping term and is a measure of the ratio of energy dissipated as heat, to maximum energy stored in the material during one cycle of oscillation.

Damping is often the most sensitive indicator of all kinds of transitions, relaxation processes, structural heterogeneities and the morphology of multiphase systems such as crystalline polymers, polyblends and filled or composite materials. Thus, damping is very useful in determining the mechanical behavior of polymers.



4.2.5.2 Measurement. In the present study dynamic mechanical testing of polymer samples was performed on a Rheovibron Dynamic Viscoelastometer Model DDV-II. The block diagram for this instrument is shown in Figure 4.10. In this instrument the sample is clamped between strain gages and subjected to a small sinusoidal tensile strain at a fixed frequency. The value of  $\tan\delta$  can be read directly off the instrument and the storage and loss moduli can be calculated from instrument readings and samples' dimensions.

Measurements are generally made as a function of temperature at one of the four fixed frequencies: 3.5, 11, 35 or 110 Hz.

The the present study,  $\tan\delta$  of polystyrene and polycarbonate films was measured as a function of temperature and load history. The range of temperature studied was from liquid nitrogen temperature<sup>1</sup> to the glass transition temperature of the polymer. The frequencies used were 3.5 and 35 Hz. The results obtained are discussed in the following chapters.

#### 4.2.6 Differential scanning calorimetry

Glass transition temperature of polystyrene and polycarbonate films was measured on a DuPont 990 thermal analyzer.

---

<sup>1</sup>It was found necessary to calibrate the pyrometer of this instrument for the temperature reading below 0°C. This was actually done by using an external thermometer and a millivoltmeter.

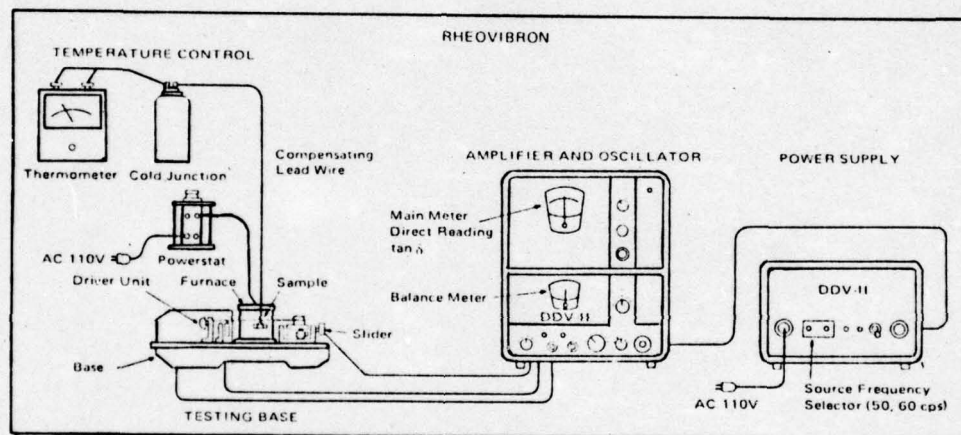


Figure 4.10 Block diagram of the Rheovibron dynamic visco-elastometer [12].



#### 4.2.7 Microscopy

Bausch and Lomb's optical microscope fitted with a polarizer and slot compensator was used to characterize polymer orientation by measuring the birefringence.

#### 4.2.8 Fatigue in polymers

4.2.8.1 Introduction. Material fatigue behavior is a property of materials which is extremely important to the design engineer. Fatigue has been extensively studied in metals, whereas its study in polymers has been limited. Even though the studies on fatigue in bulk polymers have been carried out, the mechanism at work during fatigue processes are little understood. Most of this study has progressed along the paths paralleling the study of fatigue in metals, which has been in the area of crack initiation, crack propagation and ultimate failure. However, such macroscopic phenomena along with the microscopic phenomena of crazing, shear banding and plastic flow, are insufficient to give a complete picture of fatigue processes in polymers. So far, no study has been reported which deals with the fatigue process from a very basic level, which is the molecular level. One of the objectives of this research, therefore, has been to study the molecular behavior of cyclically fatigued amorphous glassy polymer films.

4.2.8.2 Method. For the present study load controlled low cycle fatigue of polymer samples was conducted on the Instron testing

machine model TMS. The number of cycles to which these samples were fatigued depended on the amount of load applied, which was usually such that the polymer films remained within their elastic limit. To determine the yield load, load elongation curves were obtained for both polystyrene and polycarbonate film samples. All fatigue tests were conducted below the yield point to establish fatigue behavior and obtain fatigued samples. The fatigued films thus obtained were then studied by IR, FTS and Rheovibron. They were also examined under the optical microscope as well as scanning electron microscope, to detect any crazes, cracks and microvoids.

#### 4.3 Materials

##### 4.3.1 Polystyrene

Initial studies were conducted on commercial atactic biaxially oriented polystyrene (TRICITE). These TRICITE films were obtained from Dow Chemical Company, Midland, Michigan. These films had a thickness of 3 mil and 5 mil.

Subsequent study was conducted on polystyrene films manufactured in our own laboratory from pellets obtained from the following two sources:

- (i) Cellomer Associates, Webster, New York
- (ii) Dow chemical Company, Midland, Michigan.

The pellets obtained from Dow Chemical Company are well characterized [117]. These films were manufactured as follows:

Polystyrene pellets were dried under vacuum for 12 hours at 80°C.



Dried pellets were poured into a copper mold which was placed on a chrome-polished stainless steel sheet. Another similarly polished sheet was placed as a cover. The mold was then placed on a hot platten (at 250°C) of a hydraulic press. The pellets in the mold were allowed to soften for 2 minutes at this temperature of 250°C and then pressed at a pressure of 275 psi. This pressure was maintained for 10 minutes, after which it was released. The mold was then removed from the platten and cooled by blowing air. Polystyrene sheets thus obtained were about 5 mil thick.

Both oriented and uniaxially oriented polystyrene films were used in the present study. The uniaxially oriented films were obtained by stretching 2" wide and 1" long polystyrene samples in Instron hot box attached to the Instron machine. The films were drawn at 102°C and a draw rate of 8 in/min. These samples were drawn to a draw-ratio 250%, 300%, 400%, 500%, and 600%. Samples of appropriate dimensions were cut from these oriented films for studies by IR, FTS, etc.

#### 4.3.2 Polycarbonate

Polycarbonate films (Lexan<sup>®</sup>) were obtained from General Electric Company, Mt. Vernon, Indiana. These were unoriented films of 3 mil thickness.

Both unoriented and uniaxially oriented polycarbonate films were used. The uniaxially oriented films were obtained by stretching 2" wide and 2" long polycarbonate film samples in an Instron hot box attached to the Instron machine. The films were drawn at 150°C and a draw rate of 8 in/min. Drawn films were quenched by blowing air to prevent any crystallization. The films thus obtained had a draw ratio of 200%, 250% and 300%. Samples of appropriate dimensions were cut from these oriented films for studies by various techniques.

## CHAPTER V

### RESULTS AND DISCUSSIONS OF ATACTIC POLYSTYRENE UNDER TENSILE STRESS, CYCLIC FATIGUE AND IN CRAZING CONDITIONS

In this chapter various results obtained from atactic polystyrene of different orientations and under various conditions, viz., tensile stress, in fatigued and crazed conditions, will be discussed. Summary of the discussion of results will be presented at the end of each section.

#### 5.1 Results and Discussion: 0.0045" Thick TRICITE Film

##### 5.1.1 Stress-strain results

Figures 5.1 and 5.2 show the stress-strain behavior of the TRICITE film along the machine direction and across the machine direction, respectively. Strain rate applied in each case is 0.05 inch/minute, which is nearly equal to the loading rate applied during the dynamic infrared studies. The breaking stress and strain obtained from these curves are 10,800 psi and about 3.1%, respectively. These stress-strain curves indicate hard and brittle characteristics of this film, as discussed in Table 1.1.

Figure 5.3 shows the stress-strain curve of annealed TRICITE film, which was annealed under nitrogen atmosphere for 45 minutes at 70°C. The breaking stress in this case is about 10,100 psi, which is



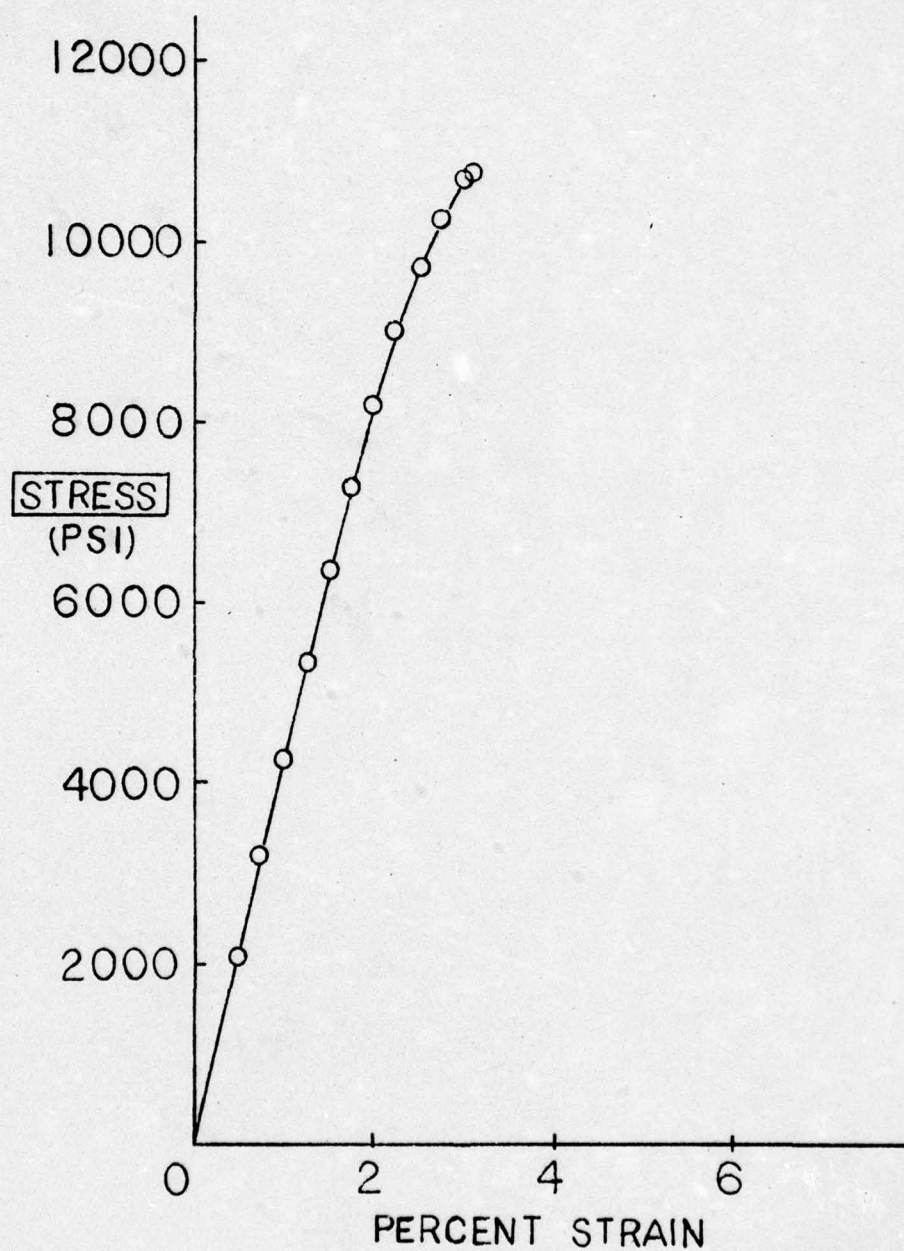


Figure 5.1 Stress-strain curve of 4.5 mil thick TRICITE film cut along the machine direction. Gage length - 2", Strain rate - 0.05 in/min.

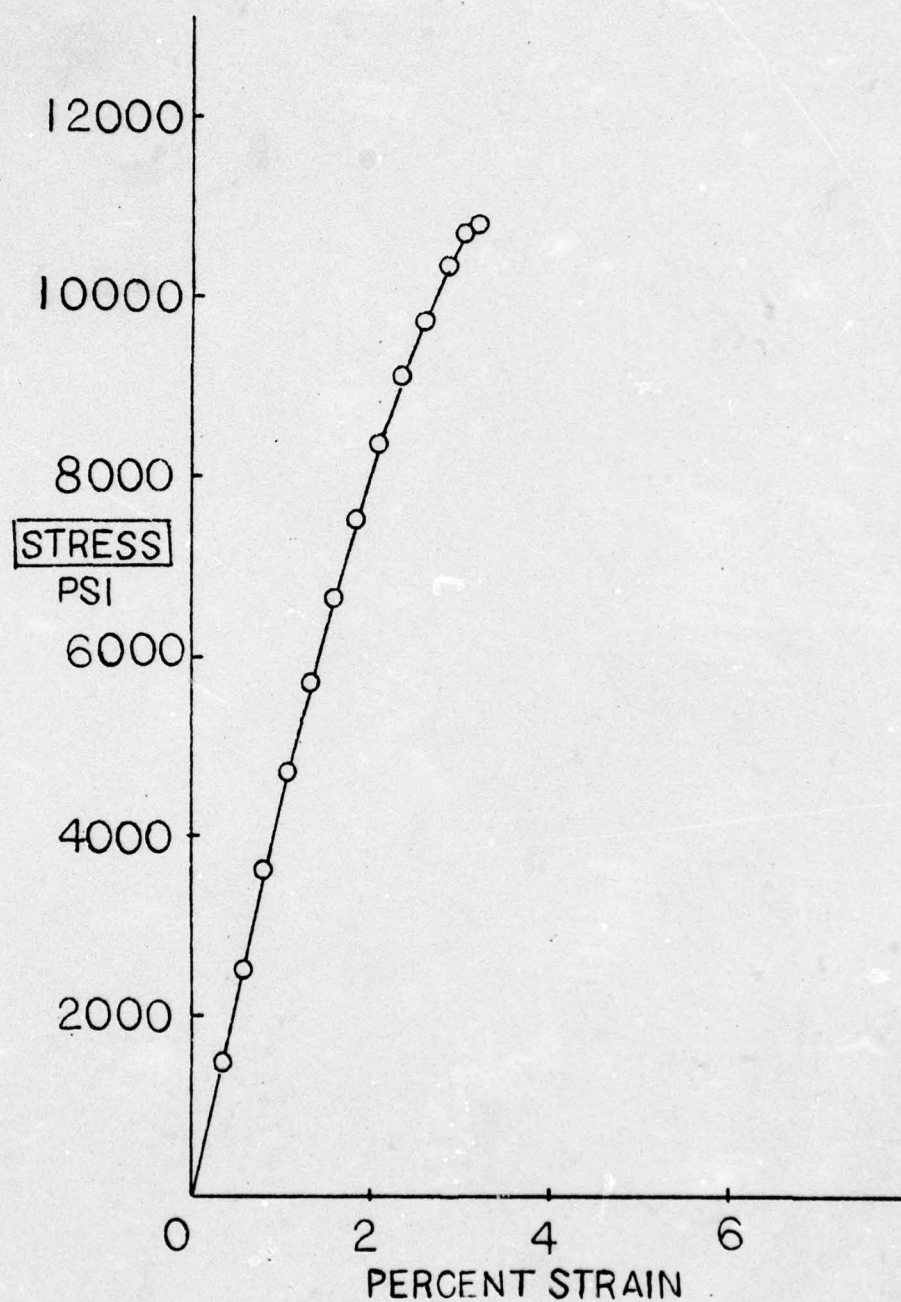


Figure 5.2 Stress-strain curve of 4.5 mil thick TRICITE film cut along transverse direction. Gage length - 2", strain rate - 0.05 in/min.



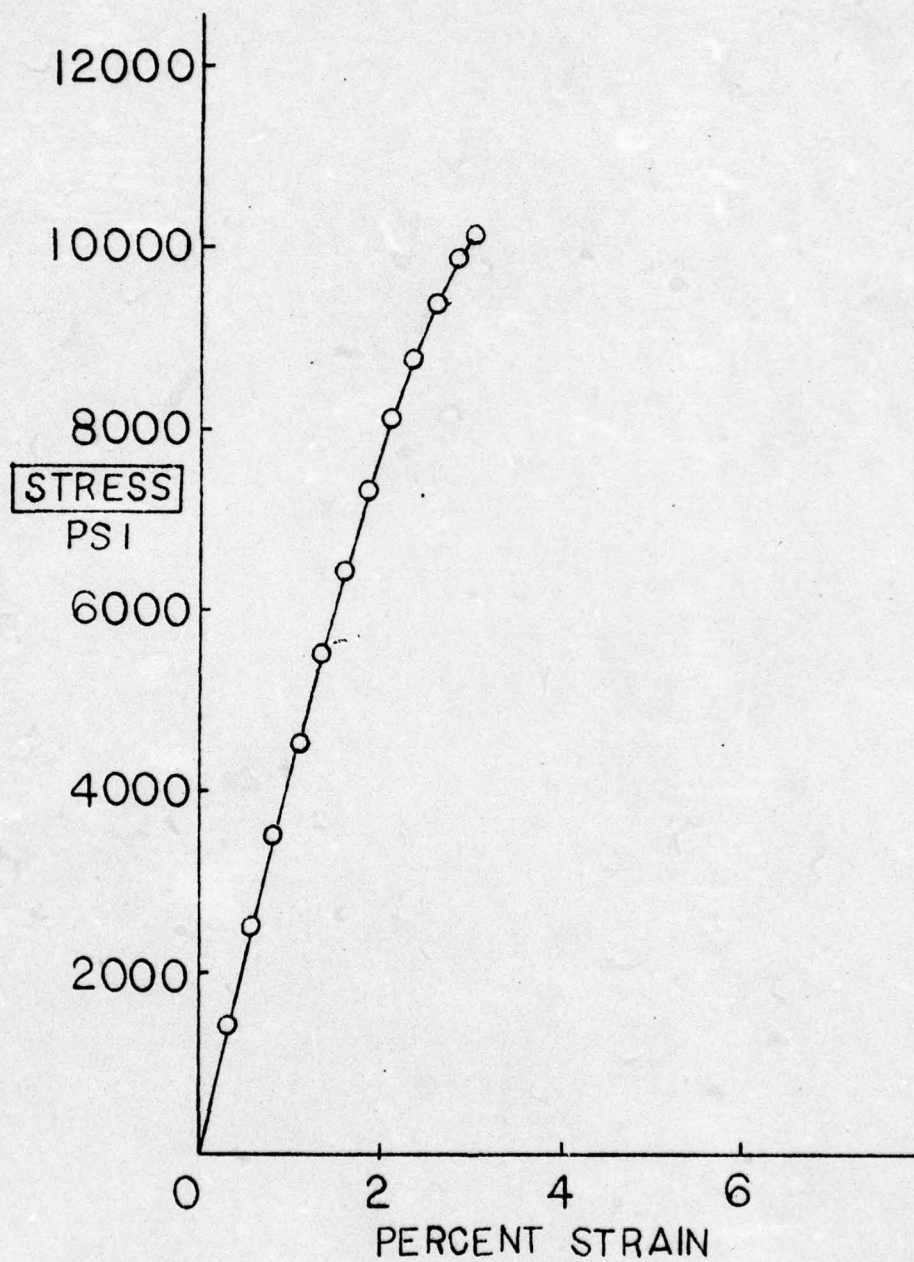


Figure 5.3 Stress-strain curve of 4.5 mil thick annealed TRICITE film. Gage length - 2", strain rate - 0.05 in/min.

only slightly lower than the one for unannealed TRICITE film. There is no difference in the breaking strain. From these stress-strain curves we may infer that Young's moduli of these films is about the same along its length and width, and the biaxial orientation along these two directions is also equal or near-equal. In the case of annealed TRICITE film, perhaps the quick annealing process reduces some orientation (at least, from the film surface) and also removes certain frozen-in stresses.

An important observation made during stress-strain tests on the Instron machine was that these films fractured in bands, as if several crazes had coalesced. Such behavior is generally observed in composite materials. These films did not show any shear banding or necking even at this low strain rate of 0.05 in/min. These observations and the evidence from IR results, which will be discussed in the following sections, suggest that an orientation gradient exists through the thickness of these films. This effect in polystyrene has been shown previously through birefringence measurements by Gurnee [118].

#### 5.1.2 Dynamic IR results

Initial dynamic infrared studies were concentrated on IR bands of PS occurring at 1182, 1154, 1110, 1067 and  $903\text{ cm}^{-1}$ , which are in the fingerprint region of infrared spectrum. Investigation of these bands was carried out, primarily, on the basis of past experience on semicrystalline polymers, viz., polypropylene and poly(ethylene terephthalate), where skeletal backbone bonds were found to be



the most stress-sensitive. In polystyrene such skeletal C-C stretching mode is assigned to IR absorption bands occurring at  $\sim 1067$  and  $1182\text{ cm}^{-1}$  (Table 3.1). Therefore, these bands were an obvious choice for the present investigations.

Figures 5.4 through 5.8 show the above mentioned infrared bands under no stress and stress of 888, 1776, 2666, 3555 and 6222 psi, respectively. The broken lines in each figure represents the spectra obtained from the stressed sample. Starting from Figure 5.4, each successive figure shows increased band distortions on an increase in stress level. It is emphasized here that each time a new sample was used to avoid previous stress effects. Furthermore, these band distortions may seem small but they are real and reproducible and they increase with increased stress on the specimen.

Figure 5.9(a) shows additional IR bands included in the present study. These bands are 1602, 1582, 1490 and  $1445\text{ cm}^{-1}$ . The assignments for these and the aforementioned bands have already been discussed in Chapter III. The IR spectra shown in Figure 5.9(a) and (b) were obtained from the TRICITE film stressed to 8000 psi (74% of the breaking stress).

A comparison of IR bands in Figures 5.4 through 5.9 reveals that the distortions become pronounced as stress is increased. The band distortions are maximum at 74% of the breaking stress. This stress level lies within the nonlinear region of the stress-strain curve shown in Figure 5.1. It may be pointed out here that Figures 5.8 and 5.9 also include the IR bands obtained after removing the imposed stress. These bands are shown by dotted lines. As can be seen in

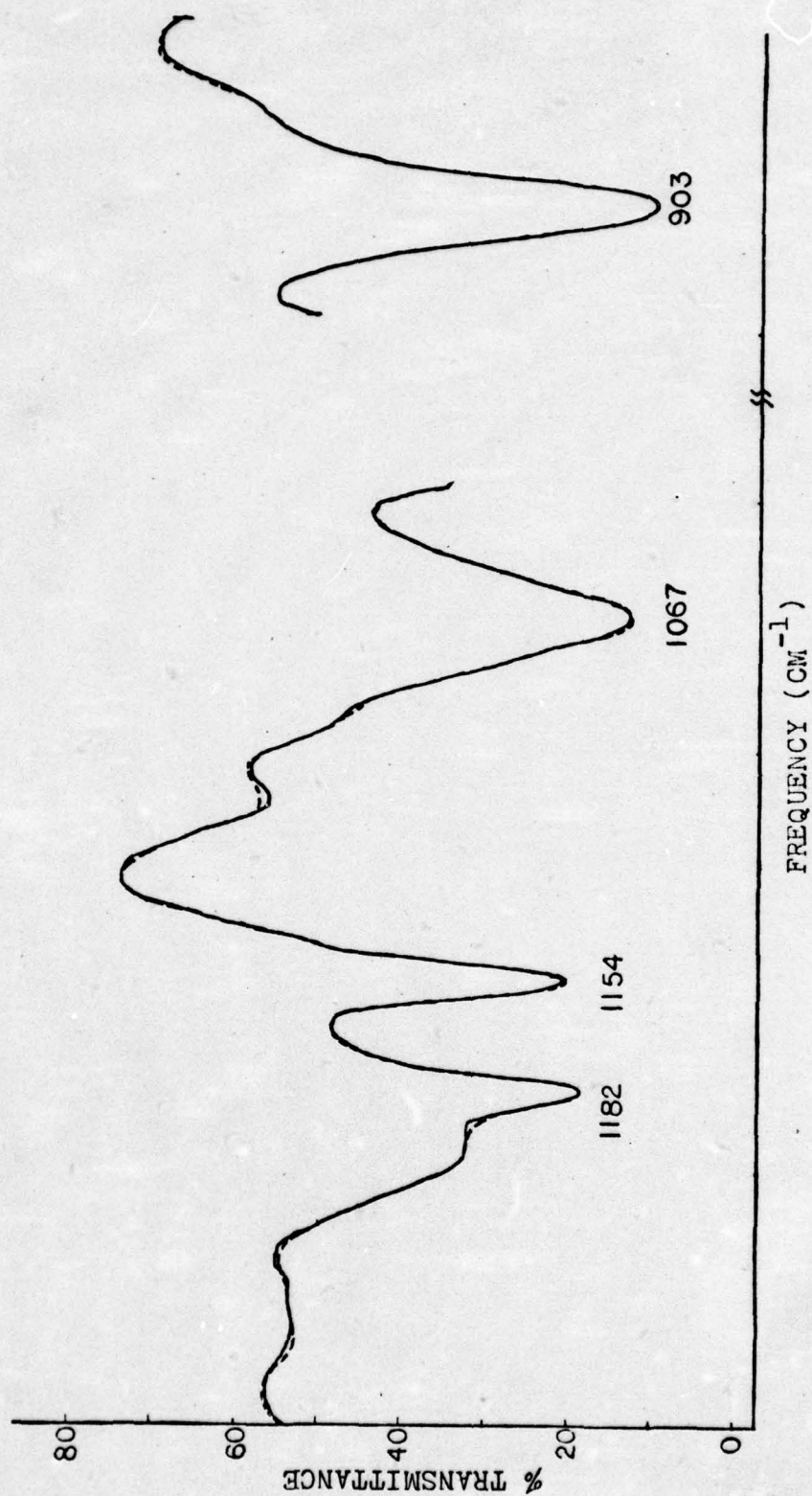


Figure 5.4 IR spectra of 4.5 mil thick TRICITE film under no stress (—) and stress of 883 psi (---). Abscissa expansion 1:5.



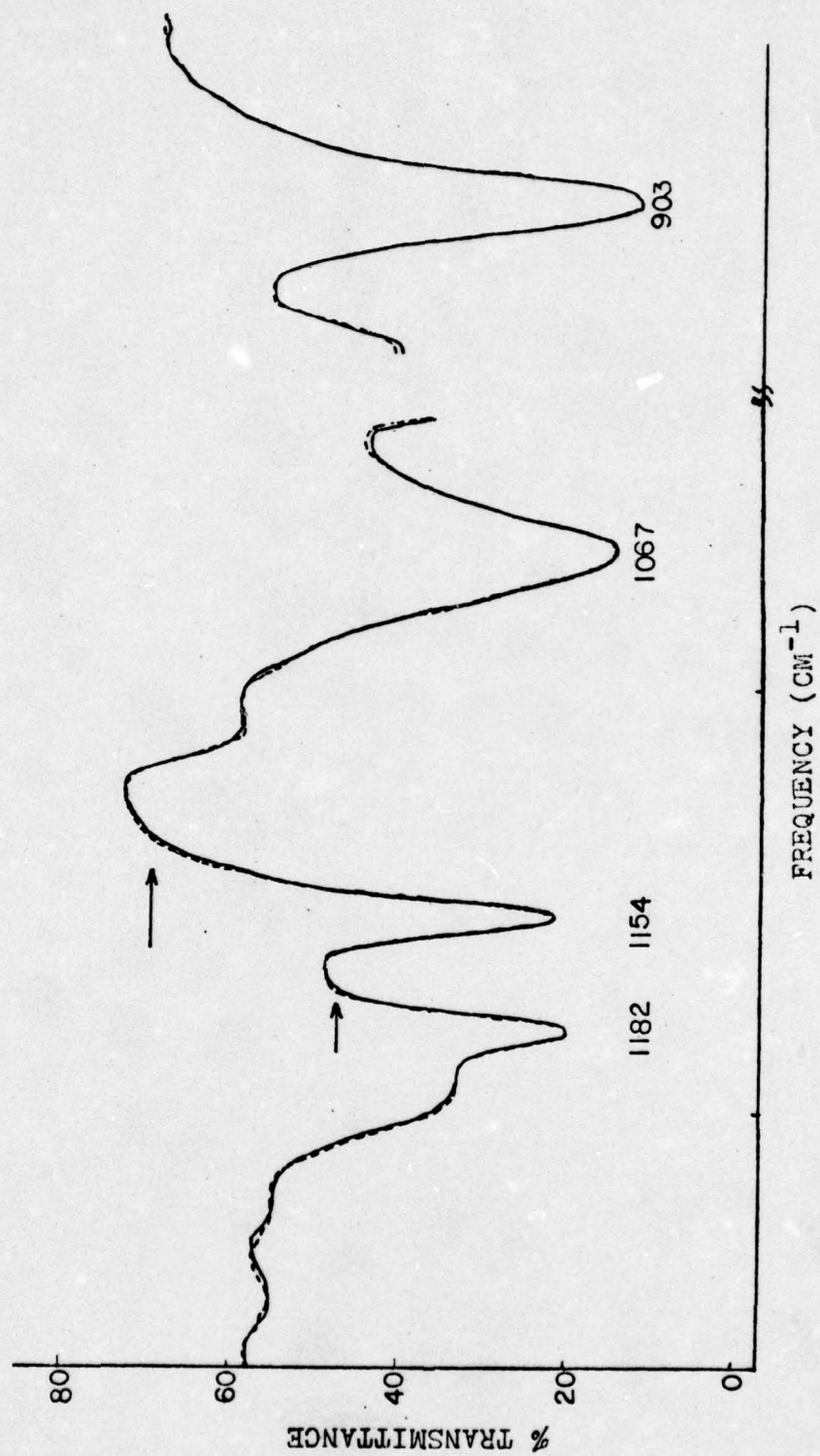


Figure 5.5 IR spectra of 4.5 mil thick TRICITE film under no stress (—) and stress of 1776 psi (---).

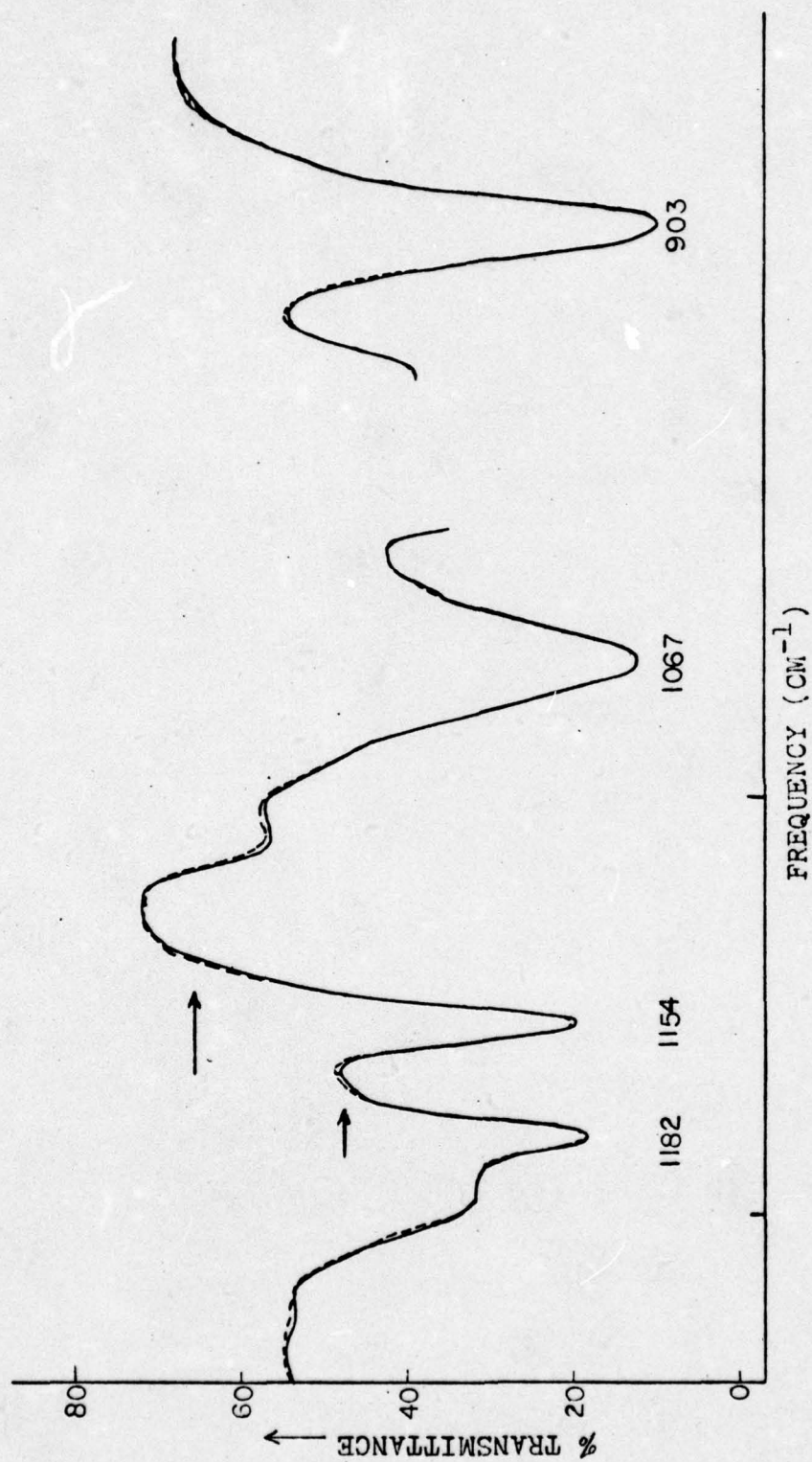


Figure 5.6 IR spectra of 4.5 mil TRICITE film under no stress (—) and stress of 2666 psi (---).



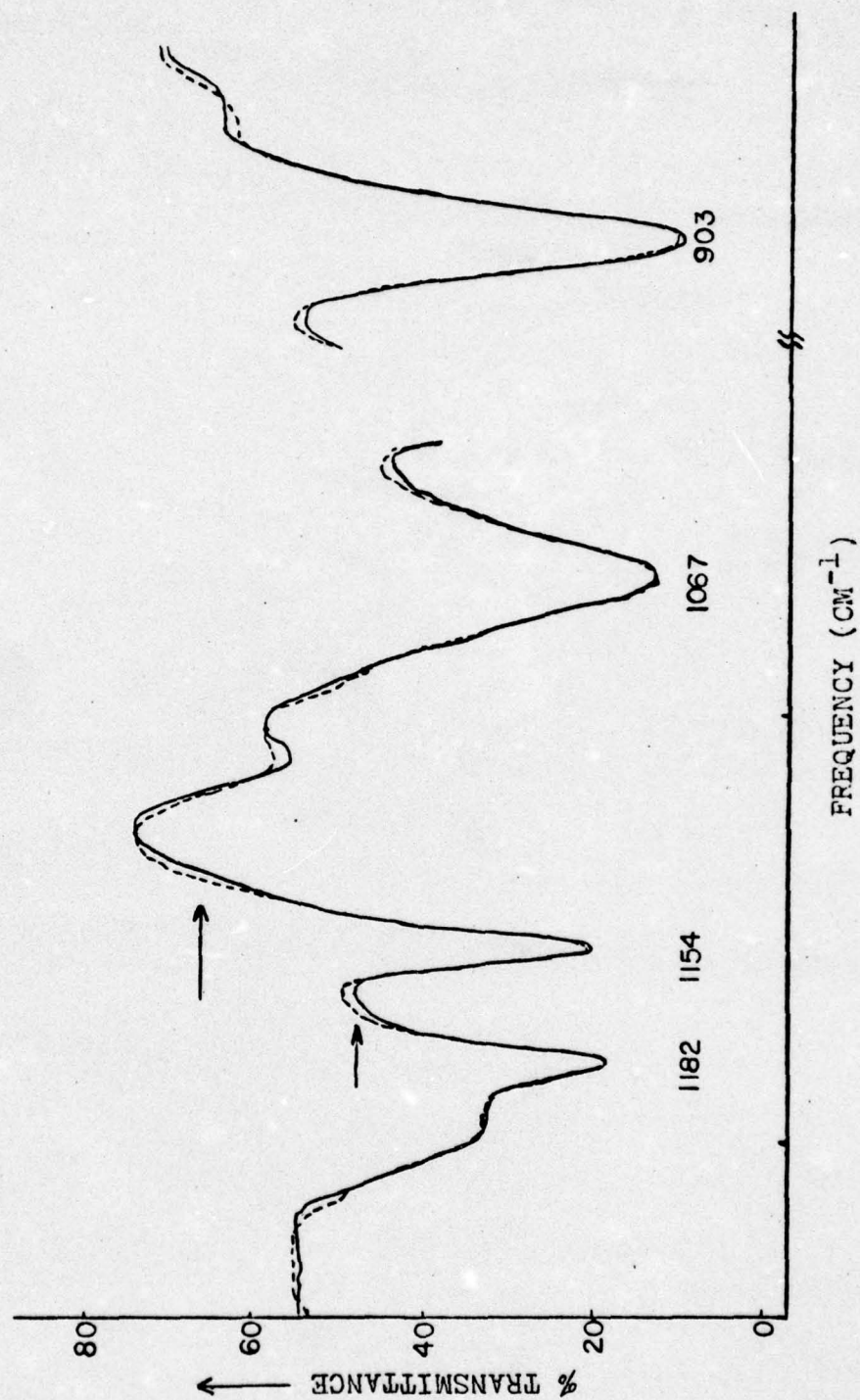


Figure 5.7 IR spectra of 4.5 mil thick TRICITE film under no stress (—) and stress of 3555 psi (---).

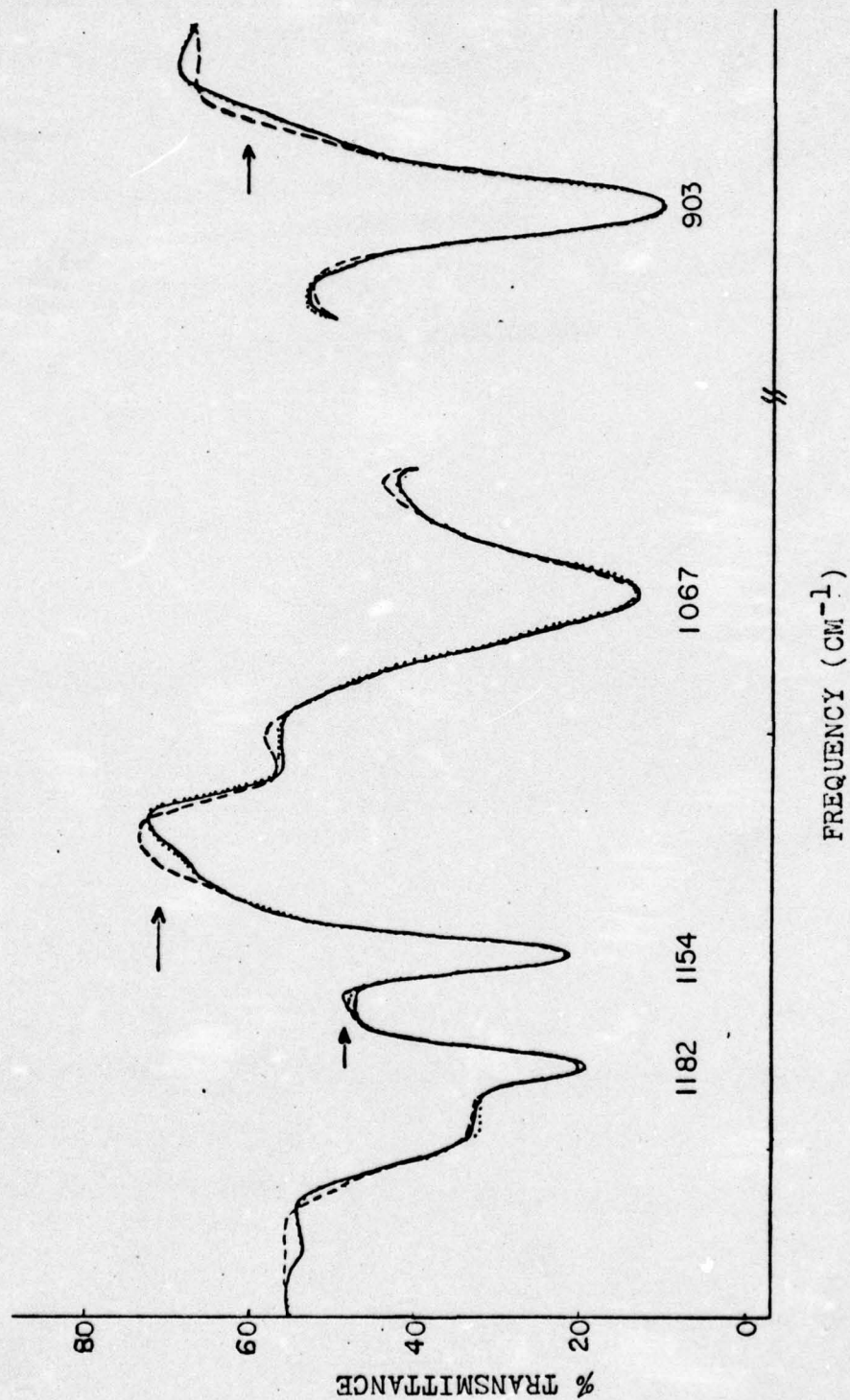


Figure 5.8 IR spectra of 4.5 mil thick TRICITE film under no stress (—) and stress of 6222 psi (---).



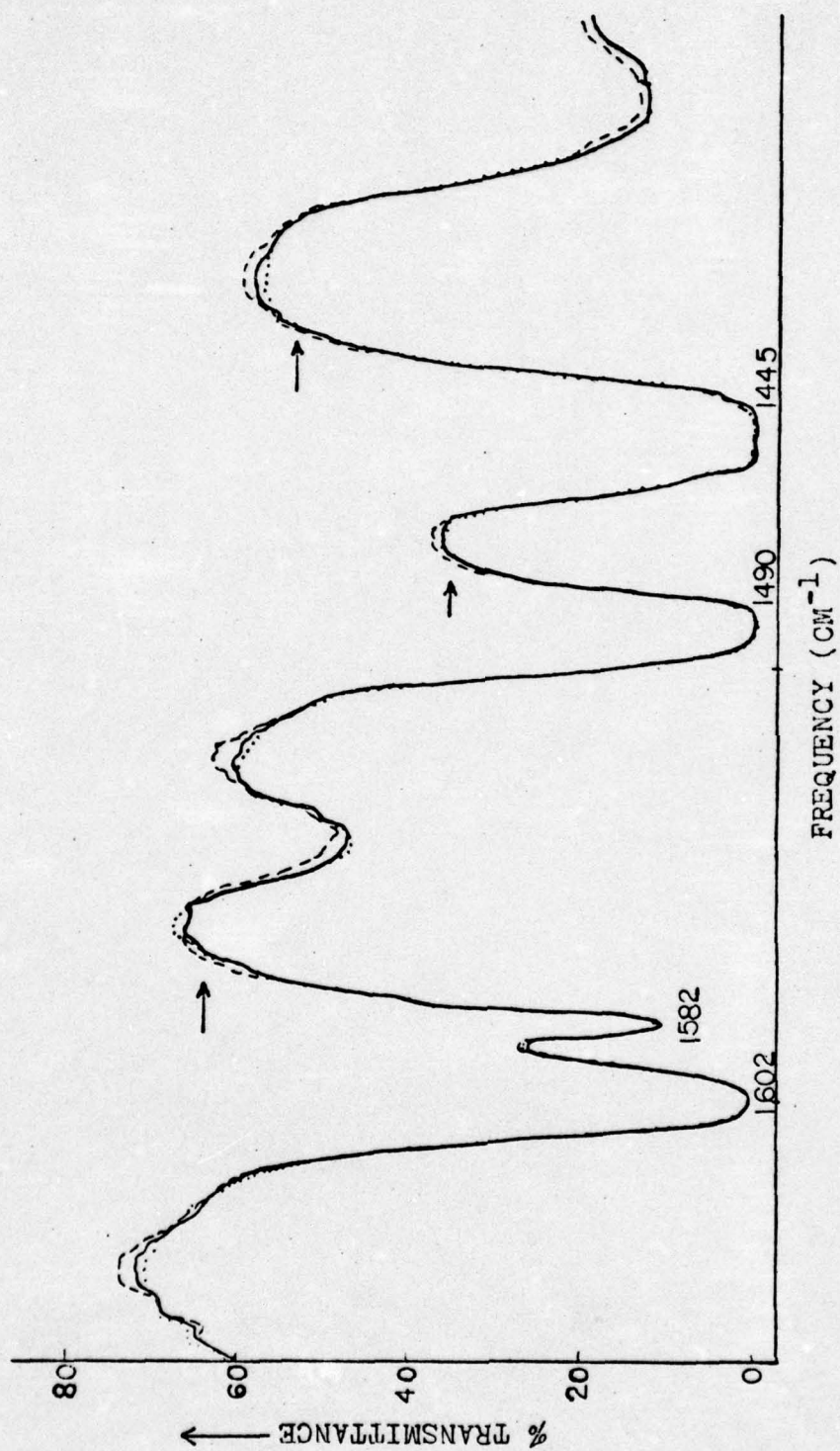


Figure 5.9 (a) IR spectra of 4.5 mil thick TRICITE film under no stress (—), stress of 8000 psi (---) and on stress removal (...).

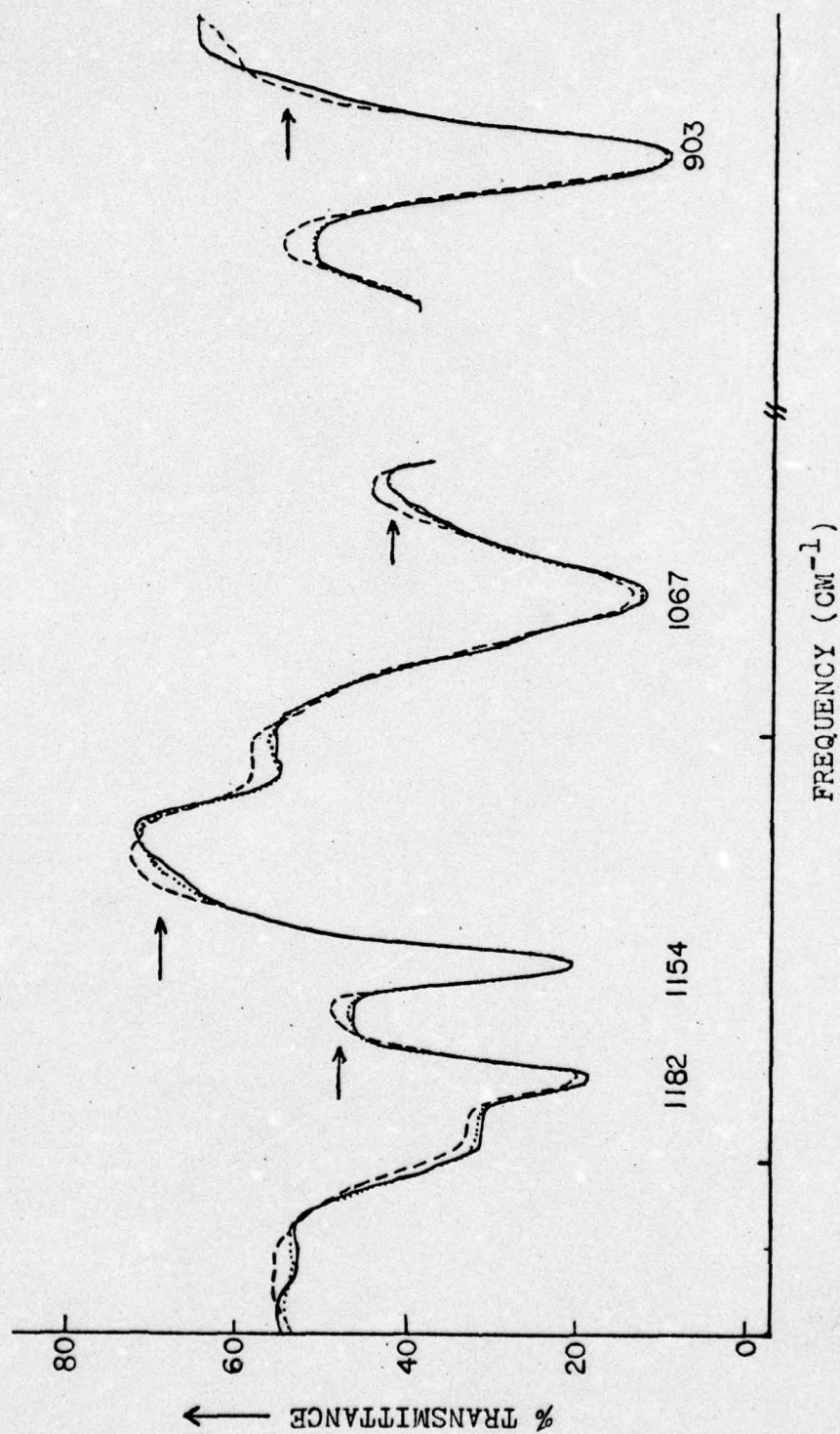


Figure 5.9 (b) IR spectra of 4.5 mil thick TRICITE film under no stress (—), stress of 3000 psi (---) and on stress removal (....).



these figures, band deformations recover mostly but not completely. Though most chains are stressed elastically, yet it appears that certain chains are permanently affected, causing some observed distortions to remain on stress-relieved films. A comparison of dotted line IR bands in Figures 5.8 and 5.9 reveals that permanent distortions are more at higher stresses than at lower stresses. This is expected because the stress-strain curve of these films is linear at lower stresses and deviates from linearity as stress is increased.

In order to obtain a quantitative estimate of relationship between the observed band deformations and imposed stresses on the sample, Zhurkov's technique (discussed in Section 2.1) of measuring the overstressed bonds has been applied to measure band deformations of  $1154\text{ cm}^{-1}$  IR band. The areas under the deformed portion of the band and symmetrical undeformed band are measured by a polar planimeter. The fraction of deformed band is obtained by finding a ratio of deformed band area to undeformed band area. The data thus obtained are presented in Table 5.1.

A graph between the fraction of deformed  $1154\text{ cm}^{-1}$  band and the applied stress is shown in Figure 5.10. This graph shows a linear relation between the amount of band deformation and the imposed stress on the sample. The  $1154\text{ cm}^{-1}$  band is assigned to out of plane vibrations of the benzene ring. The linear increase in band deformation of this band with increase in stress can be explained from the molecular viewpoint as follows:

Polystyrene chains consist of bulky phenyl side groups on their backbone. When any stress is applied, a certain amount of mobility

Table 5.1 Band Distortion of  $1154\text{ cm}^{-1}$  Band Under Stress: 0.0045" TRICITE Film

Stress (psi)	Area under de- formed portion of the band (sq. in.)	Area under sym- metrical undeform- ed portion of $1154\text{ cm}^{-1}$ band (sq. in.)	Fraction of deformed band
888	0.001	0.306	0.00327
1776	0.0035	0.298	0.01174
2666	0.0050	0.288	0.01736
3555	0.0095	0.325	0.02923
6222	0.012	0.301	0.03987
8000	0.016	0.301	0.05316



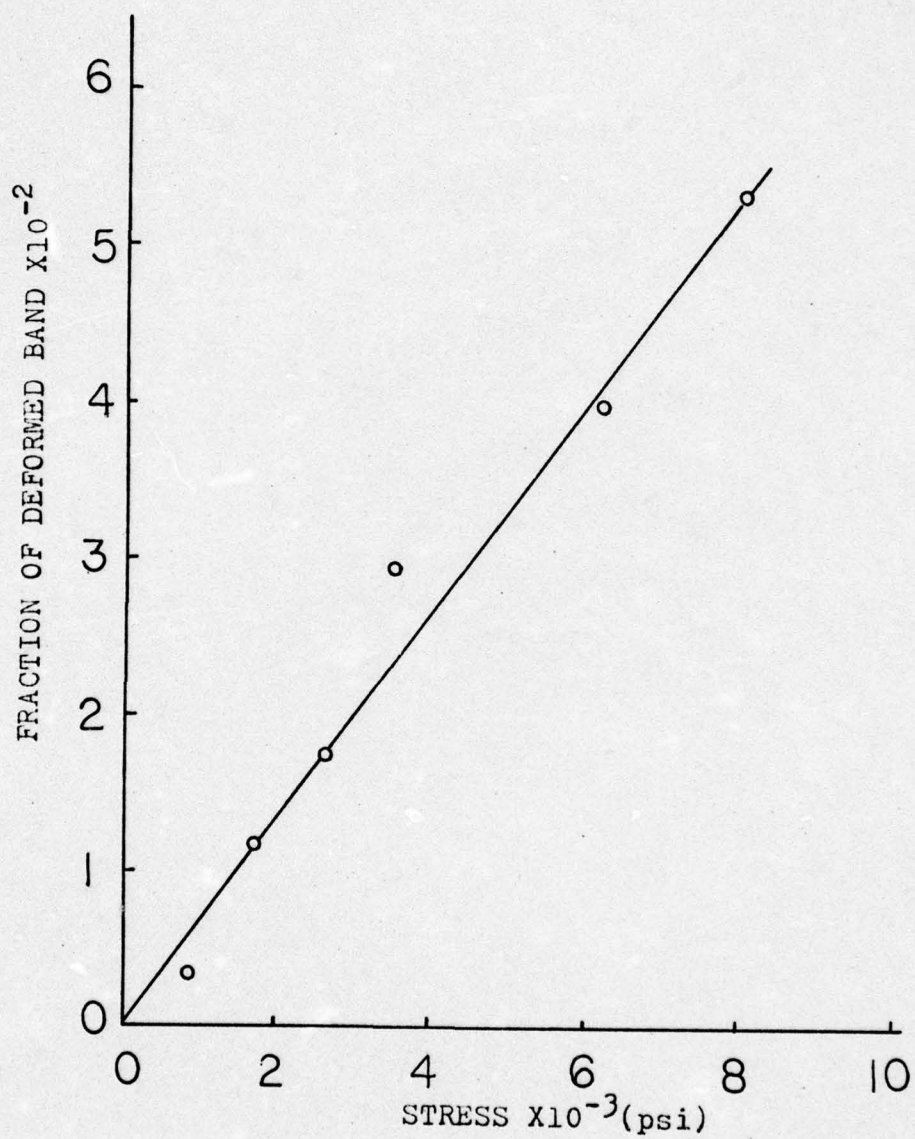


Figure 5.10 Deformed IR band ( $1154\text{ cm}^{-1}$ ) fraction vs. applied stress plot for 4.5 mil thick TRICITE film.

occurs in response to the imposed stress. This causes bulky phenyl side groups on certain chains to interfere with similar groups on the neighboring chains. An increase in stress causes additional chain mobility and, therefore, increased side group interference. Figures 5.8 and 5.9 show that a certain amount of these distortions are non-reversible on removal of stress from the sample. This indicates that, originally, some of the phenyl side groups and certain segments might be frozen-in in unfavorable conformations. Under stress these groups stress-relieve themselves by rearranging to more favorable conformations. As imposed stress is increased, many more side groups undergo such rearrangements. Therefore, even on removal of stress certain IR bands remain partially distorted, indicating non-reversible conformational and configurational rearrangements and a change from the initial molecular state (in the unstressed state). Thus the deformation of  $1154\text{ cm}^{-1}$  IR band toward higher frequency indicates the existence of interphenyl interference and removal of residual (frozen-in) stresses under stress.

An analysis similar to the one conducted for  $1154\text{ cm}^{-1}$  band was performed for  $1182\text{ cm}^{-1}$  IR band which has been assigned by Krimm to  $\nu(\text{cc})$  helix, i.e., carbon-carbon stretch in the helical portion of the polystyrene chain. The analysis of distortions of this band has produced interesting and novel results. Table 5.2 presents data obtained from  $1182\text{ cm}^{-1}$  IR band.

These data have been plotted in Figure 5.11, which indicates that increased numbers of bonds participate or are affected by an increase in stress on the sample. This relationship is almost linear up to a



Table 5.2 Fraction of  $1182\text{ cm}^{-1}$  IR Band Deformation Due to Stress

Figure	Stress (psi)	Area under deformed portion of band (sq.in.)	Area under symmetrical portion of band (sq.in.)	Fraction of deformed band
5.4	888	0.0005	0.127	$3.937 \times 10^{-3}$
5.5	1776	0.0010	0.101	$9.90 \times 10^{-3}$
5.6	2666	0.0025	0.121	$2.07 \times 10^{-2}$
5.7	3555	0.0050	0.116	$4.31 \times 10^{-2}$
5.8	6222	0.0002	0.099	$2.00 \times 10^{-3}$
5.9	8000	0.0003	0.100	$3.00 \times 10^{-3}$

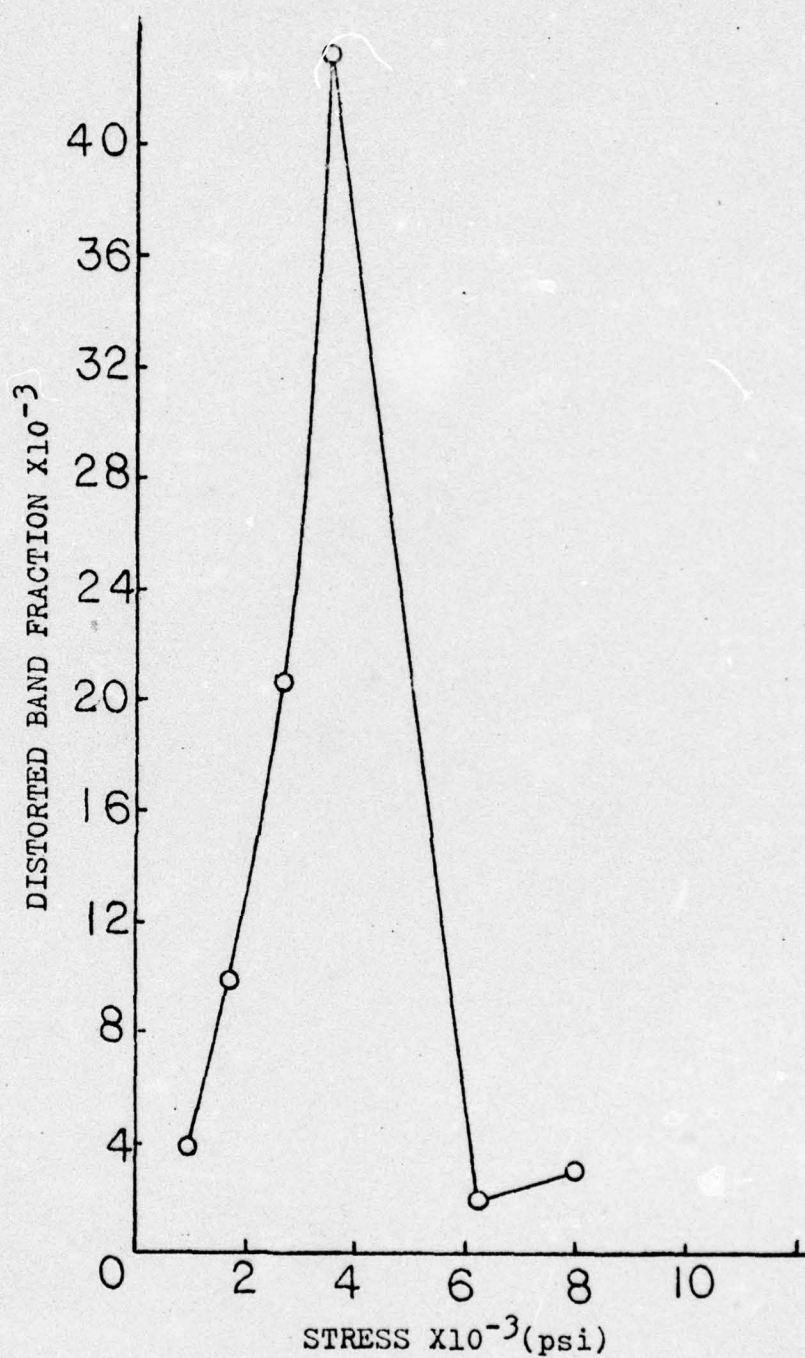


Figure 5.11 Distorted IR band ( $1182\text{ cm}^{-1}$ ) fraction vs. applied stress plot for 4.5 mil thick TRICITE film.



stress level of 3555 psi. Thereafter, the fraction of participating bonds drops off to a smaller fraction, then begins to increase again with increased stress. Since this IR band is assigned to  $\nu(\text{cc})$  in the helical portion of the polymer chain, an attempt to explain this sort of phenomena gives a new concept about the molecular behavior under stress. It appears that certain helical segments of the atactic polystyrene chains begin to bear the stresses and get taut. After they have reached their maximum extendable length, any further increase in stress then causes portions of PS chains to slip, rearrange and possibly break. This leads to a sudden drop in the fraction of affected bands at 3555 psi. Perhaps, a large number of such changes contribute toward the plastic deformation observed in the stress-strain curve of these polymers. This deformation, or the nonlinearity in the stress-strain curve shown in Figure 5.1, begins to show at about 5000 psi. At the molecular level the process seems to begin at an even earlier stress level and a large number of such processes accumulate to show up as a deviation from linearity in the stress-strain curve. Thus, there is a correlation between the molecular behavior under stress and the overall stress-strain behavior of the polymer.

Figures 5.12(a) and (b) illustrate the distortions of IR bands when TRICITE film is subjected to a stress of 7111 psi in transverse direction. These distortions are also observed at various stresses below 7111 psi, but only the distortions at maximum stress level of 7111 psi ( $\sim 70\% \sigma_B$ ) are presented here.

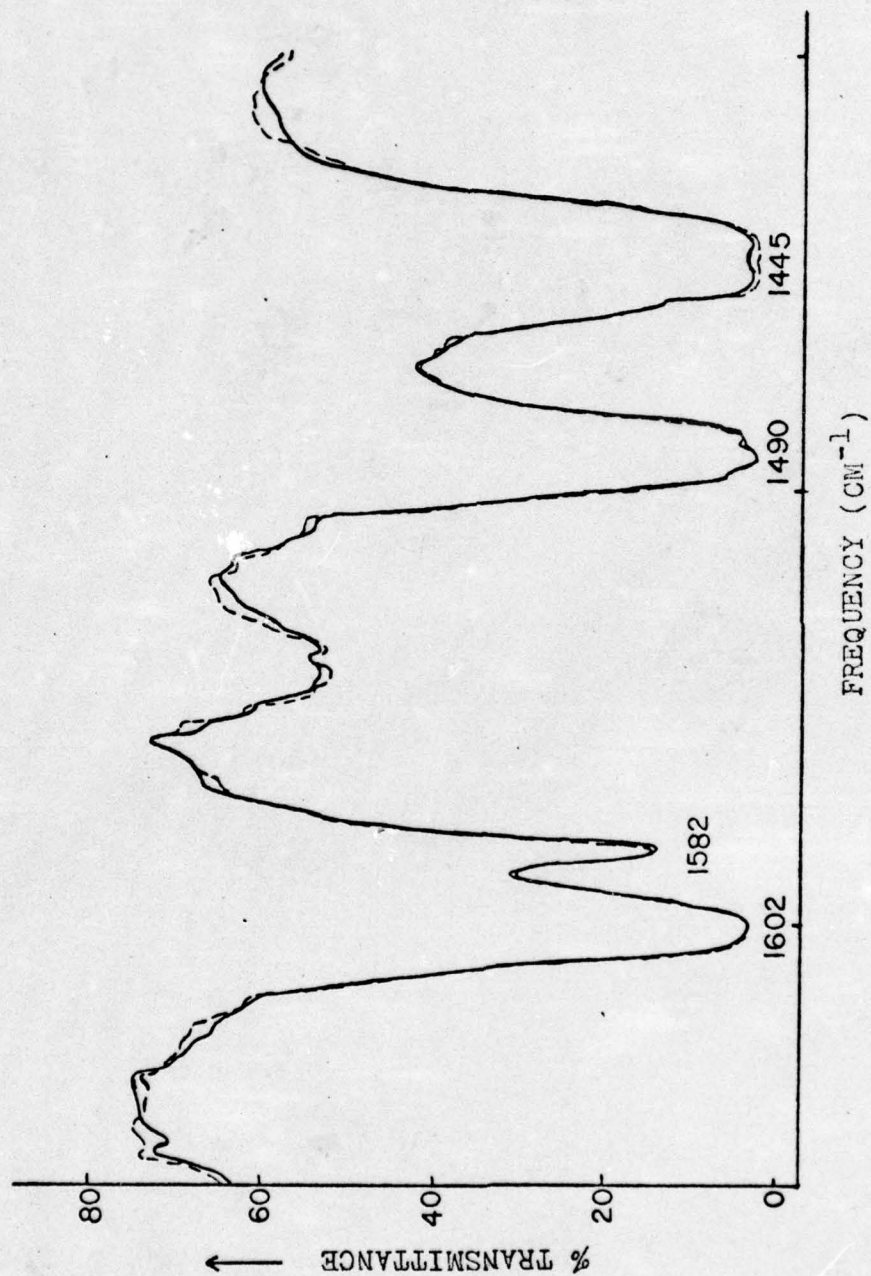


Figure 5.12 (a) IR spectra of 4.5 mil thick TRICITE film under no stress (—) and stress of 7111 psi (---) in the transverse direction.



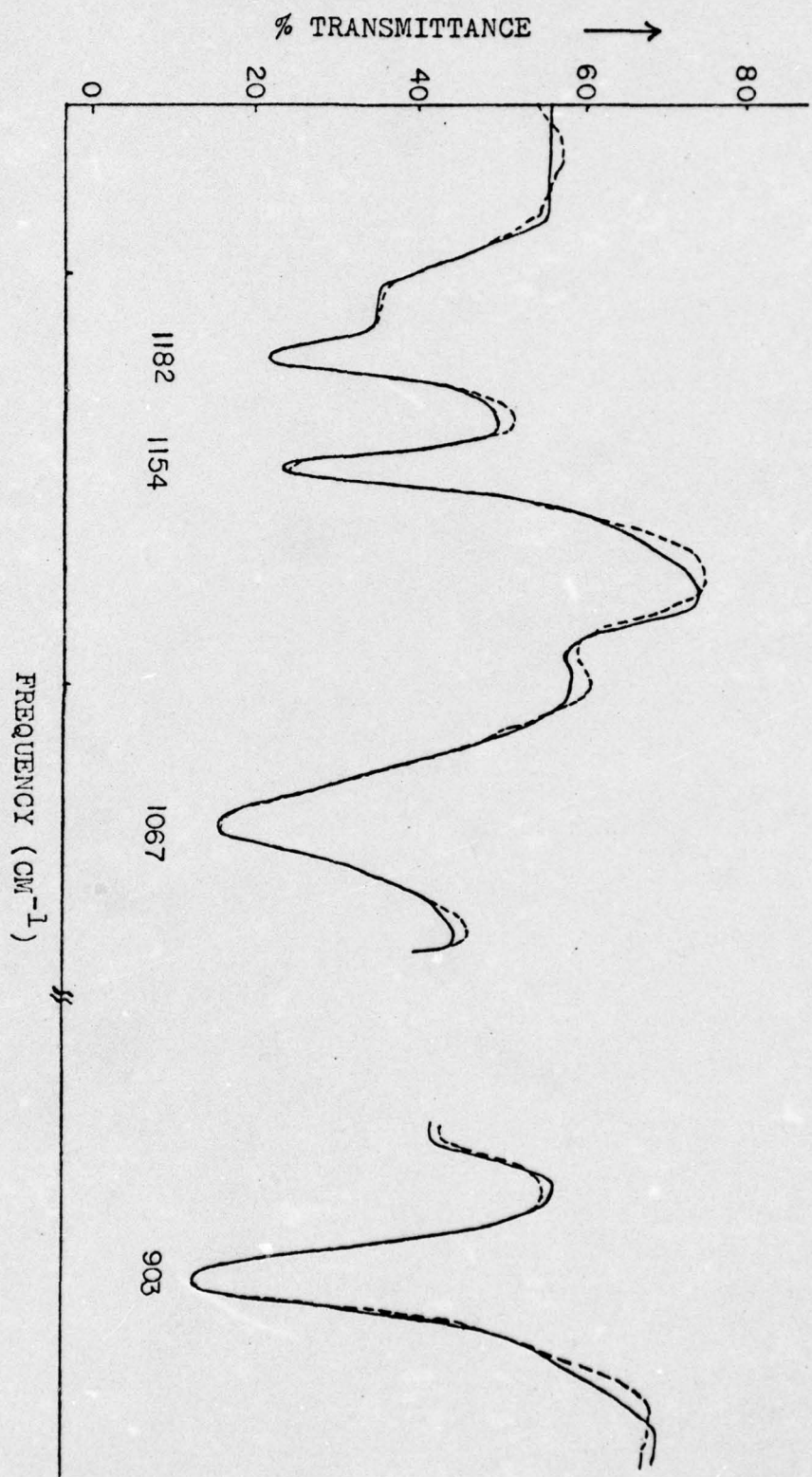


Figure 5.12 (b) IR spectra of 4.5 mil thick TRICITE film under no stress (—) and stress of 7111 psi (---) in the transverse direction.

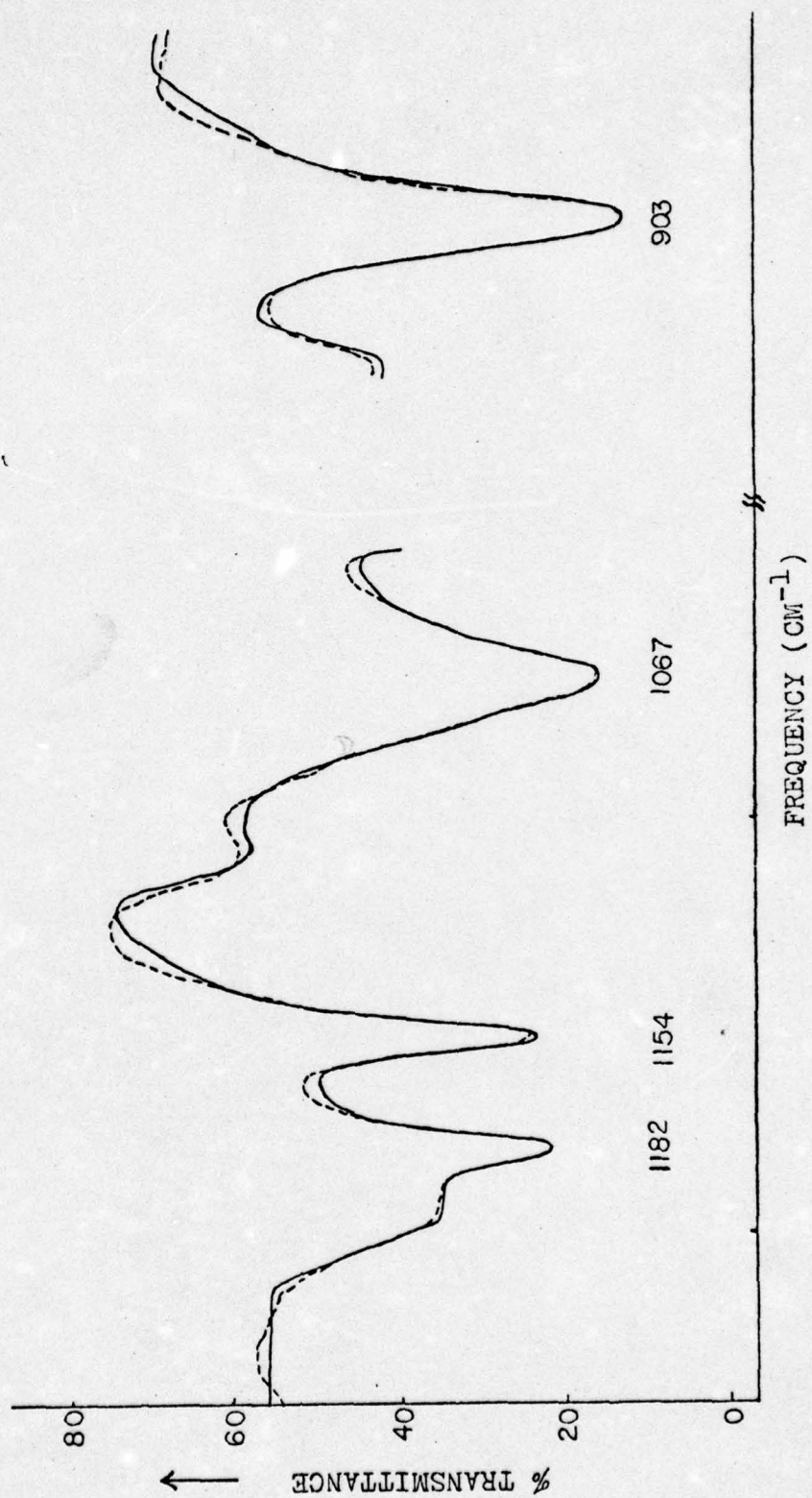


Figure 5.12 (b) IR spectra of 4.5 mil thick TRICITE film under no stress (—) and stress of 7111 psi (---) in the transverse direction.



Figures 5.13(a) and (b) show the IR absorption bands of annealed TRICITE films obtained under no stress and stress of 6666 psi. These films have been annealed under nitrogen atmosphere at 70°C for 45 minutes. Figure 5.13(b) shows that the distortions of the band at  $1154\text{ cm}^{-1}$  are significantly reduced. There is no deformation of the  $1182\text{ cm}^{-1}$  IR band. It appears that the annealing process improves the packing of chains and load is borne by the chains as if they are in a tight bundle.

### 5.1.3 Summary

(a) The orientation of molecular chains along two mutually perpendicular directions appears equal.

(b) The deformation of  $1154\text{ cm}^{-1}$  IR band exhibits a linear relationship with the applied stress, indicating an increase in interphenyl group interference under stress. Such interference appears to arise mostly from stress-relieving of frozen-in stresses in these thick films possessing orientation gradient through their thickness.

(c) Deformation of  $1182\text{ cm}^{-1}$  IR band indicates a linear increase in the number of backbone bonds participating in the load bearing mechanism. But as stress is increased on the sample, the number of such backbone bonds decreases suddenly at a threshold stress of 3555 psi, suggesting breakage of these bonds and/or transfer of stresses to the surrounding chains. Thus, the nonlinearity of the stress-strain curve seems to be related to the bond breakage processes occurring at the molecular level.

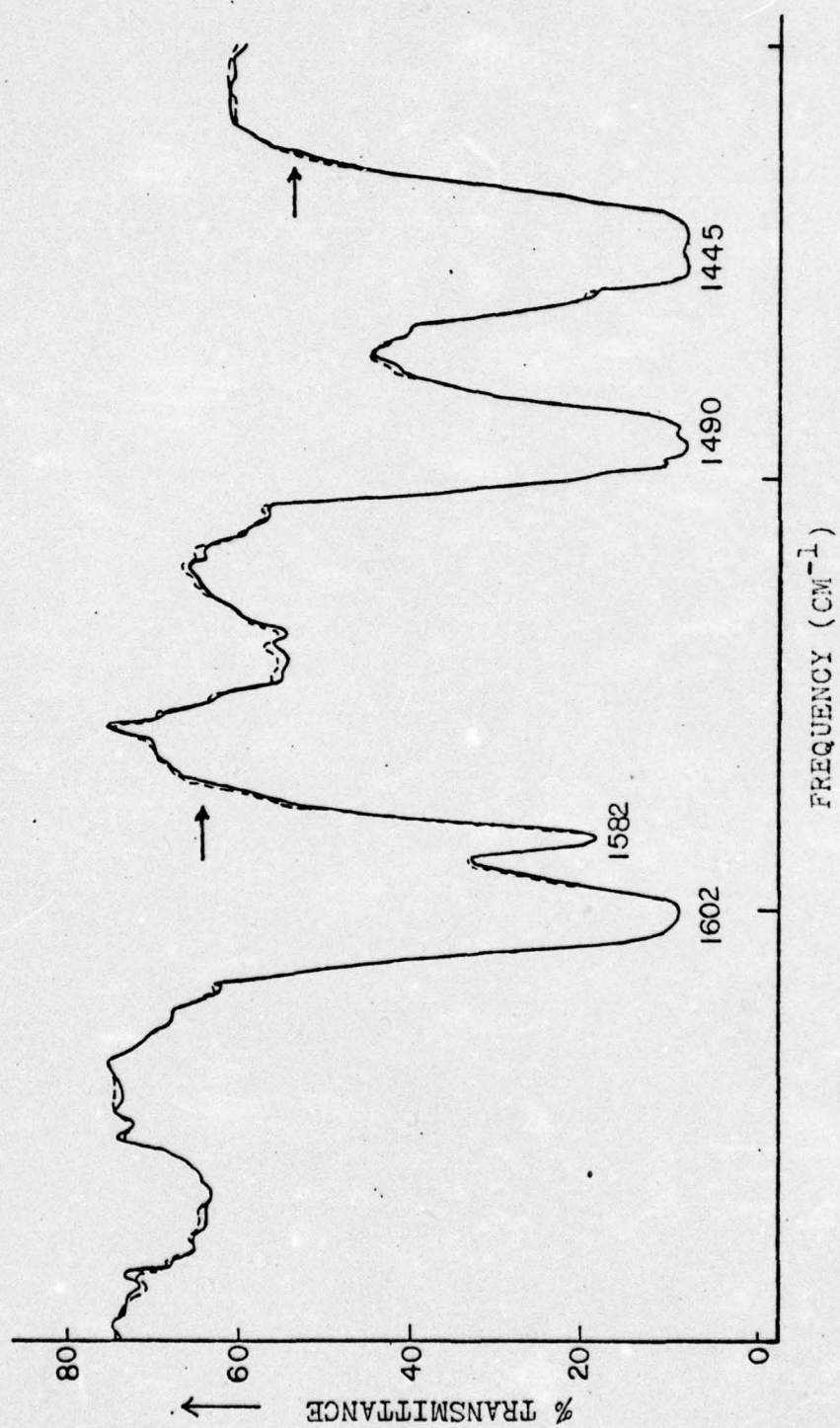


Figure 5.13 (a) IR spectra of 4.5 mil thick annealed TRICITE film under no stress (—) and stress of 6666 psi (---).



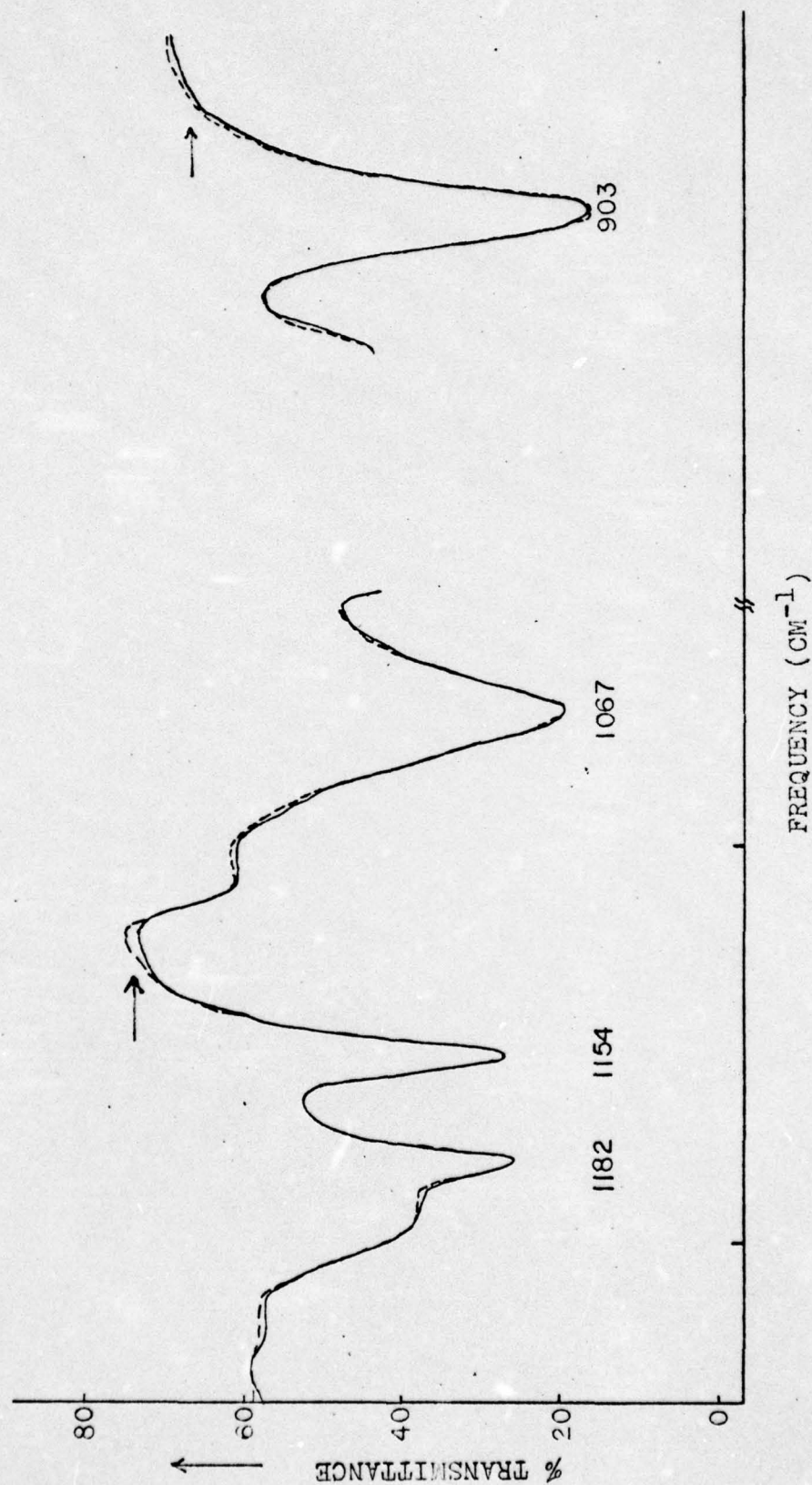


Figure 5.13 (b) IR spectra of 4.5 mil thick annealed TRICITE film under no stress (—) and stress of 6666 psi (---).

(d) Annealing removes the frozen-in stresses and improves the packing of PS chains, causing stresses to distribute over a large number of chains. This results in relatively uniform stress distributions over the backbone bonds. Reduction of  $1154\text{ cm}^{-1}$  band deformation indicates lesser interphenyl interferences in annealed films under stress.

(e) Amount and type of band deformations observed along the two mutually perpendicular directions is about the same.

## 5.2 Results and Discussion: 0.003" Thick TRICITE Film

### 5.2.1 Stress-strain results

Figure 5.14 shows the stress-strain curve for 3 mil thick TRICITE film, which has been studied extensively in the present research. The two strain rates employed to obtain these curves are 2 in/min and 0.05 in/min; the latter corresponds to the strain rate applied during DIR studies. These films are also tested in the transverse direction. The Young's modulus of 3 mil TRICITE film is the same along both directions, indicating almost perfect biaxial orientation. Stress-strain curve in Figure 5.14 shows that at very low strain rates 3 mil TRICITE films behave like tough polymers, undergoing a strain of almost 40% before fracture. This behavior indicates that microstructure in these films must have high free volume which allows the PS chains with bulky phenyl group to slip past one another in response to an imposed stress. This free volume will also help to reduce inter-chain interactions under stress. It has been observed during stress-strain tests that these films form shear-bands before the



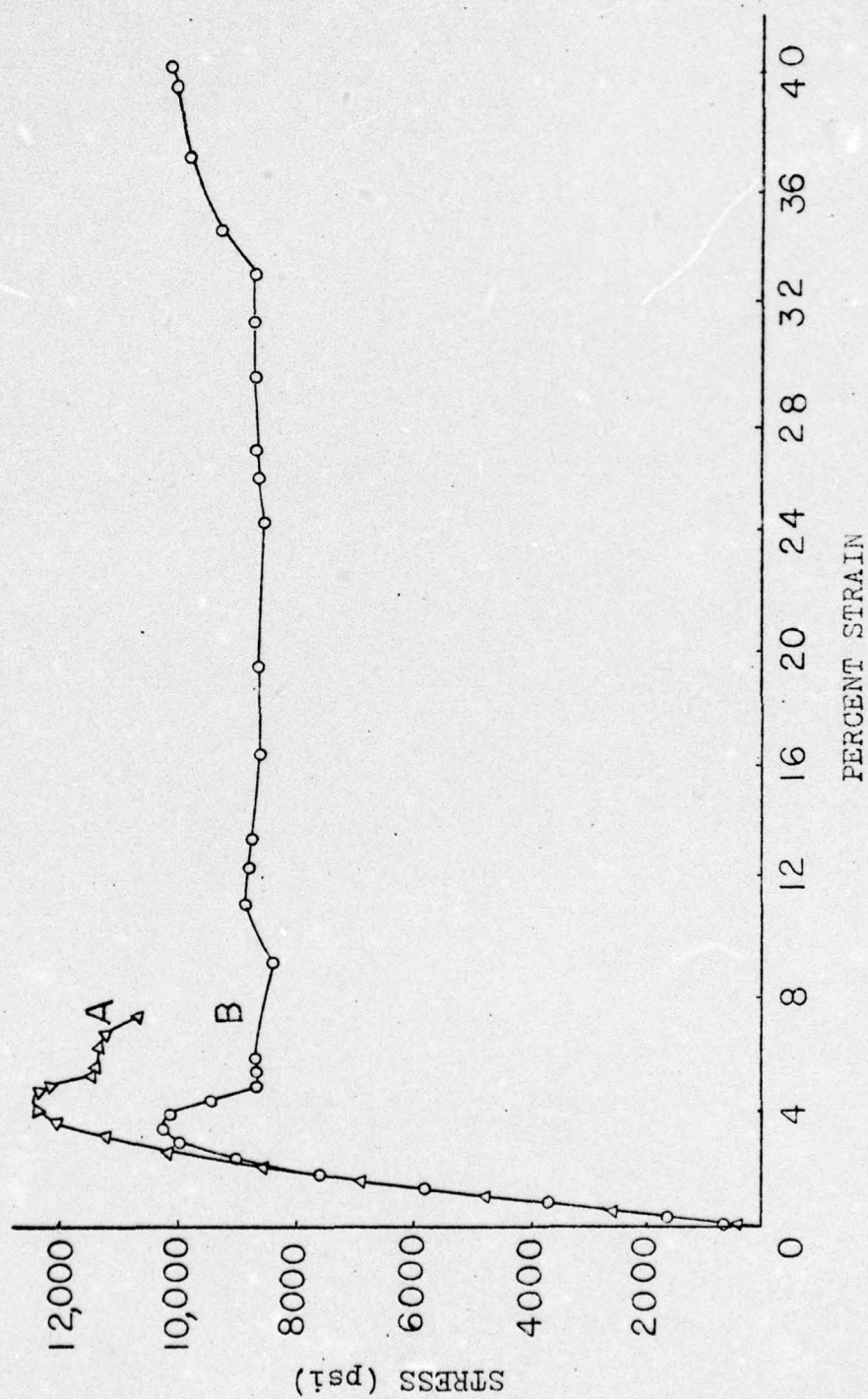


Figure 5.14 Stress-strain curves of 3 mil thick TRICITE films at strain rates of 2 in/min (Curve A) and 0.05 in/min (Curve B). Gage length = 2 inches in both cases.

development of a 'neck' at a stress of about 6700 psi, where the plastic deformation starts and shows up as a nonlinear region on the stress-strain curve.

### 5.2.2 Dynamic IR results

5.2.2.1 Ramp loading. As these films exhibit shear bands at stresses near 6700 psi, they are ramp loaded to ~6333 psi (just below the above mentioned stress level). The IR absorption bands under no stress, stress, and on removal of stress are shown in Figures 5.15(a), (b) and (c). These figures cover the entire infrared spectra of polystyrene. They also include the spectra obtained on reloading the films to the same stress-level after letting them relax for 2 hours. The IR spectra obtained after stressing the same film over again is the same as obtained after stressing the polymers the first time.

Figure 5.15(a) shows a reduction of percent transmittance on loading, indicating that increased numbers of oscillators show absorption. In this figure it is not possible to estimate any shifts of IR bands on stressing or stress-removing. However, there is a positive, though small, increase in transmittance from which we can conclude that the film sample in this test undergoes thickness changes on stressing. On restressing the film the IR spectra recorded is the same as obtained by stressing it the first time. Figure 5.15(b) shows a similar effect in IR bands at 1602, 1582, 1488 and  $1445\text{ cm}^{-1}$ . In addition, an interesting phenomenon is observed in these films, is that on application of stress the IR bands at 1582,  $1445\text{ cm}^{-1}$  distort toward the higher frequency, while on removal of stress the distortions in these bands are toward the low frequency side. This can be described



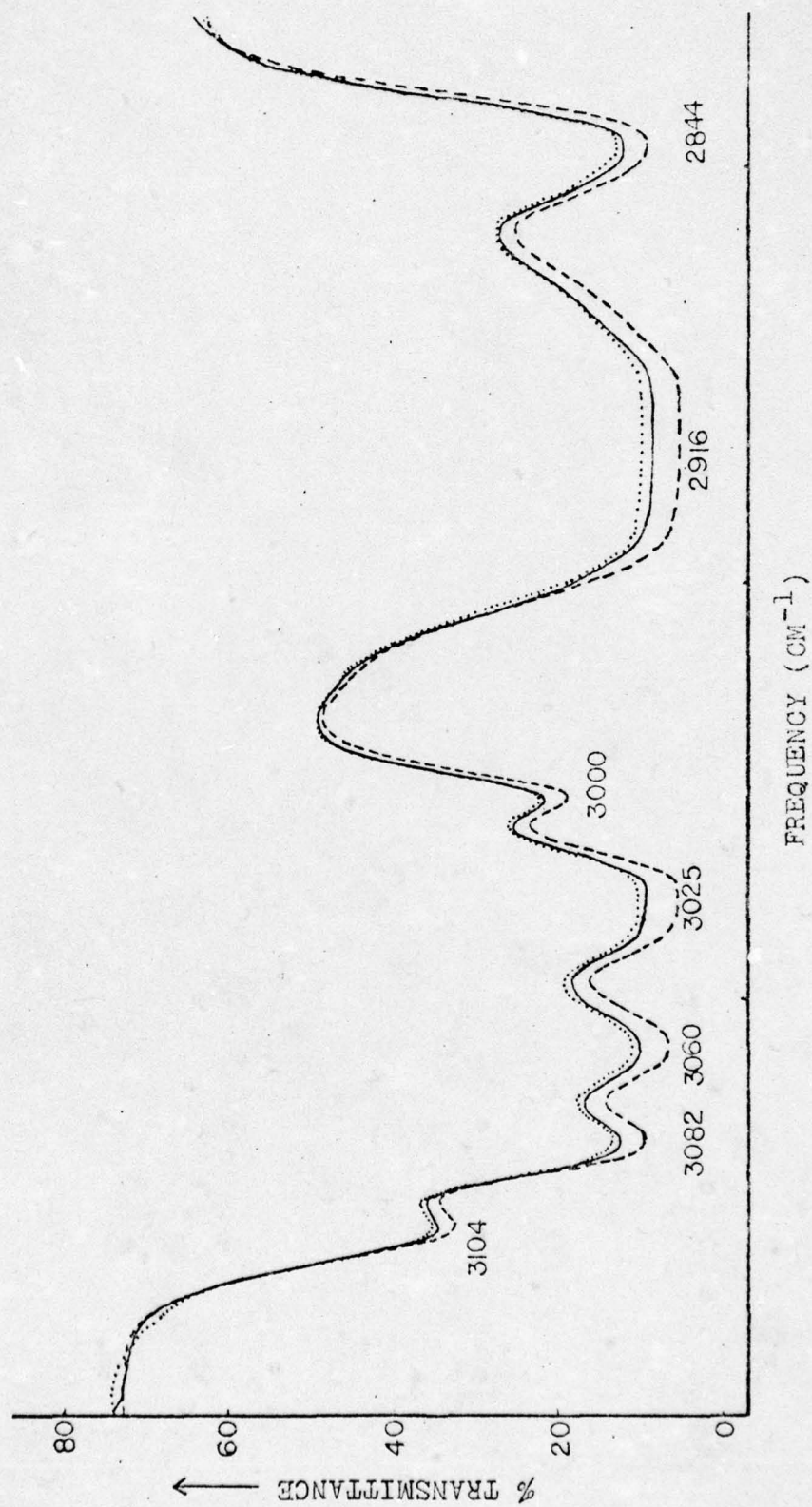


Figure 5.15 (a) IR spectra of 3 mil thick TRICITE film under no stress (—), stress of 6333 psi (---) and on stress removal (...).

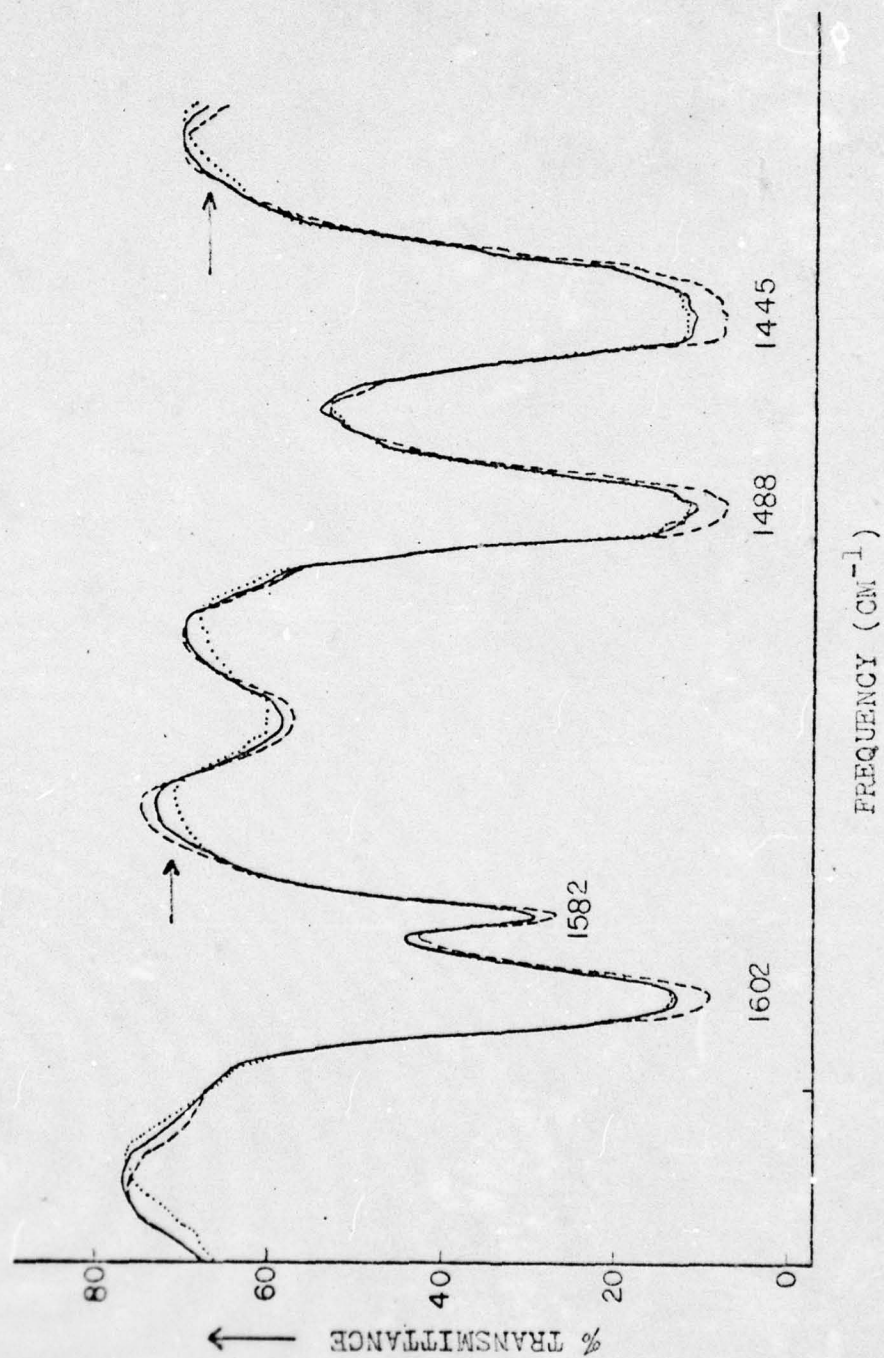


Figure 5.15 (b) IR spectra of 3 mil thick TRICITE film under no stress (—), stress of 6333 psi (---) and on stress removal (....).



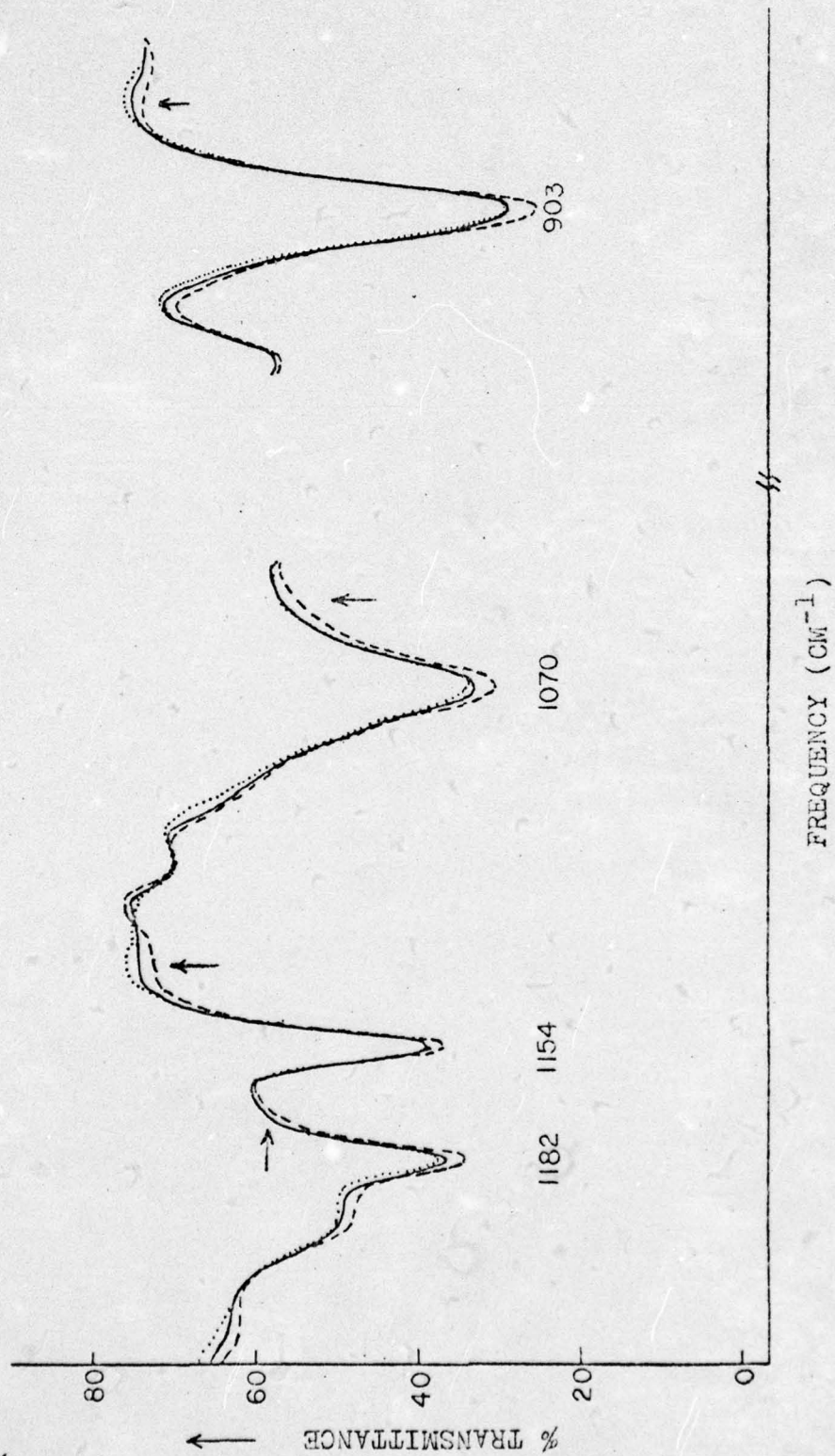


Figure 5.15 (c) IR spectra of 3 mil thick TRICITE film under no stress (—), stress of 6333 psi (---) and on stress removal (...).

in the following manner:

Let initial state of the unstressed TRICITE film be A,

Let initial state of the stressed state of this film be B and

Let initial state of the stress-removed state of this film be C.

The unstressed films show the IR spectra for the polymer in state A. On application of stress the obtained IR spectra corresponds to state B. Removal of this applied stress shows the spectra corresponding to state C, which is difference from state A. On reloading of polymer films to the same stress, the IR spectra obtained corresponds to state B again. On loading and unloading these stressed films a few times, the IR band distortions cycle between state B and C, respectively, as mentioned above. This observation implies that the initial state of the polymer at the molecular level is changed permanently on the very first loading.

A molecular explanation of this behavior is that initially (in the unstressed state) some PS chain segments with bulky side groups are frozen-in in conformationally unstable states and some segments are physically entangled. On stressing the films, polymer chains become somewhat mobile and by such chain movements some of the unstable conformations rearrange to stable ones, while some of the entangled PS chains move about and rearrange to pull themselves out. Few such entangled chains manage to pull out while the badly entangled ones are broken during the process. Since such molecular processes are irreversible at our test conditions, the IR spectra obtained on removal of the stress is different than the one observed before application of



stress--the first time.

Figure 5.15(b) shows occurrence of A, B and C states for the IR bands at 1582 and 1448  $\text{cm}^{-1}$ . 1582  $\text{cm}^{-1}$  is assigned to the vibrations of the carbon ring while 1448  $\text{cm}^{-1}$  band is assigned to the bending modes of  $\text{CH}_2$  group and also to ring vibration modes. Deformation of both of these bands indicates extensive interferences of the bulky phenyl side group on the PS chains. The distortions of 1448  $\text{cm}^{-1}$  band occurs at low frequency side of the band, i.e., about 1440  $\text{cm}^{-1}$ , corresponding to the changes in absorption frequency of the  $\text{CH}_2$  group bending modes. These vibrational motions are expected to be affected by any changes in the internuclear distance of C-C backbone bonds, i.e., the deformation of 1448  $\text{cm}^{-1}$  band is due to intramolecular interaction. Since bending modes of  $\text{CH}_2$  groups are affected by the stress, these changes should also show up in symmetric-- $\nu_s(\text{CH}_2)$ --and asymmetric-- $\nu_a(\text{CH}_2)$  stretching modes, absorbing at 2851 and 2923  $\text{cm}^{-1}$ , respectively. Looking at these bands in Figure 5.15(a), no obvious changes are observable. However, it is quite likely that any such changes are too small to be seen in the superimposed spectra and these deformations may actually be observed through FTIR 'computer-subtracted' spectra, which can plot even the minute changes in the absorption frequencies. These FTIR 'subtraction' spectra are actually obtained and do show the stress effect on the above mentioned bands. FTIR results are explained in detail in a later section.

Figure 5.15(c) shows distortions in 1154  $\text{cm}^{-1}$  band occurring toward lower frequency on stressing and toward higher frequency on stress-removal. This behavior of 1154  $\text{cm}^{-1}$  band is different than the

one observed for this band in the case of 0.0045" thick TRICITE film. This difference can be ascribed to different kinds of interchain interactions taking place in these two types of films. This behavior is actually expected on the basis of a quite different type of stress-strain response of the two films at low strain rates. An observation of state C for  $1154\text{ cm}^{-1}$  IR band indicates that in these films, too, some frozen-in stresses are removed on loading the very first time. The band at  $1070\text{ cm}^{-1}$  also shows some distortions on the low frequency side.

Since  $1070\text{ cm}^{-1}$  IR band is a combination band of CH stretching of the phenyl ring and C-C stretching mode of backbone chain, the frequencies of both vibrational modes are affected to some extent. This, along with the observed deformation of  $1154\text{ cm}^{-1}$  band, point toward the dominant role of phenyl side groups in the stress bearing processes of the polystyrene chains.

5.2.2.2 Step loading. As 3 mil TRICITE films shear-band above 6000 psi and these shear-bands develop into a neck, leading to drawing of these films, a load-elongation behavior is recorded concurrently with the recording of infrared spectra. Figure 5.16 illustrates the load-elongation behavior of 3 mil film at various stress levels in a step loading process. It may be mentioned here that the films do creep, even though only slightly, at both 4000 psi and 6000 psi. This behavior supports our findings reported for 3 mil TRICITE films under ramp loading. The creep seen here, even at low stresses, is a result of the chain mobility, rearrangement of segments and breakage



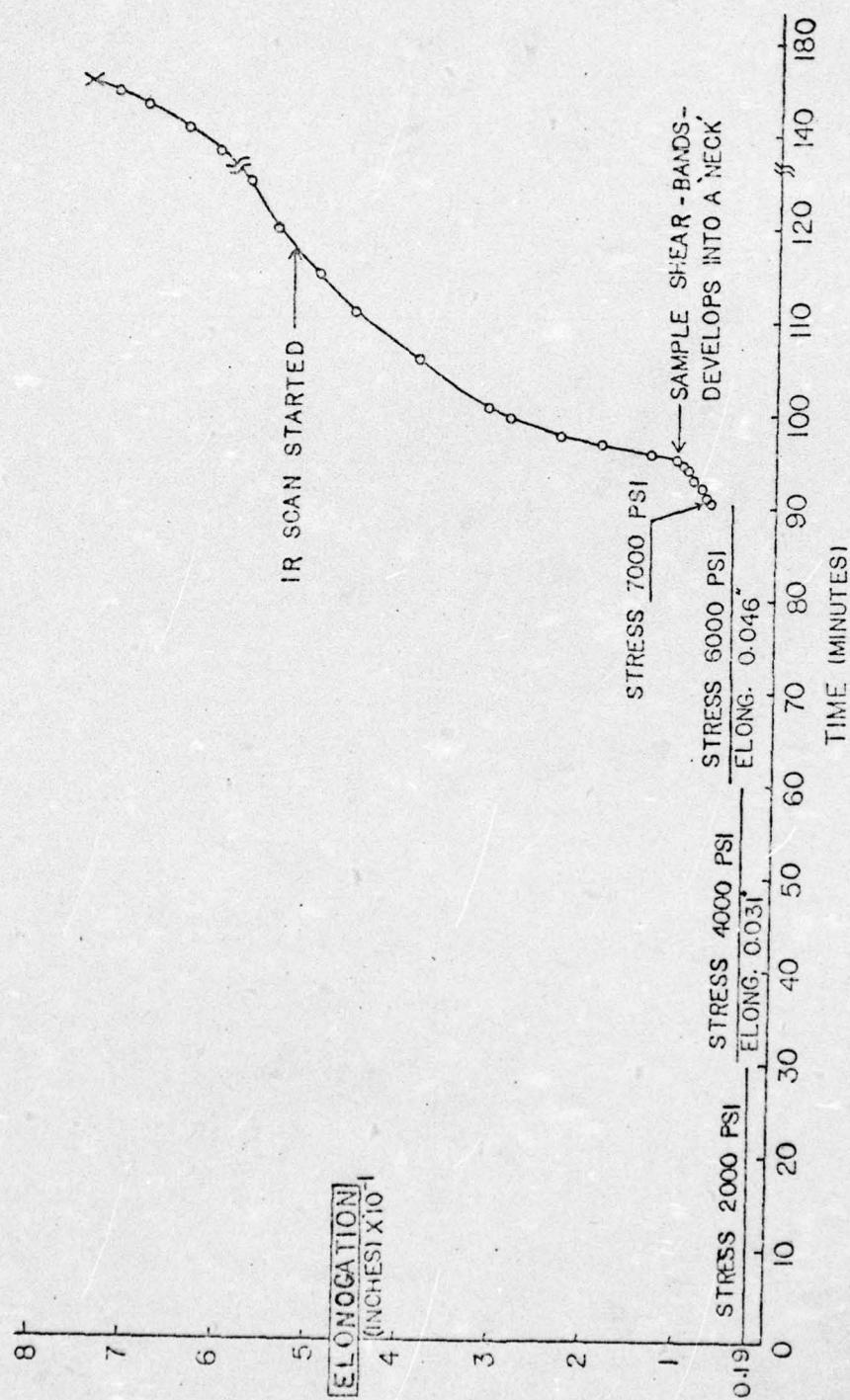


Figure 5.16 Load-elongation behavior of 3 mil thick TRICITE film at various stress levels applied in steps during the IR scans.

of taut chains under stress, causing redistribution of the imposed stress. At higher stresses, above 7000 psi, shear bands form which develop into a full-fledged neck and these films behave like a tough polymer.

Figure 5.17(a) and (b) show the IR absorption bands at no stress and stress of 2000 psi. The low frequency distortions are observable in the IR bands at 1602, 1545, 1488 and 1448  $\text{cm}^{-1}$ . Figure 5.17(b) shows almost negligible deformation of 1182  $\text{cm}^{-1}$  band, assigned to  $\nu(\text{C-C})$  helix. The deformation of 1154  $\text{cm}^{-1}$  band is quite distinct while 1072  $\text{cm}^{-1}$  band shows no deformation.

Figure 5.18(a) shows that distortions of 1582, 1545, 1488 and 1448  $\text{cm}^{-1}$  bands increase as the stress on the film is increased to 4000 psi. Figure 5.18(b) again shows quite small deformation of 1182  $\text{cm}^{-1}$  band, even at 4000 psi. Deformation of 1154  $\text{cm}^{-1}$  also increases on increasing the stress. The 1072  $\text{cm}^{-1}$  band too shows minor distortions on the low frequency side.

Figure 5.19(a) shows that 1582, 1545, 1488 and 1448  $\text{cm}^{-1}$  IR bands are further deformed on increasing the stress to 6000 psi. At this stress the deformation of 1182  $\text{cm}^{-1}$  IR band also become noticeable while the deformation of 1154  $\text{cm}^{-1}$  band further increases. Minor deformation of 1072  $\text{cm}^{-1}$  is also observed (Figure 5.19 (b)).

As seen in Figure 5.16, an application of additional stress of 1000 psi causes films to form shear-bands. On maintaining this additional stress on the film, shear-bands develop into a neck causing the films to draw extensively. This drawing process reduces the thickness of the film, thereby increasing the transmittance of the infrared



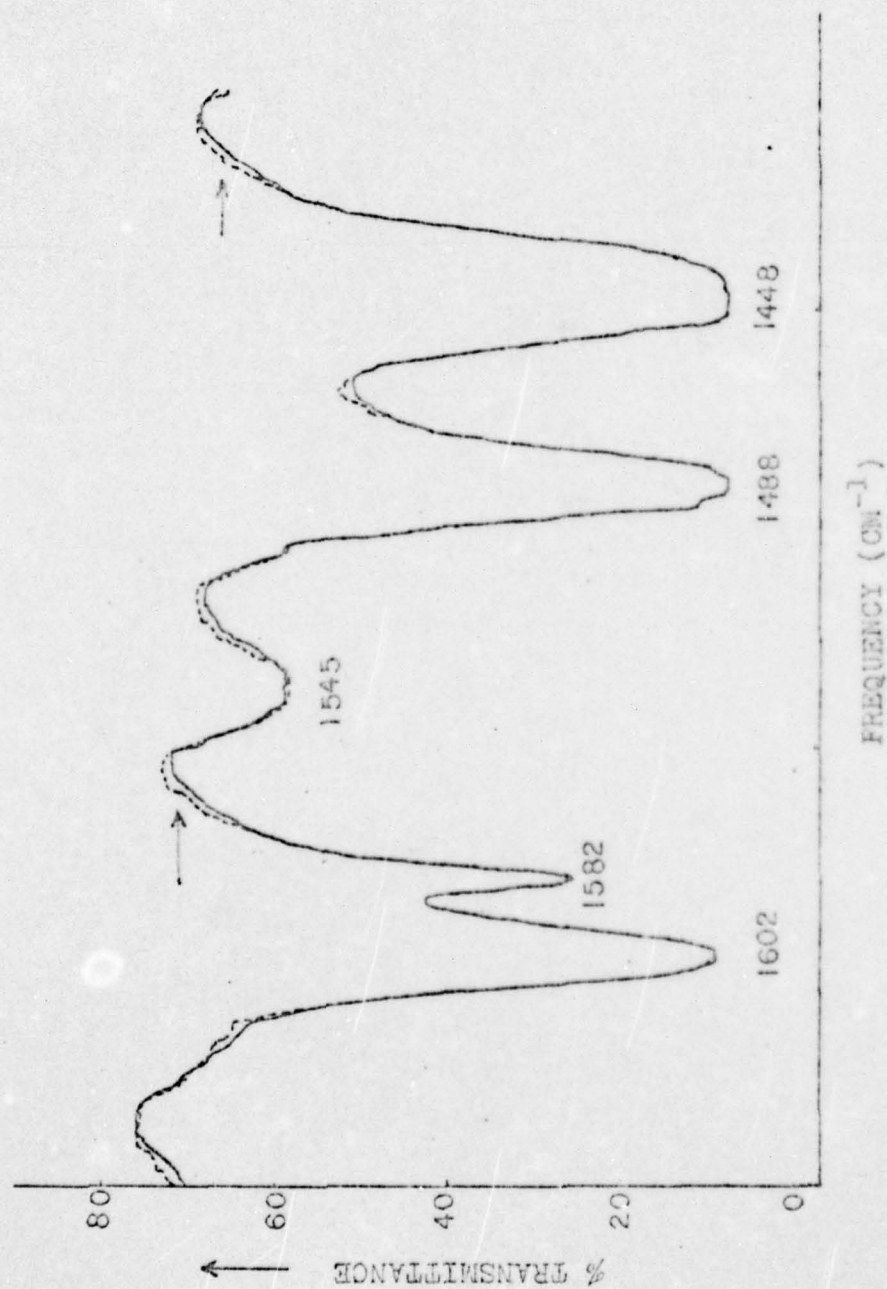


Figure 5.17 (a) IR spectra of 3 mil thick TRICITE film under no stress (—) and stress of 2000 psi (---).

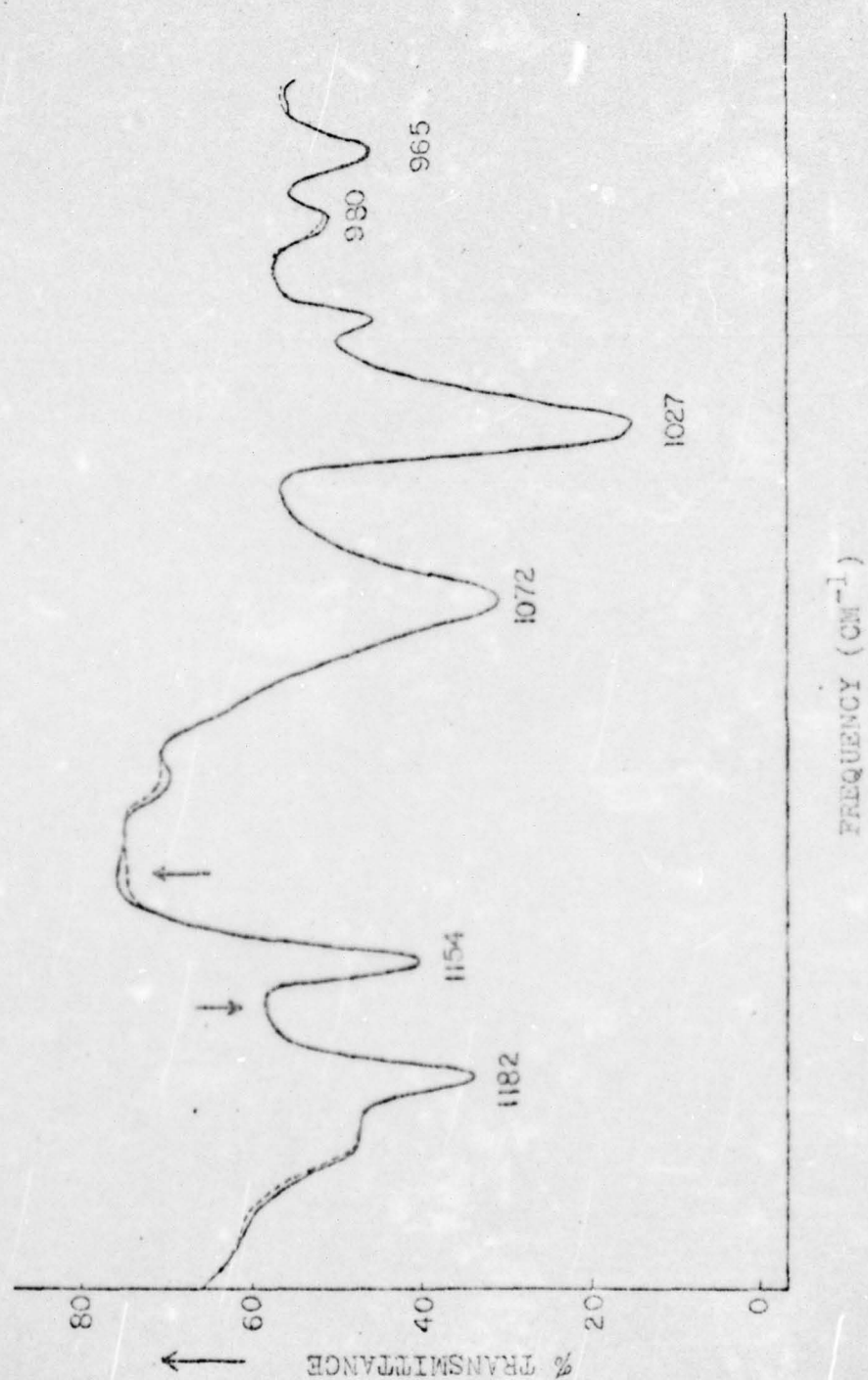


Figure 5.17 (b) IR spectra of 3 mil TRICITE film under no stress (—) and stress of 2000 psi (---).



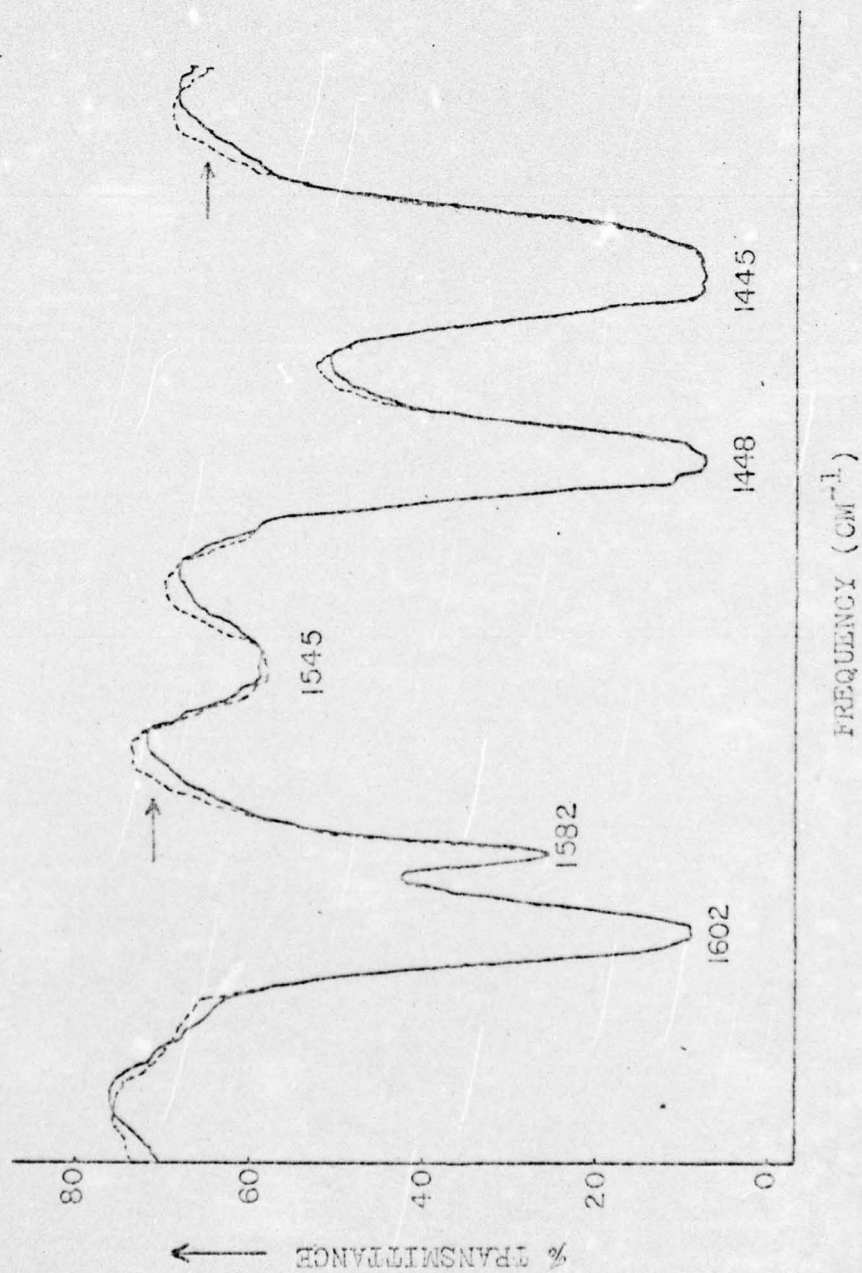


Figure 5.13 (a) IR spectra of 3 mil thick TRICITE film under no stress (—) and stress of 4000 psi (---). Stress increased on the previously stressed sample.

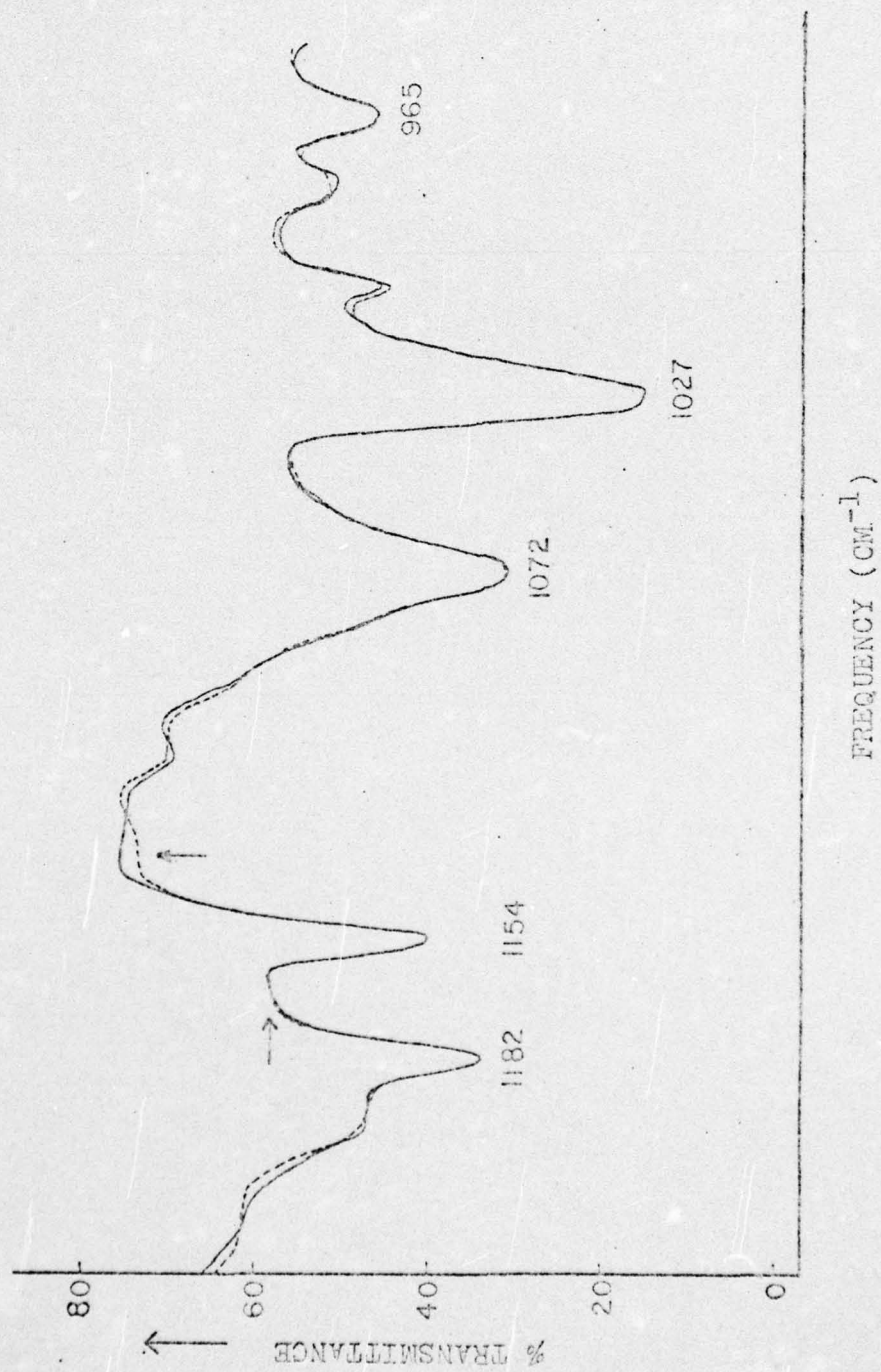


Figure 5.18 (b) IR spectra of 3 mil thick TRICITE film under no stress (—) and stress of 4000 psi (---). Stress increased on the previously stressed sample.



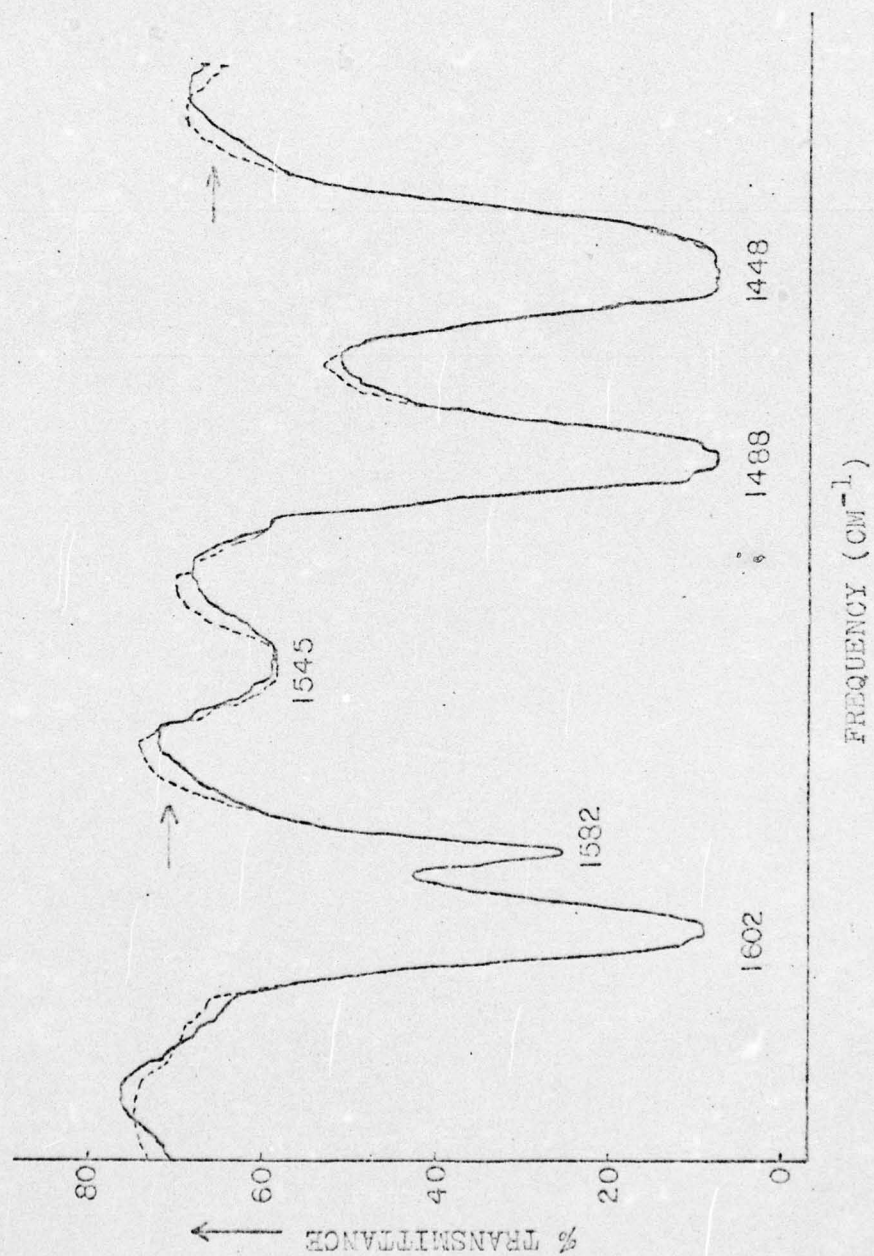


Figure 5.19 (a) IR spectra of 3 mil thick TRICITE film under no stress (—) and stress of 6000 psi (---). Stress is further increased on previously stressed sample.

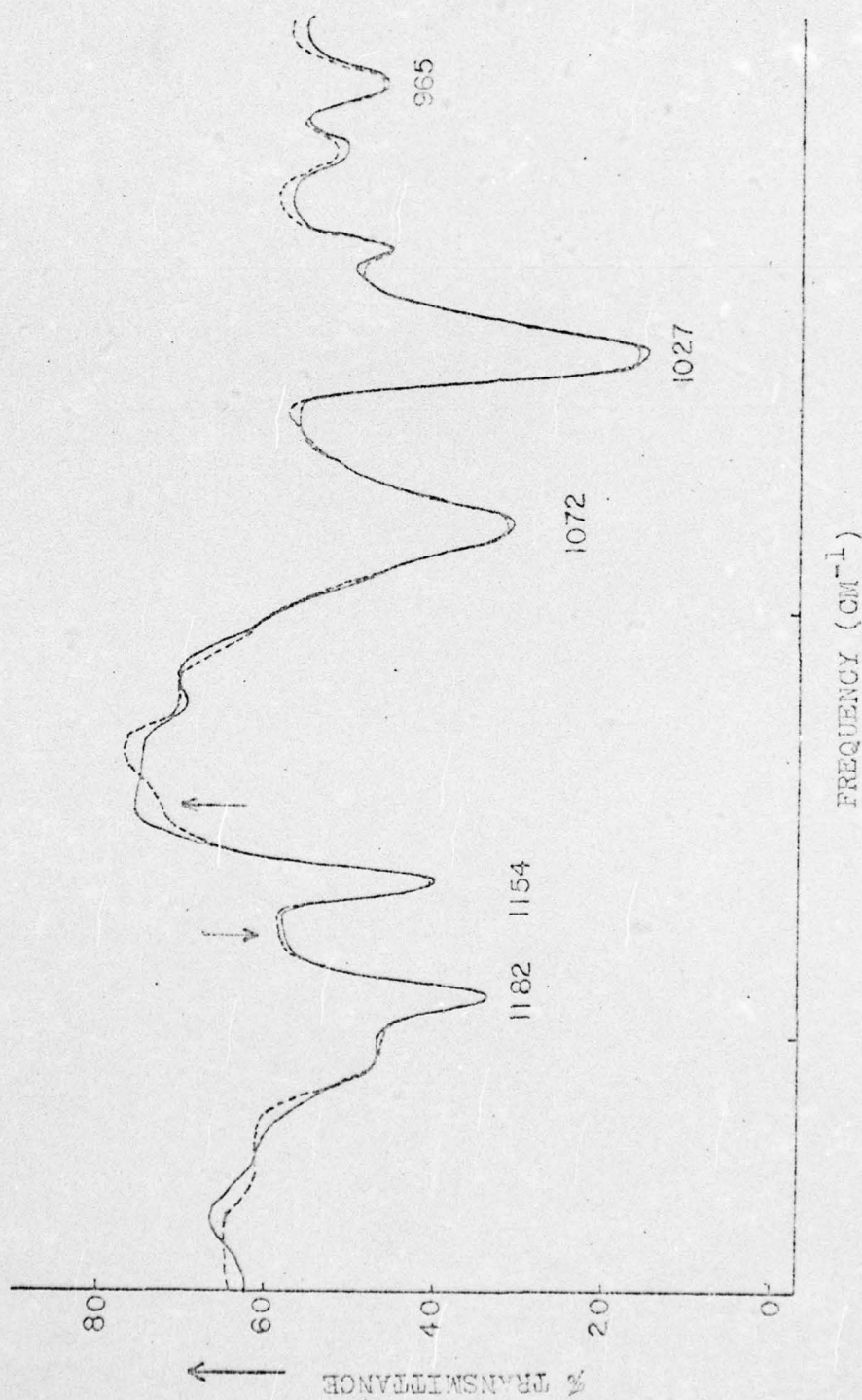
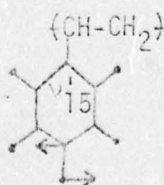


Figure 5.19 (b) IR spectra of 3 mil thick TRICITE film under no stress (—) and stress of 6000 psi (---). Stress is further increased on previously stressed sample.



bands. Therefore, it is not possible to exactly superimpose the IR bands obtained under no stress and understress. Nevertheless, by comparing these bands one can acquire a qualitative information about the band distortions. With this purpose in mind spectra obtained during the creep process at a strain of about 27% and an engineering stress of 10,000 psi are shown in Figures 5.20(a) and (b), respectively. The band deformations of 1582, 1545, 1488, 1448, 1182 and 1154  $\text{cm}^{-1}$  IR bands are quite obvious. It is not possible to make out whether 1072  $\text{cm}^{-1}$  band deforms or not.

From the results shown in Figures 5.17 to 5.20 it is evident that most of the changes observed in IR bands are related to various vibrational modes of the phenyl ring. These changes appear to have been caused by the interferences between the phenyl groups on the neighboring chains and between phenyl groups and the main chain atoms on the adjacent chains. The 1154  $\text{cm}^{-1}$  band in Figures 5.17 through 5.20 shows continuous increase in its distortions with an increase in stress on the film sample. This illustrates the increase of interchain interactions. This band is assigned to the bending modes of C and H atoms in the phenyl ring as shown below:



$B_1$ , bending mode of benzene ring

AD-A035 474

UTAH UNIV SALT LAKE CITY DEPT OF MATERIALS SCIENCE --ETC F/6 7/3  
MOLECULAR BEHAVIOR STUDIES OF GLASSY POLYMERS UNDER STRESS.(U)  
NOV 76 W O STATTON

AF-AFOSR-2827-75

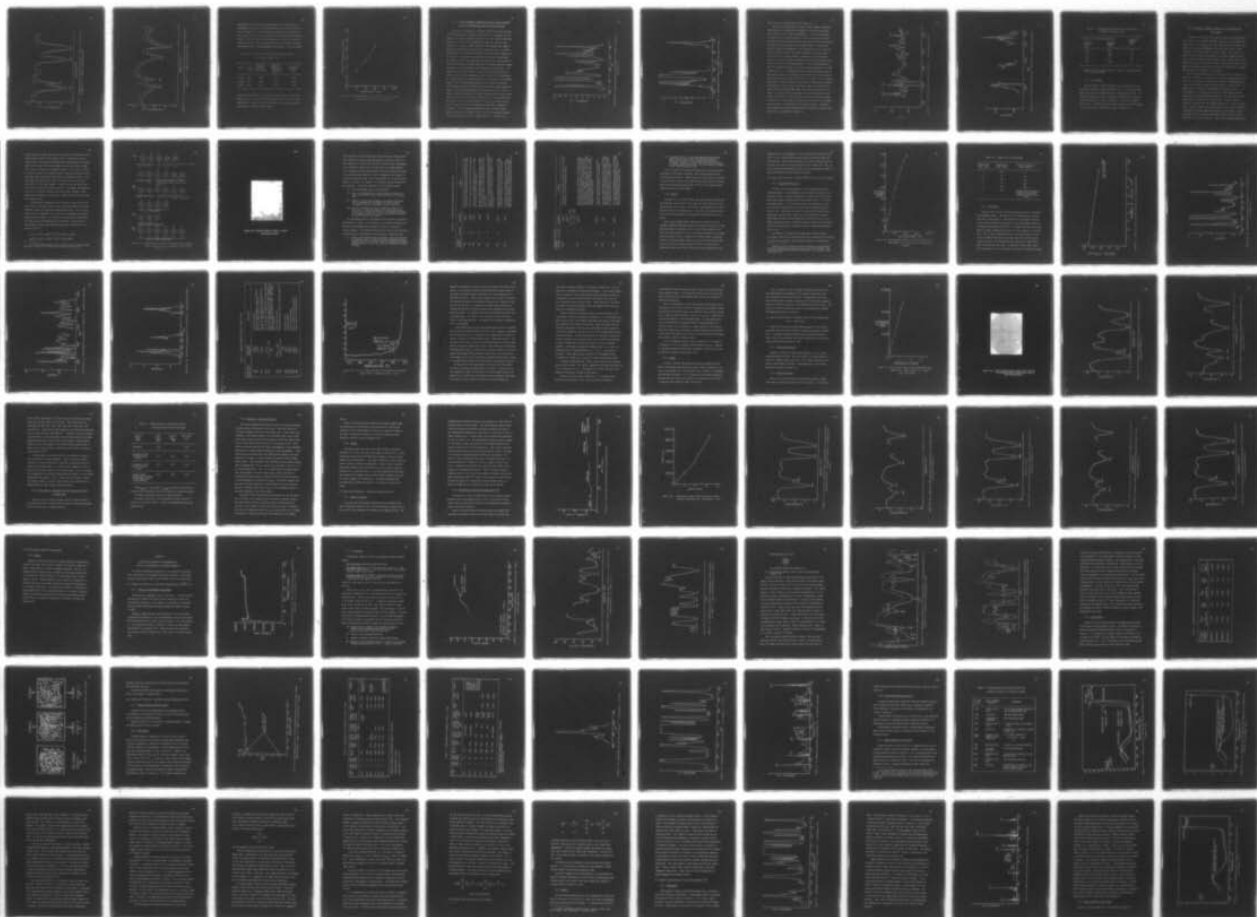
UNCLASSIFIED

UTEC-76-274

AFOSR-TR-77-0047

NL

3 OF 4  
AD A035474







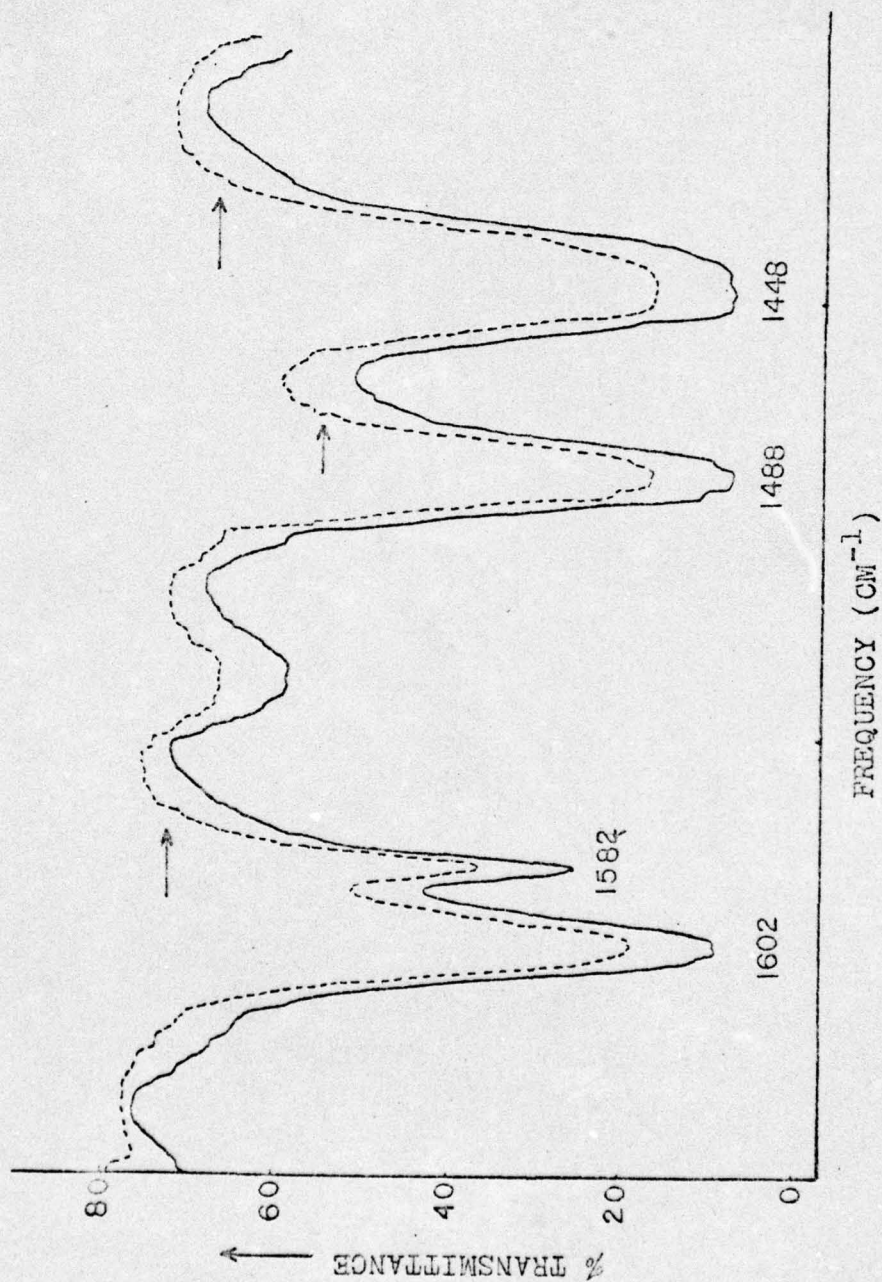


Figure 5.20 (a) IR spectra of 3 mil thick TRICITE film under no stress (—) and stress of 10000 psi (---). Sample is strained up to 27%.



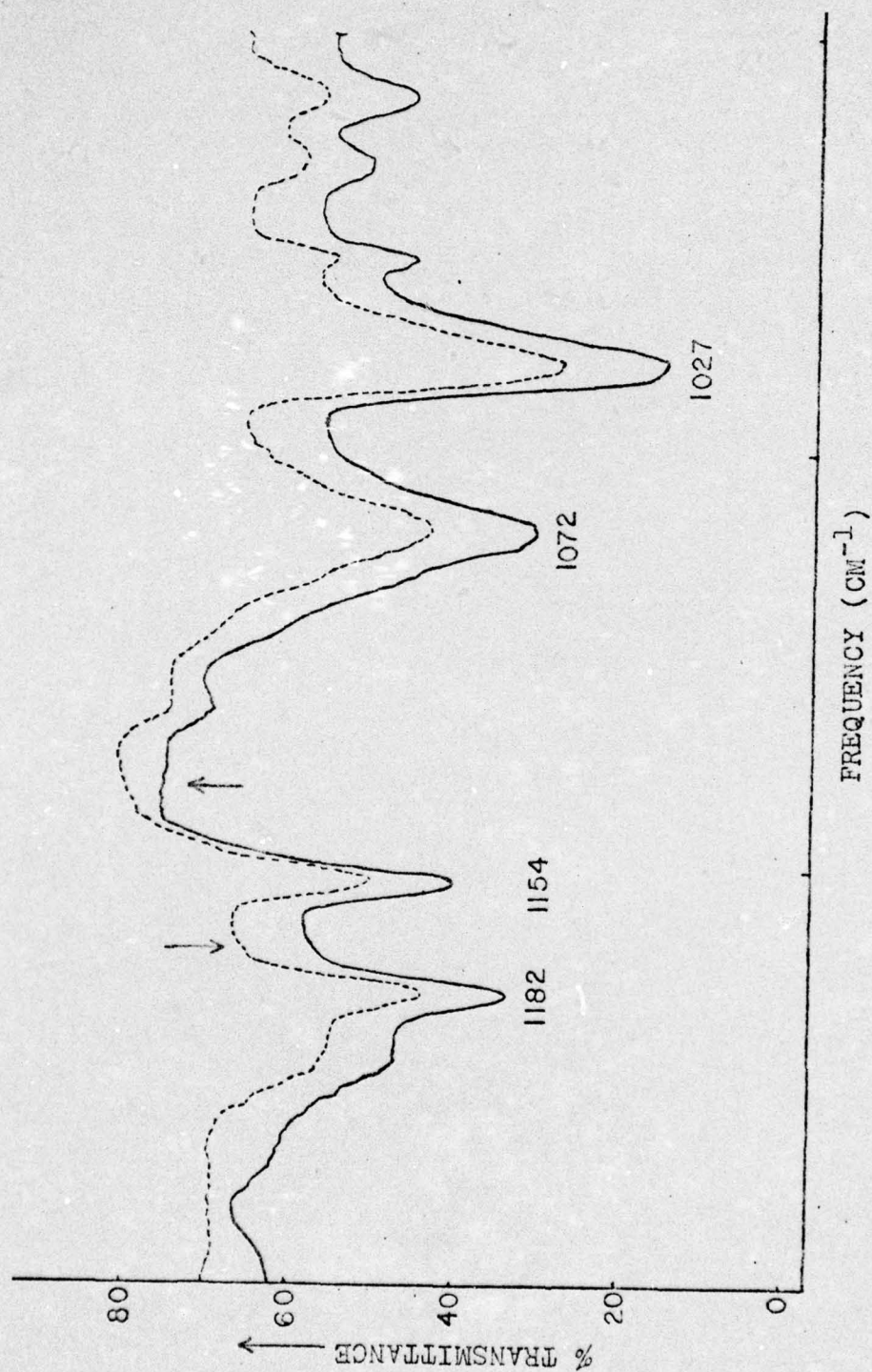


Figure 5.20 (b) IR spectra of 3 mil thick TRICITE film under no stress (—) and stress of 10000 psi (---). Sample is strained up to 27%.

When polymer chains move about, phenyl groups will interact with neighboring chains which will affect mostly the para position of the ring. Frequencies of various vibrational modes due to this part of the ring are expected to show a shift in the IR spectra obtained under stress. Table 5.3 below lists the measured area under the distorted portion of the band, area of complete band and calculated fraction of the distorted band. Area measurements were made by a polar planimeter.

Table 5.3 Fraction of  $1154\text{ cm}^{-1}$  IR Band Deformation Due to Stress on TRICITE Film

Figure	Stress (psi)	Area Under Distorted Portion of Band (sq in)	Area Under Symmetrical (Undeformed) IR Band (sq in)	Fraction of Deformed Band
5.17(b)	2000	0.005	0.151	0.033
5.18(b)	4000	0.009	0.155	0.058
5.19(b)	6000	0.013	0.149	0.087

Fraction of deformed band vs. stress has been plotted in Figure 5.21. Here again (as in  $1154\text{ cm}^{-1}$  band for 0.0045" TRICITE film), the band deformation is linearly related to the stress, indicating increase in the interchain interactions with stress.



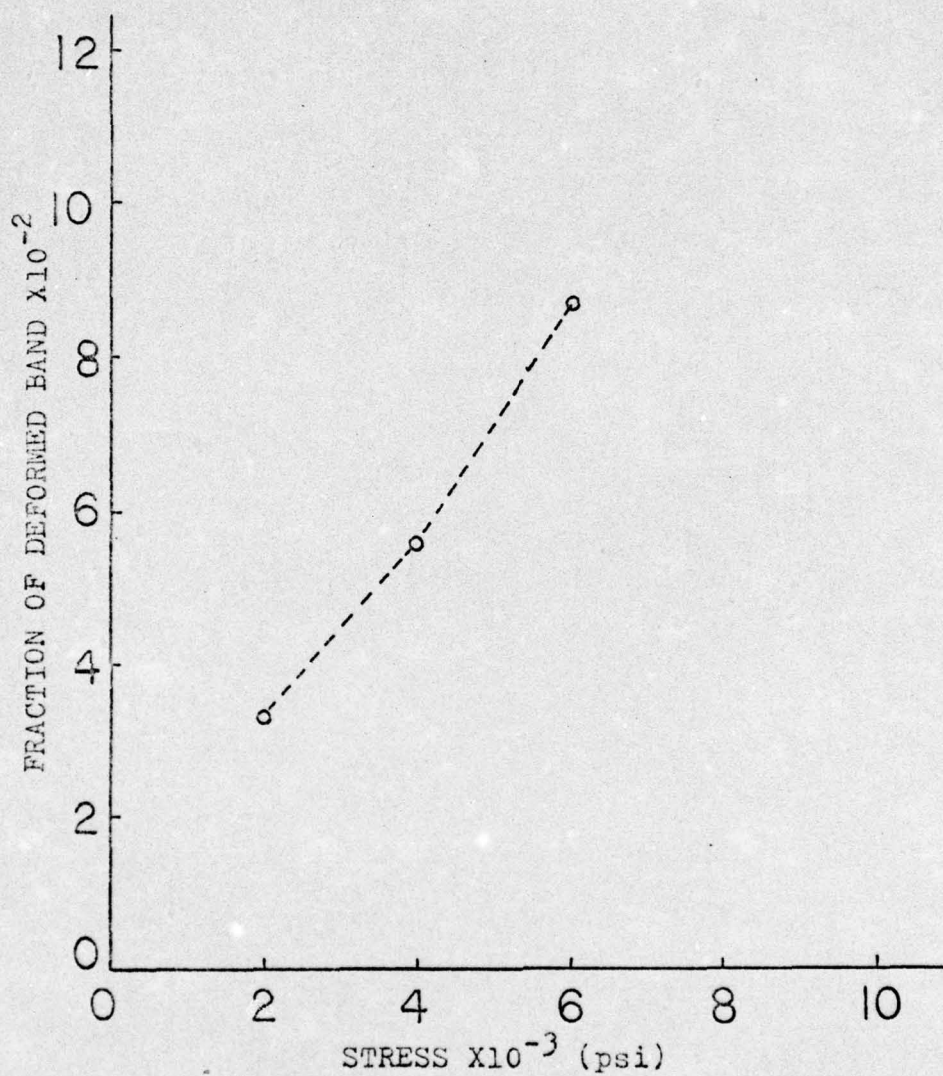


Figure 5.21 Deformed IR band ( $1154\text{ cm}^{-1}$ ) fraction vs. applied stress plot for 3 mil thick TRICITE film.

### 5.2.3 Fourier transform infrared spectroscopy results obtained from 3 mil TRICITE films under no stress and stress

IR spectra of unstressed and stressed TRICITE films were obtained on FTIR spectrometer and stored in the memory of its computer for the purpose of plotting subtraction spectra. The 3 mil TRICITE films were strained up to 3.5%, which related to a stress of  $\sim 9000$  psi from Figure 5.14. However, actual stress will vary somewhat from 9000 psi because of differences in strain rate in these two cases. A superimposed spectra of stressed and unstressed film is shown in Figures 5.22 (a) and (b). The broken lines show IR bands obtained from stressed PS sample. Figure 5.22(a) shows the IR bands between  $1700$  and  $800\text{ cm}^{-1}$ . The band distortions previously observed in IR spectra obtained through the Perkin Elmer instrument are also observable in FTIR spectra. The bands at  $1370$ ,  $1325$  and  $1310\text{ cm}^{-1}$ , which had not been previously recorded on Perkin Elmer spectrometer, were recorded on FTIR spectrometer. These bands show distortions/changes in the spectrum of a stressed sample. The FTIR superimposed spectra does not show any frequency shifts because certain minor shifts may be masked by intense absorption bands. The spectra were scanned at a resolution of  $2\text{ cm}^{-1}$ . This, of course, limits our capability to observe resolved peaks or bands unless shifts in orders of  $2\text{ cm}^{-1}$  or more take place. An obvious question in any reader's mind at this point may be: Why the experiments are not run at a resolution of  $0.5\text{ cm}^{-1}$  which the instrument is capable of providing. This was indeed considered but due to limited storage space available on the magnetic disc at the time of these experiments it was not feasible to go to a higher resolution. Therefore, the



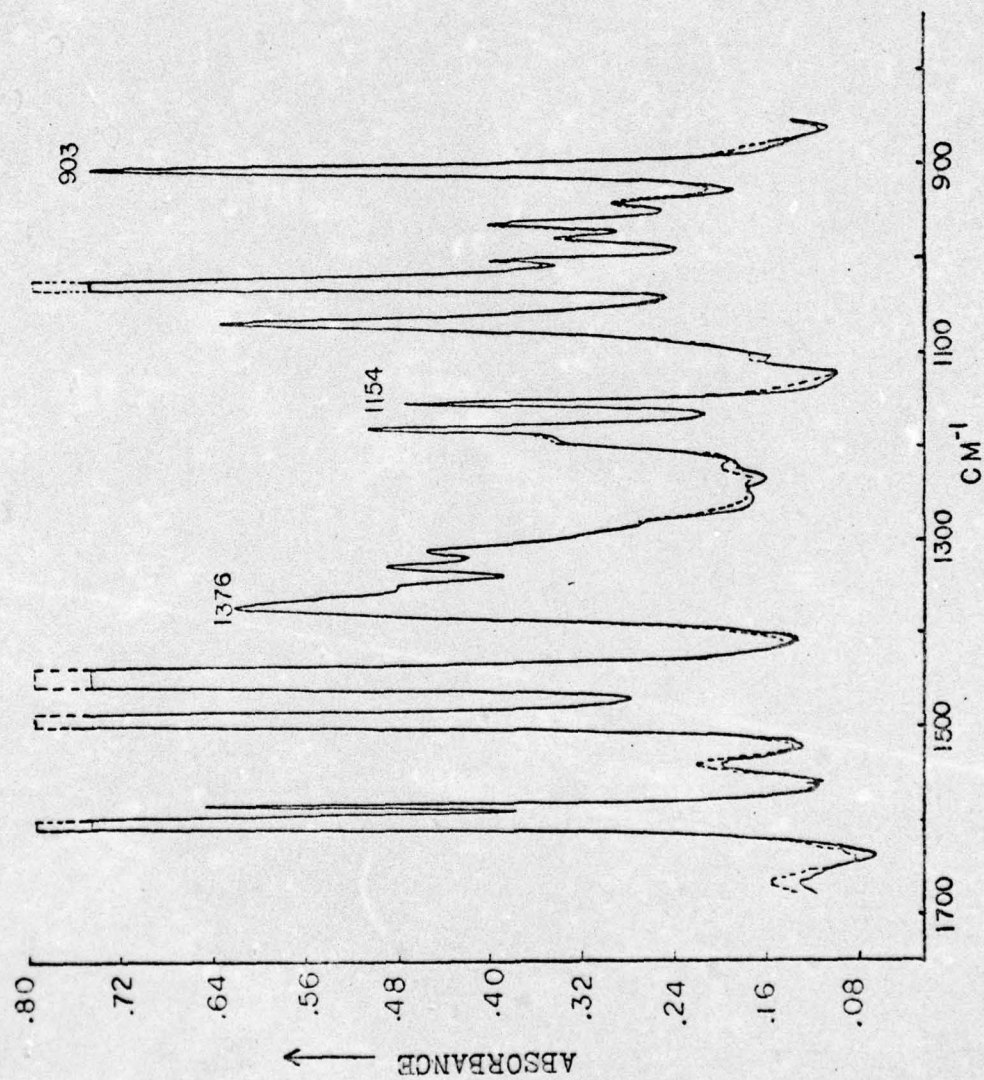


Figure 5.22 (a) Superimposed FTIR spectra of TRICITE film under no stress (—) and stress (---).

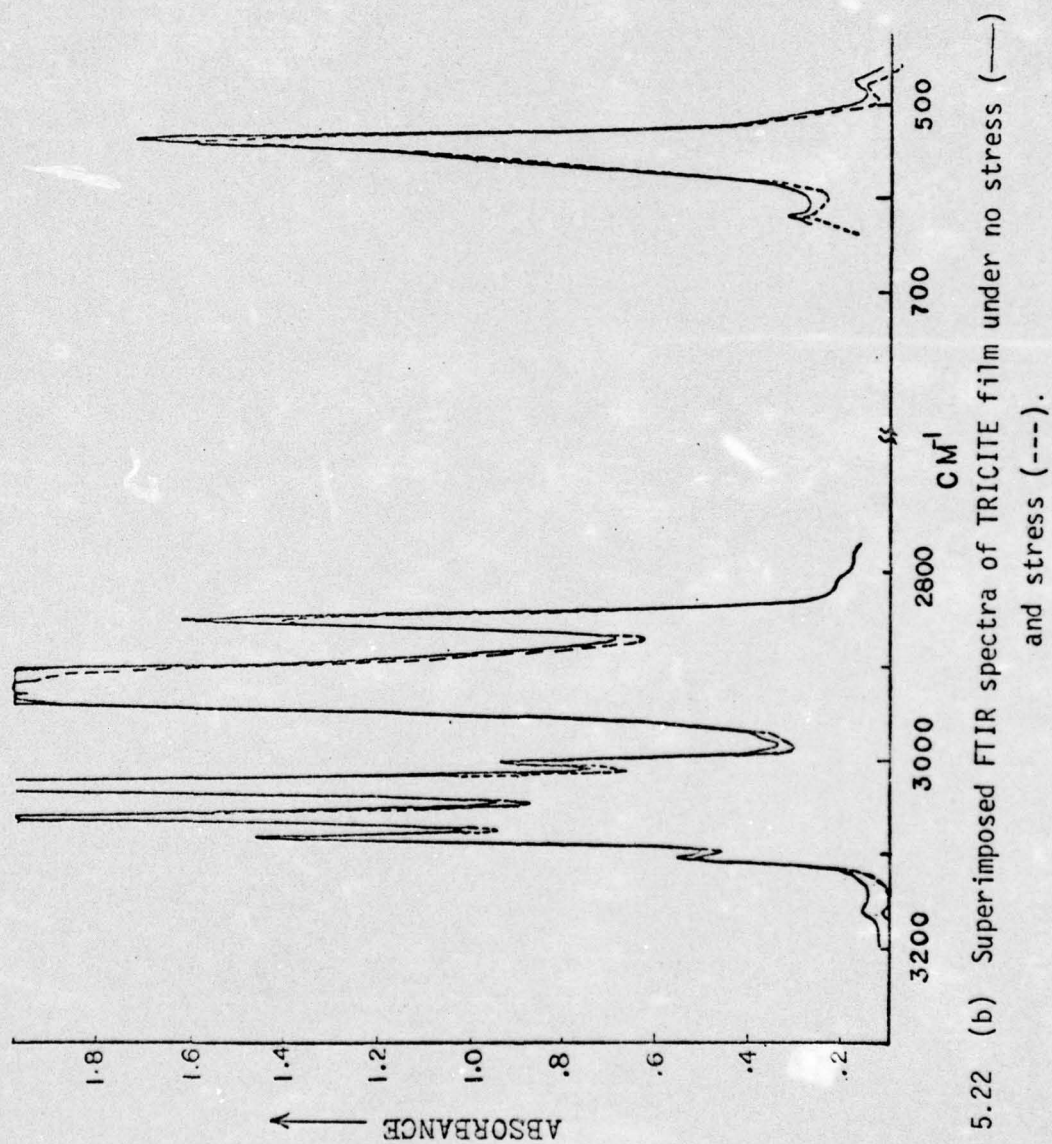


Figure 5.22 (b) Superimposed FTIR spectra of TRICITE film under no stress (—) and stress (---).



author had to be satisfied with  $2\text{ cm}^{-1}$  resolution.

The infrared spectra shown in Figure 5.22(b) reveals information about additional IR bands--540 and  $2850\text{ cm}^{-1}$ --which show splittings due to possibly small shifts in frequencies. From the superimposed IR spectra shown in Figure 5.22(a) and (b) one may almost anticipate the pattern of bands that will develop on actual subtraction of unstressed sample spectra from the stressed sample spectra. As discussed earlier, certain vibrational modes are affected due to stress and certain oscillators absorb at different frequencies in the IR spectra. This causes the IR bands to deform. Therefore, in the subtraction spectra it should be possible to separate such IR bands resulting from the stress effects on the polymer chains. This is indeed observed in the FTIR subtraction spectra. From the superimposed spectra in Figures 5.22(a) and (b) it is expected that in the subtraction spectra weak IR bands would appear at low frequency side of 906, 1154, 1310 and toward high frequency side of 1376, 1492 and  $1602\text{ cm}^{-1}$  bands. This is actually observable in Figures 5.23(a) and (b) showing (stressed-88% unstressed) FTIR spectrum. Besides these anticipated changes this spectrum also shows splittings of 3082, 3060, 2850, 1602, 1492, 1448 and  $540\text{ cm}^{-1}$  IR bands. The causes of these splittings have been modeled and are presented in Appendix A. Some of the causes of these splittings are due to change in the distribution of the absorption band, shift in frequencies and change in intensities of the absorption bands. Frequencies of the additional IR bands emerging due to the effect of stress on the TRICITE film are presented in Table 5.4.

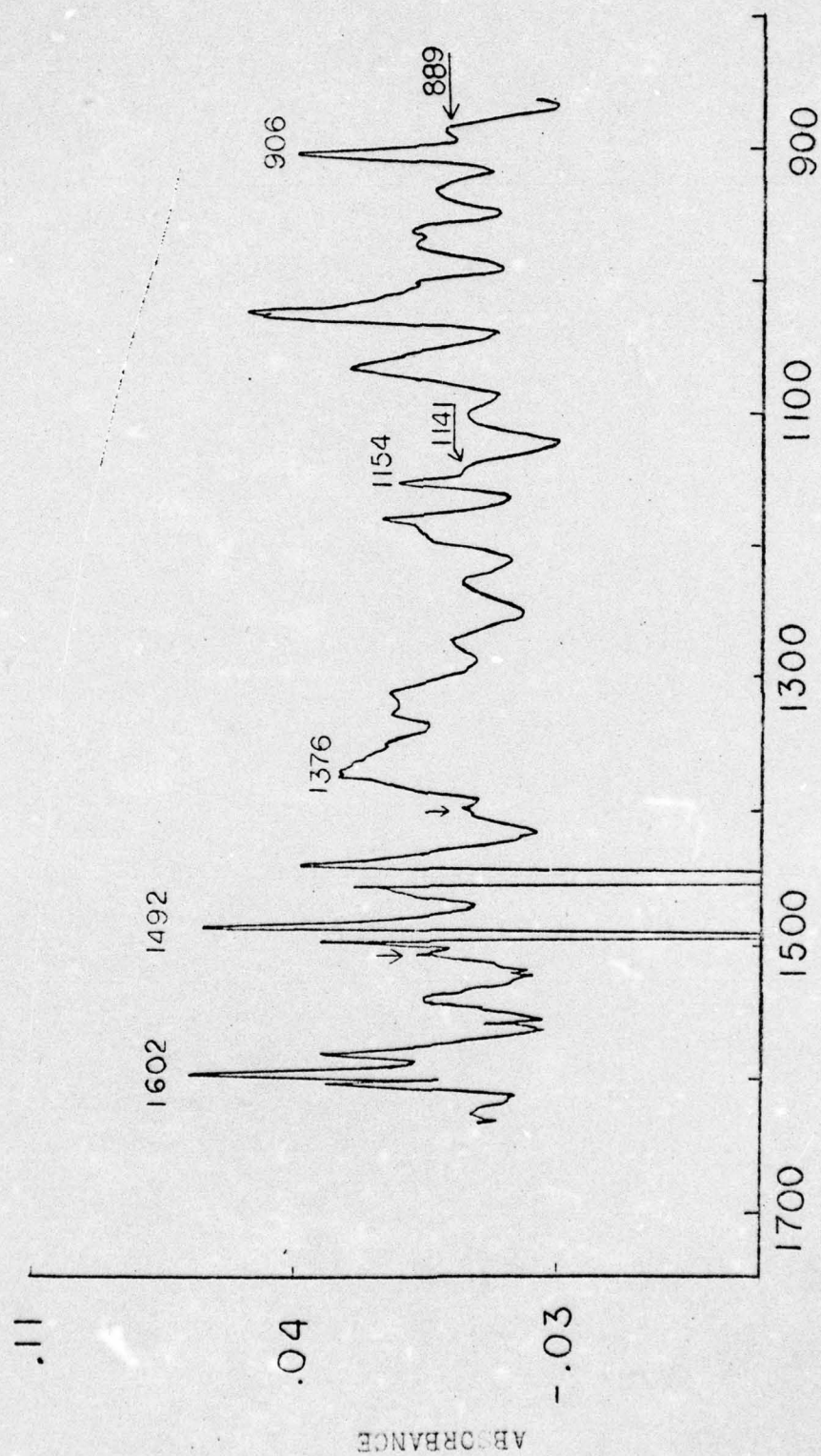


Figure 5.23 (a) FTIR subtraction spectrum of TRICITE film. (Stressed-88% unstressed)



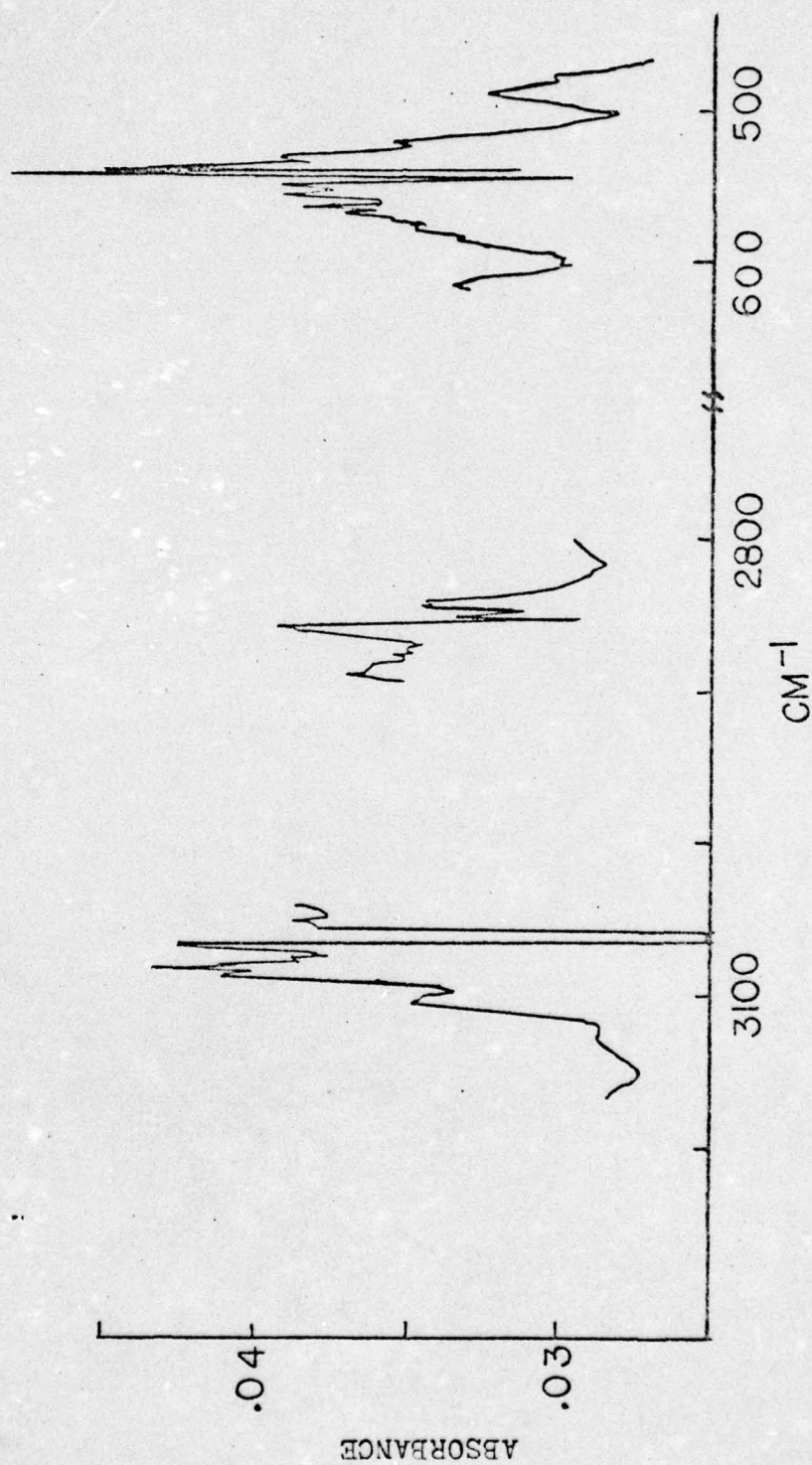


Figure 5.23 (b) FTIR subtraction spectrum of TRICITE film. (Stressed-88% unstressed)

Table 5.4 Frequency Shifts Observed from FTIR Spectra of TRICITE Films Under Stress

Frequency of IR Bands Obtained from		Frequency <sup>†</sup> Shift (cm <sup>-1</sup> )
Unstressed TRICITE (cm <sup>-1</sup> )	Stressed TRICITE (cm <sup>-1</sup> )	
1492	1506	14
1376	1400	24
1154	1141	-13
906	889	-17

<sup>†</sup>These shifts have been measured in relation to the frequencies of IR absorption peaks.

#### 5.2.4 X-ray results

The mean Bragg distance calculated from the outer halo in the diffraction pattern of unstressed TRICITE film is 4.79 Å, which lies within the range (4.67-4.85Å) reported in the literature [114]. This distance increases to 4.92 Å in the case of TRICITE film strained to 2.75% (equivalent to a stress of 9600 psi). Since the increase is rather small, a hypothesis test has been conducted to prove the validity of these results. This test is shown in Appendix B.



5.2.5 Discussion: Molecular behavior of 3 mil TRICITE film  
under stress

A comparison of stress-strain curves of these films obtained both at low and high strain rates indicates a tough and a brittle behavior, respectively. This suggests that, even though biaxial orientation decreases the physical entanglements and aligns the PS chains, chain slippage is facilitated only at low strain rates. This leads to the belief that bulky phenyl side groups on the polymer backbone obstruct any instantaneous response to an external stress, whereas these groups conform at sufficiently low strain rates. Nevertheless, extensive inter-phenyl interferences must occur due to chain slippage which is indeed observed through the dynamic infrared studies.

The IR data obtained during ramp loading of PS films suggests the following: Initially, the polymer has a certain microstructure in which there are loose segments, extended chains, physical entanglements and certain chain segments frozen-in conformationally unstable state. The author called this molecular arrangement of the polymer State A. An IR spectrum of PS film obtained from state A shows certain specific shapes of the infrared absorption bands which are associated with the characteristic absorption of its oscillators. However, when the spectrum is obtained from the stressed polymer film, certain IR bands deform, thereby suggesting the transformation of the initial molecular arrangement to another state called state B by the author. In this arrangement certain chains are extended and bear the load while the previously taut chains are broken. Some of the entangled segments are

able to pull out while others are snapped in the process. In addition, chains rearrange themselves in response to the imposed stress by breaking weaker Van der Waals' bonds and achieve their preferred conformation or low energy state. Thus, an application of stress on the sample causes certain irreversible changes, viz., untangling of chains, chain scission, removal of frozen-in stresses, and conformational rearrangements. An overall effect is a change in the arrangement of PS chains from their initial state A. This has been well-demonstrated by the IR spectrum obtained from the same film after removing the imposed stress which shows certain band distortions (different than in state B above) while mostly following the spectrum obtained from the initial state A. The author calls this state of the sample as state C. On restressing the sample to the same level as before the IR spectrum obtained is the same as from state B. Another spectrum obtained after removal of stress for the second time shows no changes from the spectrum and distortions noticed on removing the stress the first time.

From other IR spectra (not shown in this chapter) it is found that state C of the sample depends on the stress imposed in state B. Any increase of stress on the sample in this state gives a different spectrum under stress and on removal of stress. This is not surprising because any increase in stress further rearranges the structure and causes additional nonreversible changes, as mentioned earlier. Evidence for this has been given by Figure 5.11, as well as by an increase in the Bragg distance in stressed PS film. It is, perhaps, this behavior of the polymer chains at the molecular level which displays a nonlinear region in the stress-strain curve, after reaching a threshold stress.



Dynamic IR studies of step-loading process show that an increase of stress from the previous stress level on the sample causes additional band distortions. This agrees very well with the above discussion for ramp-loaded films where any increase in stress changes both states B and C.

So far, we have only discussed the amount and pattern of band distortion in the IR spectra of PS films under no stress and varying amount of stress under two types of loadings. We have not discussed the origin of these band distortions in PS films. From the results obtained so far, it appears that almost all IR bands which show distortions or splittings in the FTIR subtraction spectra are related to various vibrational modes of the phenyl side group. This reiterates that these groups interact extensively under stress and cause changes in the molecular orbitals of various groups in the polymer chains. Such changes are generally responsible for shifting the absorption frequencies of various vibrational modes arising from these groups. If such shifts are large enough, they show up as shoulders or even separate IR bands. However, when these shifts are very small, they are only observable in the computer-subtracted FTIR spectra as band splittings.

In our results we find that IR band at  $1154\text{ cm}^{-1}$  exhibits the most distortions and they increase linearly with stress. This band is assigned to  $\nu'_{15B_1}$  mode, i.e., the bending mode of C and H atoms located in the para position with respect to the main chain substitution position. This suggests that when stress is applied highly entangled PS chains try to move about to rearrange themselves under load. However, such PS

chain motions are highly restricted due to partial interlocking<sup>1</sup> of the phenyl groups located on the adjacent chains. Under stress some of these partial interlockings are broken due to conformational rearrangements of the phenyl groups and breakage of weak Van der Waal's bonds. This allows localized chain slippage or motion. Since stress is borne by certain extended chain segments, some of these may actually get taut and break, thus transferring their stress to neighboring chains. This will cause more Van der Waal's bonds to break and thus impart still more mobility to PS chain segments. However, during such chain movements certain phenyl groups may not be able to rearrange conformationally and will, therefore, obstruct any further chain slippage. These groups may be deformed or displaced as a result, but will act as strong interlocking points.

If phenyl groups indeed partially interlock in this way, while PS chains try to slide under stress, such interlocking points will be distributed randomly throughout the microstructure of PS. This is so because of various sequences, viz., isotactic, syndiotactic and atactic, present in the PS chains. As a result of strong partial interlocking at certain points and interferences at the others, we should expect the vibrational modes listed below and depicted in Figure 5.24 to be affected the most:

$$\nu_1(A_1), \nu_{6A}(A_1), \nu_{19A}(A_1), \nu_2'(A_1), \nu_{6B}(B_1), \nu_{9B}(B_1), \\ \nu_{19B}(B_1), \nu_{14}(B_1), \nu_{15}'(B_1) \text{ and all the } B_2 \text{ modes.}$$

---

<sup>1</sup>For partial interlocking to occur phenyl groups on adjacent chains should be in appropriate conformation as shown in Figure 5.25.



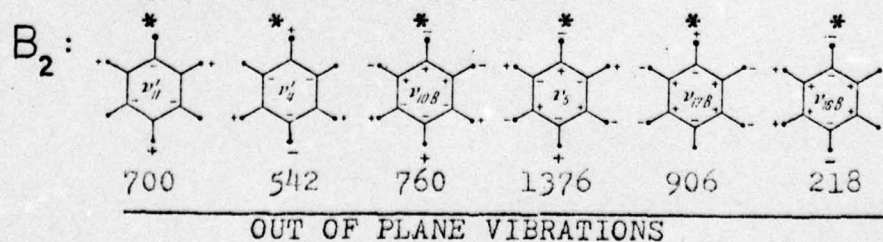
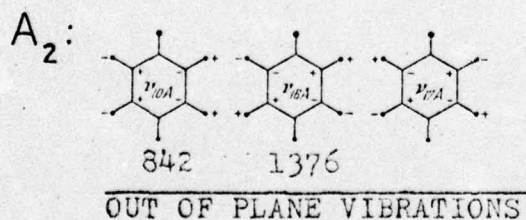
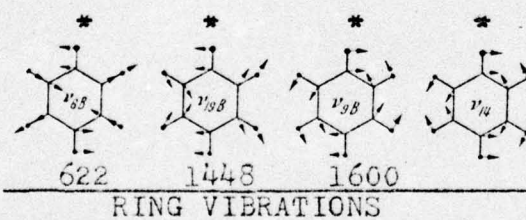
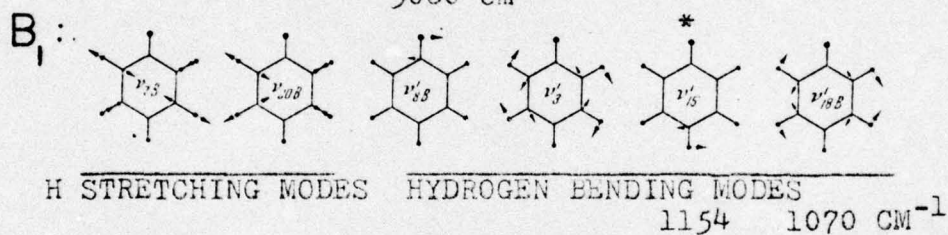
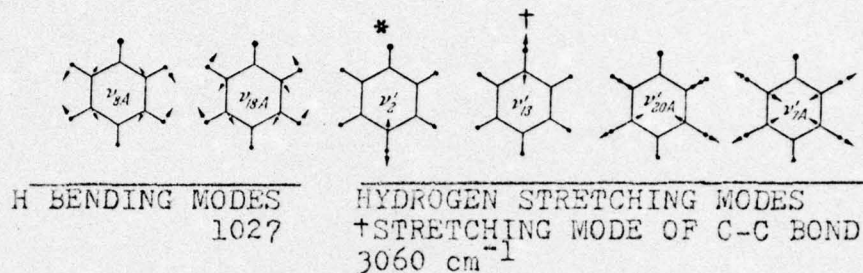
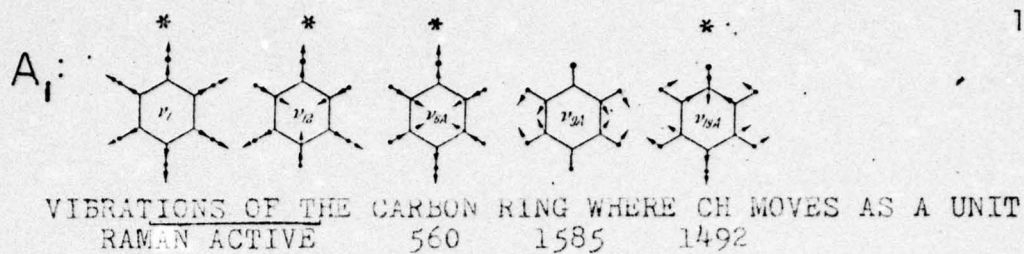


Figure 5.24 Approximate normal modes of monosubstituted benzene. Various modes expected to be affected by stress are marked by \*.

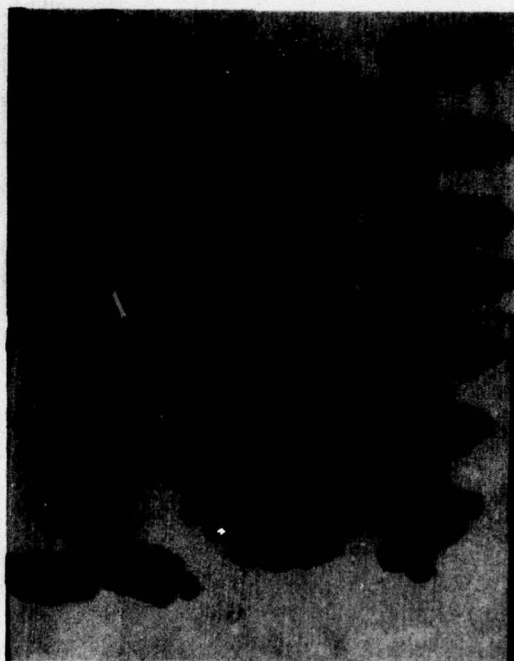


Figure 5.25 Molecular model of highly oriented polystyrene chains.



The frequencies of these vibrational modes along with comments about the influence of stress on these frequencies is given in Table 5.5. From table 5.5 it is clear that all the vibrational modes anticipated to be affected by phenyl group interferences are indeed affected. It is suggested that the backbone bonds of PS chains also participate in the load bearing mechanism. This is evidenced by the changes incurred by IR bands at 1182, 1376, 1450 and  $2851\text{ cm}^{-1}$  on stressing the sample. Of course, the changes in the backbone related IR bands are not prominent. This can be attributed to the following causes:

- (i) Only few backbone bonds are overstressed.
- (ii) Most of the backbone bond related changes are masked by large scale effects on the vibrational modes of the phenyl ring.
- (iii) Some of C-C stretching frequencies are mixed with vibrational frequencies of the phenyl ring and thus absorb at somewhat different wavenumbers in the IR spectra.
- (iv) Part of the changes observed in shapes and peaks of IR bands due to vibrational modes of the phenyl groups may, in fact, be a manifest of increase in internuclear distance of the backbone bonds, which causes non-bonded interactions of the bulky phenyl side groups.

The mean Bragg distance calculated from the scattering pattern of polystyrene is  $\sim 4.80\text{ \AA}$ . This distance is associated with both intramolecular and intermolecular distances [119] and it increases in stressed samples. This indicates that any one or both of the following mechanisms may be responsible for this increase in Bragg distance:

- (a) Certain chain segments extend themselves under the influence of external stress. During this process interphenyl interactions occur, causing phenyl groups to deform and rearrange conformationally in such a way that the intraphenyl distances increase.

Table 5.5 Stress-affected Infrared Bands of TRICITE Films

IR Band Frequency	Intensity	Assignment	Comments
560	S	$\nu_{6A}(A_1)$	Multiple splittings observed in FTIR indicating interlocking and/or interferences of the phenyl side groups
622	VW	$\nu_{6B}(B_1)$	Too weak to observe any changes in the IR on stressing.
700	VS	$\nu_{11}(B_2)$	The out-of-plane bending modes are expected to change due to stress and this indeed occurs.
760	VS	$\nu_{10B}(B_2)$	The out-of-plane bending modes are expected to change due to stress and this indeed occurs. Changes in both of these bands suggest strong interferences/locking of phenyl groups.
906	M	$\nu_{17B}(B_2)$	This is also an out-of-plane bending mode and is most affected by stress. A number of these vibrational modes are highly affected and show up as a separate band at 889 $\text{cm}^{-1}$ in the FTIR spectra.
1154	MW	$\nu_{15}^i(B_1)$	Highly affected by stress as expected. Certain vibrational modes absorb at 1141 $\text{cm}^{-1}$ and show up as separate band on stressing in FTIR subtraction spectra.
1376		$\delta(\text{CH}_2)$	The effect on this band appears to be due to change in the molecular orbital interactions. Some of these modes begin to absorb in the IR at higher frequency under stress and show up as additional band at 1400 $\text{cm}^{-1}$ .



Table 5.5 (continued)

IR Band Frequency	Intensity	Assignment	Comments
1450		$\delta(\text{CH}_2)$	This band is also highly affected by stress and shows splittings in the FTIR subtraction spectra.
	S	$\nu_{19B}(B_1)$	
		$\nu_{11} + \nu_{10B} = 1460$ $\nu_4 + \nu_{17B} = 1446$	
1493	S	$\nu_{19A}(A_1)$	This mode is due to vibrations of the carbon ring in which CH groups move as a unit. Of course, the movement of this group located in the para position will be affected by the presence of other chains in the close proximity. Therefore, we expect some of these modes to absorb at higher frequencies. This is actually observed in the FTIR subtraction spectra. Some modes are absorbed at higher frequency and show up as a separate band at 1506 $\text{cm}^{-1}$ .
1602	W	$\nu_{9B}(B_1)$	This band shows splittings in the FTIR subtraction spectra, suggesting interphenyl interferences.
2851	MS	$\nu_s \text{CH}_2$	This band is anticipated to be affected, provided the force constants of C-C-C backbone bond change. Since some splittings are actually observed in this band in FTIR subtraction spectra, it is suggested that stress is transmitted through certain backbone bonds.
3061	MS	$\nu_2'(A_1)$	This band shows splittings due to stress in FTIR spectra indicating that hydrogen stretching modes of phenyl ring are affected due to interferences or partial interlocking of interchain phenyl groups.

- (b) The chains also try to rearrange themselves by breaking weaker Van der Waal's bonds, holding them together. Since phenyl groups act as hindrance during any chain slippage or movement, PS chains move away from one another to overcome these obstructions. This will cause an increase in the intermolecular distance.

Thus, the IR and X-ray results indicate that stresses are distributed over a large number of polymer chains through many partially interlocked phenyl groups. These interlocks act as physical crosslinks in the structure, restrict chain mobility and cause certain chain segments to be stressed more than others, which, in turn, deform certain phenyl groups more than the others.

#### 5.2.6 Summary

The study of 3 mil TRICITE films under ramp-loading and step-loading conditions reveals that in both cases the initial molecular state of the polymer is disturbed. Any molecular rearrangements are irrecoverable on removal of imposed stress. Furthermore, the deviation from the initial state increases on increasing the applied stress on the sample.

Most of the infrared bands affected by an imposed stress are related to various vibrational modes of the phenyl side groups, in that only those modes are affected in which C and H atoms located on the para position participate. This is an important outcome of the present study and suggests that in oriented state several phenyl side groups located on adjacent polymer chains are in partially interlocked state. Any external stress on these oriented PS films is transmitted to individual polymer chains which attempt to relieve themselves of the



imposed stress by rearrangements. This induces certain chain mobility which, in turn, highly distorts certain phenyl groups and breaks some interlockings. This molecular behavior of PS chains affects mostly the electronic structure at the para position of the phenyl ring. Thus, it can be concluded that mechanical behavior of the polystyrene polymer is highly dictated by the bulky phenyl side groups.

### 5.3 Results and Discussion: Fatigued TRICITE Films of 3 mil. Thickness

#### 5.3.1 Load-elongation results

2" wide and 6" long specimens of 3 mil thickness were used for fatigue purposes. A load-elongation curve as shown in Figure 5.26 was obtained on such a specimen to determine the "upper-load" level, up to which these samples remained within their elastic limit, i.e., within the Hookean region. This figure shows that the nonlinearity in the curve develops at about 50 lbs and upward and the specimen breaks at about 70 lbs. Even though the number of cycles before fracture were determined at several upper loads, the author preferred to fatigue these samples at 50% of the breaking load at which the curve is still within the elastic region.<sup>1</sup> Table 5.6 shows the number of cycles before fracture at various loads. The data in Table 5.6 have been plotted in Figure 5.27.

The fatigued PS samples were scanned under scanning electron microscope to detect any crazes that might have developed due to fatigue. No crazes were observed in these samples fatigued up to 2500 cycles.

---

<sup>1</sup>Because of the viscoelastic nature of polymers a certain amount of plastic deformation is occurring even in the elastic region. The author has already demonstrated this phenomena at the molecular level in Section 5.1.2.

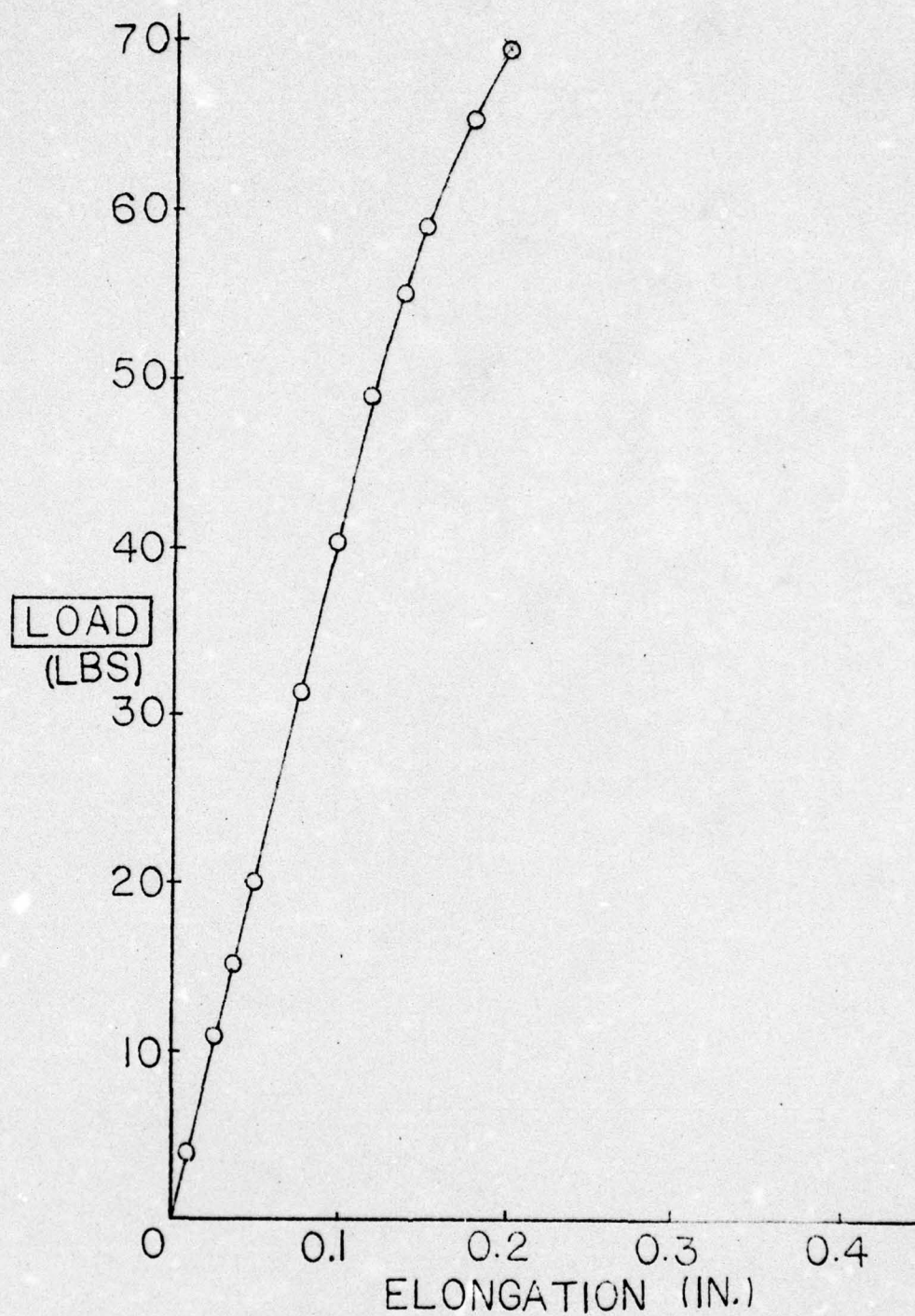


Figure 5.26 Load-elongation curve of 3 mil thick TRICITE film.  
Gage length - 6 in, width - 2 in., strain rate -  
4 in/min.



Table 5.6 Fatigue Data of PS Specimens

Minimum Load Level (lbs)	Maximum Load Level (lbs)	Number of Cycles Before Fracture
5	60	9
5	55	24
5	50	290
5	45	635
5	40	900
5	35	Sample did not fracture up to 2500 cycles and was studied by various techniques.

### 5.3.2 FTIR results

Figures 5.28(a) and (b) show the superimposed spectra of fatigued and unfatigued samples. The distortions in the bands occur near the base line of these spectra. These distortions are somewhat different in the intensity than the ones observed in the superimposed spectra of stressed and unstressed TRICITE film. It appears that some oscillators absorb at higher frequency while others at lower frequency in the same band. This is quite probable because of the fatigue process in which certain extended chains bearing the load become taut during repeated loading and break, thus transferring the stresses over other chains, which too become taut and break. In addition, certain chains which are tangled badly will also break while some slack or loose chain loops

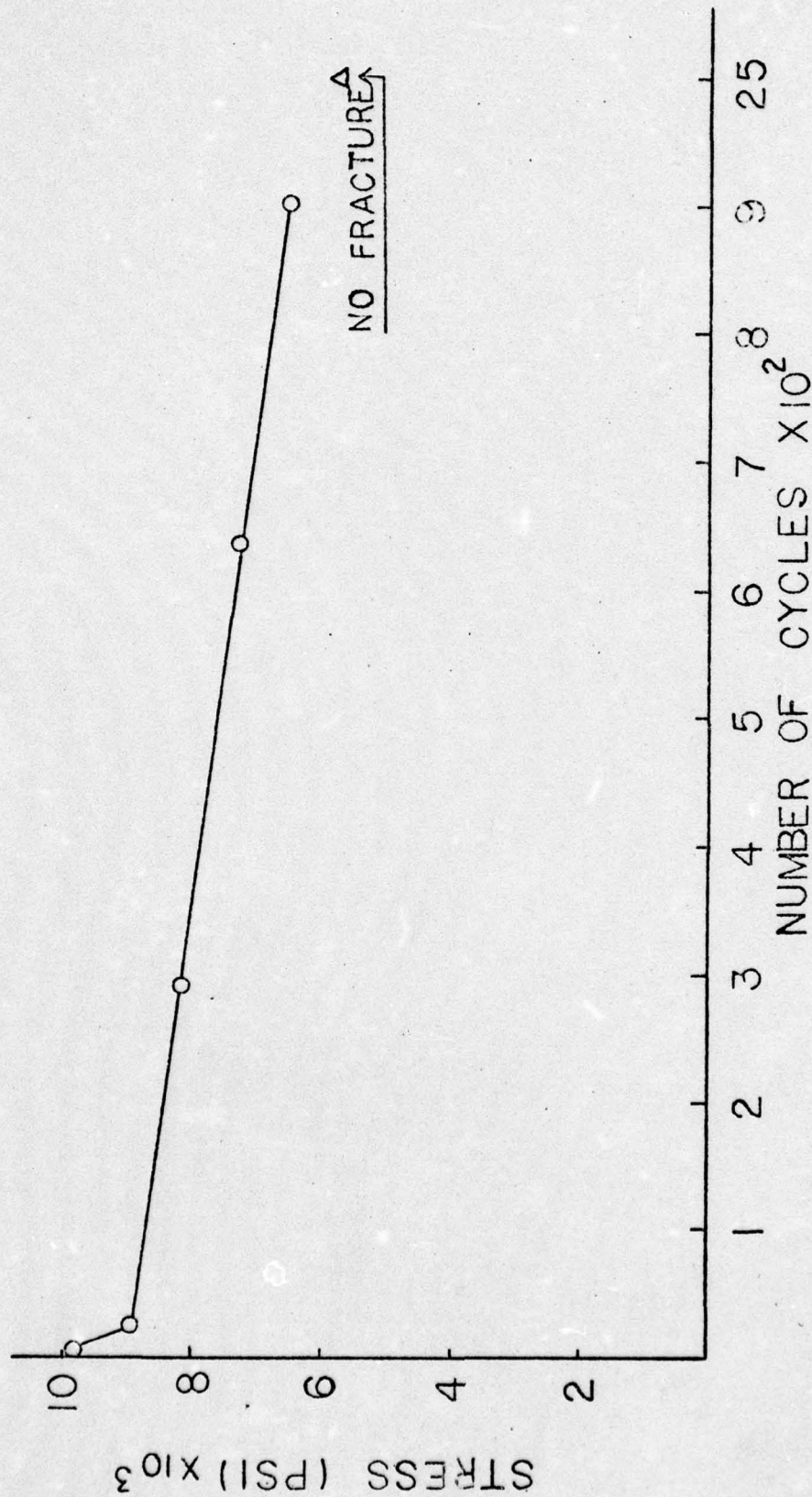


Figure 5.27 Stress vs. number of cycles to failure for 3 mil thick TRICITE film.



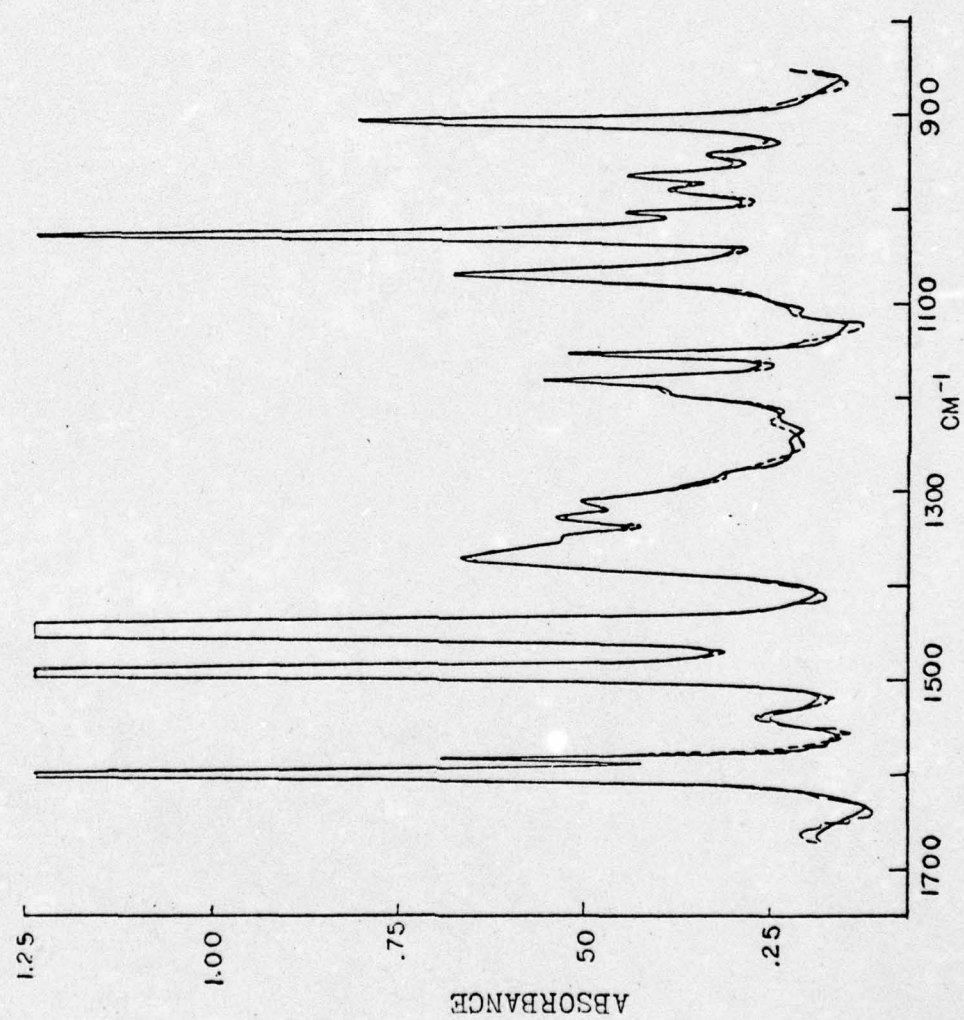


Figure 5.28 (a) Superimposed FTIR spectra of unfatigued (—) and fatigued (---) 3 mil TRICITE film.

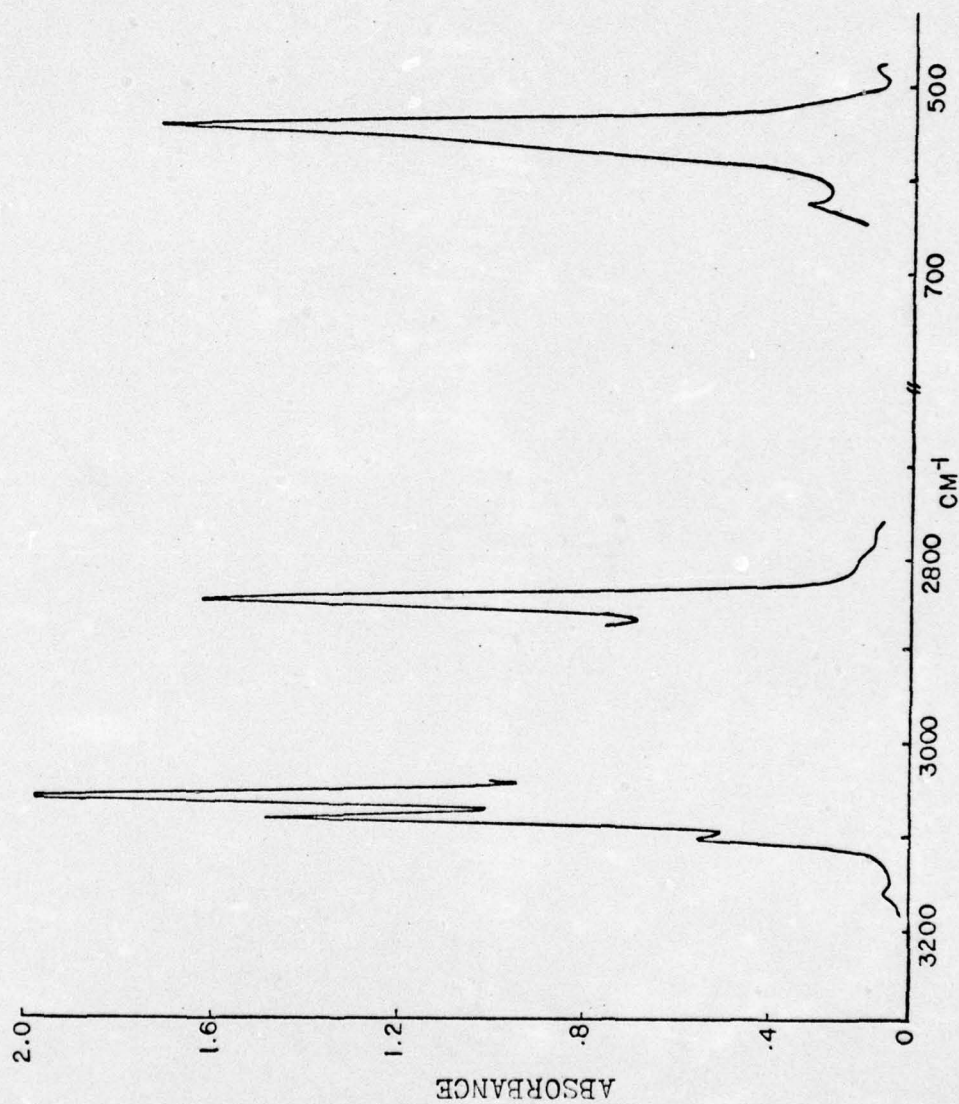


Figure 5.28 (b) Superimposed FTIR spectrum of unfatigued and fatigued 3 mil TRICITE film. No changes observed due to fatigue.



and entanglements may become tight. In order for the chains to rearrange under repetitive load-unload situations, certain Van der Waal's bonds will be broken imparting mobility to the chain segments.

In the superimposed FTIR spectra no distortions are noticeable in IR bands at 540, 2850, 3060 and 3082  $\text{cm}^{-1}$  (see Figure 5.28(b)). Several computer-subtracted FTIR spectra were recorded to detect minute changes caused by the fatigue process but only (fatigued-90% unfatigued) FTIR spectrum is shown here in Figure 5.29(a) and (b). Various changes observable from this spectrum are listed in Table 5.7.

#### 5.3.3 X-ray results

The mean Bragg distance of about 4.80 Å calculated for the unfatigued TRICITE film shows a decrease of  $\sim 0.10$  Å in cyclically fatigued (to 2500 cycles) TRICITE sample. This negative shift in  $d_{\text{Bragg}}$  is conclusive as indicated by the hypothesis test shown in Appendix B. In contrast to the decrease in interphenyl and intraphenyl distances the half width (variation about the mean distance) corresponding to the outer halo of the fatigued sample shows an increase.

#### 5.3.4 Dynamic mechanical loss results

Figure 5.30 shows a plot of  $\tan \delta$  vs. temperature for unfatigued and cyclically fatigued (to 2500 cycles) TRICITE film. The  $\tan \delta$  readings are obtained by conducting the test at a frequency of 3.5 Hz.

#### 5.3.5 Discussion: 3 mil fatigued TRICITE films

FTIR results show that fatigue process has caused changes in the

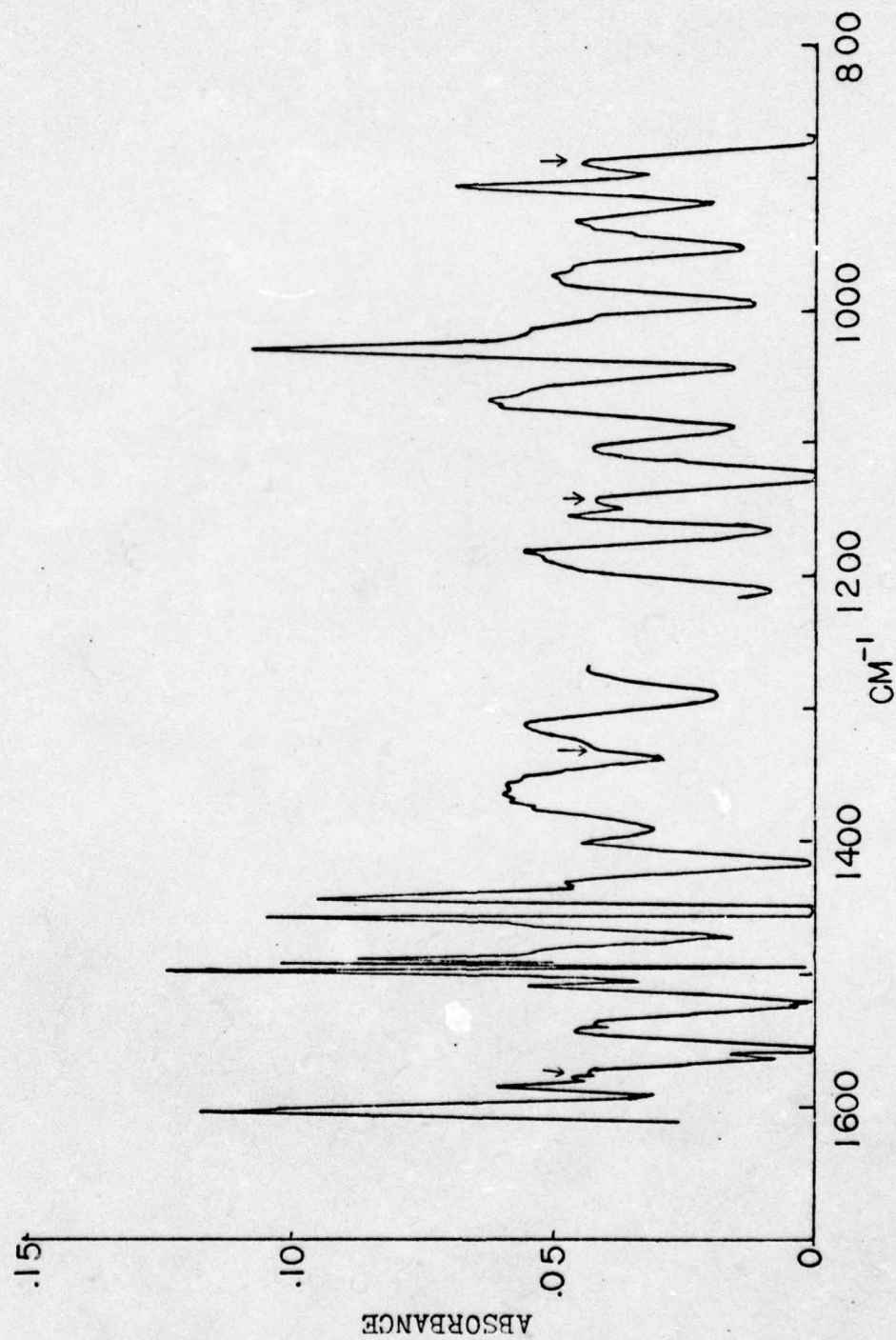


Figure 5.29 (a) FTIR subtraction spectrum of 3 mil TRICITE film. (Fatigued-90% unfatigued)



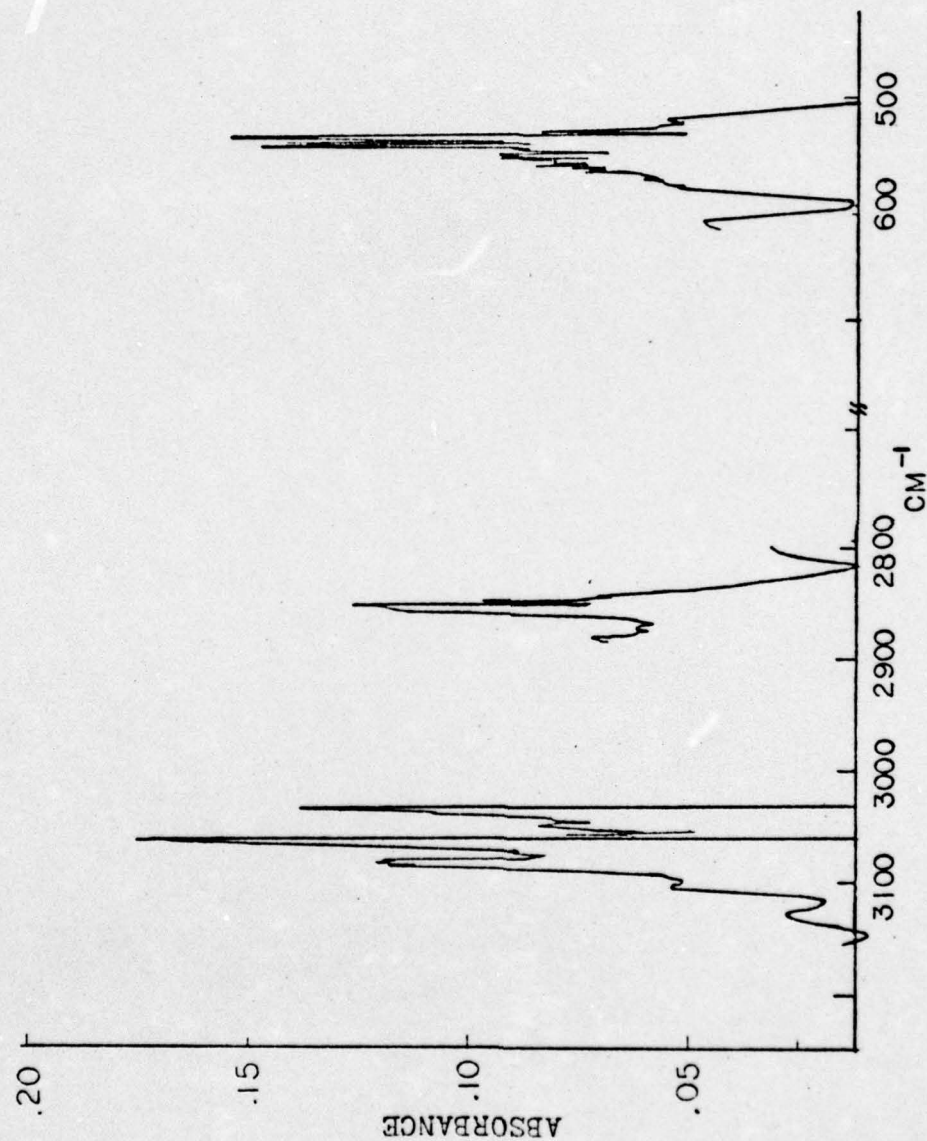


Figure 5.29 (b) FTIR subtraction spectrum of 3 mil TRICITE film. (Fatigued-90% unfatigued)

Table 5.7 Fatigue-affected IR Bands of TRICITE Films

IR Band Frequency ( $\text{cm}^{-1}$ )	Vibrational Assignment	Observation
540	$\nu_4(B_2)$	Multiple splittings Part of the band shifts to lower frequency at $888 \text{ cm}^{-1}$ . Shift amount is $-18 \text{ cm}^{-1}$ . Part of the band shifts to lower frequency at $1145 \text{ cm}^{-1}$ . Shift amount is $-9 \text{ cm}^{-1}$ . Part of the band is contributed by fatigue process. Part of the band appears at a higher frequency of $1400 \text{ cm}^{-1}$ . Shift amounts to $24 \text{ cm}^{-1}$ . Rest of the band is resolved into bands at 1352, 1358, 1365, 1371, $1376 \text{ cm}^{-1}$ . Shows strong splitting. Two additional bands appear at 1489 and $1509 \text{ cm}^{-1}$ .
906	$\nu_{17B}(B_2)$	
1154	$\nu'_{15}(B_1)$	
1310	$\nu'_3(B_1)$	
1376	$\nu_5 + \nu_{16} A = 1390$ $\delta(\text{CH})$	
1448	$\delta(\text{CH}_2), \nu_{19}(B_1)$	Negligible effect Negligible effect. Weak splitting observed. Medium intensity splitting observed. Medium intensity splitting observed.
1478	$\nu_{19A}(A_1); \nu_4 + \nu_{17A} = 1505$	
1585	$\nu_{9A}(A_1)$	
1602	$\nu_{9B}(B_1)$	
2850	$\nu_s(\text{CH}_2)$	
3062	$\nu_{20B}(B_1)$	
3083	$\nu'_2(A_1)$	



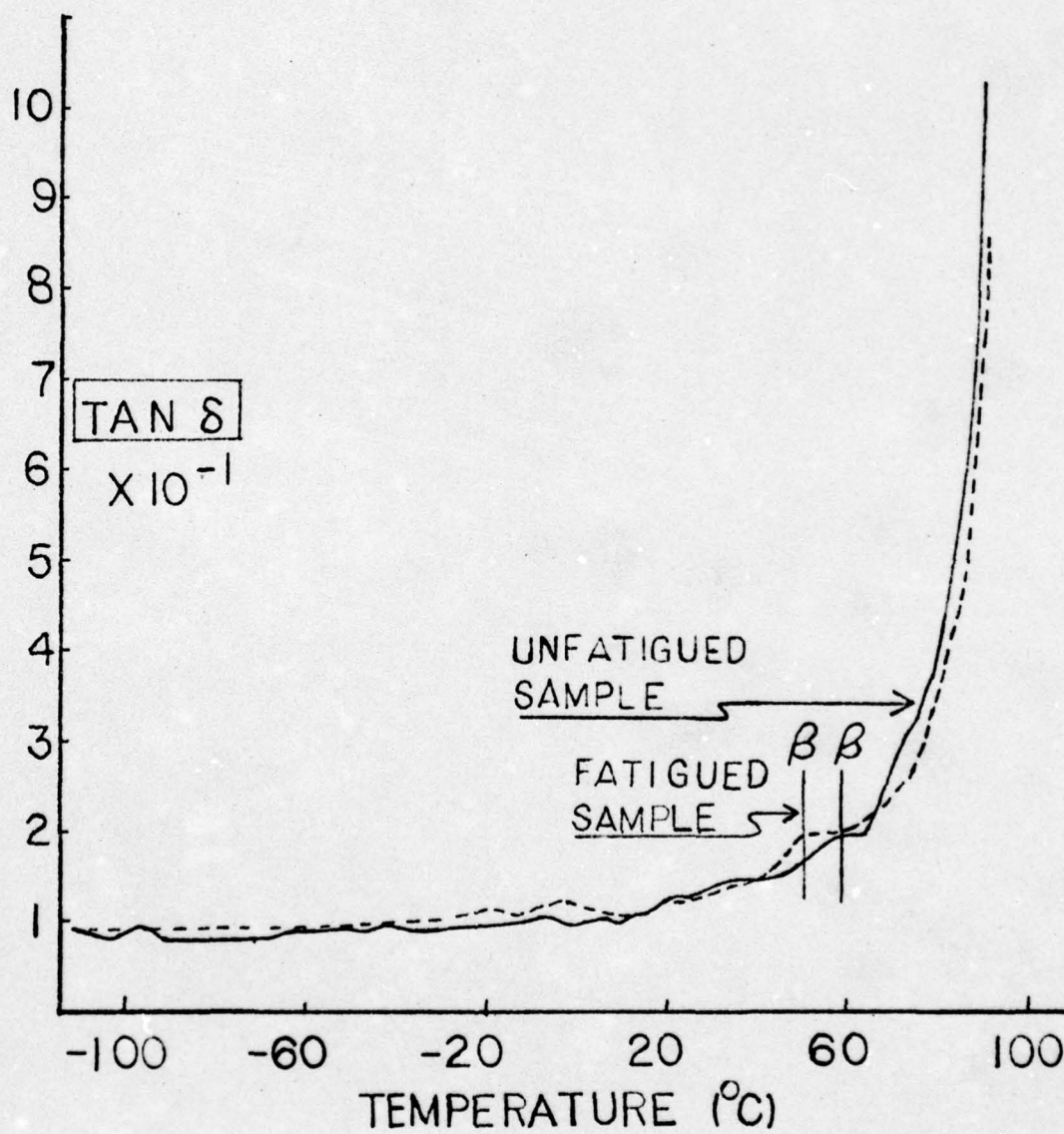


Figure 5.30 Tan  $\delta$  vs. temperature plot for fatigued and unfatigued TRICITE films. Frequency of test - 3.5 Hz.

absorption frequencies of various vibrational modes of the phenyl side groups. The IR bands associated with bending and stretching modes of  $\text{CH}_2$  groups and bending modes of CH groups also show frequency shifts and band distortions. These results suggest that fatigue has modified the internal and external environment (intrachain and interchain interactions) of PS chains. It appears that several chain segments have tautened during cyclic fatigue and many of the entangled and taut segments are broken. In addition, many weak bonds between the chains have also been broken. This results in an increase in free volume and, hence, in the chain mobility. The intensity of interphenyl interferences is also reduced.

X-ray results point out that the average Bragg distance is decreased in cyclically fatigued TRICITE film by  $\sim 2.16\%$ . However, measurement of half width, which is an indication of the spread about the mean distance, is greater in fatigued samples than in unfatigued samples. This increase in half width is actually anticipated because of the fact that certain taut chain segments move closer to one another while the highly entangled chains remain in their initial position. Wecker et al. [119] suggest that Bragg distance related to outer halo is due to two types of distances; one is due to intraphenyl distances and the other to atoms in the phenyl group and the main chain atoms in the neighboring chains.

On the basis of these assignments of the outer halo the author believes that perhaps two mechanisms are operating. According to the first mechanism, weaker Van der Waal's and some backbone bonds may be broken by cyclic exercise of the sample causing loosening of the structure, which, in turn, enables PS chains to rearrange themselves,



resulting in a better packing, like the one in Figure 5.25. This reduces both intraphenyl and interchain distances. In the second mechanism, an increase in free volume caused by bond breakage and chain rearrangement allows increased motions of the phenyl rings about the axis connecting them to the main chain. These motions will also help to improve the packing of benzene rings and thereby reduce the interchain and intraphenyl distances.

Before discussing the rheovibron data a brief discussion of the relaxations in atactic polystyrene is presented. It is well-known that most polymers show a small number of discrete loss peaks in their dynamic mechanical loss (anelastic) spectrum. These loss peaks arise at different temperatures and have been associated with the rotation of side groups attached to the main chain or to the limited motions within the chain backbone. Because these motions are intimately connected to chemical structure of the polymer chain, their intensity and position, in terms of temperature at which these occur, varies in different polymers. These peaks are generally referred to as  $\alpha$ ,  $\beta$ ,  $\gamma$  and  $\delta$  relaxation peaks or correspondingly as  $T_g$ ,  $T < T_g$ ,  $T \ll T_g$  molecular processes. These peaks are best resolved at low frequency tests, preferably at or below 1 Hz, such as in torsion pendulum test [120].

In atactic polystyrene the  $\beta$  peak is observed just below the main glass transition peak. This peak is generally quite weak, even when the test is performed at 1 Hz. The temperature at which this peak occurs depends on the thermal history of the polymer.

Various scientists have ascribed the  $\beta$  ( $T < T_g$ ) peak to the oscillation of the phenyl ring. Such oscillations involve the

coordination by several intrachain phenyl groups and the phenyl groups on the adjacent chains. Such cooperative motions will, of course, depend on the tacticity of the backbone chain and the free volume available for such motions.

The  $\tan \delta$  measurements in the present study are conducted with an anticipation that if chain scission or breaking of Van der Waal's bonds occur during the fatigue process, one should be able to observe changes in the intensity and/or location of the  $\beta(T < T_g)$  peak in comparison to similar measurements on the unfatigued sample. In the present study the dynamic mechanical measurements made on fatigued TRICITE film show an increase in the intensity of  $\beta$  peak, as well as its shift toward lower temperatures, indicating increased cooperative oscillations of the phenyl side groups due to better molecular packing and increased free volume available in fatigued sample.

It may be suggested here that such an experiment, if conducted at a frequency of 1 Hz, will perhaps yield even better results. However, in the present study the author had instrumental limitations and could not employ a frequency of less than 3.5 Hz.

#### 5.3.6 Summary

IR results indicate that polymer chains are stressed and interphenyl interferences occur during the cyclic (tensile) fatigue, up to 50% of the breaking load. X-ray results show a decrease in intraphenyl and interchain distances. This is backed up by the dynamic mechanical measurements which exhibit an increase in the intensity and a shift of  $\beta$  relaxation peak toward the lower temperatures.



Thus, a reduction in the intraphenyl distances must result from the conformational rearrangements of the phenyl groups about their axis connecting them to the main chain. The decrease in the inter-chain distance must be caused by breakage of taut and highly entangled chains and extension of others in the direction of tensile stress. This results in a better packing of PS chains, even though cyclic fatigue has damaged the molecular structure.

#### 5.4 Results and Discussion: Unoriented Atactic PS Film Under Stress and in Crazed State

Atactic PS films used in experiments discussed in this section were made from Dow's resin (S-109) by techniques discussed in Section 4.3.1. The weight average and number average molecular weights of these S-109 films are 193,000 and 182,000, respectively, which gives a molecular weight distribution of 1.06.

##### 5.4.1 Stress-strain results

Figure 5.31 shows the stress-strain behavior of  $\sim 5$  mil thick, unoriented atactic PS film. The films break in a brittle manner at a stress of  $\sim 4850$  psi and a strain of  $\sim 1.2\%$ . These films exhibit extensive crazing before fracture. Crazes appearing on one of these specimens are shown in Figure 5.32.

##### 5.4.2 Dynamic IR results

Figure 5.33 (a) and (b) show the IR absorption bands of these films under no stress and stress of 3775 psi ( $0.78 \sigma_B$ ). This stress

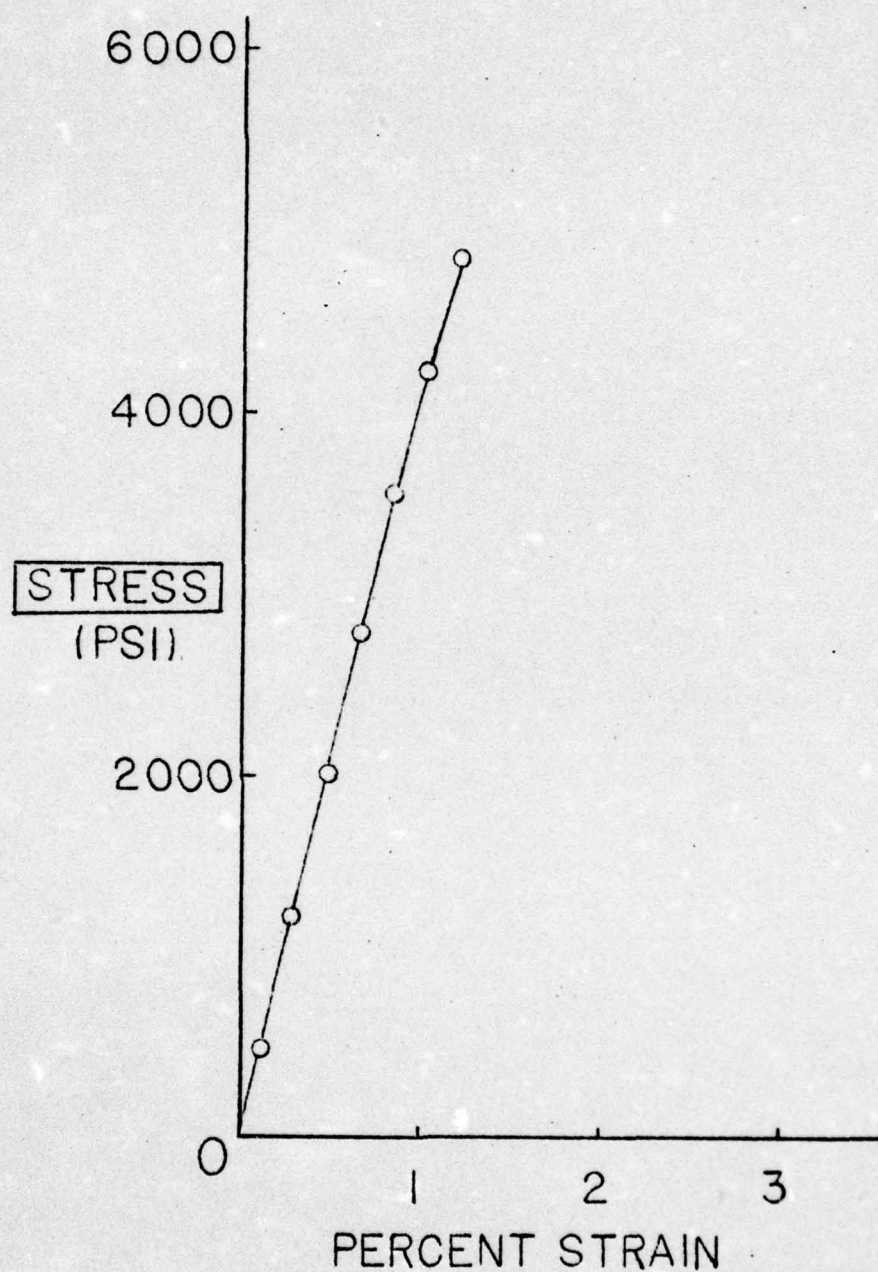


Figure 5.31 Stress-strain curve of unoriented atactic polystyrene film. Gage length = 2 in., strain rate = 0.05 in/min.



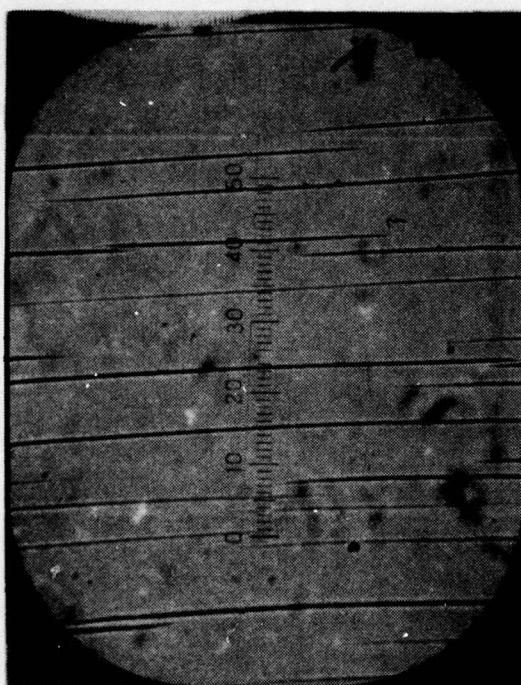


Figure 5.32 Crazes observed during stress-strain testing of unoriented atactic polystyrene films in the Instron machine.

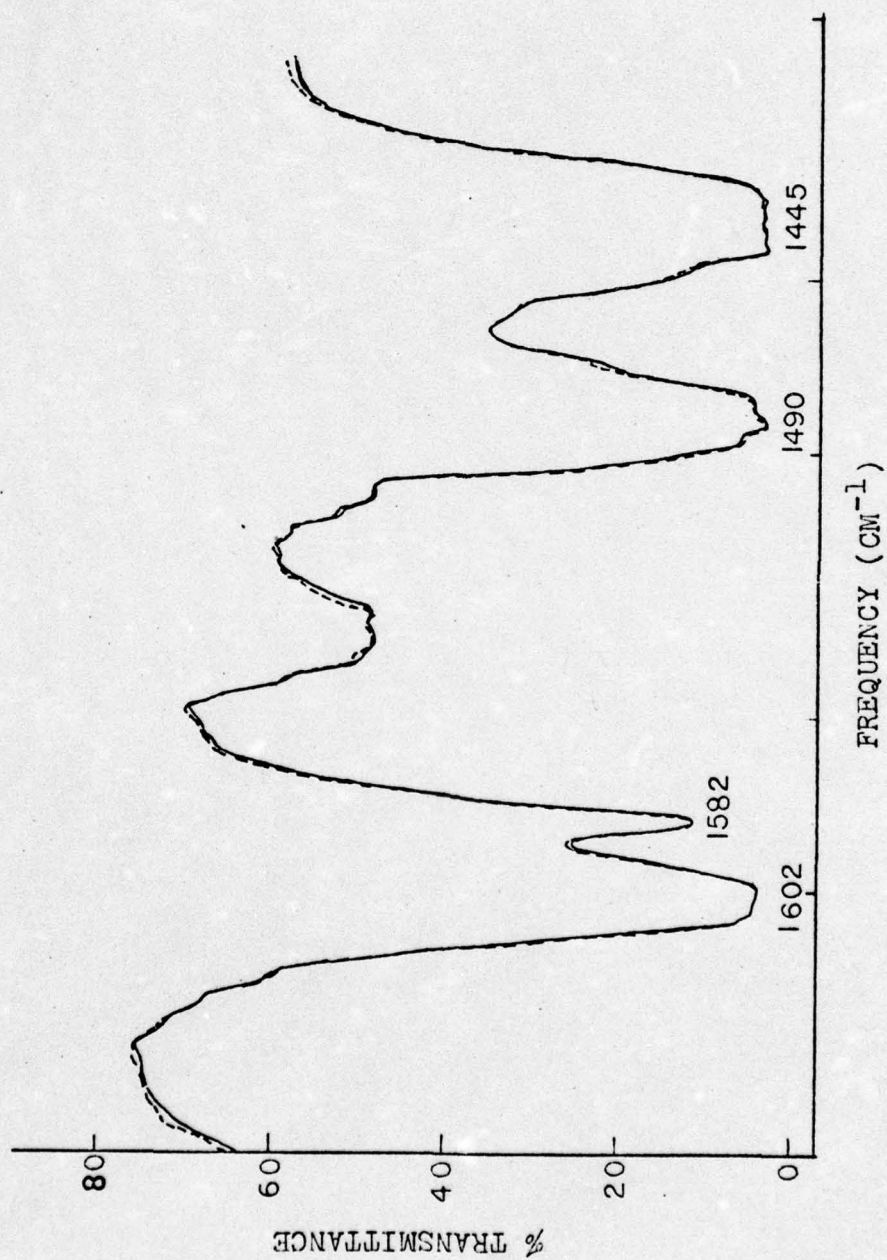


Figure 5.33 (a) IR spectra of unoriented atactic polystyrene film under no stress (—) and stress of 3775 psi (---).



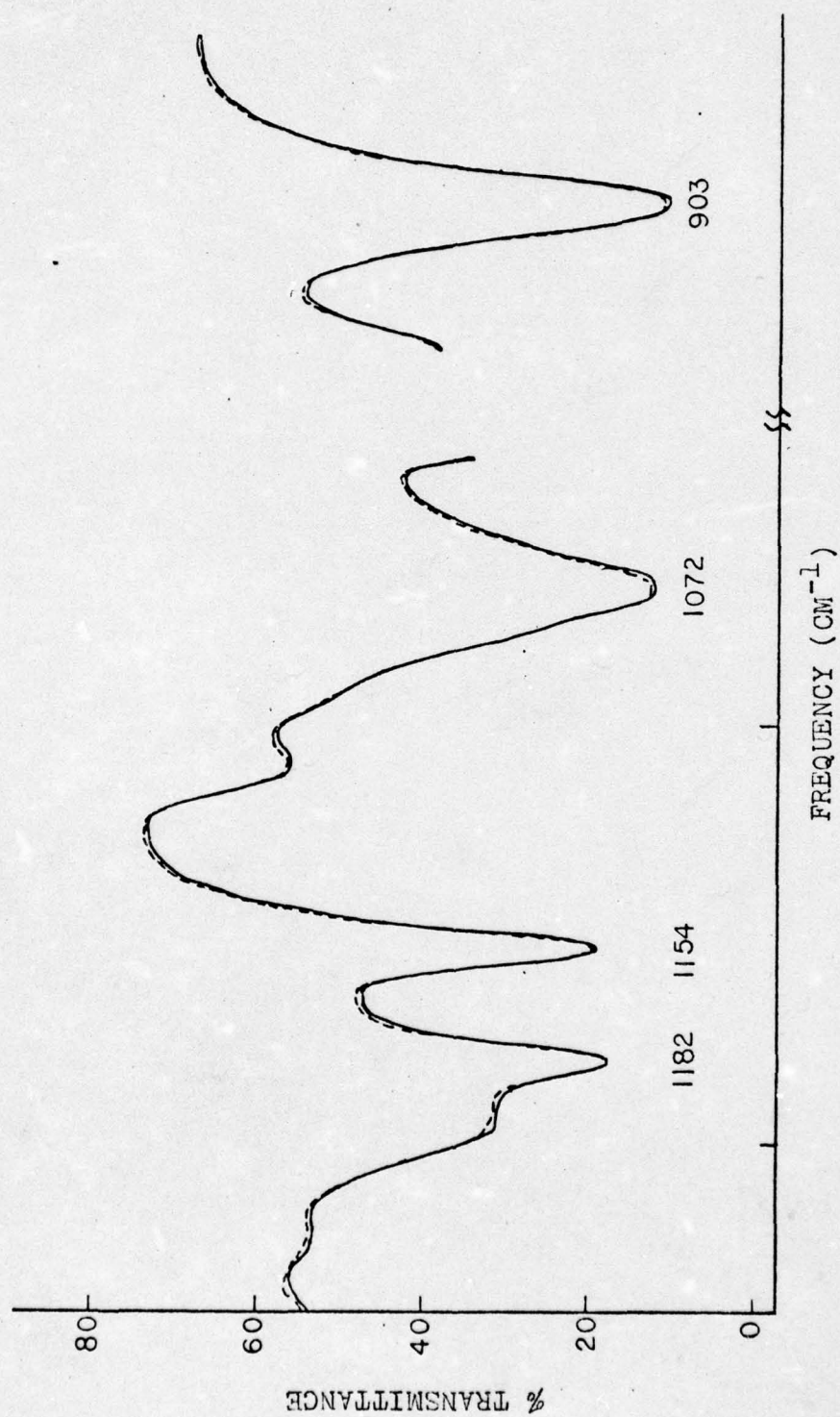


Figure 5.33 (b) IR spectra of unoriented atactic polystyrene film under no stress (—) and stress of 3775 psi (---).

level appears to be within the linear region of the stress-strain curve and no crazes are observed in these films at this stress. The band distortions of various IR bands in these figures are similar to the ones observed in the case of 0.0045" TRICITE films. Though the band distortions of 1602, 1582, 1445, 1182, 1154, 1072 and  $903\text{ cm}^{-1}$  IR bands appear to be minor, they are real. The distortions of  $1154\text{ cm}^{-1}$  band in this figure are similar to the ones observed at 888 and 1776 psi in 4.5 mil TRICITE film. Such similarities suggest similar arrangement of PS chains in both cases. In the unoriented films, PS chains are assumed to be highly entangled because of their random arrangement. This will make it impossible for chains to rearrange by slippage. Therefore, any application of stress on such a rigid molecular structure will cause the chains to break apart by breaking weaker interchain bonds, as well as backbone bonds. Such molecular processes appear to be responsible for the crazing phenomenon observed at the macroscopic level. Onset of nonlinearity in the stress-strain curve may also be related to development of crazes in these unoriented PS films. In the present research, the author seeks to investigate if these molecular processes actually cause crazes. For this purpose unoriented PS films are solvent-crazed by immersing them in ethanol for about 5 minutes and then flexing them a few times. Since only very fine crazes appear, and any craze-related differences may be very minute in the IR spectrum, specimens are studied by FTIR subtraction spectrum.

#### 5.4.3 FTIR results: Crazed vs. uncrazed atactic polystyrene

Figure 5.34 shows the (crazed-95% uncrazed) FTIR spectrum. The



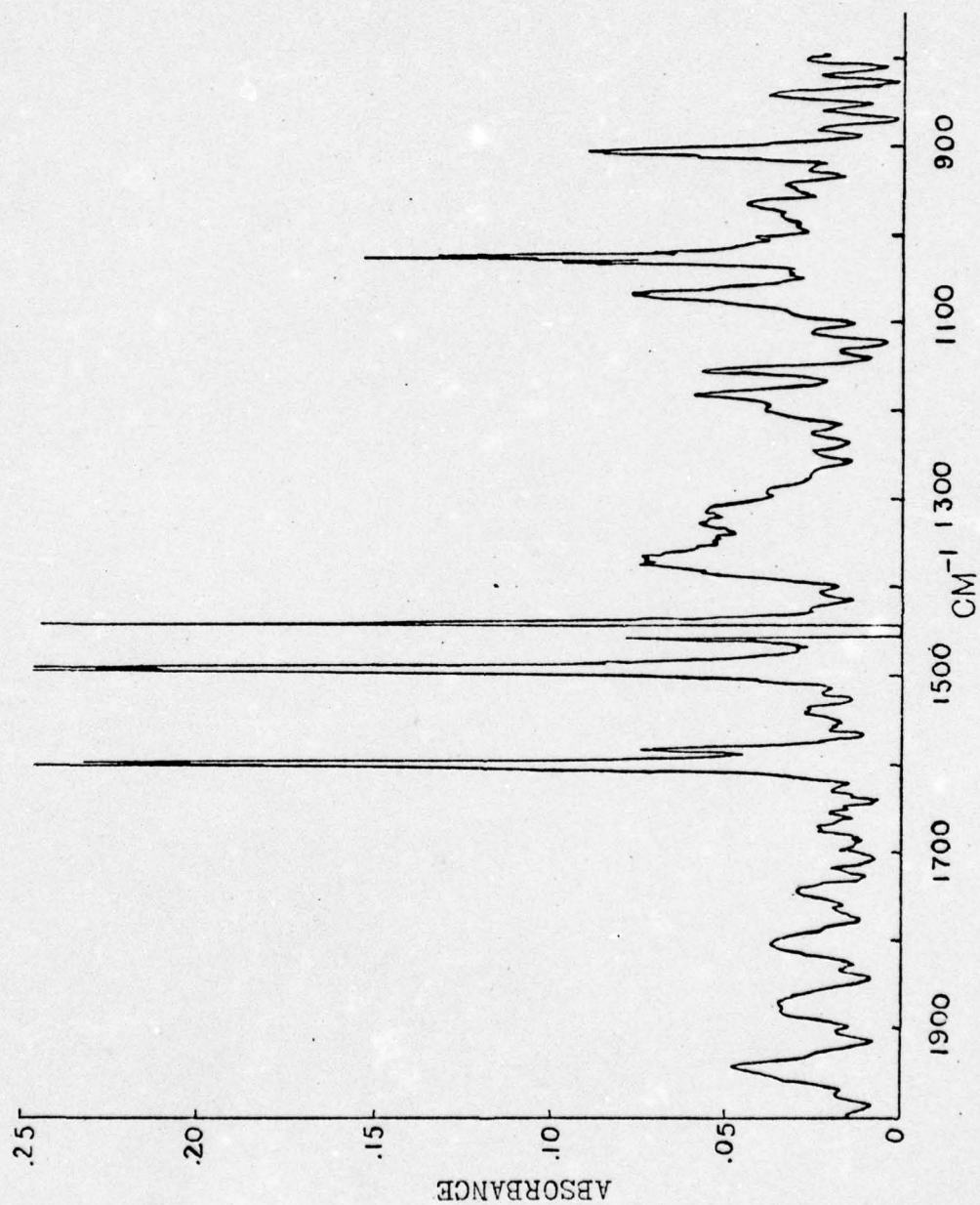


Figure 5.34 FTIR subtraction spectrum of uncrazed atactic polystyrene film.  
(Crazed-95% uncrazed)

bands at 540, 700 and  $763\text{ cm}^{-1}$  exhibit multiple splittings and, therefore, have not been drawn in this figure. Other bands which show splittings are 903, 1027, 1070, 1310, 1330, 1376, 1450, 1490, 1602 and  $1870\text{ cm}^{-1}$ . Additional IR bands emerging in the subtraction spectrum due to crazing are 880, 1130,  $1400\text{ cm}^{-1}$ . Assignments of these affected IR bands relate to the modification of the following vibrational modes: hydrogen bending modes, out-of-plane bending modes, in-plane bending modes of the CH in the phenyl ring, ring vibrations, bending mode of ( $\text{CH}_2$ ) group on the main chain, vibrations of the carbon ring where CH group moves as a unit.

The splittings, as discussed earlier, are caused by a change in the distribution of these frequencies. Since we observe extensive splitting, it can be inferred that individual polystyrene chains are under varying restrictions, i.e., certain chain segments are free to move while the others remain in the stressed state. This is evidenced by the appearance of additional bands which also emerge in the (stressed-unstressed) FTIR spectra. Thus, it seems that Van der Waals' bonds are actually broken in certain regions (where crazes appear) while remaining intact in other regions (uncrazed regions).

#### 5.4.4 X-ray results: Unoriented atactic PS under stress and in crazed state

Table 5.8 lists the Bragg distances and half widths calculated from the outer halos in the diffraction patterns of unoriented PS under no strain, strain and in crazed conditions.



Table 5.8 Bragg Distances in Unstrained, Strained  
and Stress Crazed Atactic Polystyrene

State of the Sample	Mean <sup>1</sup> $d_{\text{Bragg}}$ (Å)	Shift of $d_{\text{Bragg}}$ (Å)	Half width (cm)
Unstrained	4.75		0.30
Strained to 0.95% (70% of breaking strain)	4.91	0.16	0.38
Strained to 0.75% <sup>2</sup> (62% of breaking strain)	4.91	0.16	0.40
Stress-crazed <sup>3</sup> (stress not maintained on the sample during X-ray exposure)	4.95	0.20	0.38

<sup>1</sup>Mean  $d_{\text{Bragg}}$  is the average of  $d_{\text{Bragg}}$  calculated from equitorial, meridional and two diagonal positions on the X-ray scattering pattern.

<sup>2</sup>PS sample crazed during the X-ray exposure period.

<sup>3</sup>PS sample extensively crazed by keeping it under a strain of 0.75% for a period of 12 hours. Stress was removed during the X-ray exposure time.

#### 5.4.5 Discussion: Unoriented PS films

FTIR results obtained from crazed PS samples indicate the presence of uneven stress distribution on the chains. They also reveal that interchain interaction varies in the crazed films. X-ray results show increases in the Bragg distance of PS films under stress and in films which stress-craze during the X-ray exposure, as well as stress-crazed films not kept under stress during the X-ray exposure period. These results lead to believe that the chain rearrangements in the unoriented polystyrene are almost impossible because of high entanglements. Since there are too many obstructions and interferences hindering any chain mobility by slippage, PS chains overcome the cohesive forces through breaking them. These processes occur preferably at the polymer surfaces where inhomogeneities like air pockets, dirt particles, voids, etc. act as stress concentrators. Thus, it is these molecular processes along with rearrangements of certain phenyl groups (about the bond axis connecting the phenyl groups to the main chain) which yield increases in the intraphenyl and interchain distances. The author suggests that the uneven stresses observed in crazed PS samples are due to certain frozen-in stresses in the films, as well as to increased stresses on the chains adjacent to the crazed regions.

The overall molecular mechanism during crazes involves the separation of several chain segments from one another by breaking, mostly, the weaker cohesive forces, though some chain scission may also be involved. This, perhaps, explains the healing of crazes in polymers by raising the temperature above its  $T_g$ , at which there is an increased chain mobility, enabling large scale rearrangements of the polymer



chains.

Based on the above molecular processes the author suggests that the observation of nonlinearity in the stress-strain curve of the brittle PS films at about 3300 psi ( $0.72 \sigma_B$ ) is, perhaps, related to the onset of interchain separation. We did not observe any shear banding or necking in these unoriented films.

#### 5.4.6 Summary

Unoriented polystyrene films show crazes on their surface when stressed to a critical load and/or kept under a critical strain. These crazes result when highly entangled chains attempt to stress-relieve themselves by rearrangements. They appear preferably at the surface because it contains maximum inhomogeneities. Crazes seem to be formed when weaker cohesive forces between the chains are broken, either by a solvent or by an external stress. It is also revealed that while certain polymer chain segments free or stress-relieve themselves by crazing, other segments are overstressed. The author postulates that such overstressed chains are located in the regions surrounding the crazes.

### 5.5 Results and Discussion: Uniaxially Oriented Atactic PS

#### 5.5.1 Dynamic IR results

The stress-sensitive absorption bands were also studied in the case of 500% drawn uniaxial films. The birefringence of these films is  $\sim 2.23 \times 10^{-2}$  which represents a high degree of orientation [121]. The

perpendicularly polarized IR spectra were obtained for these films by stressing them to various levels. The load-elongation data of these films were obtained concurrently with the recording of IR spectra. The load-elongation behavior of these films, as a function of time, is shown in Figure 5.35. A stress-strain curve obtained from these data is shown in Figure 5.36. The superimposed IR spectra of 500% oriented PS film under no stress and stresses of 3375, 5400 and 8785 psi are shown in Figures 5.37 to 5.39, respectively. These figures show that increasing the stress on the sample above 5400 psi causes an increase in the percent transmittance due to thinning of the sample. This effect is due to creeping of the sample, as evident from Figure 5.35. The band distortions in these PS films at a stress of 3375 psi are minor as compared to band distortions observed in the TRICITE films. However, low frequency distortions of  $1182\text{ cm}^{-1}$  band and negative frequency shift ( $\sim 2\text{ cm}^{-1}$ ) are quite evident in Figures 5.38 and 5.39. Band distortions of  $1070\text{ cm}^{-1}$  band are also obvious in these figures. As shown in Figure 5.35 these highly oriented samples split at a stress of 10,800 psi and no additional stress can be applied.

#### 5.5.2 Discussion of uniaxially oriented atactic PS

The stress-strain data of these films show high breaking stress. Maximum strain at the breaking point is 3.5%. The shape of stress-strain curve and fibrillation of these films demonstrate polystyrene chains to be highly oriented.

Dynamic IR results obtained from 500% drawn films suggest that interchain interferences caused by the bulky phenyl side groups are



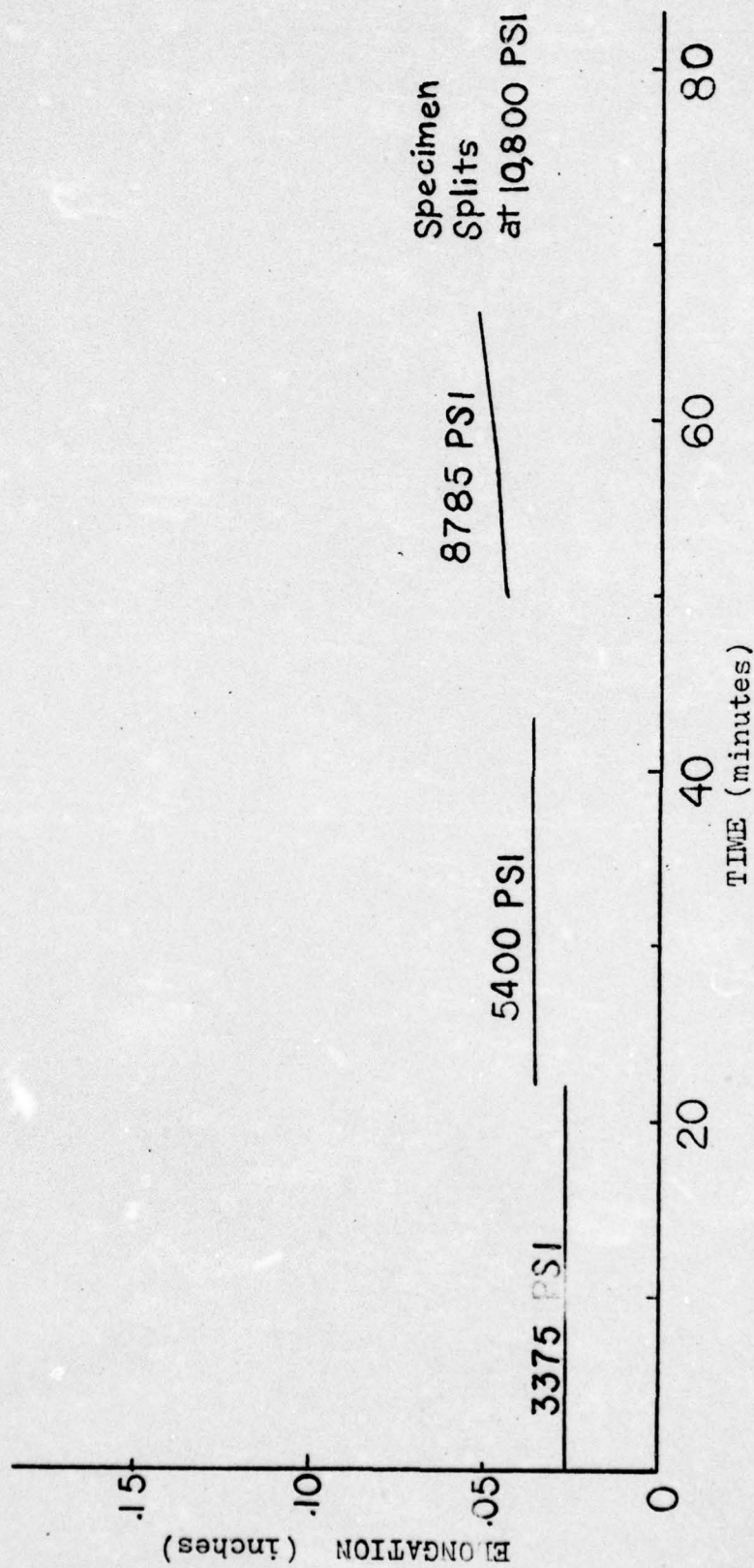


Figure 5.35 Creep response of 500% uniaxially oriented polystyrene film.

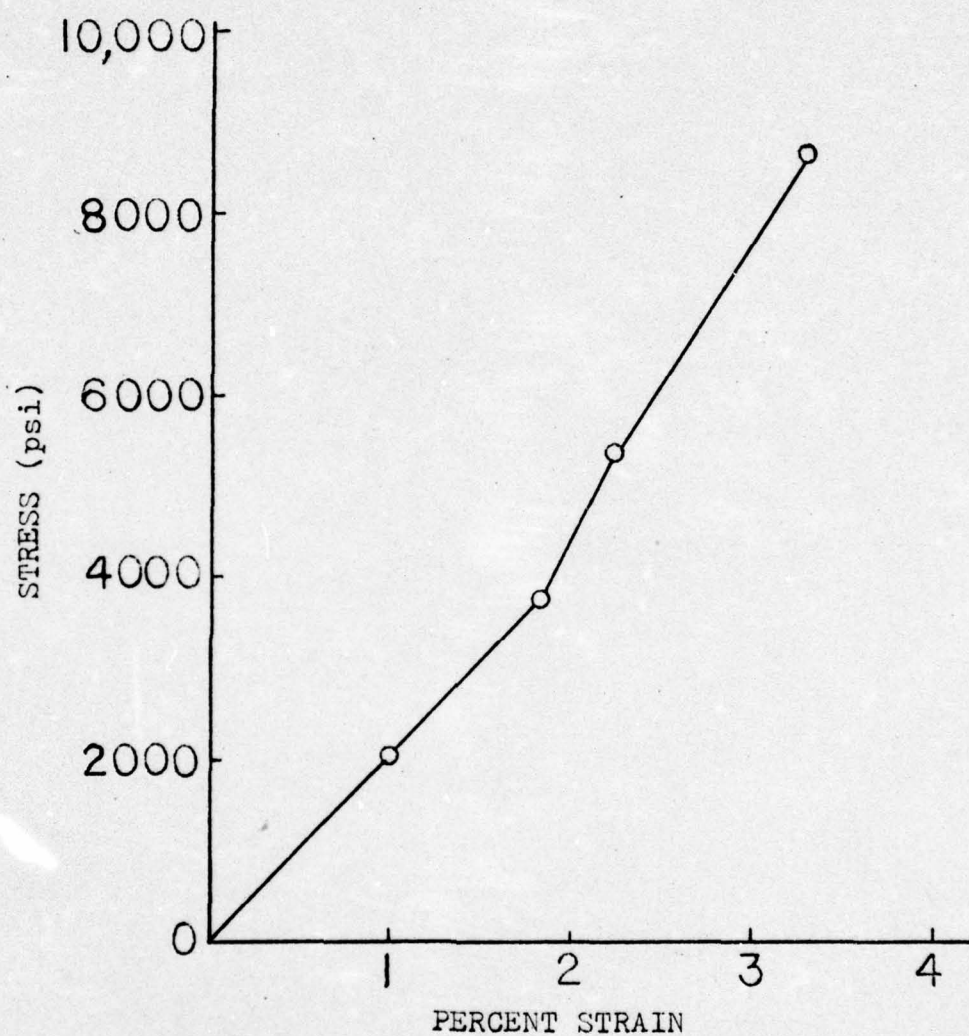


Figure 5.36 Stress-strain curve of 500% uniaxially oriented atactic polystyrene film. Gage length = 1.833".



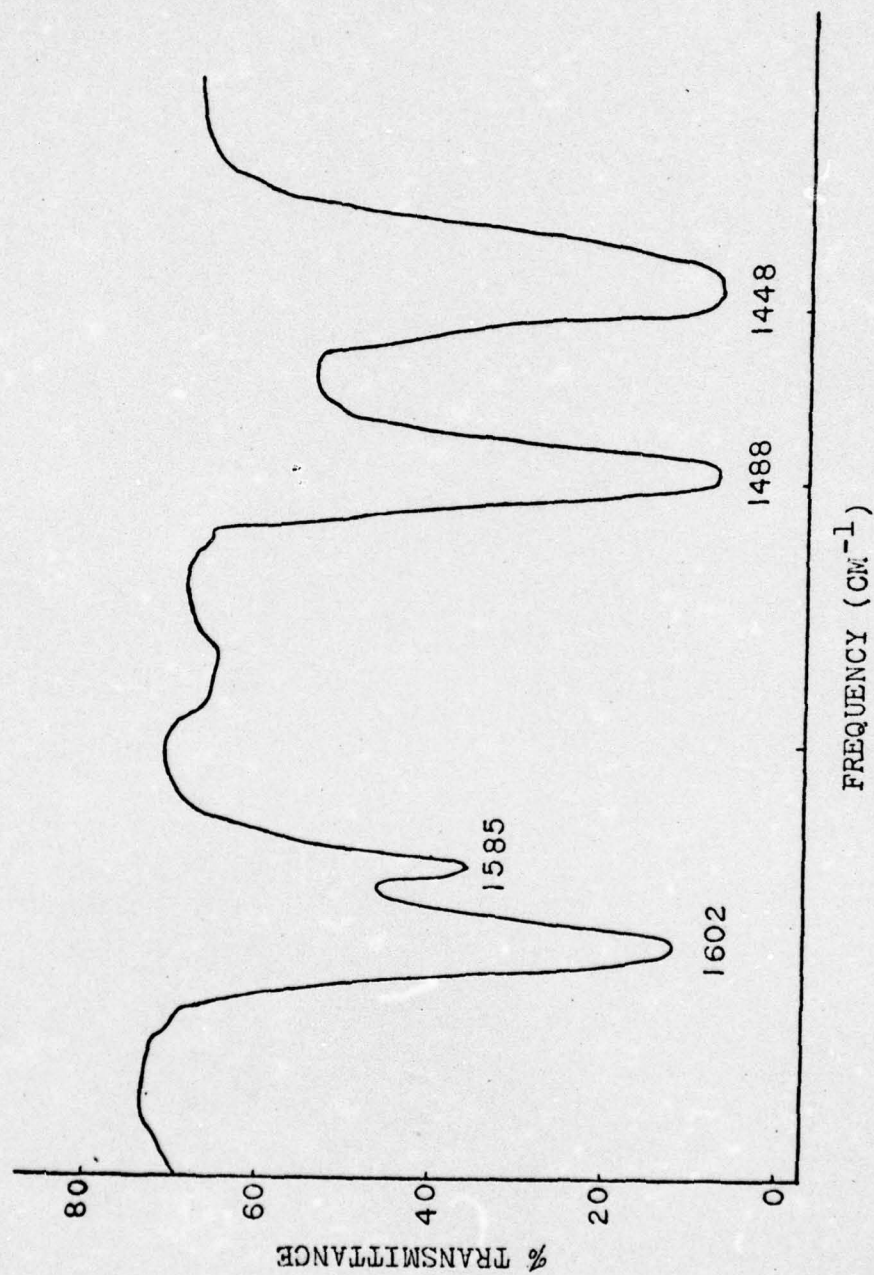


Figure 5.37 (a) IR spectrum of 500% uniaxially oriented atactic PS film under no stress and stress of 3375 psi. No change was observed in the spectrum due to stress.



Figure 5.37 (b) IR spectra of 500% uniaxially oriented atactic PS film under no stress (—) and stress of 3375 psi (---).



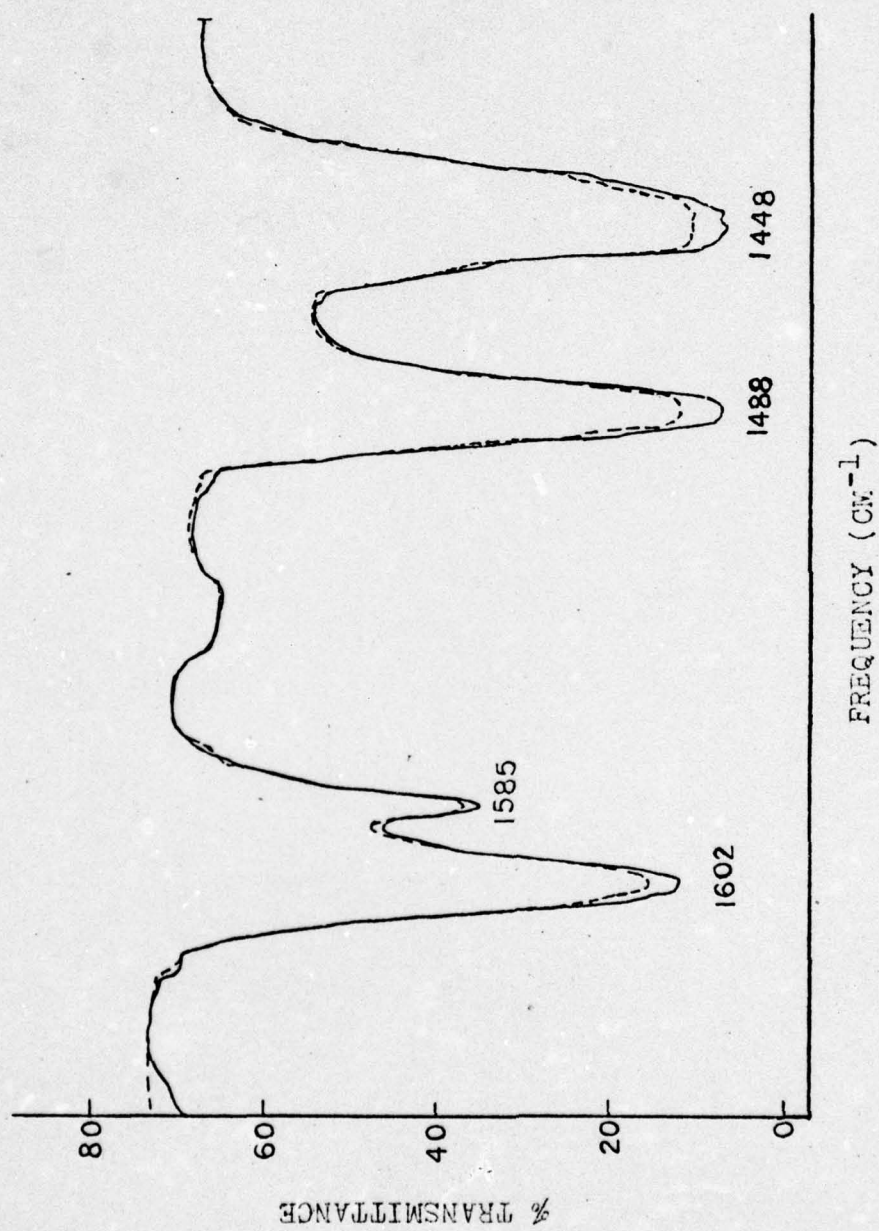


Figure 5.38 (a) IR spectra of 500% uniaxially oriented PS film under no stress (—) and stress of 5400 psi (---).

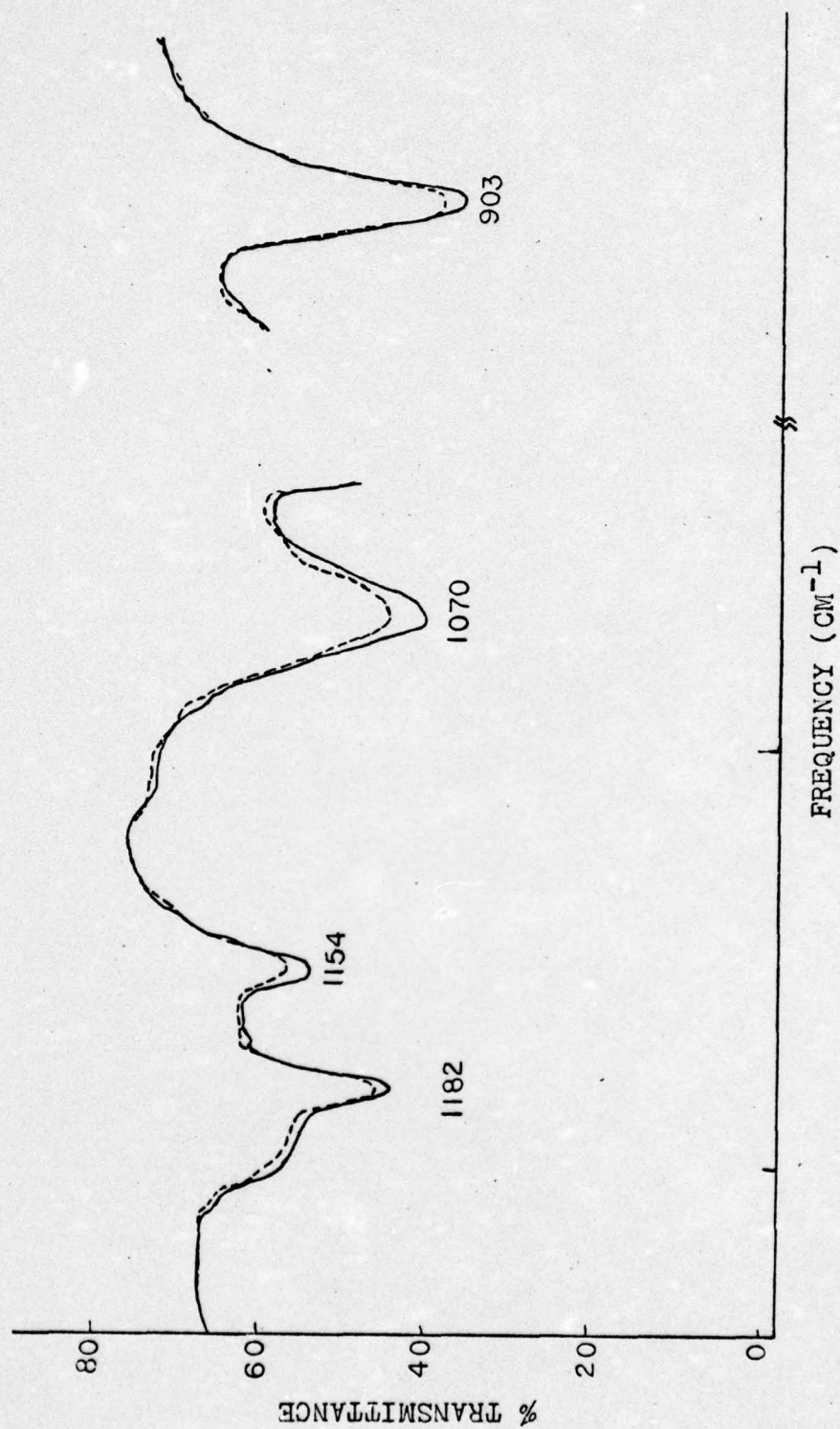


Figure 5.38 (b) IR spectra of 500% uniaxially oriented PS film under no stress (—) and stress of 5400 psi (---).



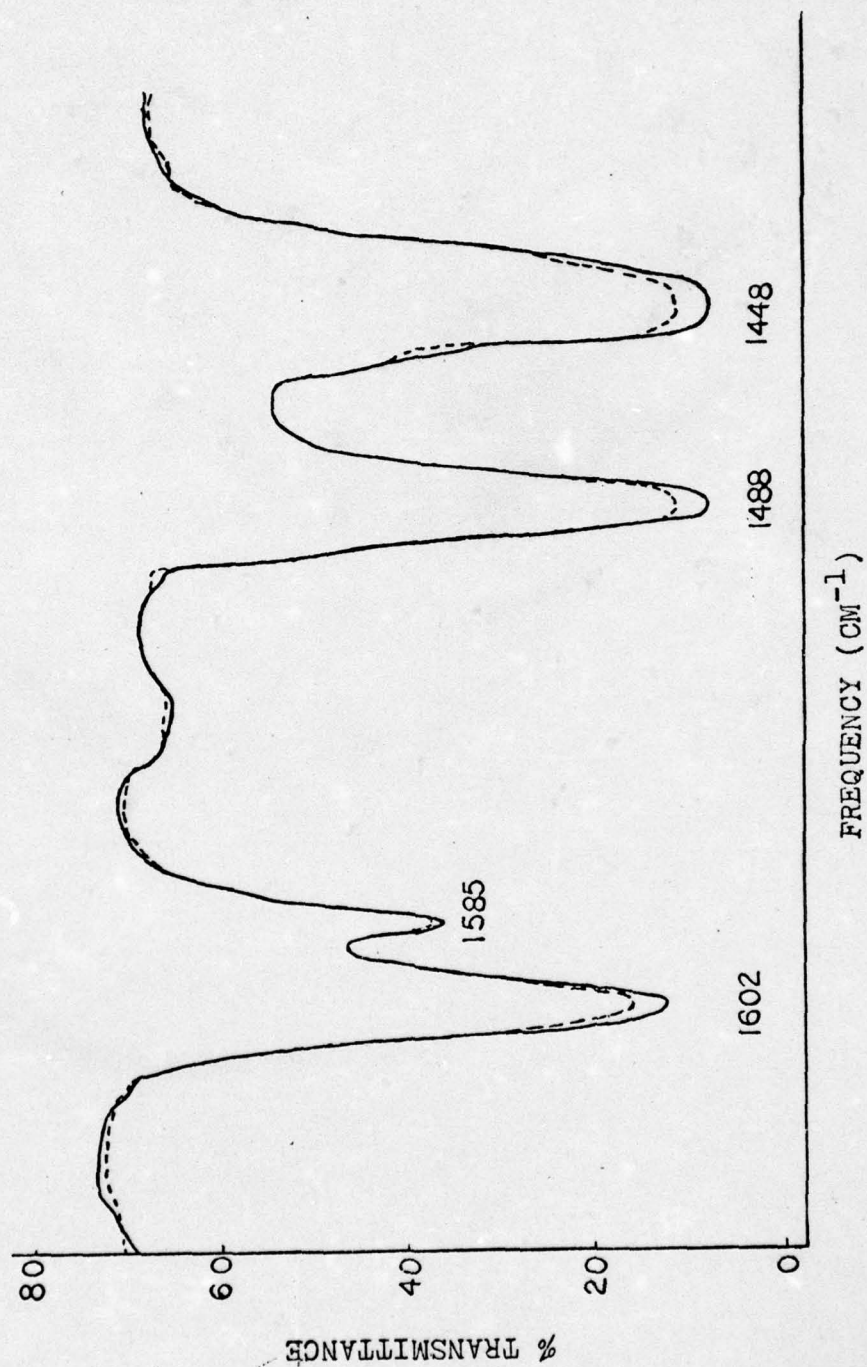


Figure 5.39 (a) IR spectra of 500% uniaxially oriented atactic PS film under no stress (—) and stress of 8785 psi (---).

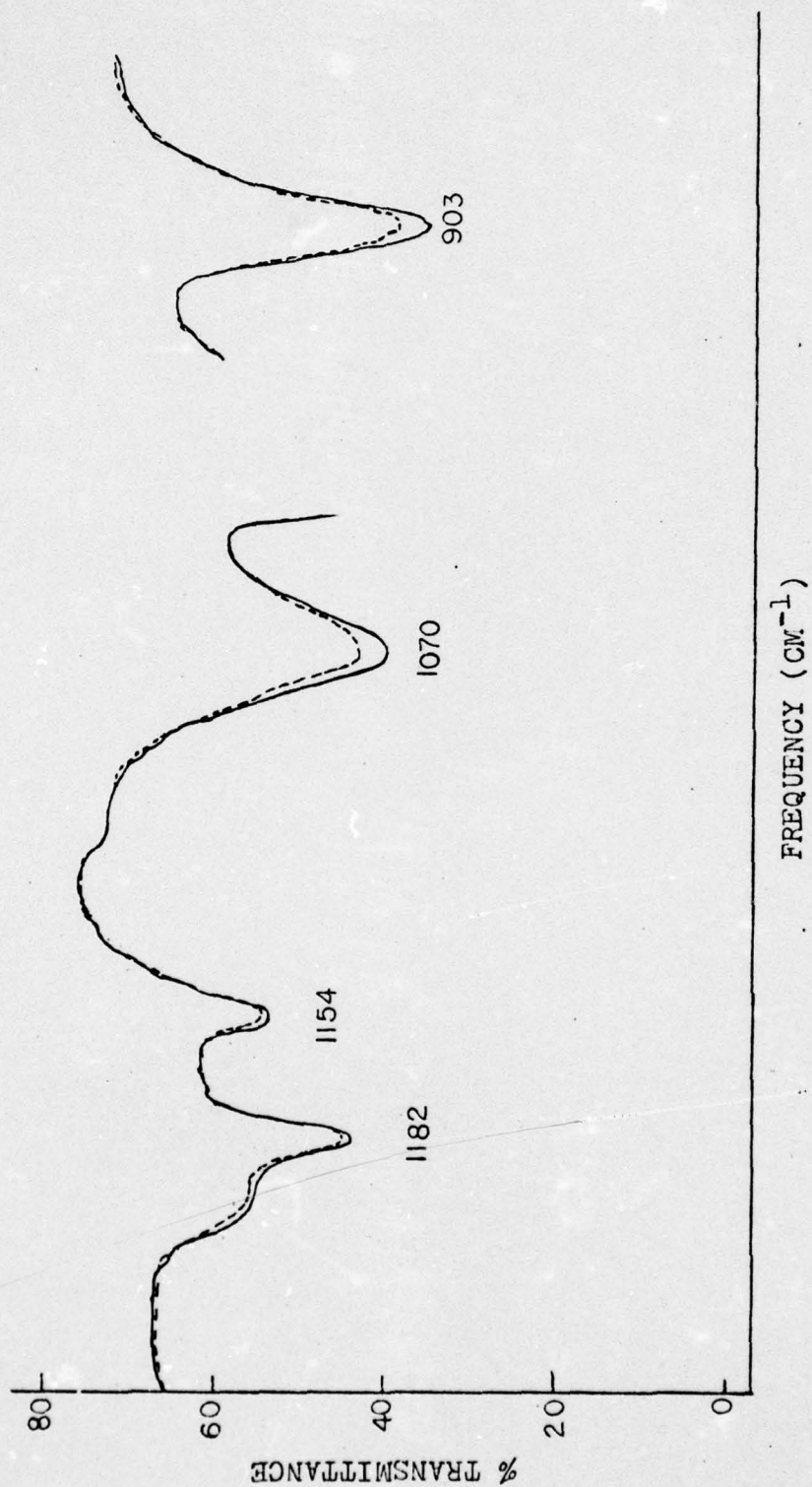


Figure 5.39 (b) IR spectra of 500% uniaxially oriented atactic PS film under no stress (—) and stress of 8785 psi (---).



considerably diminished in these uniaxially oriented films, as compared to TRICITE films under comparable stress. The frequency shifts of about  $-0.5\text{ cm}^{-1}$  of  $1182\text{ cm}^{-1}$  band and  $-2\text{ cm}^{-1}$  of  $1154\text{ cm}^{-1}$  IR bands indicate that stresses are transmitted to the backbone bonds through a network of interphenyl lockings. This mode of stress distribution abates the effect of stress on the phenyl side groups and, therefore, a shift rather than the band distortion is observed in the case of  $1154\text{ cm}^{-1}$  IR band. These results, together with the previous IR data of TRICITE films under stress, suggest that PS chains are well oriented in these samples and their alignment may be somewhat similar to the models pictured in Figure 5.24. Of course, this figure shows rather ideal alignment of the PS chains, whereas in reality there may be certain slack chain segments between the interphenyl lockings responsible for the minor distortions observed in  $1154\text{ cm}^{-1}$  band. Even though the actual orientation of PS chains may differ somewhat from the one just described, it is suggested that a large number of partial interlocking of the phenyl side groups are instrumental to an even stress distribution on most polymer chains. Since the chains are well oriented with respect to one another, they respond to an imposed stress in a collective manner (like a bundle). This way, any chain mobility is rather uniform and in large aggregates of such chains. This sort of mechanism helps to reduce high interphenyl interferences which occur when even fewer segments are able to slide past one another under the applied stress.

The author suggests that this interesting behavior of highly oriented films needs to be further explored through FTIR spectroscopy,

X-rays and dynamic mechanical measurements.

### 5.5.3 Summary

Study of the molecular behavior of highly uniaxially oriented polystyrene films shows that a better alignment of PS chains, perhaps, produces a large number of partial interphenyl couplings. This sort of network structure formed by many extended and interlocked chains helps to distribute the imposed stresses in a uniform manner over a large number of chains. These processes, in turn, reduce the slippage of individual chains past one another and hence the excessive deformations of the phenyl side groups. The stresses are, therefore, transmitted to many backbone bonds of the polystyrene chains. This type of molecular behavior may indeed be responsible for increasing the breaking stress by many times, as compared to unoriented or biaxially oriented polystyrene films.



## CHAPTER VI

### RESULTS AND DISCUSSION OF POLYCARBONATE OR (POLY-4,4'-DIOXYDIPHENYL-2,2-PROPANE CARBONATE)

The results presented and discussed in this chapter are obtained with a motivation to investigate the molecular behavior in polycarbonate (PC) under tensile stress, cyclic fatigue and in the crazed state.

#### 6.1 Results and Discussion: Unoriented polycarbonate (LEXAN<sup>®</sup>) Films

##### 6.1.1 Physical and mechanical measurements

The density of unfatigued films is 1.1976 g/ml. No birefringence are observed in these films indicating that samples are either free of residual orientations or such effects are too small to be observed. The  $T_g$  of these films obtained through Differential Thermal Analyzer is 149°C.

Figure 6.1 shows the stress-strain behavior of 3 mil thick polycarbonate film strained at a rate of 100%/minute in the Instron machine. The film dimensions used in these tests are--width: 0.5", gage length: 2". The stress-strain curve in Figure 6.1 illustrates the toughness and drawability of these PC films. Under the above test conditions the ultimate failure (fracture) of PC film occurs at a strain of about 110%.

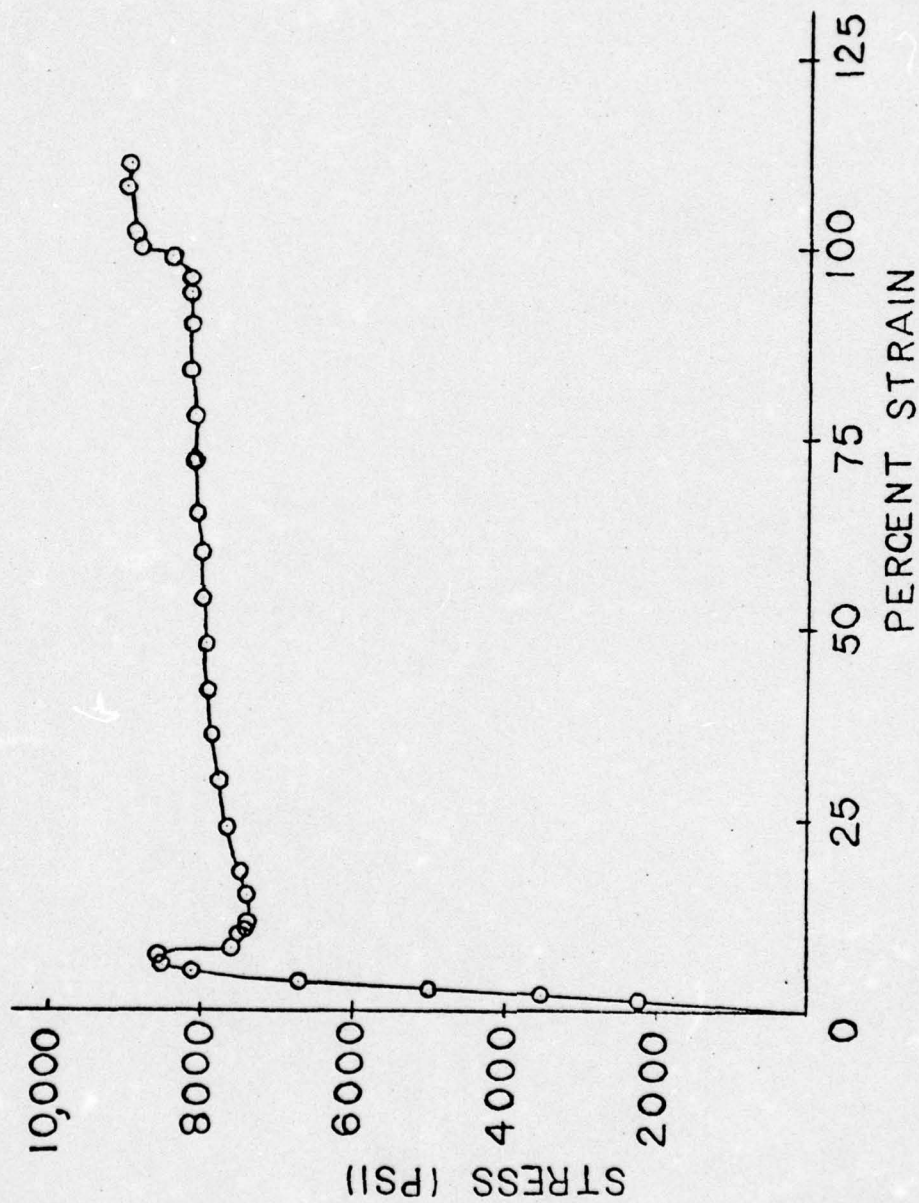


Figure 6.1 Stress-strain curve of 3 mil thick unoriented polycarbonate (LEXAN)<sup>®</sup> film.  
Gage length - 2 in., strain rate = 2 in/min.



### 6.1.2 IR results

IR absorption bands of PC films are recorded at three different stages:

The first stage--unoriented unstressed state.

The second stage--where the films have been stressed to  $\sim 6166$  psi (72% of yield stress). This stress level lies in the linear region of stress-strain curve.

The third stage--strain hardening region of stress-strain curve just before the fracture point. Engineering stress maintained on the film at this stage is 7333 psi.

Figure 6.2 shows stages 2 and 3, along with the creep behavior of the film.

Figure 6.3(a) and (b) shows the superimposed IR spectra of unstressed and stressed PC film. The stressed PC film is at stage 2, as described above. Figure 6.3(a) shows very small shifts ( $0.5\text{ cm}^{-1}$ ) in the bands at  $2965$  and  $2870\text{ cm}^{-1}$ . In addition, distortions and/or minor shifts are observed in  $1890$ ,  $1770$ ,  $1408$  and  $1362\text{ cm}^{-1}$  bands. Figure 6.3(b) shows a noticeable change in the peak shape of  $1102\text{ cm}^{-1}$  band in which absorption increases toward the low frequency. The band at  $555\text{ cm}^{-1}$  also shows slight distortion. From the band assignments for PC given in Table 3.3 we observe that the following vibrational modes associated with the above IR bands are affected due to stress.

- (a) Change in both, asymmetric and symmetric stretching vibrations of the methyl groups attached to the central carbon atom in the PC repeat unit.
- (b) Change in C=O stretching vibration.
- (c) Change in in-phase, symmetrical methyl bending mode.
- (d) Changes in the stretching modes of  $A_1$  species of the benzene ring described below where C and H atoms in the ring

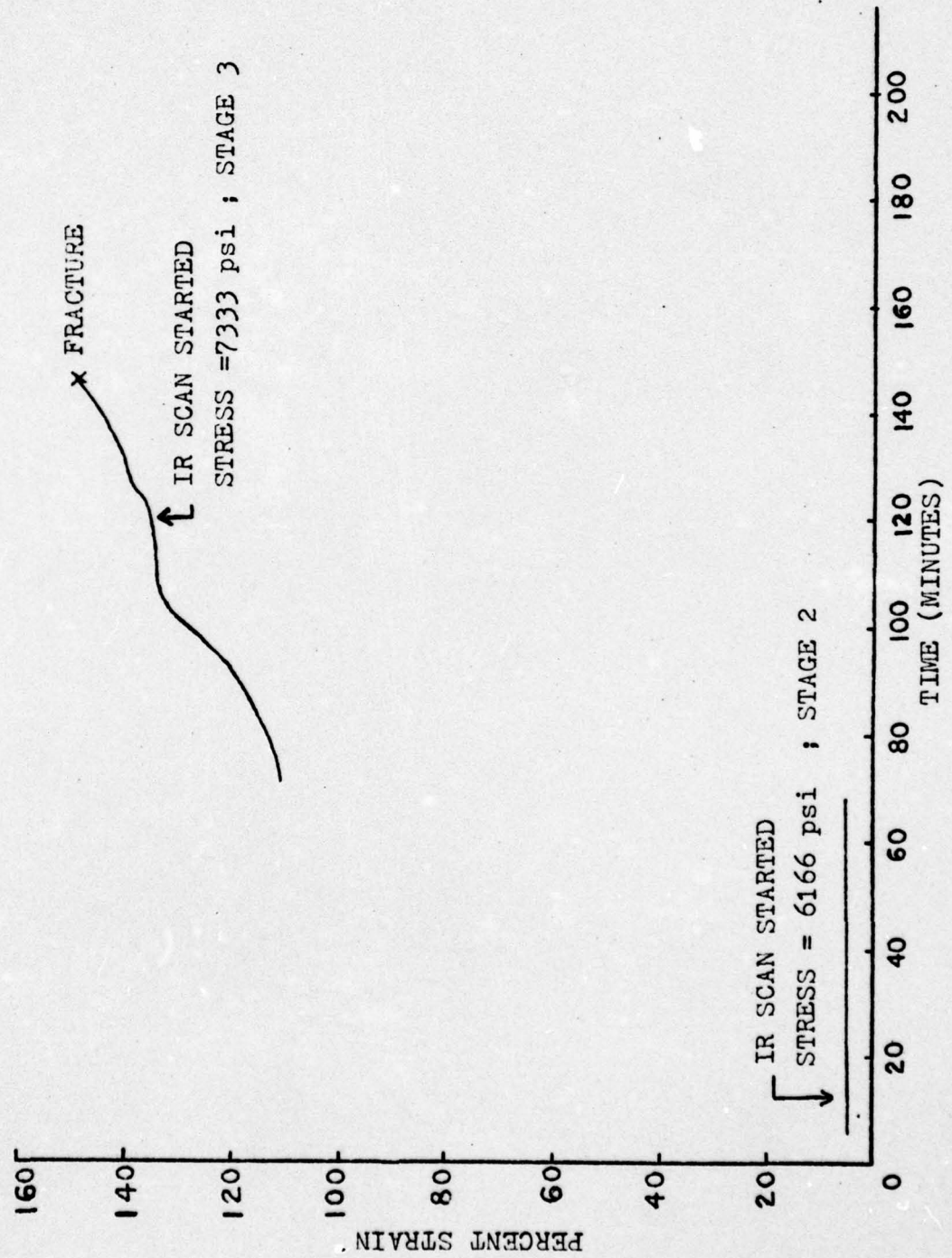


Figure 6.2 Creep behavior of unoriented polycarbonate film during the IR scans. Stage 1 is the unstressed state.



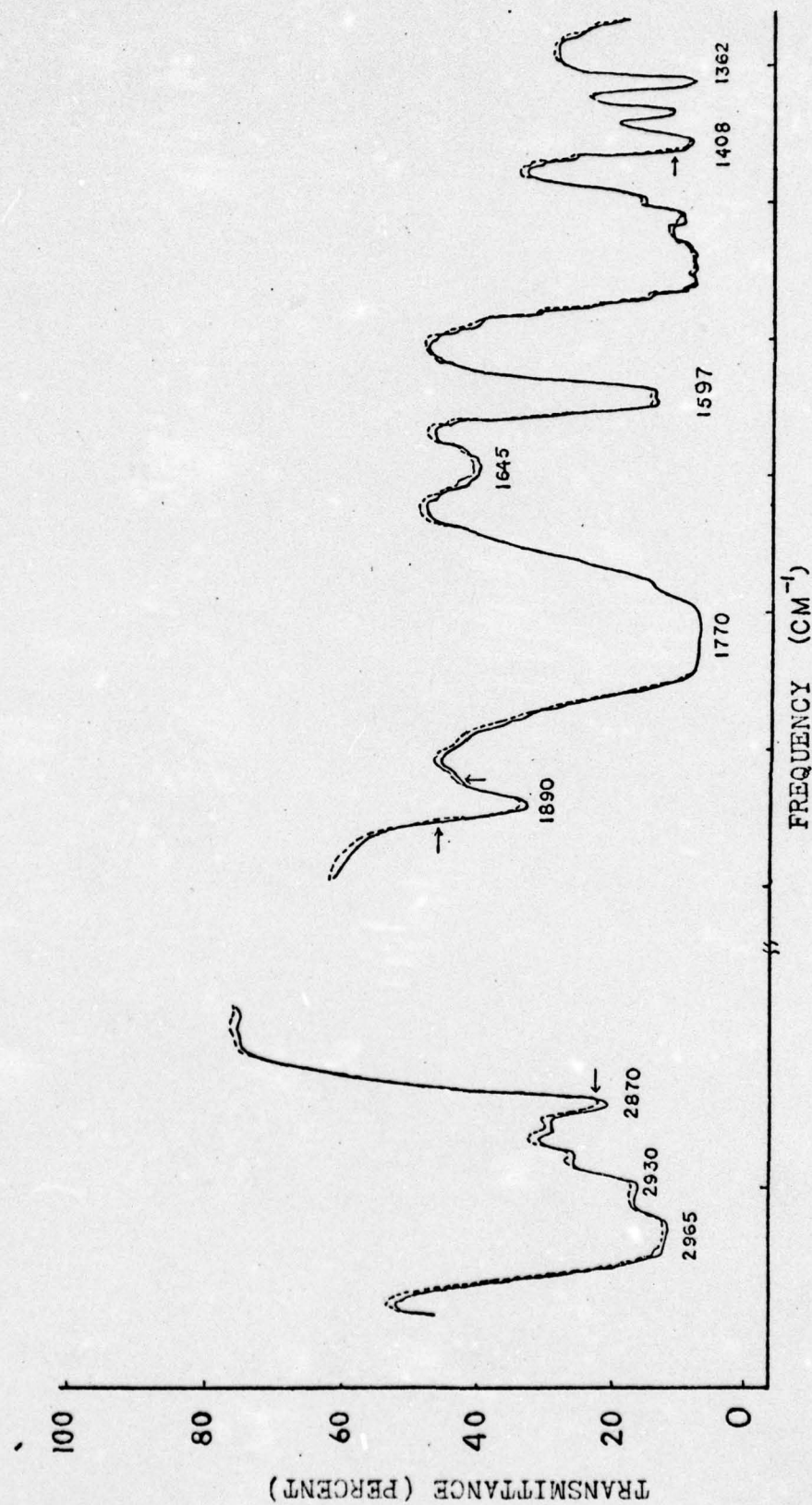


Figure 6.3 Superimposed IR spectra of polycarbonate film under no stress, i.e., in Stage 1, (—) and a stress of 6166 psi, i.e., Stage 2, (---).

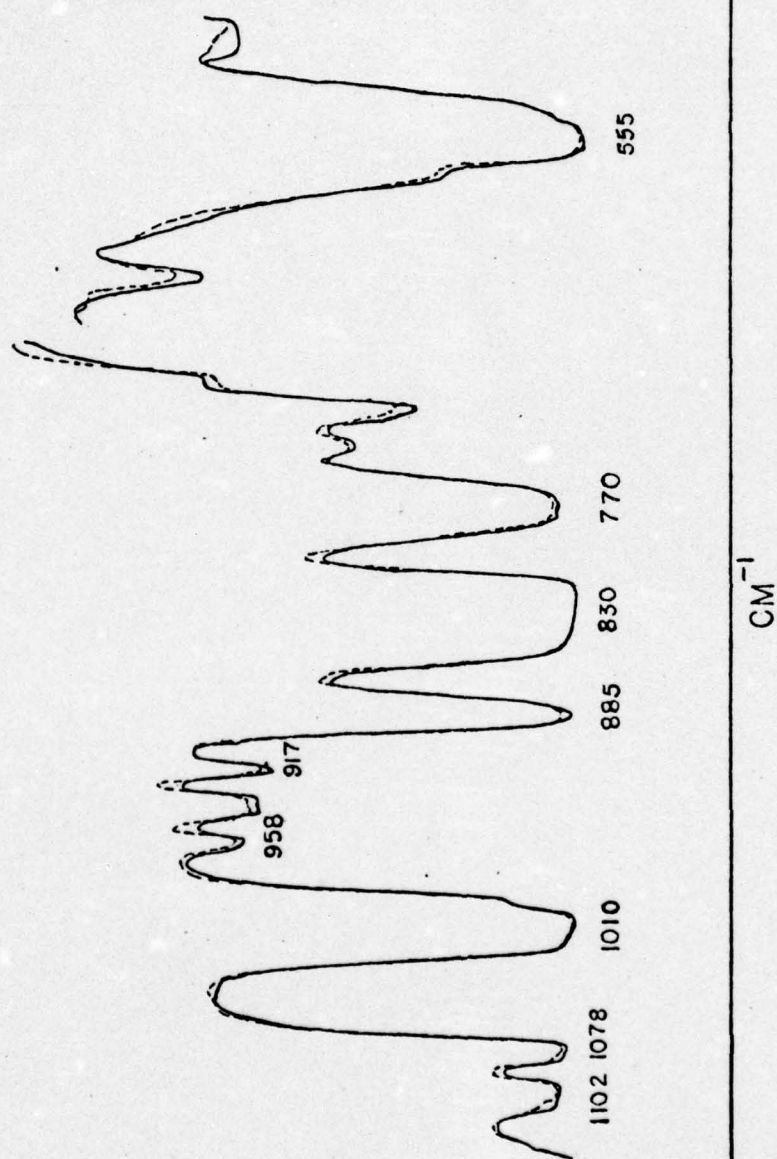
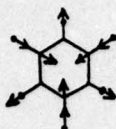


Figure 6.3 (b) Superimposed IR spectra of polycarbonate film under no stress, i.e., Stage 1, (—) and a stress of 6166 psi, i.e., Stage 2, (---).



essentially move as a unit.



$A_1$  stretching mode of the benzene ring.

- (e) Out-of-phase bending of the H atoms of p-disubstituted benzene ring.

Figures 6.4(a) and (b) show the superimposed spectra of PC film under no stress and stress, where stressed state is the stage 3 shown earlier. As seen in figure 6.2, the PC film by this stage has undergone very high strain (136%) and is reduced in thickness. As a result, there is a large increase in the percent transmittance and it is not possible to exactly superimpose the IR bands. Nevertheless, a qualitative information about the differences in IR bands can be obtained by careful comparative examination of the IR bands of unstressed and stressed PC film. Figure 6.4(a) shows very small changes occurring under stress in 2965, 2870, 1890, 1775, 1408 and 1362  $\text{cm}^{-1}$  bands, as observed in Figure 6.3(a) also. Figure 6.4(b) shows a distinct change in shape of 1102  $\text{cm}^{-1}$  IR band on stressing. A very small but noticeable difference in peak shape of 1078  $\text{cm}^{-1}$  band assigned to C-C stretch of the backbone bond is observed. Other differences are: change in peak shape of 1015  $\text{cm}^{-1}$ , shoulder distortion of 770  $\text{cm}^{-1}$  and appearance of a shoulder in 555  $\text{cm}^{-1}$  IR bands.

Thus, IR absorption bands obtained at stage 3 show only small additional changes from those observed in stage 2. From these very small IR changes observed, even at stage 3 which lies just prior to

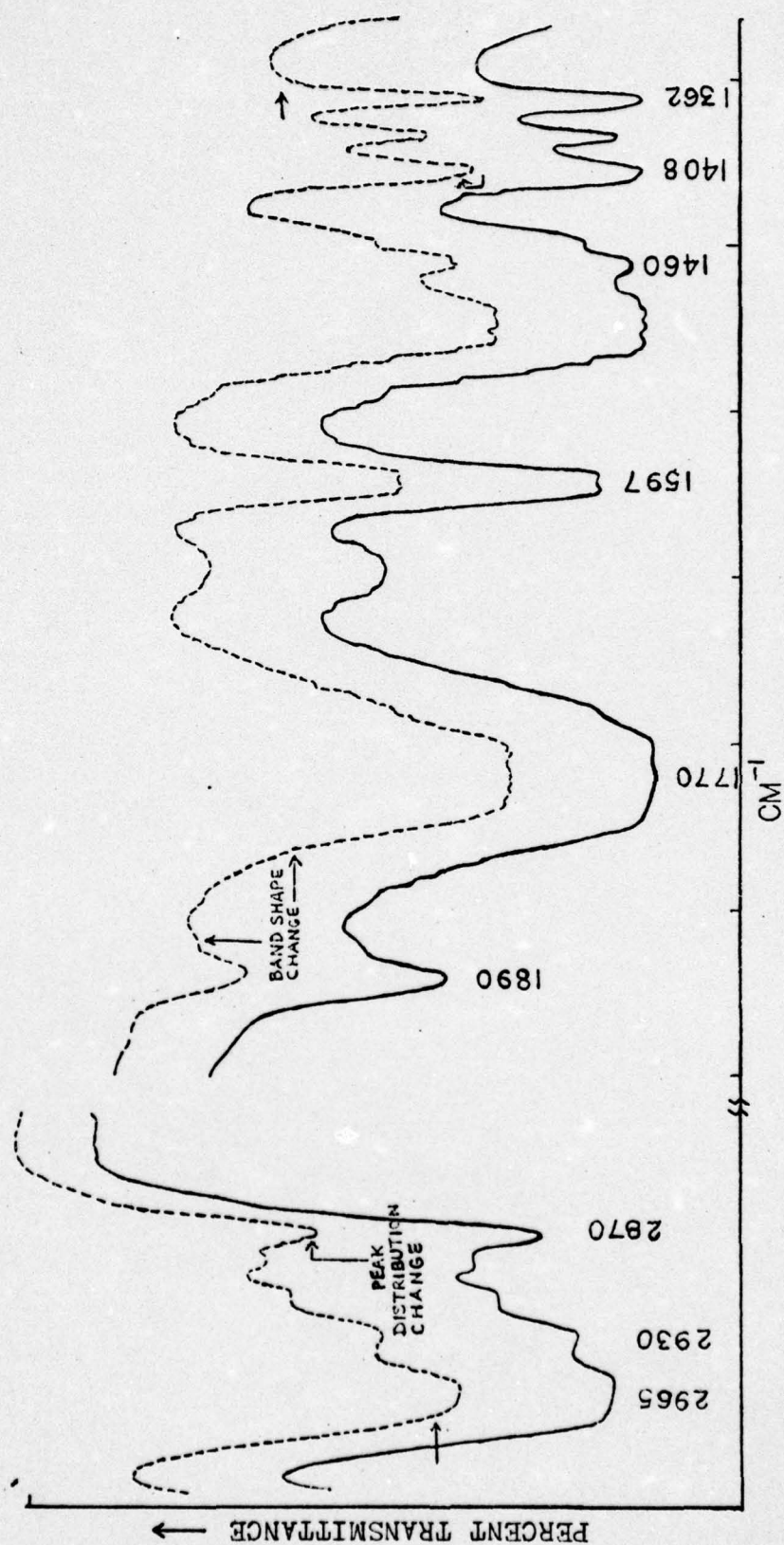


Figure 6.4 (a) Superimposed IR spectra of PC film under no stress (—) and stress of 7333 psi, i.e., Stage 3, (---). Spectra are displaced because of creep.



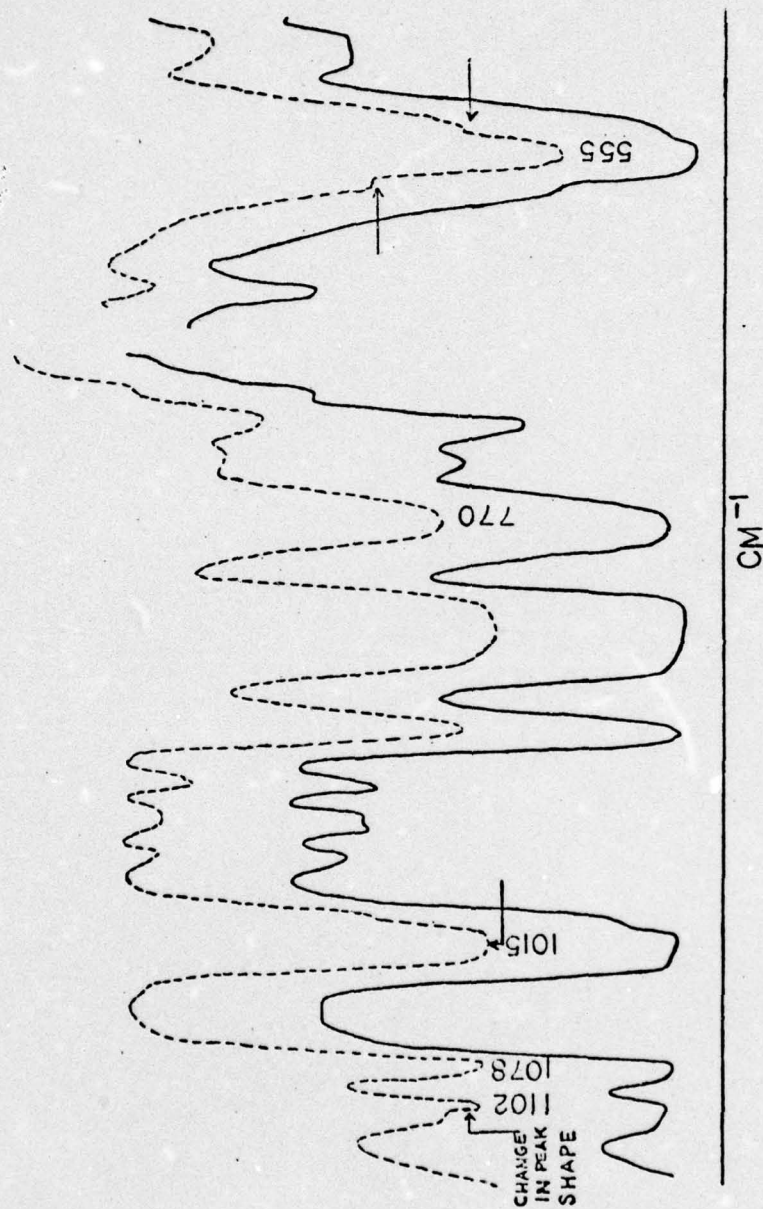


Figure 6.4 (b) Superimposed IR spectra of PC films under no stress (—) and stress of 7333 psi, i.e., Stage 3 (---). Spectra are displaced because of creep.

fracture, the author believes that in unoriented PC films the stress is distributed on a very large number of chains, therefore, no overstressed backbone bonds are observed. Most changes occur in the intermolecular and intramolecular interactions. These changes are anticipated when: (a) weak Van der Waal's bonds binding the chains together are broken during the chain slippage process and (b) the polymer chains are extended in the direction of applied stress. Thus IR results indicate that PC chains respond to applied stress by large scale chain-slippage process in which chains pull themselves out from the physical entanglements. Of course, by doing so, some of the chains extend themselves and become taut in the process. Then, any increase in stress on these taut chains will lead to breakage of their backbone bonds, and because of such molecular behavior under tension, a small shift is observed in  $1078\text{ cm}^{-1}$  IR band (assigned to C-C stretching vibration of the backbone bond). This indicates that many oscillators are absorbed at slightly different frequency, causing a change in the peak shape of this band.

### 6.1.3 X-ray results

Table 6.1 lists the Bragg distances calculated from unstrained and strained PC film (strained to 4.65%). Calculations of these distances are made from the diffractometer traces, as discussed in Chapter IV. The mean shift in Bragg distance on straining PC film is found to be  $0.544\text{ \AA}$ . The half width is also found to increase on straining the PC film. This is indicative of the increased variation about the mean Bragg distances in the strained PC films.



Table 6.1 Bragg Distances Calculated for Unstrained and Strained PC Film

Position on the Diffraction Pattern	$d_{\text{Bragg}}$ Å (unstrained PC)	Half width (cm)	$d_{\text{Bragg}}$ Å (strained PC)	Half width (cm)	Shift in $d_{\text{Bragg}}$ Å on straining
Equatorial	5.4792	0.30	4.9283	0.40	- 0.5509
Meridional	5.4789	0.30	4.9283	0.38	- 0.5506
Diagonal (1)	5.4784	0.34	4.9457	0.38	- 0.5327
Diagonal (2)	5.4761	0.34	4.9355	0.38	- 0.5416

#### 6.1.4 Discussion of the molecular behavior of unoriented PC film under stress

In the unoriented PC state the author assumes that the chains are distributed in a random manner<sup>1</sup>. The infrared results presented in the previous section indicate that on application of tensile stress, even at levels less than 72% of the yield stress, flexible polycarbonate chains begin to disengage from the entangled mass by breaking Van der Waal's bonds and by molecular rearrangements. If this stress is kept for a longer period of time, these chains respond to external stress by orienting themselves along the direction of applied stress. Since polycarbonate polymer has high free volume in its microstructure [122] and there are no bulky side groups present on the chains to cause hindrances, the chains can move about rather easily under the applied stress or strain. As a result, the stresses are distributed more evenly (than in the case of polymers with bulky side groups) over a large number of polymer chains. However, few chains which are tangled badly and cannot pull themselves out by slipping, either break or become taut. Therefore, under these circumstances, they will bear relatively more stresses. This explanation of the molecular behavior is based on relatively small shifts and distortions observed in the absorption frequencies of backbone and related IR bands. The above interpretation also derives support from the X-ray results presented in Table 6.1.

It has been suggested by Wignall and Longman [123] that the outer

---

<sup>1</sup>The author is not taking into consideration any long range order present in the amorphous structure as mentioned in the Introduction.



halo in the X-ray diffraction pattern of polycarbonate is due to average intermolecular distances in the polymer structure. The peak corresponding to these distances occurs at  $\sim 5.5 \text{ \AA}$ , as observed in our present studies. The present study shows that the intermolecular distances decrease by about 9.9% when PC film is kept under strain of  $\sim 4.14\%$  during the X-ray exposure period. This strain of 4.14% is equivalent to a stress of  $\sim 7000 \text{ psi}$  (as determined from the stress-strain curve shown in Figure 6.1). This stress amount is an approximation because there is a difference in the strain rates in these two cases (straining on the Instron vs. straining on X-ray stretching device).

On the basis of IR and X-ray data the behavior of polycarbonate chains under stress can be described by the following models. Figure 6.5(a) represents the unstressed state (Stage 1) of the unoriented films. Figure 6.5(b) represents the stressed state (stage 2) of the unoriented film. Figure 6.5(c) represents the strain hardening region (Stage 3) of PC film.

As modeled in Figure 6.5, even just before the fracture point there may be many polymer chains which are not fully extended. The fracture of such ductile material probably occurs when cracks propagate through the voids created by chain slippage and chain scission.

#### 6.1.5 Summary

IR and X-rays results point out that polycarbonate chains rearrange themselves in response to an external stress. Such rearrangements occur rather easily due to relatively high free volume available in the microstructure of this polymer. In order to stress-relieve, chains

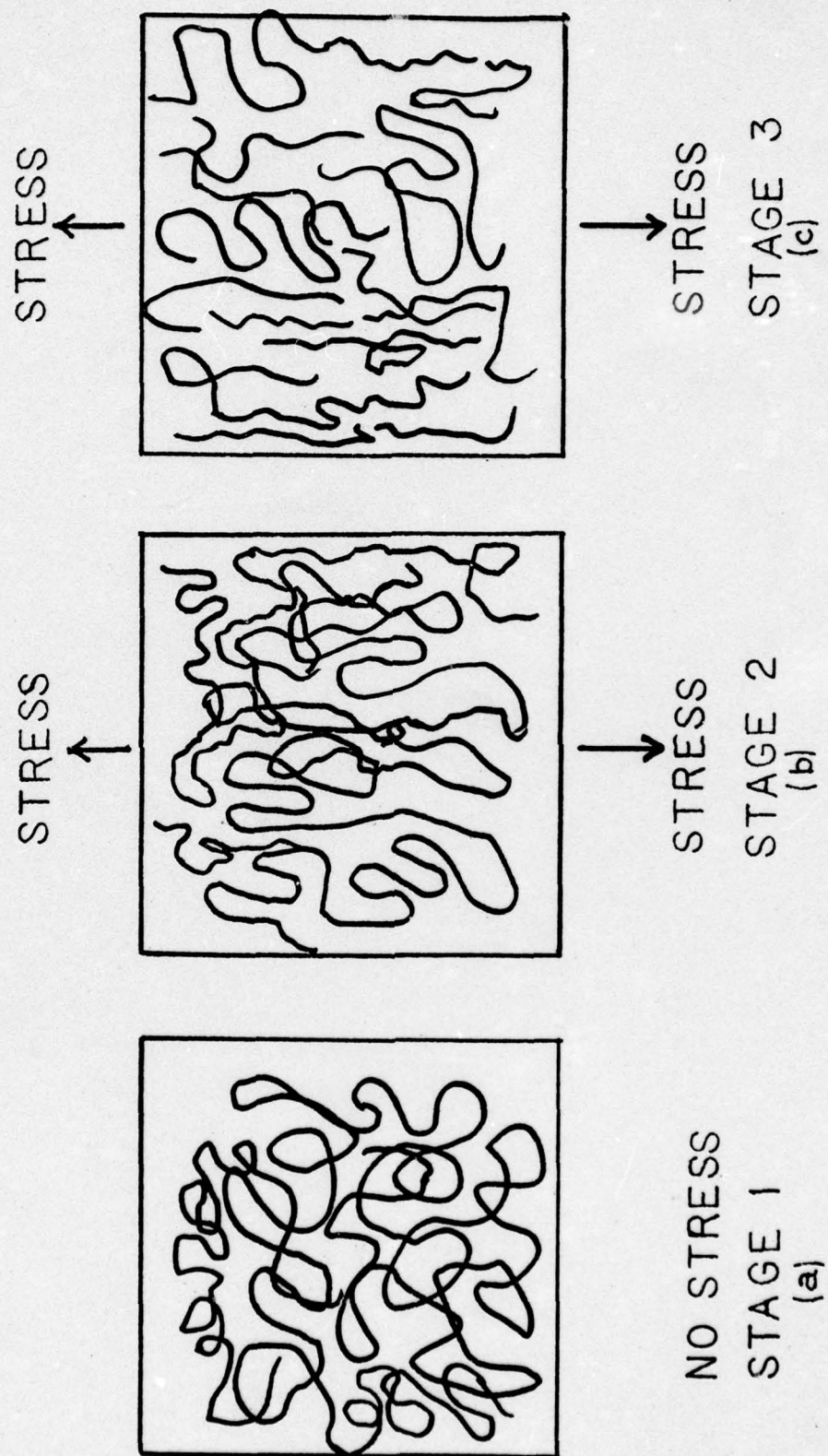


Figure 6.5 Models for the molecular behavior of PC films under no stress and on stressing.



reorient along the direction of the applied stress and thus decrease the interchain distances.

The external stress on the sample is distributed rather evenly over a large number of polymer chains.

## 6.2 Results and Discussion: Unoriented Fatigue Polycarbonate Films

### 6.2.1 Stress-strain and fatigue results

Figure 6.6 shows the load-elongation curve obtained from PC film specimens of dimensions 0.5" wide x 4" long for load-controlled cyclic fatigue on the Instron machine.

Tables 6.2 and 6.3 list the details of fatigued samples including the density results of these samples.

### 6.2.2 FTIR results

Infrared spectra of fatigued PC film sample, 108-2 listed in Table 6.2 are obtained on the Fourier Transform Spectrometer; for the purpose of comparison, a spectrum of unfatigued PC film of the same thickness (0.003") is also obtained. A superimposed spectra of fatigued and unfatigued sample is shown in Figure 6.7. However, such superimposed spectra do not show all the minute changes, such as peak shifts of less than  $1\text{ cm}^{-1}$ . Therefore, to detect these minute changes, computer-subtracted IR spectra are plotted, where different percentages of the spectrum of unfatigued sample is subtracted from the spectrum of fatigued sample. One of such subtraction spectra (fatigued-90% unfatigued) is shown in Figure 6.8. The IR bands affected by the

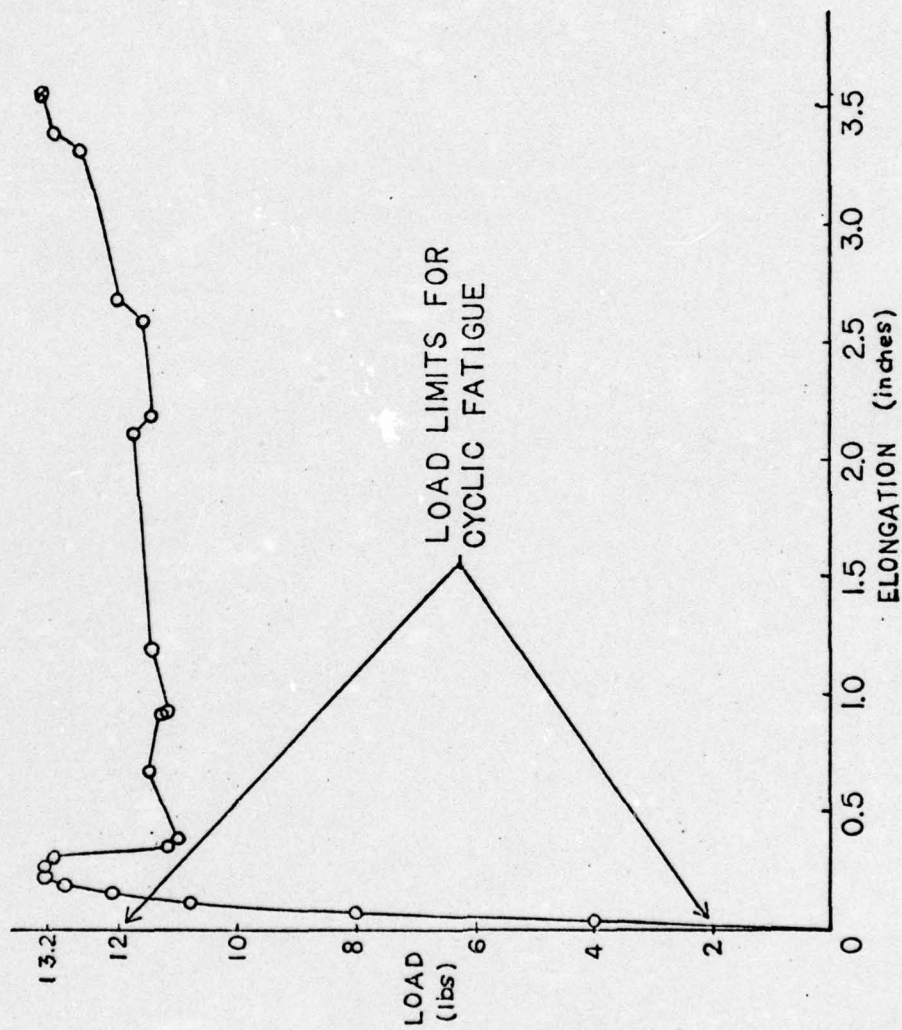


Figure 6.6 Load-elongation curve of 3 mil PC film showing load limits for the cyclic fatigue.  
Sample dimensions: width - 0.5", length - 4", strain rate - 2 in/min.



Table 6.2 Fatigue Data of PC Samples 0.5" Wide x 4" Long

Sample No.	Lower Load Level (lbs)	Upper Load Level (lbs)	No. of Cycles	Initial Elongation (in)	Elongation at end of fatigue cycle	% Change in Elongation during fatigue cycle	Sample Condition at end of cycle	Density g/ml	% Change in Density	Comments
34-5	2	12	500	-	-	-	Did not break	1.1975	0.008	Did not record elongation
34-6	2	12	1000	-	-	-	"	1.1974	0.016	"
109-1	2	12	3100	0.100	not recorded	-	"	1.1971	0.041	No crazes observed
41-1	2	12	5000	0.155	0.180	16.13	"	1.1968	0.066	"
108-2	2	11	5800	0.105	0.122	16.19	"	1.1968	0.066	"
108-1	2	11	6000	0.105	0.124	18.09	"	1.1966	0.083	Crazes observed (see Figure 2.)

Density of commercial (unfatigued) sample is 1.1976 g/ml.

Cross-head speed 2 in/min.

Load at yield = 13.2 lbs.

Table 6.3 Fatigue Data of PC Samples 1" Wide x 4" Long

Sample No.	Lower Load Level (lbs)	Upper Load Level (lbs)	No. of Cycles	Initial Elongation (in)	Elongation at end of fatigue cycle	% Change in Elongation during fatigue cycle	Sample Condition at end of cycle	Density g/ml	% Change in Density	Comments
43-4	2	23	135		Not recorded		Broke	-	-	No crazes were observed under optical microscope in all these fatigued samples
43-3	2	20	1338	0.112	Not recorded		Broke	-	-	
43-2	2	20	1000	0.102	.108	5.88	Did not break	-	-	
43-1	2	15	2000	0.072	.122	69.0	Did not break	1.1968	0.066	
43-5	2	15	2000	0.105	.170	61.9	Did not break	1.1966	0.083	
43-6	2	15	350	0.122	Not recorded		Broke	1.1975	0.050	

Density of commercial (unfatigued) sample is 1.1976 gm/ml.  
 Cross-head speed during fatigue = 4 in/min.  
 Load at yield = 27 lbs.



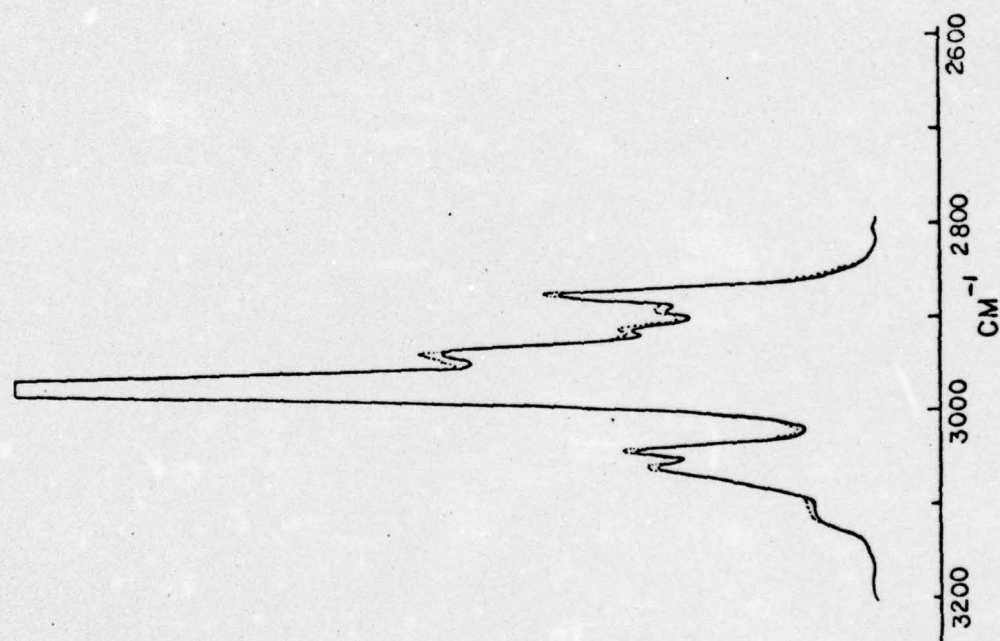


Figure 6.7 (a) Superimposed FTIR spectra of unfatigued (—) and fatigued (...) PC films.

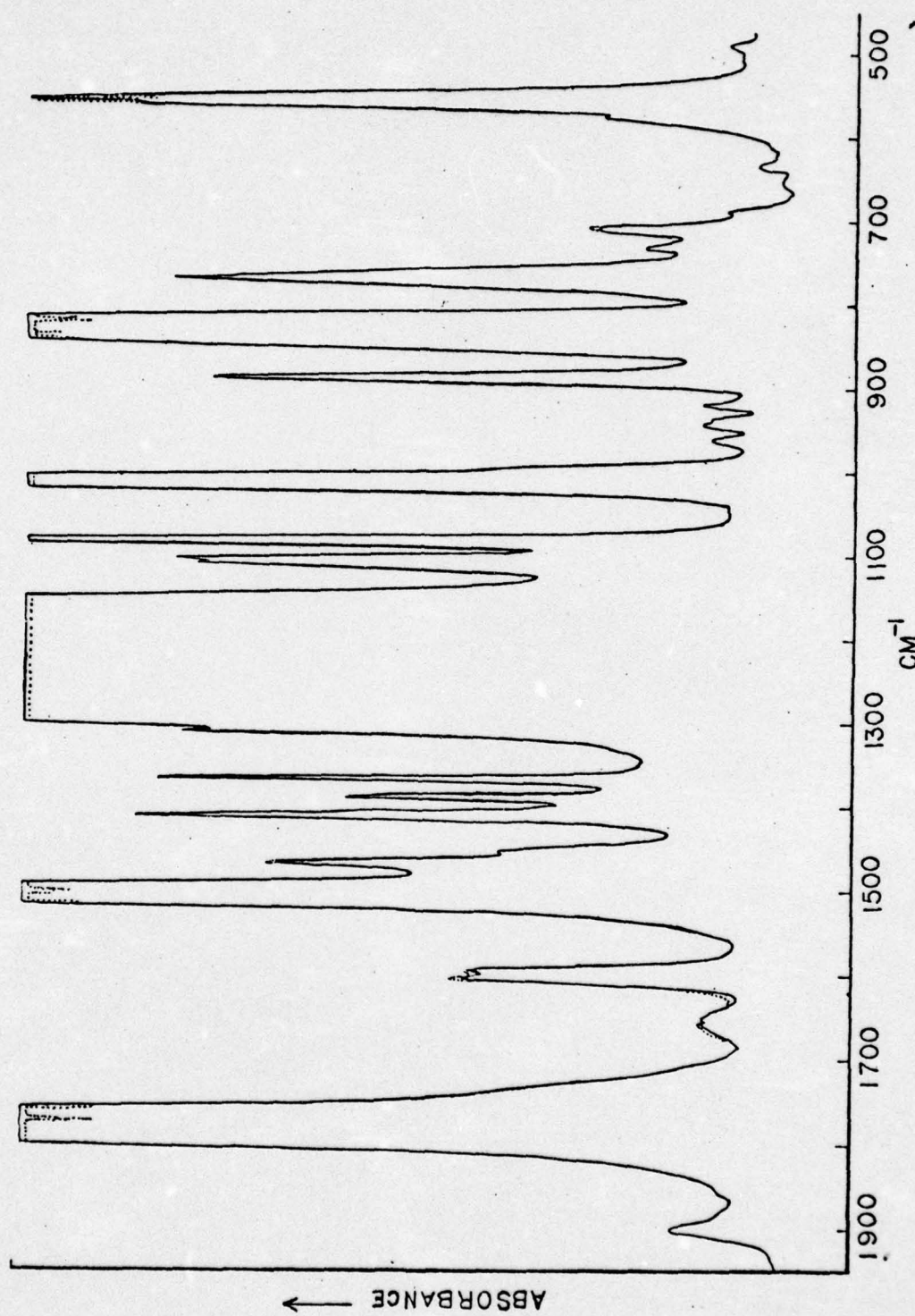


Figure 6.7 (b) Superimposed FTIR spectra of unfatigued (—) and fatigued (···) PC films.



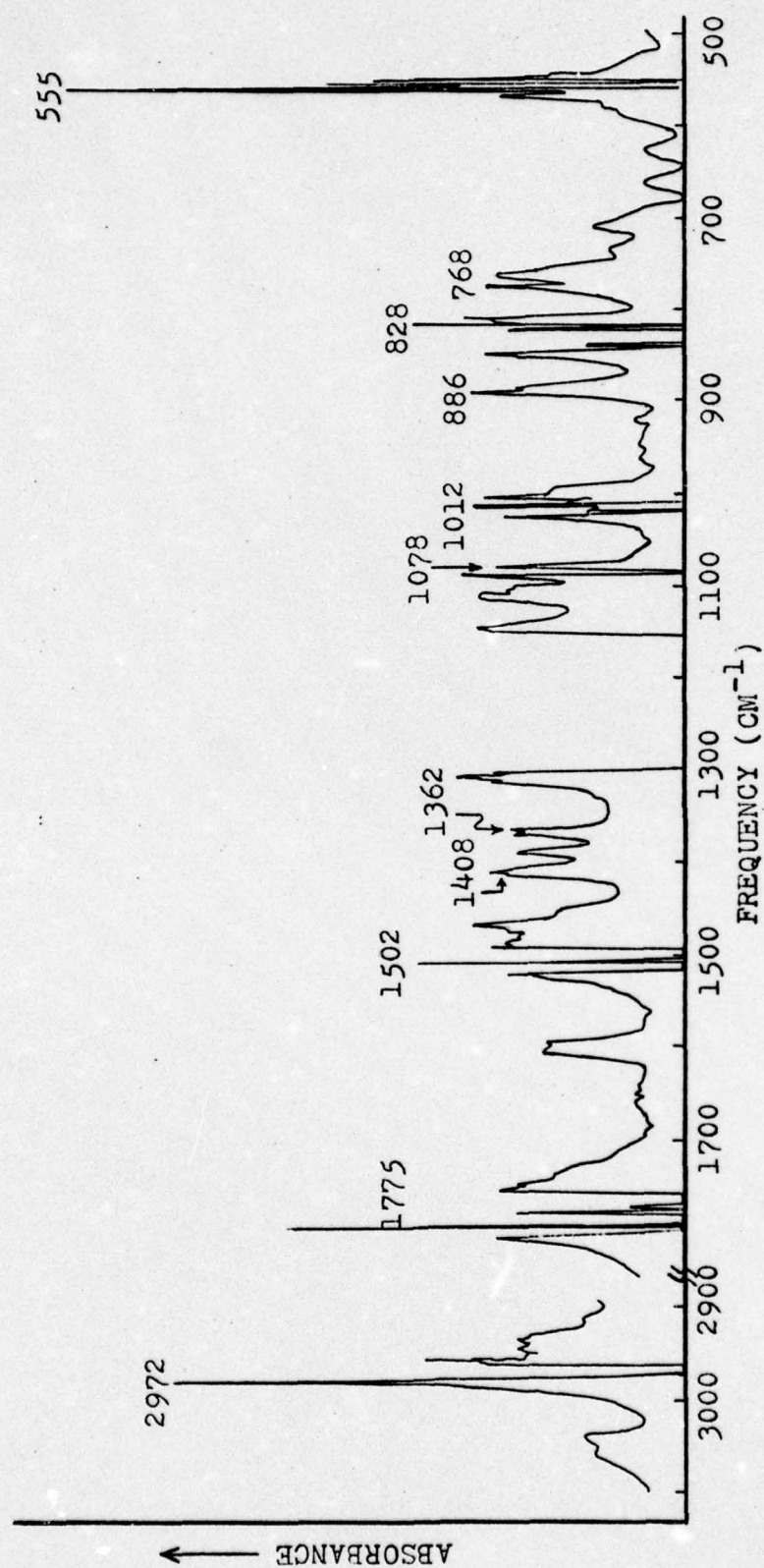


Figure 6.8 IR subtraction spectrum of polycarbonate films. (Fatigued-90% unfatigued)

cyclic fatiguing are quite obvious from this spectra and are listed in Table 6.4.

### 6.2.3 X-ray and birefringence results

The mean Bragg distance (interchain distance) obtained from cyclically fatigued PC sample (No. 108-2) shows a decrease of  $0.0636 \text{ \AA}$ . This difference is conclusive as confirmed by the hypothesis test listed in Appendix B.

The half-width of the peak due to the outer halo in the scattering pattern increases in fatigued PC sample, where the half-width is an indication of the spread about the mean interchain distance.

Birefringence measurements made on fatigued samples immediately after cyclic fatigue revealed no orientation effects because of the fatiguing process.

### 6.2.4 Dynamic mechanical loss results

Figures 6.9 and 6.10 show the  $\tan \delta$  vs. temperature plots for unfatigued PC sample (control) and samples fatigued to various numbers of cycles (shown in Tables 6.2 and 6.3). The  $\alpha$  relaxation peak in the unfatigued PC sample occurs at  $147^\circ\text{C}$ . The  $\beta$  relaxation peak<sup>1</sup> in this sample (control) is observed at  $-80^\circ\text{C}$ . The tests are conducted at a frequency of 35 Hz. Interesting features of these results are:

---

<sup>1</sup>In this work the author refers to the peak occurring at  $-80^\circ\text{C}$  as the  $\beta$  relaxation peak, even though very recently a weak peak occurring at  $\sim 110^\circ\text{C}$  (at a test frequency of 35 Hz) is being designated as the  $\beta$  peak since it fits the Matsuoka Ishida rule of  $T_\beta = 3/4 T_g$ , Boyer [124,125].



Table 6.4 Changes Observed with Bands from the FTIR  
Subtraction Spectra on Fatigued PC Samples

IR Band (cm <sup>-1</sup> )	Type of Changes Observed	Assignment
560	Multiple splitting	Out of plane bending vibration of the p-disubstituted ring
768	Splitting	Non-coordinated bands
886	Appearance of a shoulder	Non-coordinated bands
1012	Multiple splitting	A <sub>1</sub> species modes of the benzene ring.
1078	Splitting	Asymmetric C-C stretch of central carbon atom
1150-1268	Absorbs on the negative absorbance side	C-O valence vibration of $\begin{array}{c} \diagup \text{C}-\text{O}-\text{C}-\text{O}-\text{C} \diagdown \\ \quad \quad \quad \text{O} \end{array}$ group
1362	Weak splitting	Aliphatic -CH valence vibration
1408	Very weak splitting	Non-coordinated bands
1502	Multiple splitting	In plane ring vibrations of the phenyl rings
1775	Multiple splitting	C=O stretching vibration
2968	Splitting	Configuration of central C atom of the repeat unit has its effect in this reason.

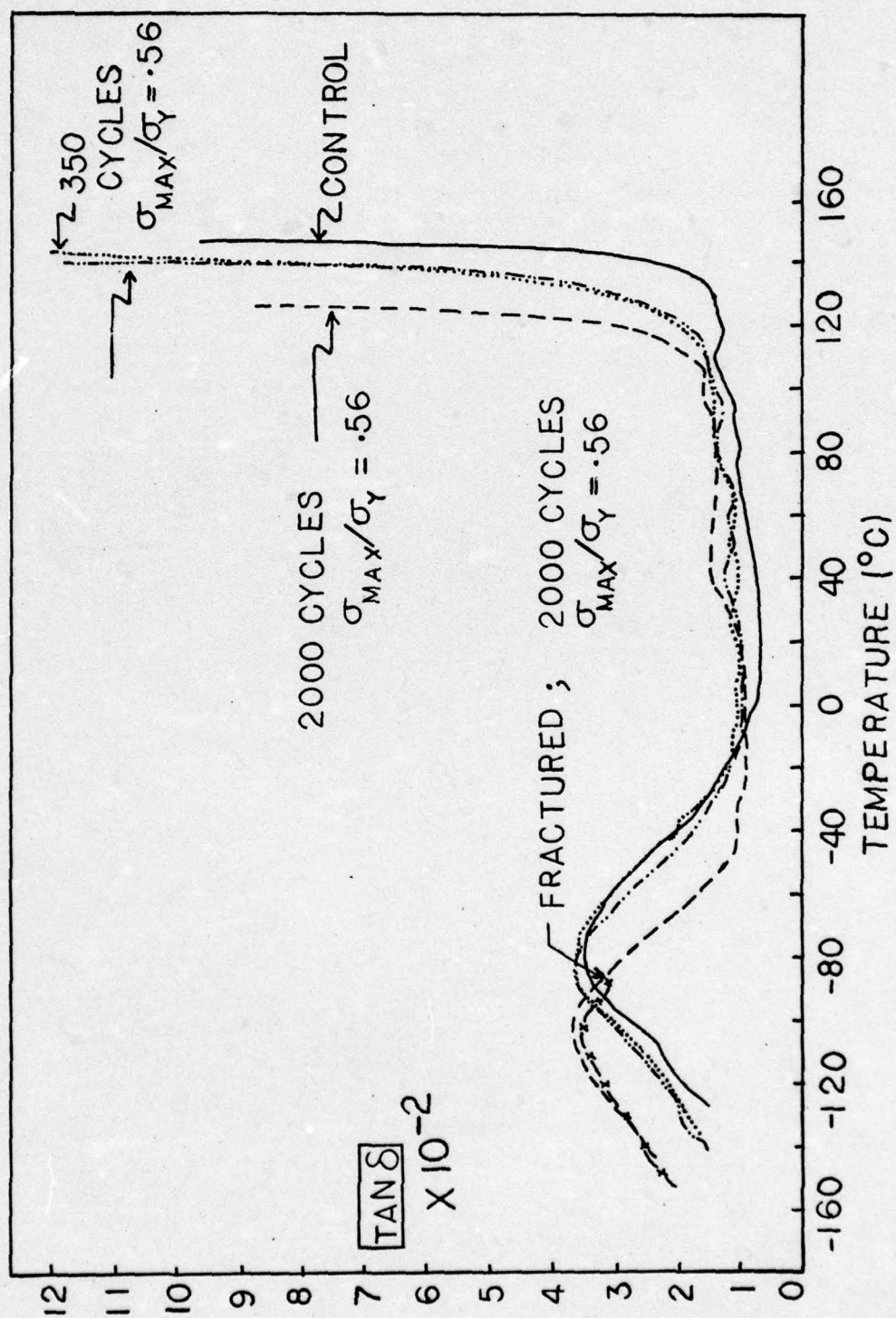


Figure 6.9 Tan  $\delta$  vs. temperature plot for unfatigued and fatigued polycarbonate films. Test frequency = 35 Hz.



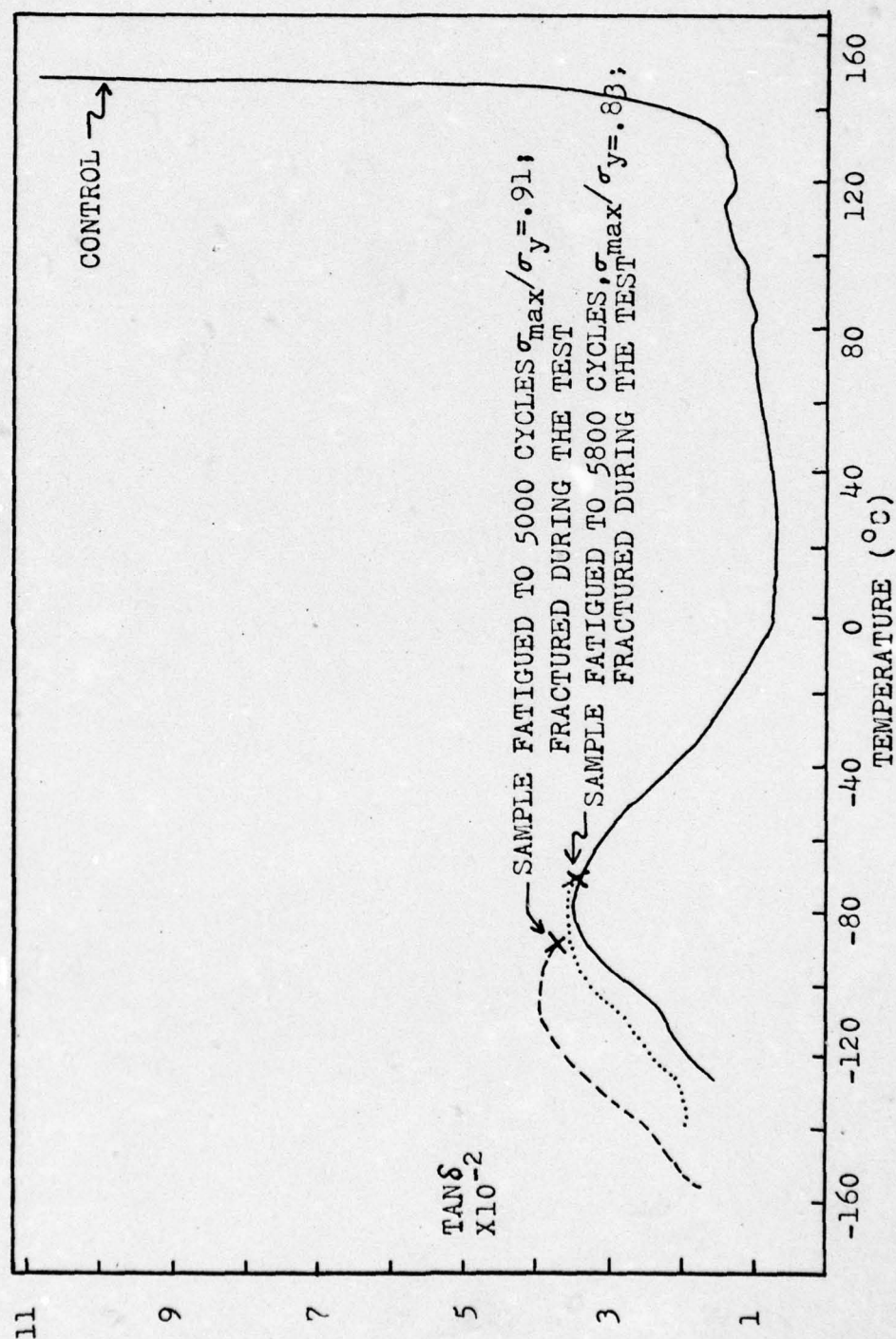


Figure 6.10 Tan  $\delta$  vs. temperature plot for unfatigued and fatigued (to over 5000 cycles) PC films. Test frequency = 35 Hz.

- (a) Samples fatigued to a large number of cycles and/or fatigued at higher stresses, fracture in the temperature range of  $-75^{\circ}\text{C}$  to  $-95^{\circ}\text{C}$  during the dynamic mechanical tests.
- (b) The  $\alpha$  and  $\beta$  relaxation peaks in fatigued samples appear at lower temperatures in comparison to these peaks in unfatigued samples. It may be mentioned here that those experiments in which the samples fractured at low temperatures have been repeated at least three times each to confirm these results. In all cases the samples fatigued to large numbers of cycles ( $> 2000$  cycles at stress levels shown in Tables 6.2 and 6.3), fracture during the tests.

The shifts toward lower temperatures of  $\alpha$  and  $\beta$  relaxation peaks observed in Figures 6.9 and 6.10 are tabulated in Table 6.5. These results are explained in the following section.

#### 6.2.5 Discussion of molecular behavior of fatigued polycarbonate samples

FTIR results indicate that the absorption frequencies of several vibrational modes are affected by fatigue process. From the changes observed in  $555$ ,  $1012$ ,  $1502\text{ cm}^{-1}$  bands it is suggested that the electronic structure of the bonds and environments of various molecular groups in the polymer chains causing the observed absorption bands has been affected. These environmental changes can be either external or internal, where external changes originate from the intermolecular interactions and the internal changes from the intramolecular effects [126]. Both of these changes, along with the factors discussed in Section 2.1.1 to 2.1.5 are known to influence the force constants and shift the absorption frequencies. In the present case these shifts are rather small but distinct and, therefore, show up as splittings in the IR bands in subtraction spectra. Changes in other IR bands,



Table 6.5 Position and Shifts of  $\alpha$  and  $\beta$  Relaxation Peaks of Samples Fatigued to Varying Number of Cycles

Sample Number	No. of Fatigue Cycles	$\frac{\sigma_{\max}}{\sigma_y}$	Temperature for $\alpha$ peak ( $^{\circ}\text{C}$ )	Shift in $\alpha$ peak ( $^{\circ}\text{C}$ ) <sup>†</sup>	Temperature for $\beta$ peak ( $^{\circ}\text{C}$ )	Shift in $\beta$ peak ( $^{\circ}\text{C}$ )	Comments
Control	0	-	145	-	- 80	-	Unfatigued sample
43-6	350	0.56	135	- 10	- 95	- 5	
43-3	1338	0.74	135	- 10	- 90	- 10	
43-1	2000	0.56	124	- 21	- 105	- 22	
43-5	2000	0.56	-	-	- 102	- 25	Sample fractured at - 87 $^{\circ}\text{C}$ .
41-1	5000	0.91	-	-	- 105	- 22	Sample fractured at - 95 $^{\circ}\text{C}$ .
108-2	5800	0.83	-	-	- 85	- 5	Sample fractured at - 75 $^{\circ}\text{C}$ .

<sup>†</sup>Shifts in peaks are measured here in relation to the peaks observed for unfatigued samples.

such as 1078, 1150-1268, 1362, 1775 and  $2968\text{ cm}^{-1}$ , indicate that the backbone bonds and bond angles of some of these chain segments have been affected. This effect is in varying degree on various chain segments. For example, certain chain segments may be fully extended by the cyclic fatigue and thus be in a taut condition by the end of the fatigue process, while the others remain in their coiled, entangled state. IR results also indicate that fatigue affects the chain backbone bonds and their bond angles.

X-ray results point out that there is a small decrease in average intermolecular distances in the fatigued samples. The average decrease is about 1.25%. This indicates that polymer chains get closer and orient in the direction of applied stress. If any orientation occurs, it is probably very low as it could not be observed during the birefringence measurements but then this instrument is not sensitive enough to pick up very small orientations. It is also pointed out here that in case of unoriented-strained PC films the average intermolecular distance decreases by about 9.9% as compared to a decrease of about 1.25% in the case of fatigued PC film.

This can be explained thus: in strained PC film the sample was kept under strain for 4 hours. In spite of the stress-relaxation which may have occurred in this duration, the net effect is a decrease of an intermolecular distance, whereas, in the fatigue process the PC film samples are strained at a rate of 2 inches and 4 inches per minute. At these strain rates the stress on the samples remains for 1 to 3 seconds during each cycle in which time not all chains are able to respond. The heavily entangled ones remain mostly unaffected,



whereas the taut ones break, but some other relaxed chains extend themselves and get taut. On repeating the fatigue cycles often large quantities of chains end up being snapped or taut, never really letting the intermolecular distances get affected as much by slippage.

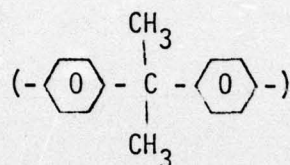
Density results of fatigued samples, shown in Tables 6.2 and 6.3, indicate small decrease in density in comparison with unfatigued PC samples. The change in density increases as the number of fatigue cycles are increased at a particular stress level or when the upper stress level is increased. The maximum change in density is -0.083% for samples No. 43-5 and 108-1 (see Tables 6.2 and 6.3). This result suggests a small increase in the free volume in the microstructure of fatigued PC samples.

Dynamic mechanical loss data tabulated in Table 6.5 illustrates the behavior of  $\alpha$  and  $\beta$  relaxation peaks in unfatigued and fatigued PC samples. The relaxation behavior of PC has been extensively studied and it is well established that  $\beta$  relaxation peak occurs at about  $-100^{\circ}\text{C}$  at a test frequency of 1 Hz. It is generally accepted that  $\beta$  peak is associated with the motion of carbonate ( $-\text{O}-\overset{\text{O}}{\underset{\text{O}}{\text{C}}}-\text{O}$ ) groups in the main polycarbonate chain [127]. However, it has also been suggested [128] that this loss peak with its maximum occurring at  $-100^{\circ}\text{C}$  consists of three overlapping curves with about the same activation energies. The loss peak in low temperature side, i.e., at about  $-145^{\circ}\text{C}$ , is related to methyl ( $-\text{CH}_3$ ) groups mobility and the other one at about  $-50^{\circ}\text{C}$  is related to the phenylene group motions while the maximum of the peak at  $-100^{\circ}\text{C}$  is due to the mobility of carbonate groups.

From measurements of dielectric properties and free volume

fraction,  $f$ , Matsuoka and Ishida [122] suggest that large value of  $f$  at  $T_g$  reflects the open packing of chains in the glassy state, which gives considerable freedom to the motion of carbonate groups.

The  $\alpha$  relaxation peak occurring at about 150°C is associated with the motions of diphenyl propane groups



and some segmental motions of PC chains [124].

From this background information the shift of  $\beta$  peak toward lower temperatures is indicative of the additional free volume generated during the fatigue process, which enables carbonate motions to occur at even lower temperatures. An indication of increase in free volume has already been suggested through density results. Also, shift of  $\alpha$  relaxation peak toward lower temperature may be attributed to an increase in free volume. Since both  $\alpha$  and  $\beta$  peaks show shifts in fatigued PC film samples, it is suggested by the author that local mode relaxation may indeed be connected with the main chain relaxations.

As already stated, Figures 6.9 and 6.10 show that highly fatigued samples fracture at about -85°C (just past the  $\beta$  peak). Figure 6.9 shows that sample 43-5, fatigued to 2000 cycles, breaks during the test at -85°C while sample 43-1, fatigued to the same number of cycles at the same stress levels, does not break during the test. This can be explained by referring to Table 6.3, which shows that initial strain during initial fatigue cycles in samples 43-1 is 0.072" as compared to



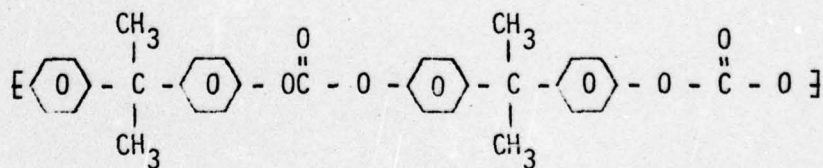
0.105" for sample 43-5. These changes may be a result of the usual variations in thickness existing in most polymer films. The percentage change in elongation between the initial and final fatigue stages of cyclic fatigue in these samples is 69 and 61.9%, respectively. Thus, we see that sample 43-5 is actually subjected to an increased strain at first, even though the percent increase in elongation during fatigue is lower by 7.1%. Based on this information, it can be stated that sample 43-5 must have sustained greater damage than sample 43-1 during the identical number of fatigue cycles. This is also indicated by a slightly greater decrease (0.017%) in the density of sample 43-5.

In the case of sample 108-2 and 41-1, the former is fatigued to 5800 cycles at  $\sigma_{\max}/\sigma_y = 0.83$  as compared to  $\sigma_{\max}/\sigma_y = 0.91$  for sample 41-1. Thus, an explanation similar to the one above also holds for the differences observed in shifts of  $\beta$  relaxation peaks in samples 108-2 and 41-1.

As shown in Tables 6.2 and 6.3, PC film samples show certain elongation during the initial cycles of fatigue process, which gradually increases during fatigue and a net increase in elongation occurs by the end of a large number of fatigue cycles. This observation suggests a possibility of microyield phenomena taking place during fatigue process.

It is suggested by the author that such an increase in elongation with increase in the number of fatigue cycles may be caused by the chain scission mechanism occurring at the molecular level. As mentioned earlier, highly entangled chains while responding to an external stress may break. In addition, taut chains may also relieve themselves

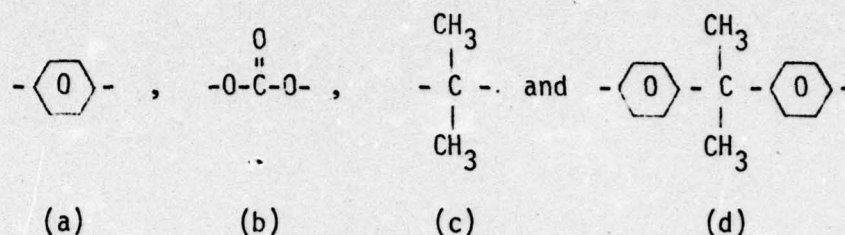
of high stresses by chain scission. As such backbone bond scissions increase, the external stress is redistributed on the remaining chains (which decrease in number). The chain scission will, therefore, tend to increase with an increase in number of fatigue cycles and, as a result, microvoids are created in the chain-ends regions. The microvoids distribute throughout the sample and contribute toward an increase in free volume. X-ray results presented earlier show a decrease of 1.25% in the intermolecular distances on fatiguing, from which we expect a slight increase in density, but actually it is not so, as evidenced by density results. Therefore, the decrease in density must have actually resulted from the microvoid formation. The latter, in fact, may also explain the dynamic mechanical loss results. An increase in number of microvoids formed due to chain scission will also be accompanied by an increase in number of free ends of PC chains. The molecular groups at these loose chain ends will contribute toward an increased mobility. The chain scission can occur by breaking any of the backbone bonds in the polymer chains, as shown below.



Dimer of polycarbonate

The end groups thus formed can be the following:





Increased presence of these end groups shown in (a), (b) and (c) above will thus cause the  $\beta$  relaxation peak to shift toward lower temperatures. Presence of diphenyl propane end groups, (d), above will cause  $\alpha$  peak to shift toward lower temperature. The shifts of both  $\alpha$  and  $\beta$  peaks<sup>1</sup> indicate an increase in free volume available for such motions.

From these molecular mechanisms occurring during the fatigue process, it is now possible to explain also the breakage of highly fatigued samples during dynamic mechanical tests.

The author suggests that PC chain mobility is significantly reduced at cryogenic temperatures and the microvoids created during the fatigue process act as stress risers which cause these samples to fracture under the sinusoidal stress.

#### 6.2.6 Summary

Taut and extended polymer chains, while responding to cyclic tensile stress, break weak Van der Waal's bonds, pull away from entanglements by rearranging and bond breakage. In subsequent cycles there is

---

<sup>1</sup>The newly recognized relaxation peak occurring at 110°C also shifts toward lower temperature in fatigued sample.

a transfer of stress to remaining adjacent chains. As the sample is worked during fatigue, some other chains become taut and they, too, break. Such breakage of backbone bonds or chain scission keeps on recurring during the fatigue process, leading to a redistribution of stresses over lesser number of chains. These chains, too, begin to tauten and break. This process of extensive chain scission during cyclic fatigue has been evidenced by a decrease in density results, as well as shifts of  $\alpha$  and  $\beta$  relaxation peaks toward lower temperatures in fatigued PC samples. This chain scission results in creation of microvoids (defect regions) throughout the microstructure of the sample, which weakens the material by lowering its stress-bearing capability. On application of additional stress or cyclic loading the microvoids located adjacent to each other possibly coalesce, forming crazes and large voids. The crazes appear on the surface and are easily noticeable. Figure 1.6 shows crazes formed in sample 108-1, cyclically fatigued to 6000 cycles. These crazes or voids are precursors to crack propagation and eventual failure.

### 6.3 Results and Discussion of Crazed Polycarbonate Films

#### 6.3.1 FTIR results

FTIR spectra of solvent crazed polycarbonate film is obtained on the Fourier Transform spectrometer. A superimposed spectra of uncrazed and crazed PC films is shown in Figure 6.11. This figure, rather obviously, shows the differences in absorption of uncrazed and crazed PC films. Crazed samples are not quite as transparent as the uncrazed



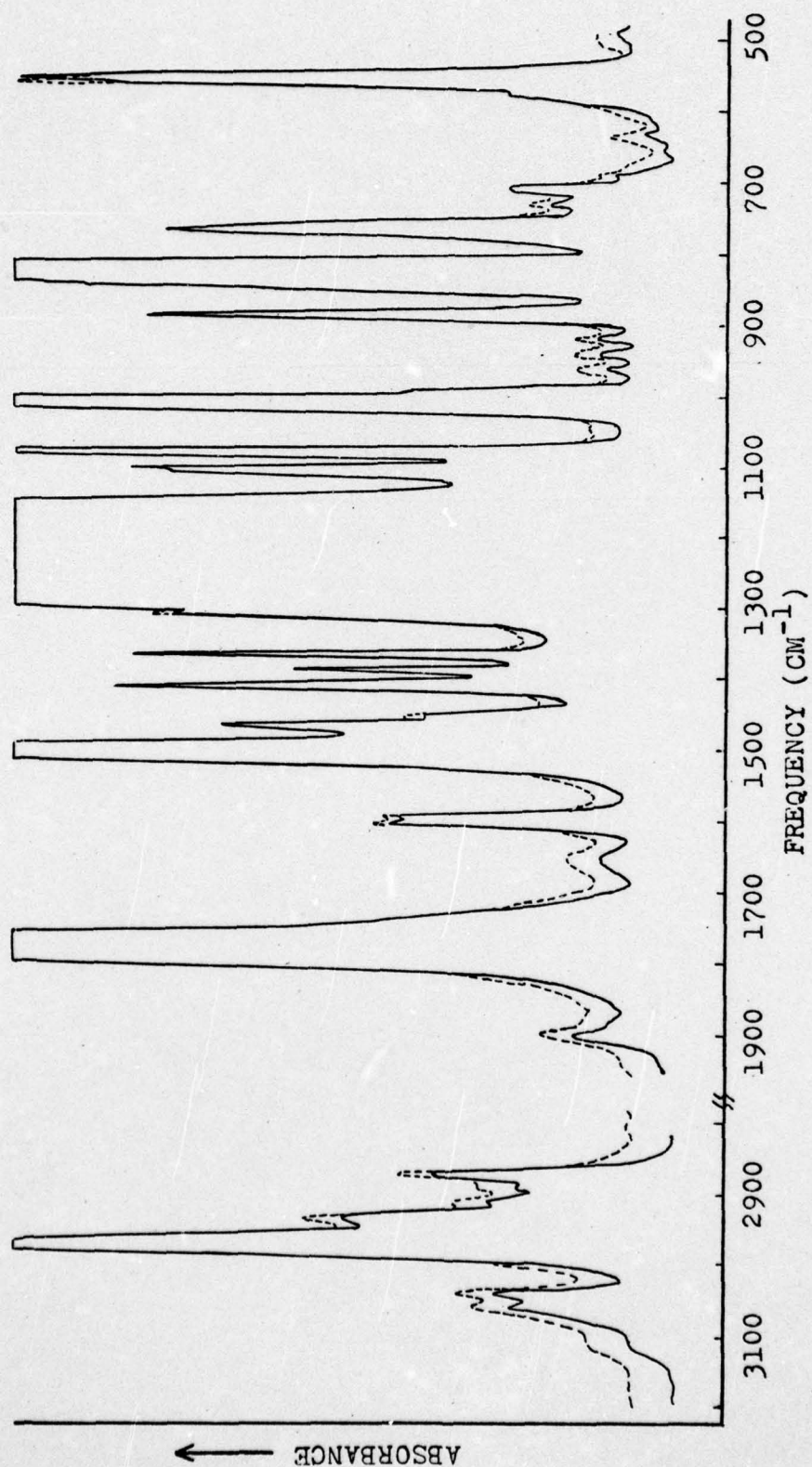


Figure 6.11 Superimposed FTIR spectra of uncrazed (—) and crazed (---) polycarbonate films.

ones. The only other difference noticeable in this figure is a shift in peak of  $555\text{ cm}^{-1}$  toward higher wavenumbers. FTIR computer-subtracted (crazed-90% uncrazed) spectrum is shown in Figure 6.12. The IR bands which show splitting are: 555, 768, 828, 1012, 1078, (1150-1268), 1408, 1502, 1775 and  $2972\text{ cm}^{-1}$ . The development of peak shift of  $555\text{ cm}^{-1}$  toward higher wavenumbers is obvious from the superimposed spectra, but there are shifts as small as a fraction of a wavenumber, which cannot be observed in the superimposed spectra, whereas, these weak shifts can be observed by subtracting an increased percentage of the spectrum of uncrazed PC film from that of crazed film. For example, the effect of crazing on the  $1362\text{ cm}^{-1}$  IR band is observable in the subtraction spectra shown in Figure 6.12.

From the comparison of (crazed-90% uncrazed) and (fatigued-90% unfatigued) FTIR spectra, it may, at first, seem that the differences in IR bands in both of these cases are similar but actually it is not so. A close and detailed study of these IR bands reveals that the two spectra are quite different. For example, the differences in IR bands at 555, 1078 and  $1775\text{ cm}^{-1}$  in these two cases are obvious. In the subtraction spectra of fatigued samples, the splittings observed in  $555\text{ cm}^{-1}$  band are too numerous, whereas in crazed samples, only one strong splitting and another very weak splitting is observed. The  $1078\text{ cm}^{-1}$  IR band in fatigued sample shows strong splitting, whereas in the spectrum of the crazed sample this band is only very slightly affected. This, itself, indicates the differences of intermolecular and intramolecular interactions in the two cases, which is indeed expected.



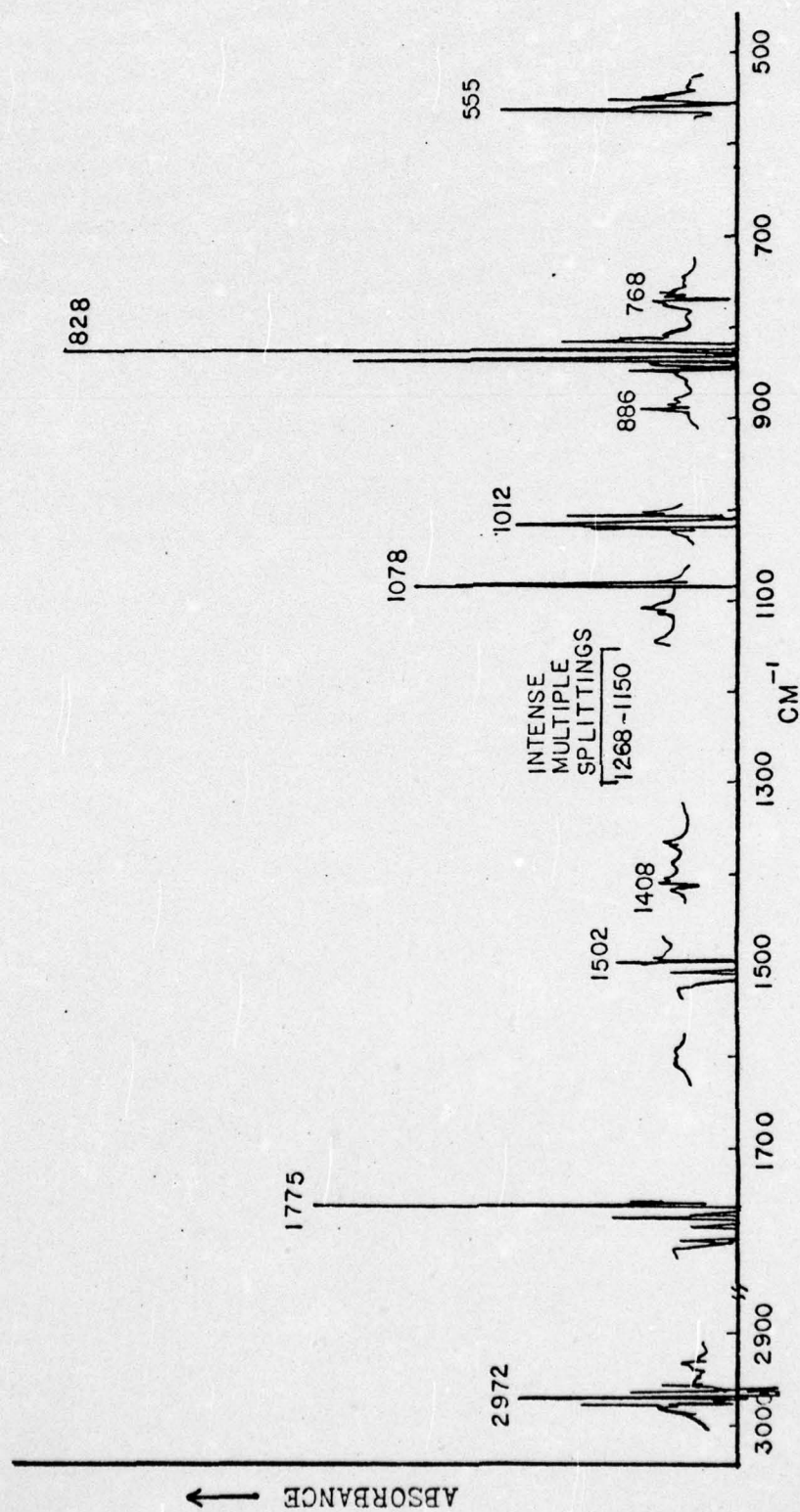


Figure 6.12 IR subtraction spectrum of polycarbonate films. (Crazed-90% uncrazed)

Based on the present IR studies on crazed and fatigued samples, the author suggests that in crazed PC samples most polymer chains try to stress-relieve themselves, but such processes depend on the location of these stressed polymer chains. The chain segments on and just below the surface of the sample bear higher frozen-in stresses and can relieve themselves of these stresses by crazing. However, the ones located within the bulk may not be able to do so. FTIR results suggest that most of the IR band changes are related to external environmental changes, i.e., intermolecular in nature. Only certain IR band changes may be ascribed to intramolecular effects. The  $1078\text{ cm}^{-1}$  IR band, shown in Figure 6.12, is only weakly affected by crazing and this effect is different than the one observed in the case of fatigued and stressed PC samples. This observation suggests that backbone bonds of most polymer chains are unaffected by crazing. A few backbone bonds which might have been under stress due to unfavorable molecular conformation are stress-relieved. Double splitting of  $2972\text{ cm}^{-1}$  band indicates asymmetric stretch of the methyl group and occurs at two distinct frequencies which can be attributed to two different types of interchain interactions in the crazed and uncrazed region of PC samples. Similar effect is demonstrated by a large and another very fine splitting of  $555\text{ cm}^{-1}$  band assigned to out-of-plane bending vibrations of the benzene ring. Other IR bands affected due to differences in intermolecular interactions are  $1775$ ,  $1502$ ,  $1408$ ,  $1012$  and  $828\text{ cm}^{-1}$ .

### 6.3.2 Dynamic mechanical loss results

Figure 6.13 shows a comparison of the relaxation spectra of



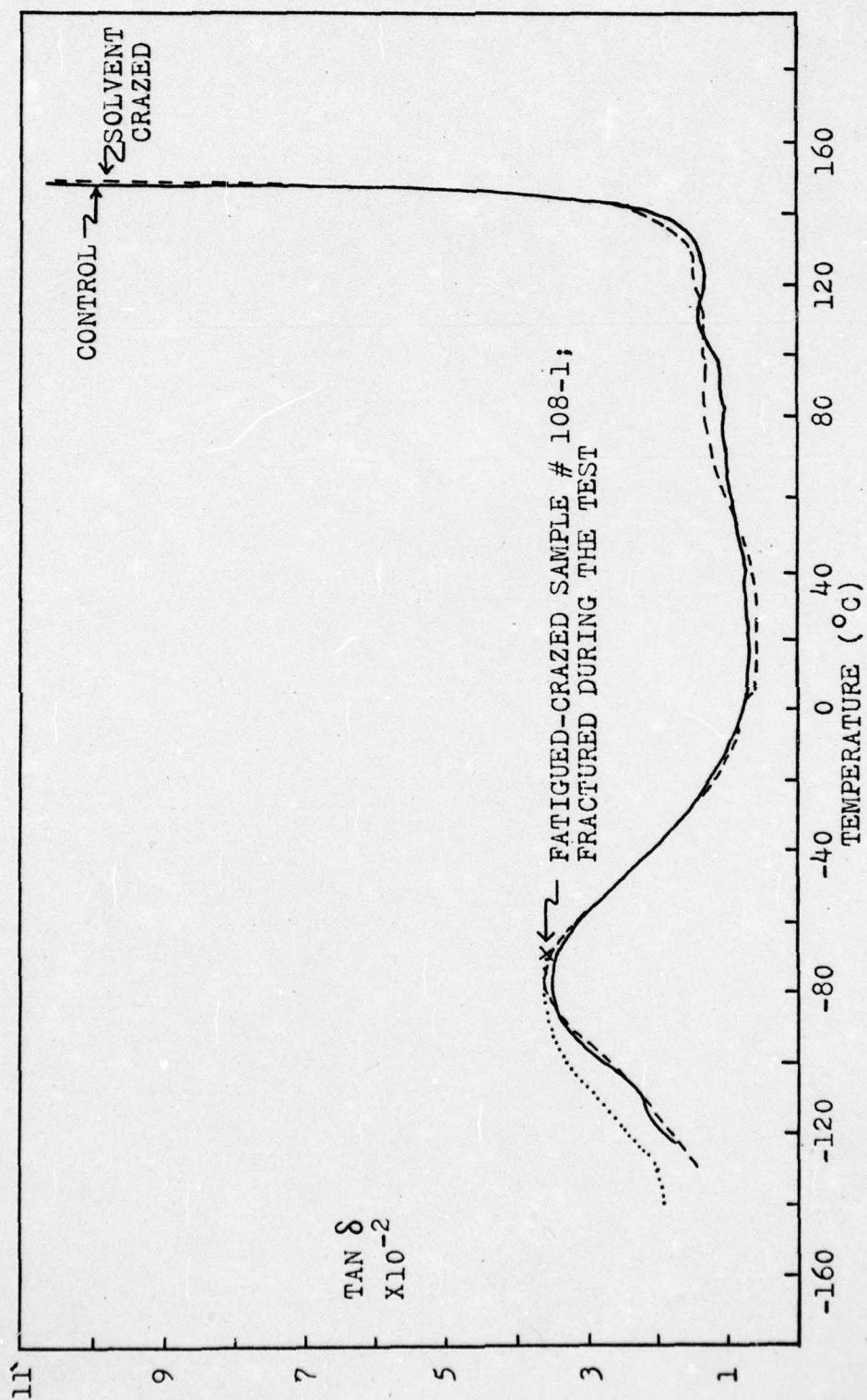


Figure 6.13 Tan  $\delta$  vs. temperature plot for fatigue-crazed and solvent-crazed PC film.  
Test frequency = 35 Hz.

AD-A035 474

UTAH UNIV SALT LAKE CITY DEPT OF MATERIALS SCIENCE --ETC F/G 7/3  
MOLECULAR BEHAVIOR STUDIES OF GLASSY POLYMERS UNDER STRESS.(U)  
NOV 76 W O STATTON

AF-AFOSR-2827-75

UNCLASSIFIED

UTEC-76-274

AFOSR-TR-77-0047

NL

4 OF 4  
AD  
A035474



END

DATE  
FILMED

3-77



OF

4

35474



MICROCOPY RESOLUTION TEST CHART  
NATIONAL BUREAU OF STANDARDS-1963-A

uncrazed (control) fatigue-crazed and solvent-crazed PC samples. It is obvious from this plot that both  $\alpha$  and  $\beta$  relaxation peaks in the uncrazed and solvent-crazed PC samples occur at the same temperatures. However, the peak occurring at  $-110^{\circ}\text{C}$  in the uncrazed sample is dispersed in the relaxation spectra of solvent-crazed sample due to certain amounts of plasticizing effect caused by the solvent, whereas, in the fatigue-crazed sample, fatigued to 6000 cycles, the  $\beta$  peak becomes broad and shifts toward the lower temperatures. The  $\alpha$  relaxation peak in this sample is unobtainable because the sample fractures during the test at  $-75^{\circ}\text{C}$ . This fracture behavior is similar to sample 108-2, fatigued to 5800 cycles, which, although does not exhibit any crazes, fractures at  $-75^{\circ}\text{C}$ .

### 6.3.3 Discussion

IR results of crazed polycarbonate films indicate that stress-relieving processes actually occur at the molecular level in crazed samples. The intermolecular interactions are modified due to crazing of films.

Dynamic mechanical loss results point out that there are differences between the fatigue-crazed and solvent-crazed PC samples from the molecular viewpoint. Fatigue-crazed samples are damaged extensively at the molecular level due to chain scission and the damage is distributed throughout the sample. The microvoids generated due to chain scission as well as due to breakage of weaker interchain bonds create weak spots and the material is locally deformed, causing crazes; whereas, the solvent-crazed samples are damaged only at the surface and



crazing is mainly due to the stress-relieving by the molecular chains in which weaker intermolecular forces are broken along with certain chain rearrangements.

Thus, it is important to make a distinction between the craze formation due to organic solvents and the craze formation due to repeated load-unload (fatigue) processes. The crazes formed under these two conditions appear to be similar at the surface but they affect the materials differently at the molecular level. Therefore, they are expected to perform quite differently under stress.

#### 6.3.4 Summary

The study of solvent-crazed and fatigue-crazed samples shows that crazes in these two samples are produced via different molecular behavior. Crazes occurring due to solvent attack and due to cyclic fatigue have the same appearance but the films in the two cases are affected differently. In solvent-crazed film samples, damage is mostly concentrated on the surface, whereas, in fatigue-crazed film samples, damage occurs on the surface as well as within the bulk. As a result, two materials behave quite differently under stress.

### 6.4 Results and Discussion: Uniaxially Oriented Polycarbonate Films Under Stress

#### 6.4.1 Stress-strain and birefringence results

Figure 6.14 shows the stress-strain curve of 300% drawn PC film. Smoothness of the curve indicates uniform flow of the molecular chains

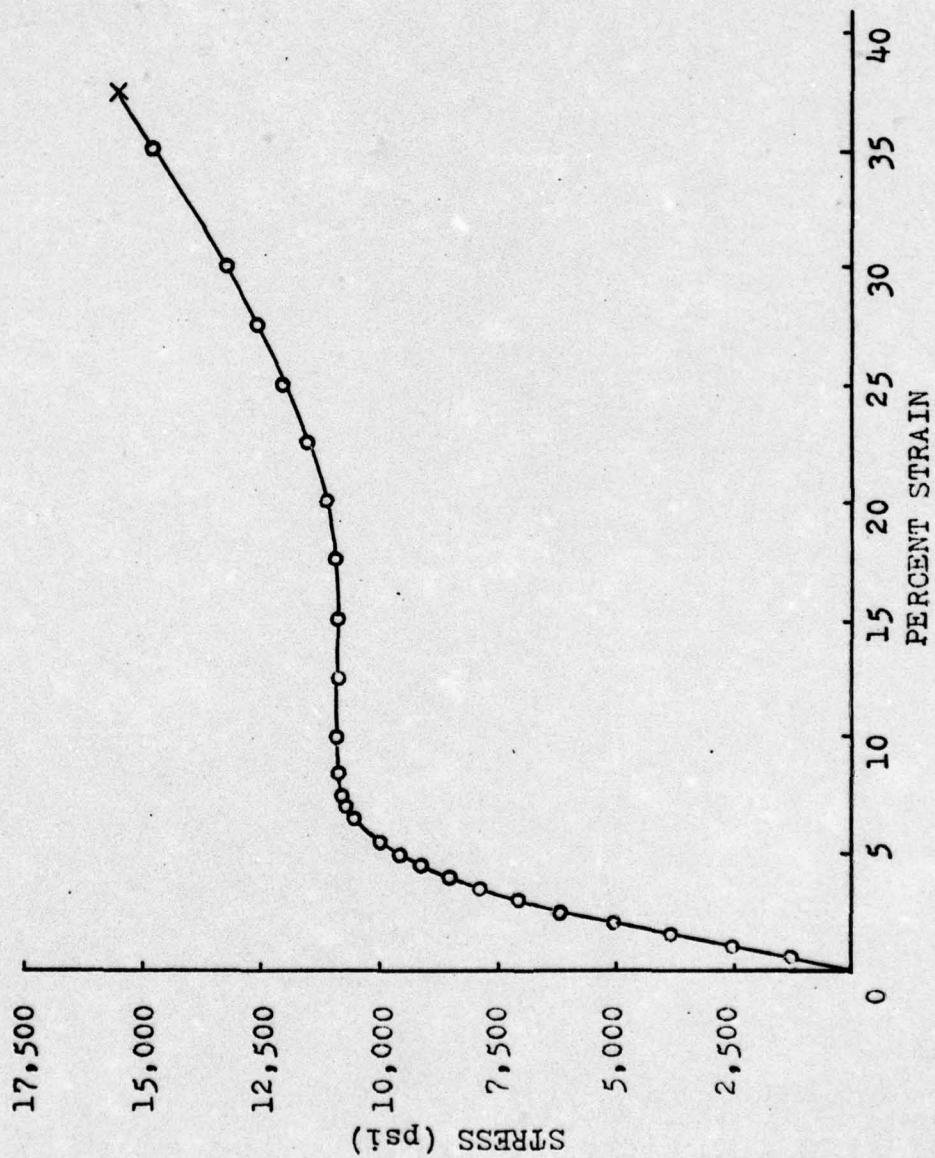


Figure 6.14 Stress-strain curve of 300% uniaxially oriented polycarbonate film.  
Gage length = 2 in., strain rate = 2 in./min.



during the test.

Birefringence of these films is 0.0212, which is indicative of the uniaxial orientation of the polymer chains.

#### 6.4.2 IR results

Oriented PC films have been studied by both conventional IR and Fourier Transform Spectroscopy. As illustrated in Figure 6.14, oriented films show uniform strain hardening. Therefore, to detect the stresses on the polymer chains, IR spectra are recorded at stress levels before which strain-hardening occurs and at stress levels in the strain-hardening region prior to fracture. Load-elongation curve recorded simultaneously during the recording of IR spectra is shown in Figure 6.15. Arrows indicate the points at which the IR scan is recorded. As it can be seen in Figure 6.15, the sample keeps on creeping at a stress of 8888 psi, at which the IR spectrum of PC film is obtained. A superimposed spectra of unstressed and stressed (up to 8888 psi) PC shows no changes, viz., frequency shifts and band distortions. The PC sample is then stressed to 11800 psi, at which extensive yielding occurs. In order to detect stressed PC chains (if any) before the fracture point, another IR spectrum was obtained at a strain of 47% (Figure 6.15). The PC sample creeps again during the recording of the IR spectrum, which takes about 20 minutes. After the scan stress is maintained on the sample which causes it to fracture at a strain of about 56%. The superimposed spectra thus obtained is shown in Figure 6.16. Various changes in IR bands evident from this figure are listed below:

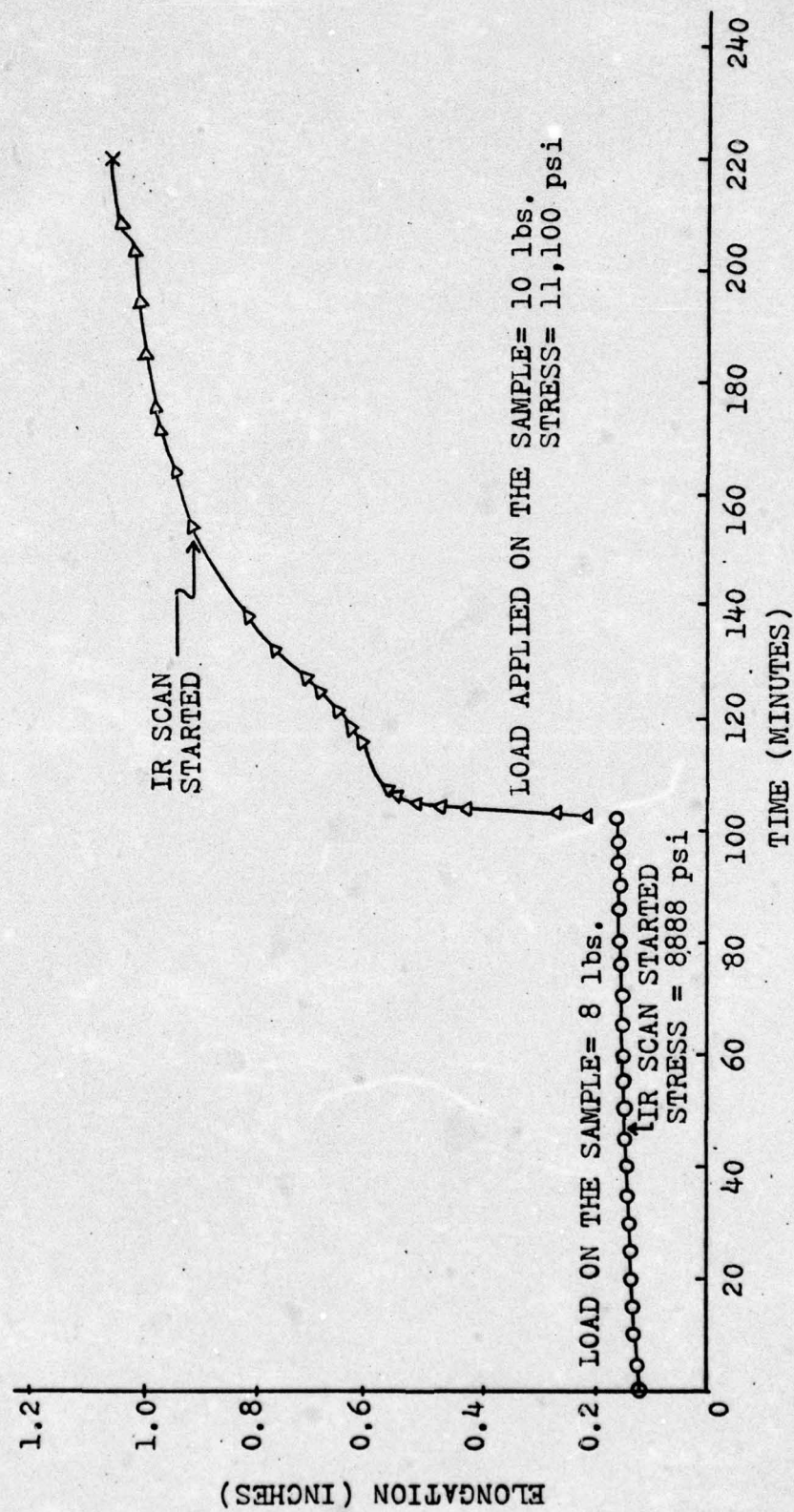


Figure 6.15 Creep behavior of 300% uniaxially oriented PC film during the IR scans. Gage length = 1.889".



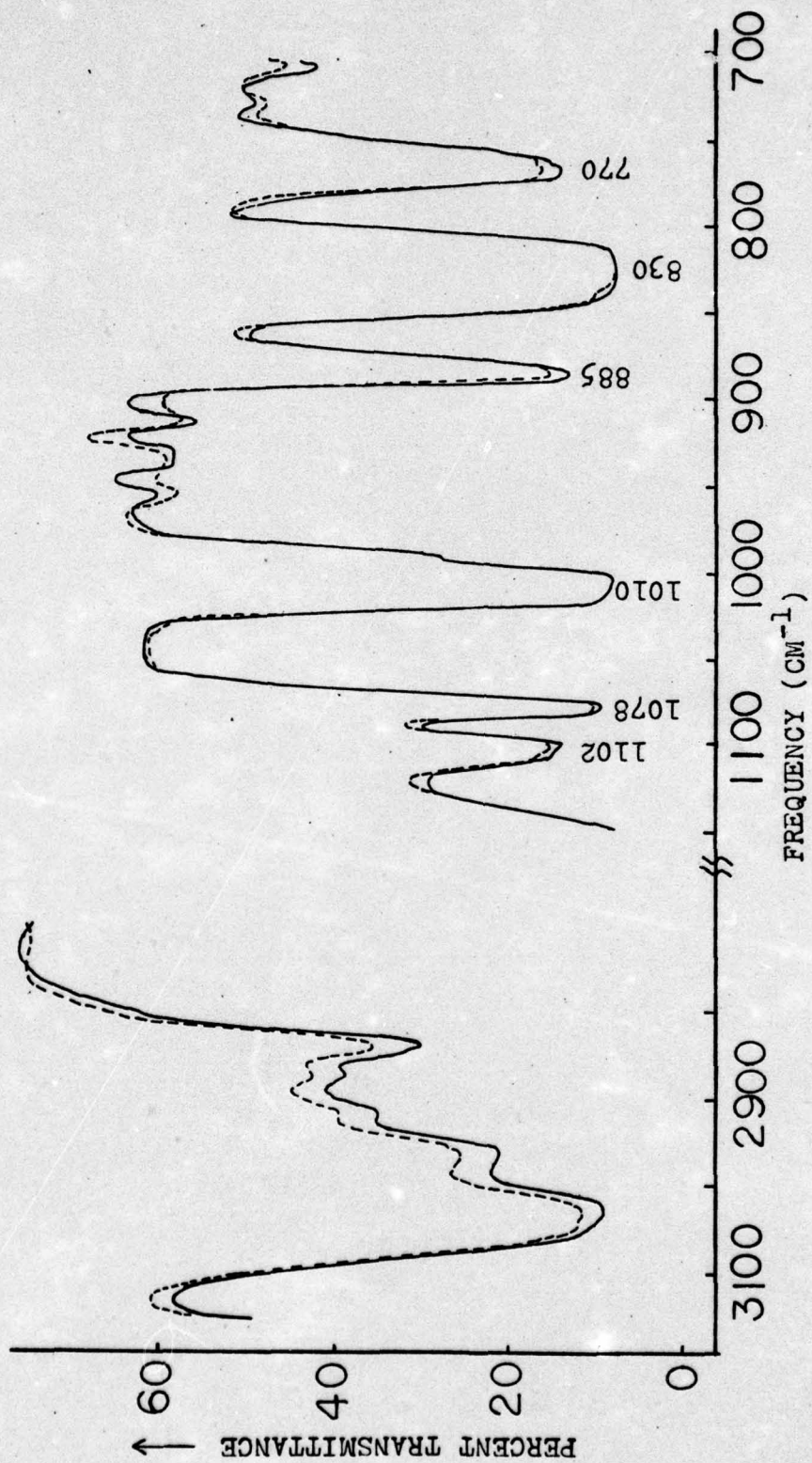


Figure 6.16 IR spectra of 300% uniaxially oriented PC film under no stress (—) and stress of 11100 psi (---).

<u>Frequency</u>	<u>Changes Observed</u>
1102 $\text{cm}^{-1}$	Change in peak shape, showing increased absorption toward lower frequency of the band.
1078 $\text{cm}^{-1}$	Very small negative band shift ( $\sim 0.5 \text{ cm}^{-1}$ ).
885 $\text{cm}^{-1}$	Band shifts ( $\sim 1 \text{ cm}^{-1}$ ) toward lower frequency.
830 $\text{cm}^{-1}$	Band shifts ( $\sim 0.5 \text{ cm}^{-1}$ ) toward lower frequency.
770 $\text{cm}^{-1}$	Band distorts on the low frequency side.

A confirmation of these and other changes in the IR bands of stressed PC (300% uniaxially drawn) films has been received from the computer-subtracted (stressed-50% unstressed)<sup>1</sup> spectrum shown in Figures 6.17(a) and (b). The PC film is strained to 5.91% in the stretching device shown in Figure 4.5 to obtain the spectrum of stressed PC film. This strain corresponds to a stress of about 10,250 psi and lies in that region of stress-strain curve where large scale yielding occurs. Figure 6.17(a) shows splittings of 2972  $\text{cm}^{-1}$  IR band assigned to asymmetric stretching mode of the methyl groups. Changes occurring in other IR bands, shown in Figure 6.17(b), are listed in Table 6.6. From the splitting patterns of 555, 886, 1012, 1078, 1775  $\text{cm}^{-1}$  bands it can be gathered that absorption frequencies of these bands have shifted toward lower wavenumbers in the IR spectra of stressed PC films. The assignments of these bands have been presented in Table 3.3. A split of 555

---

<sup>1</sup>In these oriented films (stressed-50% unstressed) FTIR subtraction spectra yields the maximum information. As already seen in Figure 6.15, these uniaxially oriented films creep significantly under the applied stress which causes considerable reduction in their thickness. Therefore, subtraction of a higher percentage of the spectrum of unstressed film shows strong negative absorptions and hence defeats our purpose of monitoring small differences in band shapes and frequencies.



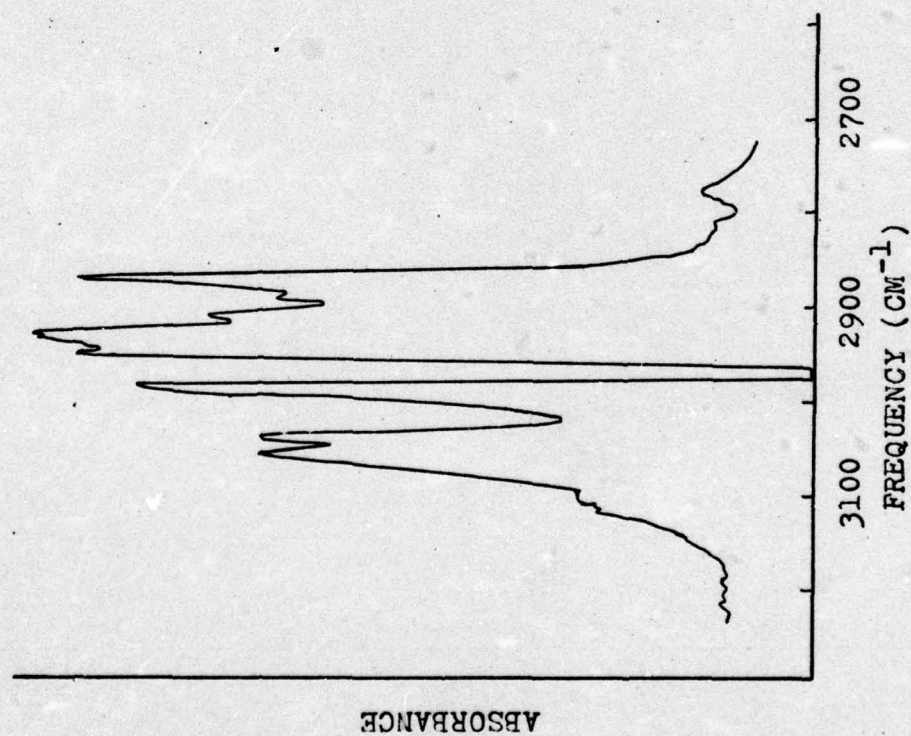


Figure 6.17 (a) FTIR subtraction spectrum of 300% uniaxially oriented PC film.  
(Stressed-50% unstressed)

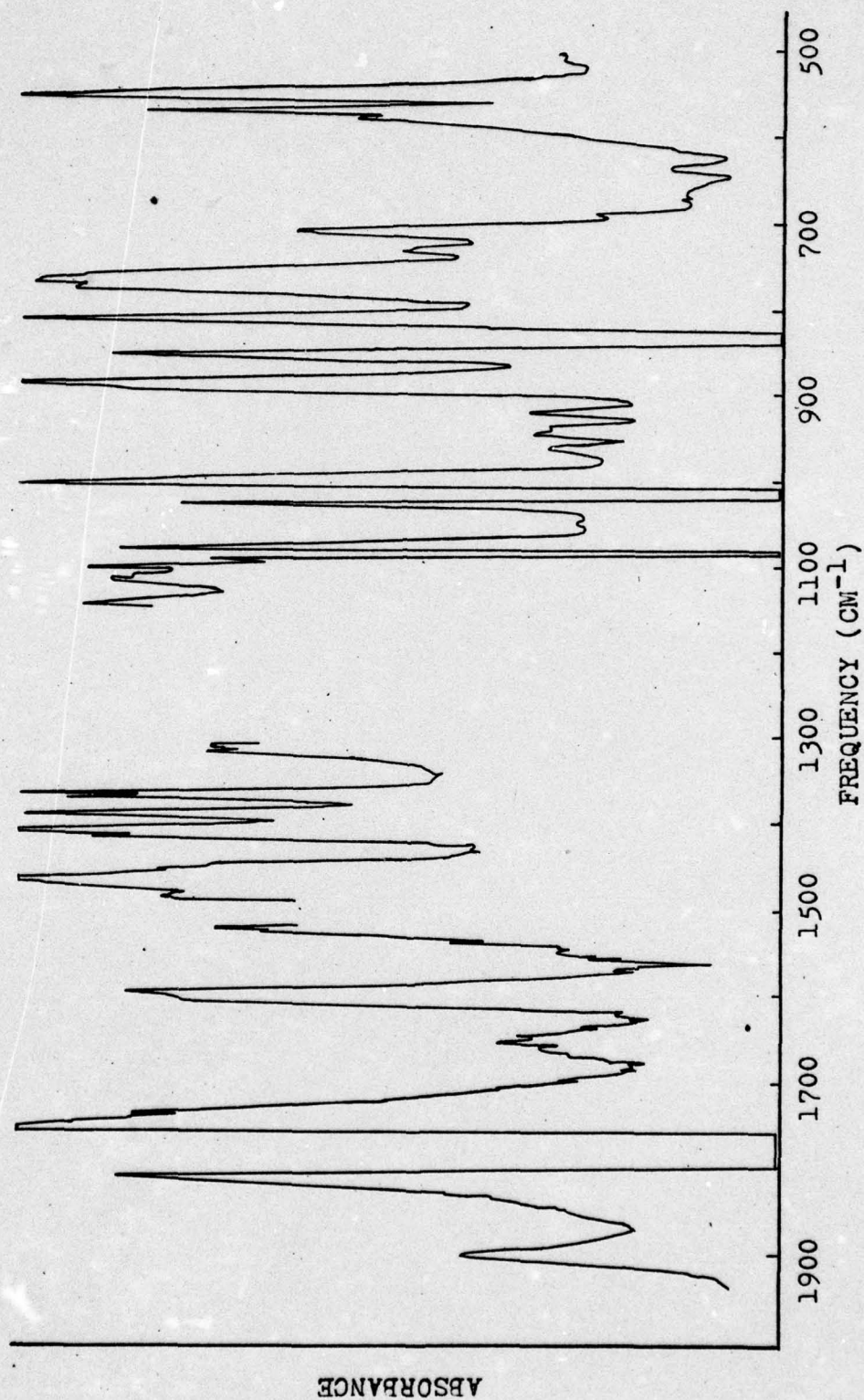


Figure 6.17 (b) FTIR subtraction spectrum of 300% uniaxially oriented PC film.  
(Stressed-50% unstressed)



Table 6.6      Changes in IR Bands of Stressed PC Films  
(Oriented)

Frequency ( $\text{cm}^{-1}$ )	Change Observed
555	Band splits with increased absorption toward lower frequency.
768	Weak shoulder appears.
829	Band splits.
886	Peak absorption distribution changes. It increases toward lower wavenumbers.
1012	Band splits.
1078	Band splits with increased absorption toward lower frequency.
1362	Weak splitting.
1408	Weak splitting.
1502	Shows strong negative absorption.
1775	Shows strong splitting with increased absorption toward lower frequency.

$\text{cm}^{-1}$  band with increased absorption toward lower frequency indicates that many oscillators are absorbing at slightly lower frequency. Similar types of behavior (splitting and frequency shifts) are also observed in 1012, 1078, and 1775  $\text{cm}^{-1}$  IR bands. The principle of these shifts has already been discussed in Sections 2.1.1 to 2.5.5.

In addition to band splittings, it is observed that major changes occur in the absorption intensities, which are caused by the thinning of the films due to creep. Such effects are quite pronounced in polycarbonate where higher free volume (as compared to most other polymers) and absence of rigid and bulky side groups impart unrestricted chain mobility which, in turn, allows PC chains to rearrange and reorient rather easily under the imposed stress.

#### 6.4.3 Discussion

As already mentioned, no changes are observed in the IR spectrum of PC obtained under a stress of 8888 psi, at which the sample shows significant creep. This behavior indicates that many entanglements must have been removed because of the orientation of these films above their  $T_g$  (glass transition temperature), making it easier for PC chains to slide past one another under stress. Thus, relatively more (as compared to unoriented PC) mobile PC chains respond to an imposed stress by extending and reorienting along the direction of the applied stress. As a result, only very few chains may get taut or overstressed to show any significant difference in stress-sensitive IR bands. Thus, it appears that at the molecular level many loops and extendable chain segments exist, even in 300% uniaxially oriented PC films.



The other IR spectrum is obtained from the PC sample strain-hardened by an engineering stress of about 11,100 psi and already strained by 48%. This spectrum shows a negative shift of about  $0.5\text{ cm}^{-1}$  in the  $1078\text{ cm}^{-1}$  IR band along with minute frequency shifts of 1102, 885,  $770\text{ cm}^{-1}$  IR bands. This indicates that most of the PC chains are highly extended under stress in the strain-hardening region of the stress-strain curve. The stresses are, therefore, distributed evenly and almost equally on these chains. This type of stress distribution dilutes the impact of the imposed stress and hence only very small ( $< 1\text{ cm}^{-1}$ ) peak shifts are observed. There can be some overstressed chains but they may be too few to cause any large negative peak shifts.

Similar stress distribution at the molecular level has also been suggested for PC films stressed up to just below the fracture point. This suggestion comes from the (stressed-50% unstressed) FTIR subtraction spectrum, which indicates small negative peak shifts as deduced from the asymmetrical splitting pattern of the stress-sensitive IR bands. The asymmetric band splitting has been modeled and shown in Appendix A.

#### 6.4.4 Summary

IR results obtained from stressing 300% uniaxially oriented samples do not show any overstressed bonds. The stresses in these samples are evenly distributed over a large number of chains. These chains relieve themselves of the imposed stresses by sliding past one another, which is easier in these films having fewer entanglements because of their orientation above the  $T_g$ .

The stresses on the strain-hardened PC films are also distributed

evenly over a large number of extended chains. This has been shown by small negative frequency shifts of the stress-sensitive IR bands. No overstressed chains have been observed even up to a point just before the fracture of these samples.

#### 6.5 Comparison of Molecular Behavior of Unoriented and Oriented PC Films Under Stress

It has been shown in Section 6.1 that in the case of unoriented PC the effect due to stress is noticeable, even at a stress level of 6160 psi ( $\sim 75\%$  of yield stress), whereas it is not so in 300% drawn PC film samples at a stress of 8888 psi ( $\sim 81\%$  of yield stress). This can be explained in terms of differences in the microstructure of unoriented and oriented PC chains. In unoriented state, molecular chains are assumed to be arranged in a random manner with high physical entanglements. In response to external stress, polymer chains try to untangle themselves and during the process some chains tauten, certain segments of tangled chains rearrange while still others, unable to pull out of the entanglements, are overstressed. These stresses cause backbone bonds to deform and intermolecular and intramolecular interactions which, in turn, affect the IR spectrum.

In the case of 300% drawn PC films the chains untangle during the orientation process (above  $T_g$ ). Polymer chains in this oriented state still have several loops and extendable segments. Applied stress causes the chains to flow in the direction of applied stress. As a result, only a few segments may tauten which does not cause any significant changes in the IR spectrum. However, the molecular behavior differs



in the yield region of the stress-strain curve, as demonstrated by the changes observed in IR bands obtained through FTIR subtraction spectrum. The molecular behavior still differs in the strain-hardening region of the stress-strain curve where the changes are noticeable, even in the superimposed IR spectra obtained on Perkin Elmer spectrometer. This indicates that many chains participate in the load bearing process at this stress level and cause significant changes in the IR spectrum. This is, of course, anticipated, because the spectrum is obtained from stressed PC samples at a point just before the fracture point on the stress-strain curve, where most chains are expected to be in taut condition.

#### 6.5.1 Summary

IR studies on unoriented and oriented PC samples reveal that in both cases stresses are almost uniformly distributed over a large number of polymer chains. It is basically the inherent mobility of polymer chains in polycarbonate which yields this result. IR studies of PC under stress, even in the region just prior to fracture, show rather uniform stress distribution on the polymer chains. If there are any taut chains at this stage, they break and redistribute the stresses over the remaining adjacent chains and are probably too few to cause any significant change in the stress-sensitive IR bands.

## CHAPTER VII

### SUMMARY AND CONCLUSIONS

#### 7.1 Summary of Research Objectives

The overall objectives of this research were to extend two new techniques --Dynamic Infrared Spectroscopy and Dynamic Fourier Transform Infrared Spectroscopy -- to the study of amorphous glassy polymers. When combined with standard polymer characterization techniques, these would give an insight into the molecular behavior of amorphous glassy polymers in the following conditions:

- (i) under tensile stress
- (ii) under cyclic fatigue
- (iii) in solvent-crazing
- (iv) in fatigue-crazing.

In these pioneering studies of molecular behavior in amorphous polymers two commercially important materials, polystyrene and polycarbonate, were chosen. The main purpose behind this selection was to learn about the molecular behavior in polymers which are very different in terms of their

- (i) chemical structure, viz., with bulky side groups vs. non-bulky side groups on their backbone
- (ii) mechanical behavior, viz., hard and strong vs. hard and tough.



## 7.2 Summary and Conclusions of Studies on Polystyrene

Study of the molecular behavior of polystyrene films under different orientation conditions, such as unoriented, uniaxially oriented and biaxially oriented films, has given us a better understanding of the stress-bearing mechanism in this polymer which has bulky phenyl side groups on its backbone chain.

The present study of infrared band distortions of TRICITE (biaxially oriented) films under stress has revealed that the phenyl side groups located on adjacent polymer chains are partially interlocked. When stress is applied on the films, it is transmitted to individual portions of the chains, causing rearrangement which is accompanied by distortions of the phenyl groups and breakage of certain interlockings. This results in an increase in local chain mobility which, in turn, is responsible for an increase in interphenyl interferences under increased stress. Such interferences have been found to be greater in biaxially oriented TRICITE films than in unoriented or uniaxially oriented films. This is due to greater free volume and hence greater chain mobility that is shown to exist in the biaxially oriented films by their much greater ability to extend before fracture.

This molecular behavior is quite dependent upon sample preparation and processing as shown by the study of 4.5 and 3.0 mil thick TRICITE films under stress.

In thicker films orientation is known to vary through the thickness of the films; the interior of thicker films is relatively less oriented than the surfaces. In the thin films the better uniformity of quenching

and orientation causes a more uniform load distribution which allows much greater extension per unit of loading. This, in turn, causes a greater distortion of phenyl side groups which causes a peak distortion toward lower frequencies. In the thick films the non-uniform orientation provides varying mobility and varying stress distribution, as shown by band distortions toward higher frequencies. This anomalous behavior is explained as a relief of stresses frozen-in during thick film's formation.

A behavior common to both thick and thin films is that stress causes irreversible changes of their initial molecular arrangements. Once stressed, a film never reverts back to its original phenyl conformations, even if the stress is in the linear part of the stress-strain curve. Similarly, each additional increment of stress causes changes which are only partially reversible. Thus, there appears to be a continuous rearrangement of the phenyl groups, chain movement by breaking Van der Waal's interactions and probable breakage of some backbone bonds. Thus, the results show the interesting conclusion that all strain at all stress levels has a component of plastic deformation at the molecular level.

Another important result of this study is that an increasing number of backbone bonds in the helical sections of atactic PS chains participate in load bearing as stress is applied. Above a threshold level, however, the number of such loaded bonds drops sharply, indicating large scale bond rupture and/or slippage causing redistribution of imposed stress. The threshold stress level at which the above drop is observed lies below the stress where nonlinearity occurs in the stress-



strain curve.

Both of the above results show that changes at the molecular level begin to occur much earlier than can be observed at the macroscopic level.

This study also shows that in highly uniaxially oriented films, chains have better interlocking arrangement of phenyl side groups than in TRICITE biaxial films. Any external stress is evenly distributed in a collective manner over a large number of chains with stresses transmitted to the backbone bonds. This is shown by a smaller distortion of the IR bands assigned to various vibrational modes of the phenyl side groups, at comparable stress levels.

In unoriented polystyrene films chains are assumed highly entangled. Since bulky phenyl side groups are involved in these entanglements, chain mobility is highly restricted. Therefore, when an external stress is applied and chains try to rearrange themselves to relieve this stress, chains must break weak interchain interactions by plastic deformation. This was shown by measurements of the X-ray pattern which indicate a greater increase in the interphenyl and intraphenyl separations than in TRICITE films under stress. This molecular behavior is accompanied by crazes on the surfaces.

Cyclic tensile fatigue of TRICITE films at 50 percent of breaking stress causes chains to rearrange themselves by breaking interchain interactions and some backbone bonds. This is shown by the IR results, X-ray measurements giving a decrease in interphenyl separations, as well as a shift in  $\beta$  relaxation peak in the dynamic mechanical loss spectrum, indicating more free volume. Thus, mechanical exercise causes

a rearrangement into better packing of the chains. This can only occur, apparently, by breakage of the most taut backbone segments, creating the anomalous situation that cyclic fatigue is causing a damaged chain structure, even though better packing occurs.

Stress-crazing and solvent-crazing, on the other hand, are quite different molecularly from the fatigue process. X-ray measurements and IR results appear more like (but not identical to) the stressed condition. In general, crazing shows a freeing and stress-relief of certain chain segments, although certain other segments appear to be overstressed. It is postulated that these overstressed segments are located in the regions surrounding crazes.

### 7.3 Summary and Conclusions of Studies on Polycarbonate (bisphenol A)

This present pioneering study of unoriented and uniaxially oriented polycarbonate films under tensile stress reveals that the load is evenly distributed over a large number of polymer chains. This result is readily understandable from the high free volume that has been shown to exist in the microstructure of this polymer. Also, the lack of bulky side groups on the polymer backbone allows high mobility of the chains. As a result, the chains rearrange themselves rather easily under the imposed stress and the load is redistributed evenly over many chains. This conclusion is reached by dynamic infrared results in which there are shifts toward lower wavenumbers of the backbone bond related IR bands peaks. Measurements of interchain distances in unoriented films by X-rays also indicate this mechanism, since interchain distances decrease by about 10% when films are subjected to 80% of the



yield stress.

Most interesting and useful results have been obtained from cyclically fatigued polycarbonate films subjected to stresses equalling 56, 74, 83 and 91% of the yield stress and to varying number of cycles. In all cases much chain scission occurs. This creates voids throughout the sample and the material is weakened. This increase in free volume is also shown by a decrease in the density of the fatigued samples. This is also further supported by our dynamic mechanical measurements which show that cyclic fatigue causes both  $\alpha$  and  $\beta$  relaxation peaks to shift toward lower temperatures. The amount of shift is dependent on the extent of damage caused to the materials during fatigue. In addition to the above large peaks, a weak relaxation occurs around 110°C in the unfatigued film sample (which has now been called the  $\beta$  peak by Boyer). This relaxation peak also shifts toward lower temperatures in the fatigued films, again indicating increase in free volume. Formation of microvoids is demonstrated by the fact that many highly fatigued samples fracture at cryogenic temperatures during dynamic mechanical measurements. Fracture occurs because chain mobility at these temperatures is reduced and the microvoids act as stress risers under the sinusoidal stress. In addition to chain scission and microvoid formation, some stressed chains also exist in fatigued film samples, as shown by weak splitting of  $1078\text{ cm}^{-1}$  IR band assigned to the asymmetric stretch of the C-C-C backbone bond.

Comparisons of fatigue-crazed and solvent-crazed film samples show that these crazes are produced via a different molecular behavior. This is determined from the relaxation spectra in which both  $\alpha$  and  $\beta$

relaxation peaks are unaffected in the solvent-crazed film samples, whereas in the fatigue-crazed samples there is a shift of  $\alpha$  and  $\beta$  peaks toward lower temperatures. In addition, only the fatigue-crazed samples fracture at cryogenic temperatures. Also, solvent-crazing causes a dispersion of the weak relaxation peak (occurring at about 110°C in uncrazed samples), indicating a certain amount of plasticizing effect by the solvent.

#### 7.4 Comparison of Polystyrene and Polycarbonate Polymers

In this section similarities and difference in the structure and molecular behavior of atactic polystyrene and polycarbonate (bisphenol A) under the studied conditions are presented in tabulated form in Table 7.1.

#### 7.5 Comparison of Present Studies with Studies on Semicrystalline Polymers

In PET samples the dynamic infrared technique demonstrated the existence of overstressed bonds by showing the peak shifts in 1-2  $\text{cm}^{-1}$  range along with distortions in the low frequency region of the 976  $\text{cm}^{-1}$  band. Such overstressing of bonds occurs in the tie molecules which bear very high stresses during any loading process. The 976  $\text{cm}^{-1}$  IR band studied by Mocherla and Statton has been assigned to  $\delta(\text{CCC})$  vibrational mode. Other backbone bonds in the structure of PET shown in I below,

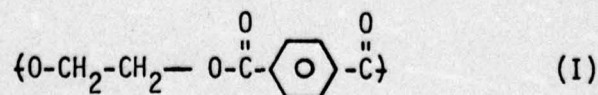




Table 7.1 Comparison of Atactic Polystyrene and Polycarbonate Polymers

	PS	PC
Type of polymer	addition	condensation
Type of side groups	bulky and rigid phenyl side groups	non-bulky-CH <sub>3</sub> side groups
Mechanical behavior	brittle in unoriented state	strong and tough in unoriented state
Density	1.04 to 1.06 g/ml	1.20 g/ml
Fractional free volume ( $\Delta \alpha T_g$ )	0.11	0.16 [124]
Glass transition temperature	80°C	149°C
Bragg spacing due to outer halo	$\sim 4.67 \text{ \AA}$ ascribed to both interphenyl and intraphenyl distances	$\sim 5.47 \text{ \AA}$ ascribed to interchain distances only
Molecular weight of repeat unit	104 [130]	254 [130]
Repeat unit length	$2.21 \times 10^{-10} \text{ m}$ [130]	$10.75 \times 10^{-10} \text{ m}$ [130]
Molecular area	$74.1 \times 10^{-20} \text{ m}^2$ [130]	$32.9 \times 10^{-20} \text{ m}^2$ [130]
Bonds/nm <sup>2</sup>	1.35 [130]	3.04 [130]
Effect of tensile stress on IR bands	Highly distorts bands assigned to vibrational motions of phenyl side groups	Peak shifts are observed in IR bands related to backbone bonds

Table 7.1 (continued)

	PS	PC
Type of stress distribution in (i) unoriented state	(i) non-uniform due to strong interphenyl interferences and highly restricted chain mobility	uniform distribution because of higher chain mobility in all cases
(ii) biaxially oriented state	(ii) non-uniform because of high interphenyl interferences	
(iii) uniaxially oriented state	(iii) relatively even distribution because of increased alignment of PS chains and, therefore, increased number of interphenyl lockings	
Recovery of IR bands on removal of stress	Mostly but not completely at stresses even before the yield point	not determined
Effect of tensile stress on Bragg distance	increases	decreases
Effect of cyclic fatigue (i) on IR bands	(i) IR bands related to vibrational motions of phenyl groups are affected indicating changes in intermolecular and intramolecular interferences	(i) Backbone related IR bands show small peak shifts toward lower frequency indicating stressing of many chains
(ii) Bragg spacing	(ii) decreases, indicating better packing resulting from fatigue process	(ii) decreases very slightly



Table 7.1 (continued)

	PS	PC
(iii) $\alpha$ relaxation peak	(iii) no shift	(iii) shifts toward lower temperature
(iv) $\beta$ relaxation peak	(iv) shifts toward lower temperature	(iv) shifts toward lower temperature
(v) Density	(v) not determined	(v) decrease in fatigued samples
(vi) Crazes	(vi) not observed	(vi) observed
(vii) At Molecular level	(vii) breakage of interchain interaction, conformational changes, removal of frozen-in stress	(vii) breakage of interchain interactions and breakage of backbone bonds or chain scission
Effect of Crazing		
(i) Bragg spacing	(i) increases in stress-crazed unoriented sample	(i) not determined
(ii) relaxation behavior	(ii) not determined	(ii) no shift of $\alpha$ & $\beta$ relaxation peaks, however, a weak peak occurring at $-110^{\circ}\text{C}$ in uncrazed samples disperses over large temperature range due to plasticizing effect of the solvent

Table 7.i (continued)

	PS	PC
(iii) IR bands	(ii) Phenyl group related vibrational modes are affected indicating presence of some stressed chains even in solvent-crazed samples	(iii) the effect on IR bands is quite weak. No peak shift observed in the IR bands assigned to various vibrational motions of the backbone bonds. However, weak splittings are observed in the case of several bands. The phenomena needs further investigation.



have not been studied. Since FTIR was available during the present study, this author obtained FTIR spectra from PET film sample (film C described in Chapter II) under stress and no stress. At strains above 5%, which correspond to a stress of 25,000 psi, FTIR superimposed spectra shows formation of shoulders on the low frequency side. The peak shift at this point should be about  $1\text{ cm}^{-1}$  as determined from Figure 2.7, which is not actually observed in the superimposed spectra. Nevertheless, this  $976\text{ cm}^{-1}$  band splits in the computer-subtracted (stress-95% unstressed) FTIR spectrum. This indicates that splittings are a valid way of determining the changes occurring at the molecular level and these may even be resolvable if spectra are obtained at a resolution of  $0.5\text{ cm}^{-1}$ . The spectrum of unstressed PET is shown in Figure 7.1 and the subtraction spectrum (stress-95% unstressed) in Figure 7.2. It can be seen in these spectra that a large number of bonds associated with the backbone of the PET chain are affected by an imposed stress (as indicated by observed splittings). In the case of amorphous polymers splittings have been found to be quite numerous and rather intense. This difference is explainable on the basis of high stresses applied on amorphous film samples as compared to relatively low stresses applied on PET film samples which have extremely high tensile modulus. Distribution of stresses over a rather large number of chains also reduces the impact of applied stresses as compared to stresses being borne by only a few bonds and becoming, therefore, highly overstressed.

Thus, the present brief study by FTIR confirms the validity of the earlier work in this laboratory using the conventional instrumentation.

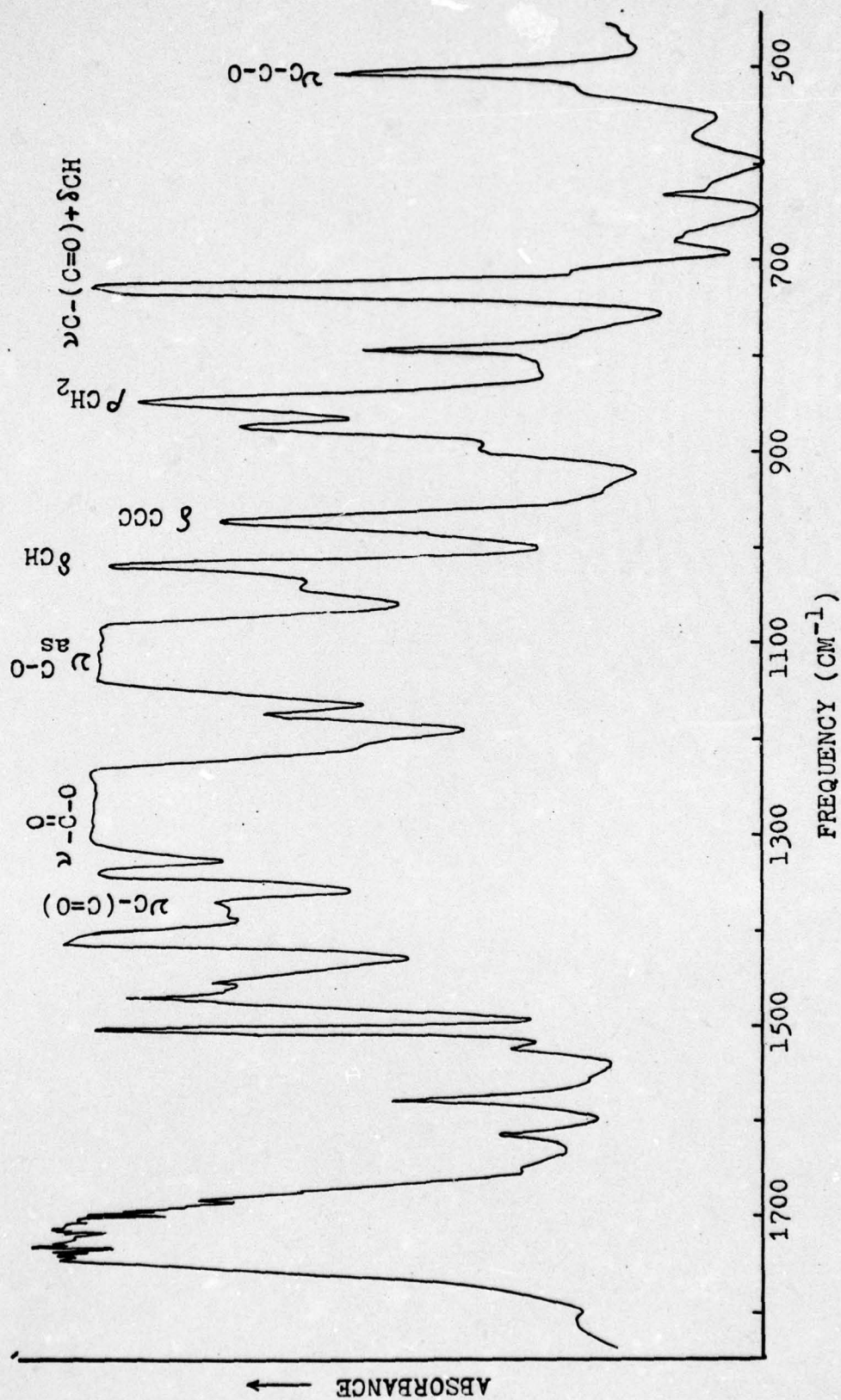
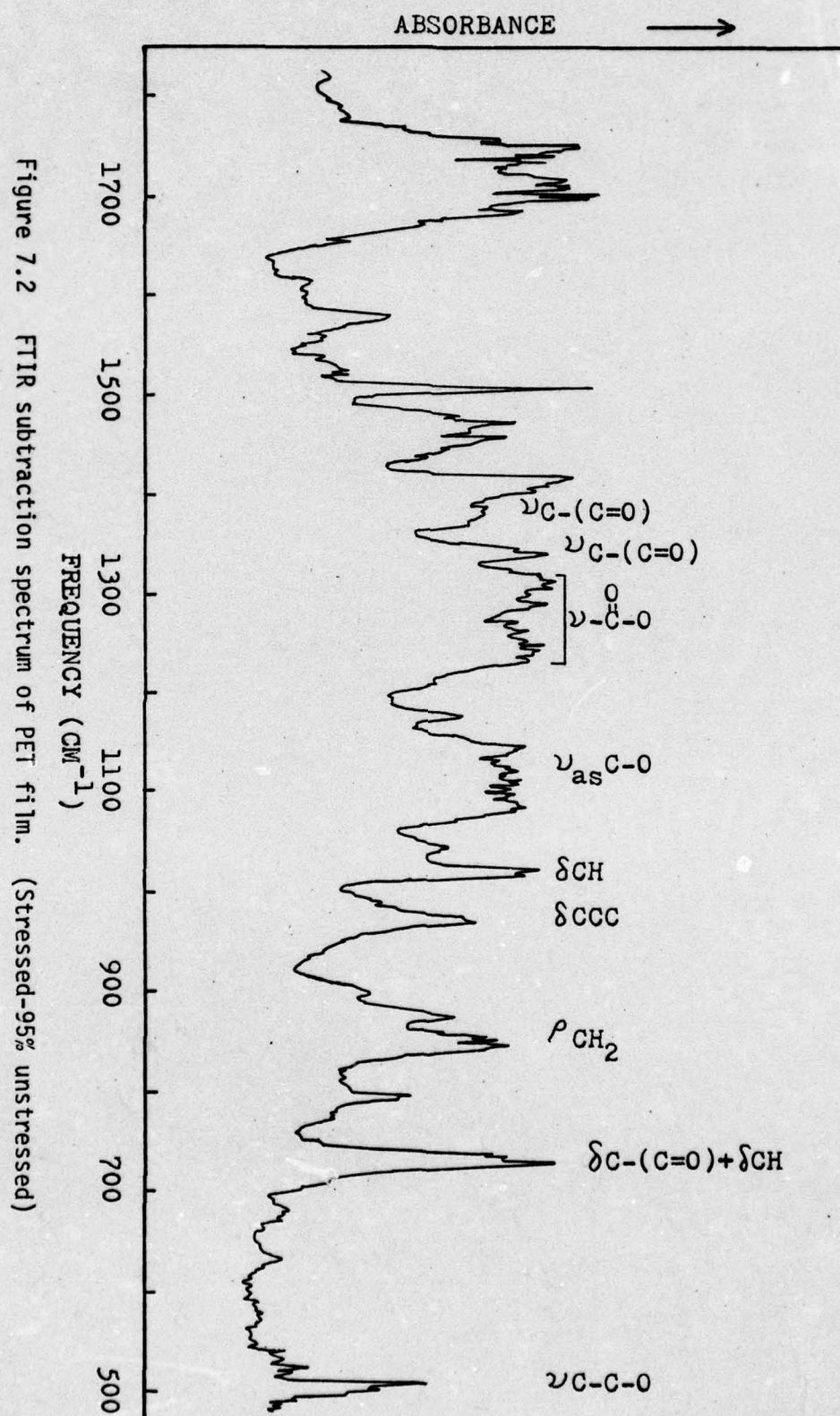


Figure 7.1 FTIR spectrum of unstressed PET film.





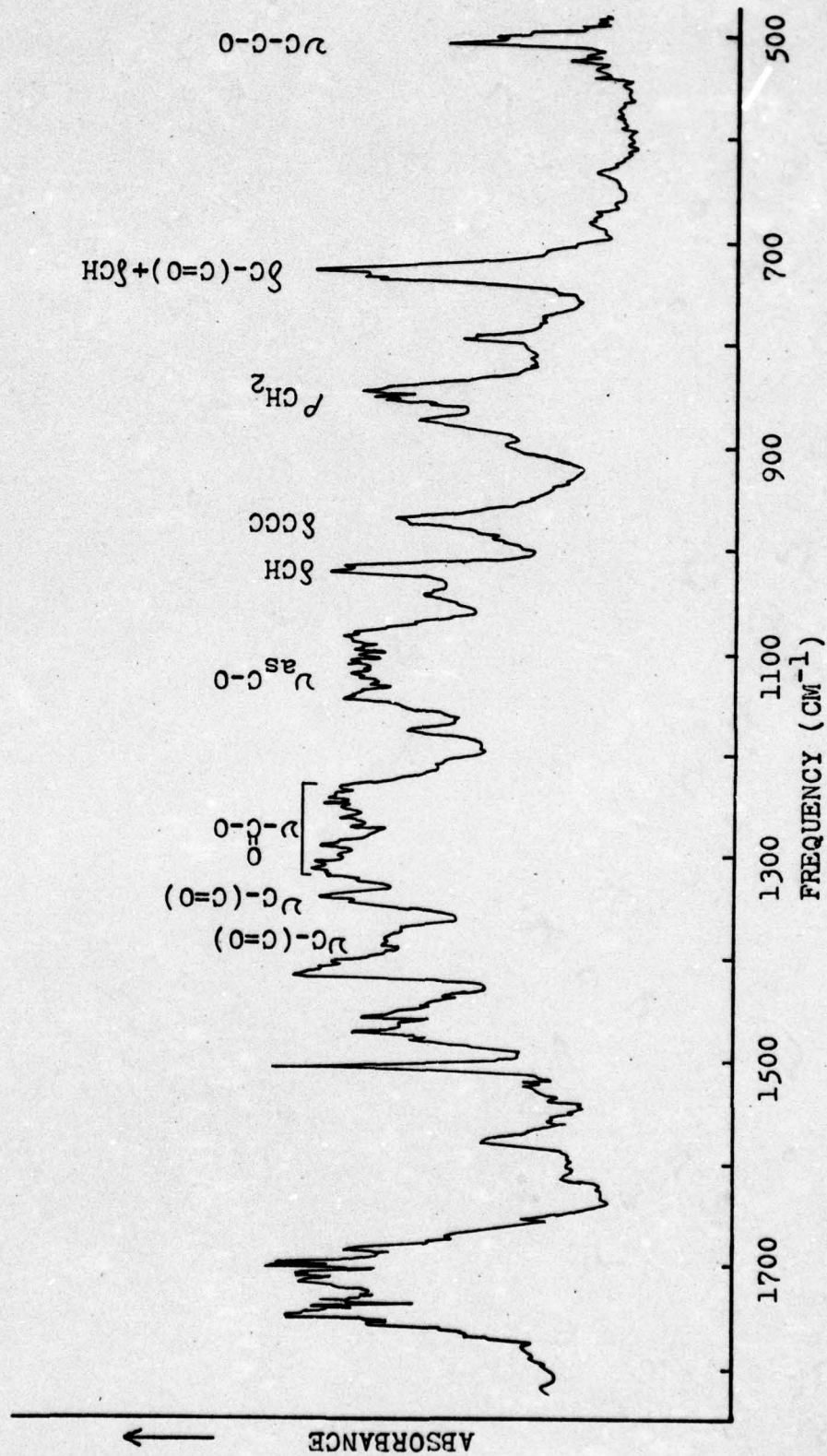


Figure 7.2 FTIR subtraction spectrum of PET film. (Stressed-95% unstressed)



The present study also indicates how many more absorption bands are readily available for detailed analysis than can be conveniently handled by the earlier technique, and that very subtle and perhaps seemingly inconsequential changes can be cataloged by means of the computer-subtracted FTIR spectra.

#### 7.6 Recommendations for Further Research

At this point the author recommends the following research as desirable to answer some new questions that have arisen during the present work.

1. It has been discovered by the author that stressed polymer chains exist in crazed polymer samples and these are postulated to exist in the regions surrounding crazes. Since the IR technique has now been well established for studies of the molecular behavior in both semi-crystalline and amorphous polymers, this author suggests that this method should also be employed to study molecular level stresses ahead of propagating cracks, as well as in the regions surrounding crazes. This can be achieved rather easily by focusing the infrared beam through a beam condenser on to these regions. For such purposes Fourier Transform Infrared Spectroscopy will be required because of the miniscule area of concern.
2. Laser Raman spectroscopy is another very powerful tool which can complement the IR results in studying molecular level processes taking place in polymers under various external conditions. This technique was, in fact, briefly explored by the author. However, these experiments were hampered because of the lack of proper stretching and sample

mounting device needed for the present experimental set-up available at the Chemistry Department of the University of Utah. This technique can be particularly useful in unraveling the molecular behavior under tensile stress and fatigue conditions in bulky or thicker polymer samples.

3. The strong interactions caused by partial interlocking of phenyl side groups in PS can, perhaps, be reduced by increasing the interchain distances and by increasing the free volume in the microstructure of this polymer. This can be achieved by adding plasticizer which will provide a more complete insight into the nature of these interactions.
4. In polycarbonate samples significant amounts of chain scission occur during fatigue. The author recommends that chain scission mechanism proposed here may be correlated by the studies of molecular weight distributions in unfatigued vs. fatigued PC samples. These studies, when correlated with dynamic mechanical measurements, can give an insight to the extent of molecular chain scission occurring during the fatigue process. Similar studies are also recommended for the polystyrene polymer.



## APPENDIX A

### MODELING OF BAND SPLITTINGS IN FTIR SPECTRA

In order to understand the causes of IR band splittings observed in the FTIR subtraction spectra, the author assumed certain shapes of the curves, preferably Gaussian curve, which the IR absorption bands generally follow and modeled several subtractions under different conditions.

Figure A-1 shows the subtraction performed when the distribution of the curve changes. In this case 80% of the broken line curve was subtracted from the solid line curve to normalize intensity differences between the two curves. This resulted in a difference curve shown by dotted lines.

Figure A-2 exhibits a different behavior. In this case a broad curve and its resolution into three Gaussian curves has been modeled. Here a 100% subtraction of broken line curve from the solid line curve results in two small peaks represented by dotted lines. Such behavior has been observed in certain IR bands in the FTIR subtraction spectra.

Figure A-3 again illustrates the type of splitting anticipated when oscillators intensely absorb at a certain frequency, exhibiting a sharp intensity peak. Here 50% of the broken line curve has been subtracted from the solid line curve. The result is a single splitting of the curve with symmetrical shoulders.

Figure A-4 represents a situation in which the curve is slightly

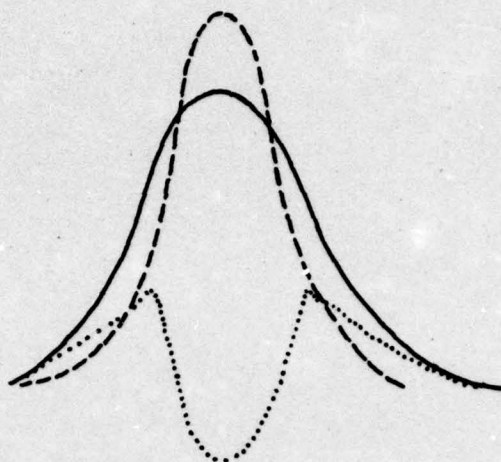


Figure A.1 Model for single band splitting resulting from change in peak distribution.

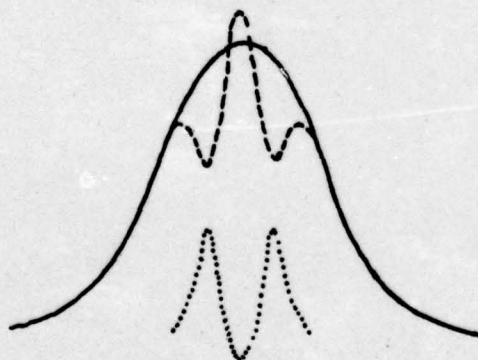


Figure A.2 Model for double band splitting resulting from change in peak distribution.



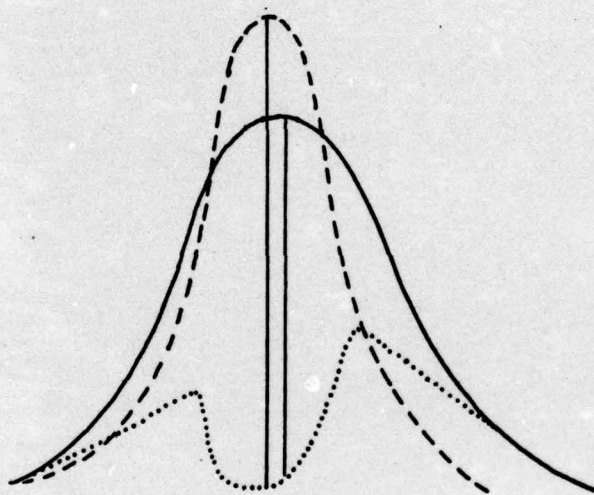


Figure A.3 Model for non-symmetrical single band splitting resulting from change in peak distribution and position.

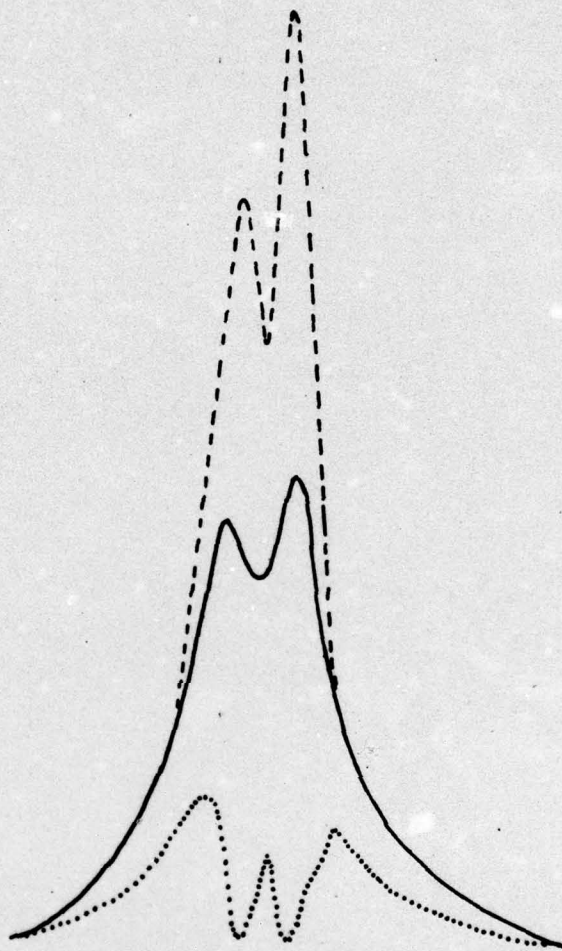


Figure A.4 Model for double band splitting due to peak shift.



shifted toward a certain direction. In this case solid line curve is shifted toward the right direction. An 80% subtraction yields a resultant curve which is split non-symmetrically.

Figure A-5 shows another case in which the shorter peak of the two in the broken lined curve is shifted toward the right side. A 50% subtraction of the broken line from the solid line curve yields a dotted line curve as the difference, which is similar to a double splitting observed in certain IR bands during the FTIR subtraction spectra.

It is pointed out that all or some of the situations mentioned here may actually occur in many IR bands in the computer-subtracted FTIR spectra. However, the examples given here are quite magnified, whereas in the case of actual FTIR subtraction spectra, such changes are rather small.

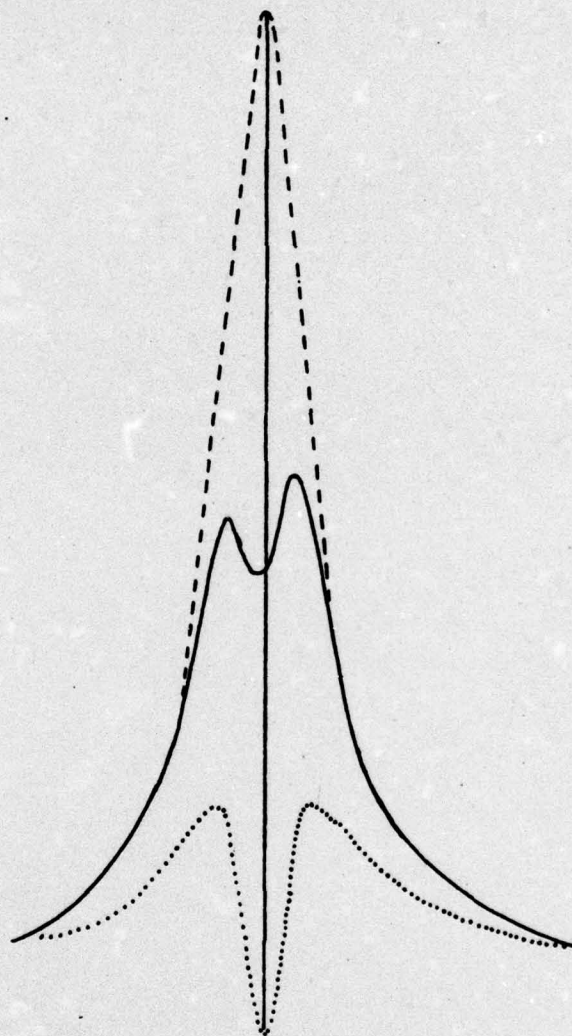


Figure A.5 Model for single band splitting due to band resolving and peak shift.



## APPENDIX B

### HYPOTHESIS TESTING

A test of hypothesis was carried out to prove the validity of the small changes in the  $d_{\text{Bragg}}$  caused by tensile stressing and cyclic fatigue of TRICITE films.

The hypothesis testing method used here is the one which tests the sample means when the true means and variances are unknown. It was assumed here that experimentally measured values follow a normal distribution. It was also assumed that the two variances are unknown. The testing here is shown for  $d_{\text{Bragg}}$  in cases of unstressed and stressed films of TRICITE;  $d_{\text{Bragg}}$  in case of fatigued and unfatigued TRICITE film;  $d_{\text{Bragg}}$  for unfatigued and fatigued polycarbonate films.

The test characteristic is

$$t_0 = \frac{\bar{x}_1 - \bar{x}_2 - \gamma}{s_p \sqrt{\frac{1}{n_1} + \frac{1}{n_2}}}$$

$\gamma$  is the difference assumed between the true  $d_{\text{Bragg}}$ .

$$s_p = \frac{(s_1^2)(n_1 - 1) + (s_2^2)(n_2 - 1)}{n_1 + n_2 - 2}$$

The frequency of the criteria characteristic is determined as

$$v = \frac{\left( \frac{s_1^2}{n_1} + \frac{s_2^2}{n_2} \right)^2}{\frac{(s_1^2/n_1)^2}{n_1 + 1} + \frac{(s_2^2/n_2)^2}{n_2 + 1}} - 2$$

$$s_1^2 = \text{variance of 1} = \frac{n_1}{\sum_{i=1}^{n_1}} \frac{(x_{1i} - \bar{x}_1)^2}{n_1 - 1} = \frac{ss_1}{n_1 - 1}$$

$$s_2^2 = \text{variance of 2} = \frac{n_2}{\sum_{i=1}^{n_2}} \frac{(x_{2i} - \bar{x}_2)^2}{n_2 - 1} = \frac{ss_2}{n_2 - 1}$$

$\mu$  represents the true mean of the particular  $d_{\text{Bragg}}$



Step	Test for $d_{\text{Bragg}}$ for unstressed & stressed TRICITE film	Test for $d_{\text{Bragg}}$ for unfatigued & fatigued TRICITE film	Test for $d_{\text{Bragg}}$ (unfatigued and fatigued) PC film
1. Sample means			
$x_1$	4.7995	4.7995	5.4781
$x_2$	4.9314	4.6954	5.4146
2. Null hypotheses	$\mu_1 - \mu_2 = \gamma$	$\mu_1 - \mu_2 = \gamma$	$\mu_1 - \mu_2 = \gamma$
3. Alternate hypotheses	$\mu_1 - \mu_2 \neq \gamma$	$\mu_1 - \mu_2 \neq \gamma$	$\mu_1 - \mu_2 \neq \gamma$
4. Criteria for rejection-fail to reject if	$ t_0  > t_{\alpha/2, \nu}$	$ t_0  > t_{\alpha/2, \nu}$	$ t_0  > t_{\alpha/2, \nu}$
5. $t_0$	0	0	0
6. Error $\alpha$	0.05	0.05	0.05
Confidence level	99.95%	99.95%	99.95%
7. Frequency $\nu$	9.5215	7.5921	3.8748
8. $t_{\alpha/2, \nu}$	2.24	2.33	3.10
9. Test	$ t_0  \not> t_{\alpha/2, \nu}$	$ t_0  \not> t_{\alpha/2, \nu}$	$ t_0  \not> t_{\alpha/2, \nu}$
10. Reject	no	no	no

CONCLUSIONS OF THE ABOVE TESTS are that null hypothesis cannot be rejected with a confidence limit of 99.95%.

$\therefore d_{\text{Bragg}} (\text{unstressed}) < d_{\text{Bragg}} (\text{stressed}) \text{ TRICITE film}$   
 $d_{\text{Bragg}} (\text{unfatigued}) > d_{\text{Bragg}} (\text{fatigued}) \text{ TRICITE film}$   
 $d_{\text{Bragg}} (\text{unfatigued PC}) > d_{\text{Bragg}} (\text{fatigued PC}).$

## REFERENCES

1. Polymer Preprints, 15(2), 1-45, 324-343 (1974).
2. J. Macromolecular Science, Pt. B, Physics, in press.
3. "ASTM Standards," American Society for Testing and Materials, Philadelphia, Pa.
4. J. V. Schmitz, Ed., Testing of Polymers, Interscience, New York, 1965.
5. L. E. Nielsen, Mechanical Properties of Polymers, Van Nostrand Reinhold Co., New York, 1962.
6. L. E. Nielsen, Mechanical Properties of Polymers and Composites, Vol. I., Marcel Dekker, Inc., New York, 1974.
7. L. E. Nielsen, Mechanical Properties of Polymers and Composites, Vol. II, Marcel Dekker, Inc., New York, 1974.
8. I. M. Ward, Mechanical Properties of Polymers, Wiley Interscience, New York, 1971.
9. A. V. Tobolsky, Properties and Structure of Polymers, John Wiley, New York, 1967.
10. J. D. Ferry, Viscoelastic Properties of Polymers, 2nd ed., J. Wiley & Sons, New York, 1970.
11. P. D. Ritchie, Physics of Plastics, D. Van Nostrand Co., Inc., Princeton, N. J., 1965.
12. E. W. Collins, J. Bares and F. W. Billmeyer, Jr., Experiments in Polymer Science, John Wiley & Sons, New York, 113 (1973).
13. T. L. Smith, Soc. Plast. Engr. Journal, 16, 1211 (1960).
14. "Encyclopedia of Polymer Science and Technology," Interscience, New York, 1968, 8, 461 (1968).
15. F. W. Billmeyer, Textbook of Polymer Science, Wiley-Interscience, New York, 1971.
16. D. K. Roylance, Ph.D. Dissertation, "An EPR Investigation of Polymer Fracture," University of Utah, 1968.



17. S. N. Zhurkov, Int. J. Fract. Mech. **1**, 311 (1965).
18. K. Jenckel, Kolloid Z., **137**, 130 (1954).
19. I. Marshall and A. B. Thompson, Proc. Roy. Soc. (London), **221A**, 541 (1954).
20. F. H. Mueller, Kolloid Z., **126**, 65 (1952).
21. R. D. Deanin, Polymer Structure and Applications, Cahners Books, Boston, Mass., 259 (1972).
22. S. J. Newman, J. Polymer Science, **27**, 563 (1958).
23. P. I. Vincent, Polymer **1**, 7 (1960).
24. J. D. Ferry and R. A. Stratton, Kolloid Z., **171**, 107 (1960).
25. G. M. Byrant, Textile Res. J., **31**, 399 (1961).
26. R. D. Andrews and Y. Kazama, J. Appl. Phys., **38**, 4118 (1967).
27. J. Skelton, W. D. Freestone, Jr. and M. M. Schoppee, J. Appl. Polym. Sci., **14**, 2797 (1970).
28. S. Raha and P. B. Bowden, Polymer **13**, 174 (1972).
29. G. M. Bartenev and S. Yu Zuyev, Strength and Failure of Viscoelastic Materials, Pergamon Press, Oxford (1968).
30. T. E. Brady and G. S. Y. Yeh, J. Macromol. Sci. (Phys.) **B9(4)**, 659 (1974).
31. R. E. Robertson, Appl. Polym. Symp. **7**, 201 (1968).
32. K. K. R. Mocherla, Ph.D. Dissertation, "Stress-Strain Behavior of Oriented Crystalline Polymers--A Molecular Approach by Dynamic Infrared Techniques," University of Utah, Salt Lake City, Utah, 1976.
33. Yu B. Zaks, M. L. Lebedinskaya and V. N. Chaldize, Polym. Sci., USSR, (English Transl.), **12**, 3025 (1970).
34. B. A. Lloyd, K. L. DeVries and M. L. Williams, J. Polym. Sci., A2, **10**, 1415 (1972).
35. S. N. Zhurkov, V. A. Zakrevskyi, V. E. Korsukov and V. S. Kukseno, J. Polym. Sci. A2, **10**, 1509 (1972).
36. A. A. Griffith, Phil. Trans. Royal Soc. A221, 163 (1920).

37. T. L. Smith, J. Polym. Sci., 32, 99 (1958).
38. P. Predecki and W. O. Statton, J. Appl. Phys., 37, 4053 (1966).
39. R. N. Haward, The Physics of Glassy Polymers, John Wiley & Sons, New York, 1973.
40. N. W. Taylor, J. Appl. Phys., 15, 943 (1947).
41. H. A. Stuart and D. L. Anderson, J. Amer. Ceram. Soc., 36, 416 (1953).
42. S. N. Zhurkov, E. E. Tomashevsky, "In Practical Basis of Yield and Fracture," Institute of Physics, London, 200 (1966).
43. J. B. Park and W. O. Statton, to be published.
44. K. L. DeVries, D. K. Roylance and M. L. Williams, J. Polym. Sci. A-1, 8, 237 (1970).
45. K. L. DeVries, D. K. Roylance and M. L. Williams, J. Polym. Sci. A-2, 10, 1415 (1972).
46. H. H. Kausch, Revs. in Macromol. Chem., 5, Pt. 2, 97 (1970).
47. Y. Kawashima, S. Shimada, H. Kashiwabara and J. Shoma, Polymer J. 5, No. 2, 135 (1973).
48. K. L. DeVries and D. K. Roylance, Prog. in Solid State Chem., J. O. McCaldin and G. Somorjai, eds., Pergamon Press, New York, 283 (1973).
49. A. Peterlin, J. Polym. Sci., Pt. C, 32, 297 (1971).
50. R. P. Wool and W. O. Statton, J. Polym. Sci., Polymer Phys. Ed., 12, 1575 (1974).
51. K. K. R. Mocherla and W. O. Statton, Symp. for High Polym. Phys., Seoul, Korea, 1 (1975).
52. A. N. Gent, J. Mater. Sci., 5, 925 (1970).
53. A. N. Gent, J. Macromol. Sci., B8 (3-4), 597 (1973).
54. R. J. Oxborough and P. B. Bowden, Phil. Mag. 28(3), 547 (1973).
55. I. Narisawa, J. Polym. Sci., A-2, 10, 1789 (1972).
56. G. Menges and R. Riess, Plast. and Polym. 42, No. 159, 119 (1974).



57. S. Rabinowitz and P. Beardmore, CRC Crit. Revs. in Macromol. Sci., 1, 1 (1972).
58. R. P. Kambour and A. S. Holik, J. Polym. Sci., A-2, 7, 1393 (1969).
59. P. Behan, M. Bevis and D. Hull, Phil. Mag., 24, 1267 (1971).
60. R. P. Kambour and R. Russer, General Electric Co. Report No. 70-C-360.
61. R. P. Kambour, Polymer 5, 143 (1964).
62. J. Murray and D. Hull, Polymer 10, 541 (1969).
63. D. Hull, J. Mater. Sci., 5, 357 (1970).
64. P. Beardmore and T. L. Johnston, Phil. Mag., 23, 1119 (1971).
65. W. Whitney and R. D. Andrews, J. Polym. Sci., C, 16, 2981 (1965).
66. S. S. Sternstein and F. A. Meyers, J. Macromol. Sci.-Phys., B8 (3-4), 539 (1973).
67. A. S. Agron, R. D. Andrews, J. A. Godrick and W. Whitney, J. Appl. Phys. 39, 1899 (1968).
68. P. B. Bowden, Phil. Mag., 22, 455 (1970).
69. P. B. Bowden and S. Raha, Phil. Mag., 22, 463 (1970).
70. T. E. Brady and G. S. Y. Yeh, J. Appl. Phys., 42, 4622 (1971).
71. W. Whitney, J. Appl. Phys., 34, 3633 (1963).
72. T. E. Brady and G. S. Y. Yeh, J. Mater. Sci., 8, 1083 (1973).
73. J. N. Sultan and F. J. McGarry, Polym. Eng. and Sci., 14, No. 4, 282 (1974).
74. D. W. Van Krevelen, Properties of Polymers-Correlations with Chemical Structure, Elsevier Publishing Co., New York (1972).
75. R. Zbinden, Infrared Spectroscopy of High Polymers, Academic Press, New York (1964).
76. S. N. Zhurkov, V. I. Vettegren, V. E. Korsukov and I. I. Novak, Proceedings of Second International Conference on Fracture, Brighton, England, April 1969.
77. R. P. Wool, "Molecular Mechanics of Polymers by Dynamic Infrared Techniques," Ph.D. Dissertation, University of Utah, Salt Lake City, Utah (1974).

78. A. I. Gubanov, Mekhanika Polimerov, 4, 608 (1967).
79. A. I. Gubanov, Mekhanika Polimerov, 3, 771 (1967).
80. V. I. Vettegren and I. I. Novak, J. Polym. Sci., A-2, 11, 2135 (1973).
81. S. N. Zhurkov, V. I. Vettegren, V. E. Korsukov and I. I. Novak, Fizka, Tuerdого Tela, 2, 290 (1969).
82. V. A. Kosobukin, Soviet Phys.--Solid State, 14, No. 9, 2246 (1973).
83. A. I. Gubanov and V. A. Kosobukin, Mekhanika Polimerov, 4, 586 (1968).
84. J. Reynolds and S. S. Sternstein, J. Chem. Phys., 41, 47 (1964).
85. S. L. Cooper, Polymer Conference Series, University of Utah, Salt Lake City, Utah (1973).
86. N. L. Alpert, W. E. Keiser and H. A. Szyamanski, IR Theory and Practice of Infrared Spectroscopy, A. Plenum/Roseeta, ed., New York (1970).
87. R. H. Boyd and S. M. Breitling, Macromolecules, 5, 279 (1972).
88. T. Miyazawa, J. Chem. Phys., 35, 693 (1961).
89. B. Szigeti, Royal Soc. Proc. Series A, 252, 217 (1959).
90. B. Szigeti, Royal Soc. Proc. Series A, 258, 377 (1960).
91. A. A. Maradudin, Defects and the Vibrational Spectrum of Crystals, (Russ.), Moscow (1968).
92. V. I. Vettegren and V. A. Kosobukin, Optics and Spectroscopy, 31, 311 (1971).
93. V. A. Kosobukin, Mekhanika Polimerov, 4, 579 (1971).
94. V. K. Mitra, R. H. Baughman and W. M. Risen, Jr., Office of Naval Research Technical Report No. 75-02, December 1975.
95. S. I. Veliev, V. I. Vettegren and I. I. Novak, Mekhanika Polimerov 3, 433 (1970).
96. C. Y. Liang and S. Krimm, J. Polym. Sci., 27, 241 (1958).
97. J. R. Katz, Z. Phys. Chem., A125, 321 (1927); Trans. Faraday Soc., 32, 77 (1936).



98. S. Krimm and A. V. Tobolosky, Textile Res. J., 21, 805 (1951).
99. P. Outer, C. I. Carr and B. H. Zimm, J. Chem. Phys., 18, 830 (1950).
100. A. Charlesby, J. Polym. Sci., 10, 201 (1953).
101. K. A. Grirov, O. I. Kandotov and A. V. Kotov, Zhurnal Prik. Spekt., 17, No. 6, 1074 (1972).
102. S. Krimm, C. Y. Liang, G. B. B. M. Sutherland, J. Chem. Phys., 25, 549 (1956).
103. C. Y. Liang, S. Krimm and G. B. B. M. Sutherland, J. Chem. Phys., 25, 543 (1956).
104. S. Krimm, Fortschr. Hochpolym.-Forsch. Bd., 2, 51-172 (1960).
105. M. Kobayashi, K. Tsumura and H. Tadokoro, J. Polym. Sci., A-2, 6, 1493 (1968).
106. M. Takeda, K. Iimura, A. Yamada and Y. Imamura, Bull. Chem. Soc. Japan 33, 1219 (1960).
107. R. F. Boyer, Encyclopedia of Polymer Science and Technology, John Wiley, New York, 13, 259 (1970).
108. H. Schnell, Plast. Inst. Trans. J. (London), 28, 143 (1960).
109. W. Brügel, An Introduction to Infrared Spectroscopy, John Wiley, New York (1962).
110. Sadtler Standard Spectra, Sadtler Research Labs, Philadelphia (1970).
111. J. B. Bates, Science 191, No. 4222, 31 (1976).
112. R. J. Bell, Introduction to Fourier Transform Spectroscopy, Academic Press, New York (1972).
113. W. H. Warhus Co., 406 Rowland Park Blvd., Wilmington, Delaware.
114. R. F. Boyer, Encyclopedia of Polymer Science, John Wiley, New York, 13, 224 (1970).
115. H. P. Klug and L. E. Alexander, X-ray Diffraction Procedures for Polycrystalline and Amorphous Materials, John Wiley, New York, 631 (1954).
116. International Critical Tables, McGraw-Hill, New York, 3, 52 (1928).

117. J. F. Rudd, J. Polym. Sci., C-14, 3 (1966).
118. E. Gurnee, Encyclopedia of Polymer Science and Technology, John Wiley, New York, 13, 342 (1970).
119. S. M. Wecker, T. Davidson and J. B. Cohen, J. Mater. Sci., 7, 1249 (1972).
120. R. F. Boyer, Encyclopedia of Polymer Science and Technology, John Wiley, New York, 13, 277 (1970).
121. A. D. Gabaraeva, M. F. Milagin and N. I. Shishkin, Polymer Mechanics, 3, No. 6, 726 (1965).
122. Y. Ishida and S. Matsuoka, Am. Chem. Soc., Polymer Preprints, 6, No. 2, 795 (1967).
123. G. D. Wignall and G. W. Longman, J. Mater. Sci., 8, 1439 (1973).
124. R. F. Boyer, private communication.
125. R. F. Boyer, J. Polym. Sci., Polymer Symp., 50, 189 (1975).
126. M. Davies, Infrared Spectroscopy and Molecular Structure, Elsevier Publishing Co., New York (1963).
127. R. F. Boyer, Polym. Engr. and Sci., 8, No. 3, 161 (1968).
128. D. A. LeGrand and P. F. Erhardt, J. Appl. Polym. Sci., 13, 1707 (1969).
129. R. F. Boyer, Encyclopedia of Polymer Science and Technology, John Wiley, New York, 13, 293 (1970).
130. P. I. Vincent, Polymer 13, 558 (1972).